Summer 2009

Analysis of cell culture models of mammary drug transport

Joanne Elizabeth Reiland
University of Iowa

ANALYSIS OF CELL CULTURE MODELS OF MAMMARY DRUG TRANSPORT

by

Joanne Elizabeth Reiland

An Abstract

Of a thesis submitted in partial fulfillment
of the requirements for the Doctor of
Philosophy degree in Pharmacy
in the Graduate College of
The University of Iowa

July 2009

Thesis Supervisor: Professor Maureen D. Donovan

ABSTRACT

A human-derived, mammary epithelial cell culture model would allow drug transport in the mammary epithelium to be studied in greater detail while minimizing risks to mothers and nursing infants. MCF10A and primary human mammary epithelial cells (HMECs) were investigated for their utility as human, cell-based model systems for drug transport studies. Polarized monolayers are essential for transcellular flux studies of drug transporter function, and their formation was measured by transepithelial electrical resistance, immunofluorescence microscopy and vectoral flux studies. Both cell types failed to form adequately polarized monolayers despite various modifications to the cells or culture conditions.

Transporter-mediated drug uptake and efflux in MCF10A cells was measured using flow cytometry, a technique which enables the measurement of intracellular drug concentrations. The fluorescent drug, mitoxantrone, was used to assess active efflux transport by the ABC transporters ABCG2 (BCRP) and ABCB1 (MDR1). After accounting for the inter-day variability with a linear mixed effects model, inhibitor effects on intracellular drug concentrations were evident. Specific inhibition of MDR1 using verapamil increased mitoxantrone accumulation as expected; however, BCRP-specific inhibition with fumitremorgin C decreased accumulation. Flow cytometry studies on mitoxantrone uptake suggested that it is a substrate for an unidentified active uptake transporter.

PEPT1 and PEPT2 transporter functionality in MCF10A cells was evaluated using a fluorescently labeled dipeptide (A-K-AMCA). A-K-AMCA uptake showed an active component which was inhibited by a general metabolic inhibitor, the dipeptide

Gly-Gln, and the peptidomimetic cefadroxil, indicating the involvement of a peptide transporter in A-K-AMCA uptake.

Drug transporter expression levels in MCF10A cells and HMECs were measured using RT-PCR. Transporter expression levels, which were similar in the MCF10A cells and the HMECs, were compared with expression levels in lactating and non-lactating mammary epithelial cells. Low expression of BCRP, MDR1 and PEPT1 was seen in MCF10A cells, yet the effects of these transporters could still be observed in functional flow cytometry transport assays. Flow cytometry studies MCF10A cells may useful as a mammary drug transport model for transporters which have similar expression levels to lactating mammary epithelial cells.

Abstract Approved: _____
Thesis Supervisor

_____
Title and Department

_____
Date

ANALYSIS OF CELL CULTURE MODELS OF MAMMARY DRUG TRANSPORT

by

Joanne Elizabeth Reiland

A thesis submitted in partial fulfillment
of the requirements for the Doctor of
Philosophy degree in Pharmacy
in the Graduate College of
The University of Iowa

July 2009

Thesis Supervisor: Professor Maureen D. Donovan

Graduate College
The University of Iowa
Iowa City, Iowa

CERTIFICATE OF APPROVAL

_____

PH.D. THESIS

_____

This is to certify that the Ph.D. thesis of

Joanne Elizabeth Reiland

has been approved by the Examining Committee
for the thesis requirement for the Doctor of Philosophy
degree in Pharmacy at the July 2009 graduation.

Thesis Committee: _____
Maureen D. Donovan, Thesis Supervisor

_____
Douglas Flanagan

_____
Lee Kirsch

_____
Dale E. Wurster

_____
Mahfoud Assem

_____
Sarah England

To my father for his invaluable guidance and inspiration

ACKNOWLEDGMENTS

I would like to express my sincere appreciation and gratitude for the support, encouragement, and especially the guidance I received from my advisor, Dr. Maureen Donovan. I would also like to express my gratitude to my thesis committee members, Drs. Flanagan, Kirsch, Wurster, Assem and England for their assistance in the completion of my research project. In addition, I would like to thank the other faculty members of the Division of Pharmaceutics for their role in my graduate education. I am very appreciative of the staff of the excellent core facilities at the University of Iowa including the Central Microscopy Research Facility, Flow Cytometry Facility, and DNA Facility for providing essential knowledge and expertise towards the completion of my research. Also, to Dr. Robert Kerns and his lab members for advice the use their equipment, and Dr. Sarah England and Victoria Korovkina for their assistance with the cell cultures. This work could not have been completed without valuable advice from my good friend Kevin Freise.

I am deeply grateful to my friends and family. Their love and support were essential in maintaining my motivation and dedication. I would especially like to thank my parents: my mother for her unwavering belief in me, and my father for inspiring me to enter this field of study and the support and guidance he has provided along the way. Finally, I would like to thank Josh for his love and faith, which carried me through all the ups and downs along this journey.

ABSTRACT

A human-derived, mammary epithelial cell culture model would allow drug transport in the mammary epithelium to be studied in greater detail while minimizing risks to mothers and nursing infants. MCF10A and primary human mammary epithelial cells (HMECs) were investigated for their utility as human, cell-based model systems for drug transport studies. Polarized monolayers are essential for transcellular flux studies of drug transporter function, and their formation was measured by transepithelial electrical resistance, immunofluorescence microscopy and vectoral flux studies. Both cell types failed to form adequately polarized monolayers despite various modifications to the cells or culture conditions.

Transporter-mediated drug uptake and efflux in MCF10A cells was measured using flow cytometry, a technique which enables the measurement of intracellular drug concentrations. The fluorescent drug, mitoxantrone, was used to assess active efflux transport by the ABC transporters ABCG2 (BCRP) and ABCB1 (MDR1). After accounting for the inter-day variability with a linear mixed effects model, inhibitor effects on intracellular drug concentrations were evident. Specific inhibition of MDR1 using verapamil increased mitoxantrone accumulation as expected; however, BCRP-specific inhibition with fumitremorgin C decreased accumulation. Flow cytometry studies on mitoxantrone uptake suggested that it is a substrate for an unidentified active uptake transporter.

PEPT1 and PEPT2 transporter functionality in MCF10A cells was evaluated using a fluorescently labeled dipeptide (A-K-AMCA). A-K-AMCA uptake showed an active component which was inhibited by a general metabolic inhibitor, the dipeptide

Gly-Gln, and the peptidomimetic cefadroxil, indicating the involvement of a peptide transporter in A-K-AMCA uptake.

Drug transporter expression levels in MCF10A cells and HMECs were measured using RT-PCR. Transporter expression levels, which were similar in the MCF10A cells and the HMECs, were compared with expression levels in lactating and non-lactating mammary epithelial cells. Low expression of BCRP, MDR1 and PEPT1 was seen in MCF10A cells, yet the effects of these transporters could still be observed in functional flow cytometry transport assays. Flow cytometry studies MCF10A cells may useful as a mammary drug transport model for transporters which have similar expression levels to lactating mammary epithelial cells.

TABLE OF CONTENTS

LIST OF TABLES

LIST OF FIGURES

CHAPTER 1

INTRODUCTION

There are many well known health and nutrition benefits to breast feeding for both the infant and the mother. Health advantages for the infant include a lower incidence of morbidity and mortality, improvement in infant cognitive development, and immunological benefits from the presence of immunoglobulin and complement components in the milk. There are nutritional advantages for the infant as well, including lower incidence of obesity, food allergies and diarrhea.(1) In addition, there are advantages to breast feeding for the mother, including a decreased risk of cancer and osteoporosis, mother-infant bonding, and a return to pre-pregnancy weight more quickly.(1,2) Due to these many benefits, the American Academy of Pediatrics recommends that infants be exclusively breast fed for the first 6 months (3) and, consequently, 60-90% of women in industrialized countries choose to initiate breast feeding.(1)

Despite the many benefits to breast feeding, many women are unable to or choose not to breast feed because of the risk of infant drug exposure to medications through the breast milk. More than 90% of women take at least one medication during the first month post-partum.(2) All drugs in the mother's blood are also present to some extent in the milk, and therefore, pose some exposure risk to the infant. In addition to drugs, environmental toxins and other non-medical substances may be present in the breast milk as well.(1) The majority of drugs are safe to take during breast feeding because the infant exposure risk is minimal; however, information on the safety of most drugs during breast feeding is not available. The unknown drug exposure risk, due to lack of sufficient

available information, can often causes fear of continuing medication during nursing. This fear of infant drug exposure forces many new mothers to choose between their medication and breast feeding, even when the drug is thought to be safe. Medications which are commonly taken by new mothers, and are therefore of great interest for infant drug exposure studies, include antibiotics, pain medications, anti-depressants and medication for chronic conditions such as asthma, allergy, hypertension, arthritis, diabetes, epilepsy or migraine.(1,2)

Milk to Plasma Drug Concentration Ratio

Infant drug exposure is primarily related to the extent the drug is transported into the milk by passive transport, and is commonly quantified by the milk to plasma drug concentration ratio (M/P also called the milk to serum ratio, M/S) (Equation 1.1).(4) The M/P ratio reflects the relative accumulation of drug in the milk relative to the blood. The infant serum drug concentration (Equation 1.2), a measure of infant drug exposure, is determined by the M/P ratio as well as the volume of milk consumed by the infant, the feeding interval, and the pharmacokinetics parameters in both the mother and infant, specifically the maternal dose, bioavailability and clearance.(2) Measured M/P ratios *in vivo* often reflect only a very small number of subjects and sample only a limited number of time points (often only one).(2) Therefore, depending on when in the dosing regimen the samples are taken, the M/P ratio may be over or under the average level. Ideally, M/P ratios would be determined from steady state plasma levels or from the area under the curve for a single dose, both of which would require multiple milk and plasma samples. The M/P ratio for drugs which cross the mammary epithelium solely by passive diffusion can be calculated from Equation 1.1 based on the pH-partitioning behavior of the molecule.

$$M/P = \frac{f_m f_m^{un}(S/W)}{f_p f_p^{un}}$$ Equation 1.1

Where
f_m and f_p = fraction unbound in milk and plasma respectively
f_m^{un} and f_p^{un} = unionized fractions in milk and plasma respectively
S/W = skim to whole milk drug concentration ratio (4)

$$\overline{C}^{infant} = \frac{F^{infant}}{Cl^{infant}}\left[\frac{F^{maternal}D^{maternal}}{Cl^{maternal}}\left(\frac{M}{P}\right)\left(\frac{V_{milk}}{\tau}\right)\right]$$ Equation 1.2

Where
$\overline{C}^{infant}$ = average infant serum concentration at steady state
$F^{infant/maternal}$ = infant/maternal bioavailability
$Cl^{infant/maternal}$ = ^{systemic} clearance for infant/mother
$D^{maternal}$ = daily maternal dose
M/P = milk to plasma drug concentration ratio
V_{milk}/τ = volume of milk consumed per nursing interval (2)

Milk Composition

The amount of drug in the milk is also affected by time-dependent compositional changes in the milk. Milk composition affects drug transfer significantly because only the dissolved, unbound, unionized drug is believed to passively diffuse across the plasma membrane. The ability of a drug to partition into the plasma membrane also determines the extent to which it can be passively transported, and this partitioning behavior is reflected in the oil/water partition coefficient of the drug.

Milk is a mixture of dissolved nutrients, proteins and fat globules, and a pH of 7.0 in the milk is maintained, which is slightly lower than that of the plasma, through directional H^+ ion transport.(2,4,5) This lower pH leads to the accumulation of basic (positively charged) compounds due to ion-trapping. The total protein concentration of the milk is lower than that of the plasma, around 0.9% in milk compared to 5% in plasma, and consists of predominantly caseins and whey.(2,4) The lower milk protein

concentration compared to plasma means that there is significantly less drug-protein binding in the milk, although binding in the milk does occur. Milk also has a higher lipid concentration (2-3%, 98% of which are triglycerides) than plasma.(4) Therefore, lipophilic drugs have a greater potential to accumulate in the milk. In general, drugs with low plasma protein binding, low molecular weight, high lipophilicity, and basic compounds which are charged at the lower pH value will accumulate in the milk by passive diffusion.

Milk composition changes both with the duration of breast feeding and also within each feeding interval; therefore, these can affect the measure M/P ratios as well. The mammary gland secretes colostrum, a high protein, and low fat fluid in the first 5 days of breast feeding, and even within one feeding the initial milk produced is lower in fat than the milk at the end of the feeding. The length of time the milk remains in the alveoli before removal also affects these measurements since back diffusion of the drug may occur.(6) For these reasons reported M/P ratios can vary extensively from study to study. However, since the majority of compounds are transported across the mammary epithelium by passive diffusion, pH-partitioning based models of M/P ratios will accurately predict M/P ratios for many compounds; although the milk accumulation of compounds which are transported by carrier-mediated processes will not be accurately predicted with these models.

Animal Models of Mammary Drug Transport

To address the limited ability to conduct human *in vivo* studies and the limitations of the passive diffusion model for drug transport, animal models and animal cell cultures (most commonly mouse and rat) have been used. Animal models and animal cell cultures are capable of providing more detailed information on drug transport

mechanisms; however, they may not accurately represent the carrier-mediated transport processes present in humans since transporter expression levels may be drastically different between animals and humans. For example, *in vivo* measurements of nitrofurantoin, a known substrate for BCRP (ABCG2), an efflux transporter, showed milk accumulation in rats to be nearly 75-fold greater than predicted from passive diffusion. In humans, nitrofurantoin transport into milk was found to be only 20-fold greater than expected based on passive diffusion.(1) Transport of cimetidine into rabbit milk, which is also a substrate for BCRP, was not significantly different from that predicted from passive diffusion. However, cimetidine transport into milk was almost three times greater than predicted when using a lactating rat model.(7) In addition, significant interspecies differences exist in milk composition and this further limits animal model utility for drug transport studies due to significant differences in partitioning behavior and protein binding between species.(5)

Despite the limitations of animal models, additional valuable information on drug transport can be determined using *in vitro* cell cultures utilizing mammary cells obtained from various species. *In vitro* cultures have a number of advantages over other techniques including easy and rapid measurement; the ability to study molecular mechanisms of transport, and minimizing the use of live animals.(8) Mouse mammary epithelial cell cultures (CIT3) have been used to study carrier-mediated drug transport. Nitrofurantoin was shown to have a greater basal-to-apical flux compared to the apical-to-basal direction, which suggested the presence of an efflux transporter,(9) later identified as BCRP.(10) The main disadvantages of cell culture systems are the decreased cellular differentiation and protein expression compared to *in vivo* tissues.

However, animal cell cultures also have the same disadvantage as whole animal models in that the transporter expression may differ significantly from those in the human mammary gland.

Human Mammary Epithelial Cells

Due to the limitations of *in vivo* M/P ratio measurements, the passive diffusion model, and non-human based systems, a human cell culture model of mammary drug transport would fill in some of the gaps in the understanding of drug transport in the mammary gland. A cell culture model reflective of drug transport in the human mammary gland would allow mechanistic studies of carrier-mediated transport, while better reflecting the properties of the human mammary gland. A greater understanding of the factors governing drug transport into human breast milk and improved ways to limit drug exposure to the infant are the first steps in addressing the important issue of infant drug exposure.

The human mammary epithelial cell line, MCF10A (ATCC, Manassas, VA), was selected for drug transport studies because it is a normal (untransformed), immortalized cell line derived from human fibrocystic mammary tissue.(11) MCF10A cells display normal characteristics of the mammary epithelium such as a lack of tumorgenicity, three-dimensional growth on collagen, response to hormones and growth factors (11) and they secrete some simple milk proteins. MCF10A cells also express basal/luminal differentiation markers. However, they do not secrete caseins or express aldolase C, prolactin, or progesterone receptors.(12) MCF10A cells are, therefore, a closer representation of the human mammary epithelium than the other currently available whole animal and animal cell culture models, and may allow a wide range of drug

transport studies to be performed, thus allowing greater insight into underlying transport mechanisms.

Mammary Gland Physiology

The lactating mammary gland is composed of a branching network of ducts which transport milk secreted by alveolar epithelial cells to the nipple. The alveoli are lined with a single layer of polarized epithelial cells with their apical surfaces facing the lumen of the alveoli. These cells secrete various milk components into the lumen of the alveoli. Underlying these epithelial cells are myoepithelial cells which function in milk ejection and are supported by an extracellular matrix.(13) The mammary alveoli are highly vascularized and have a high surface area to volume ratio which allows rapid solute flux across the epithelium between the milk and the blood.(4)

Mammary epithelial cells are glandular cells with a polarized morphology which is created through cell-to-cell interactions and cell attachment to the extracellular matrix.(14) The epithelial cells lining the ducts and alveoli of the mammary gland are linked through adherens junctions and tight junctions. These intercellular junctions are responsible for maintaining cell polarity and regulating the paracellular transport of ions and molecules. Barrier properties refers to regulation of the paracellular transport route, while polarization refers to the asymmetric protein distribution between the apical and basolateral membranes.(15) Barrier properties and cell polarity are determined largely by the tight junctions, which control paracellular solute transport as well as the asymmetric distribution of proteins within the cell membranes.(16) The mammary epithelium is relatively unique in the sense that the strength of the tight junctions is altered depending on the stage of lactation. The tight junctions in the mammary epithelium are loose and unorganized during pregnancy and consequently the epithelium has a high permeability.

During lactation, however, the tight junctions form a highly impermeable barrier and the paracellular transport of ions and molecules from the plasma to the milk is tightly regulated.(17)

Tight junctions contribute to cell polarity through their function as a barrier to diffusion of membrane proteins within the cell membrane. This keeps membrane proteins, such as transporters, on the cellular surface to which they were exported (apical or basolateral). The asymmetric distribution of transporters between the apical and basolateral membranes leads to a net directionality of flux for their substrates; the direction of the net flux depends on the location of the transporter and its orientation within the membrane (i.e. in which direction it transports its substrates).

The tight junctions are composed of three types of the cytosolic proteins, zona occludins (ZO) ZO-1, ZO-2 and ZO-3, which interact with actin within the cell, and the transmembrane protein, occludin, which participates in the interaction with neighboring cells.(16) Glucocorticoid hormones along with prolactin, insulin and other growth factors are known to induce tight junction formation in the mammary epithelium (18,19) and *in vitro*, the synthetic glucocorticoid dexamethasone has been shown to induce junction formation.(19) Development of a barrier to solute transport by the paracellular route through tight junction formation is essential for normal lactation (20) and is closely correlated with the onset of lactation.(21)

Epithelial cells, *in vivo*, are attached at their basolateral surfaces to an extracellular matrix (ECM), and these attachments are known to be a trigger for the generation of cell polarity.(22,23) The ECM is composed of collagen, laminin V and other fibrous proteins and glycoproteins.(24,25) The extracellular matrix (ECM) is also

an important component of the mammary epithelium, with collagen IV and laminin V being important ECM components for cell attachment and functional differentiation.(14) The basal surface of the cell attaches to the ECM while milk secretion occurs from the apical surface into the alveolar lumen.

Cell polarity and tight junction formation on tissue culture plastic is often different from *in vivo* polarity and there are also differences between cells grown as a two-dimensional monolayer in culture as compared to their growth in three dimensions *in vivo*(14). Cell growth in culture on reconstituted basement membrane, collagen or other ECM components has been shown to aid in the generation of cell polarity in 3D cultures.(26)

The integrity of tight junctions, *in vitro,* can be measured using a number of different methods. The easiest of these methods is measurement of the transepithelial electrical resistance (TEER). This method measures the resistance of the cell layer to ion flow using a set of electrodes, one placed on each side of the cell layer. Reported TEER values for a polarized monolayer of epithelial cells varies widely (from 70 to 3000+ Ωcm^2) depending on the cell line and culture conditions. In general, a TEER of $<200\ \Omega cm^2$ indicates insufficient tight junction formation allowing ions to readily pass through the low resistance paracellular pathway.(17) A TEER of over $1000\ \Omega\ cm^2$ indicates complete barrier formation and thus is desirable for models of the mammary epithelium which form very tight paracellular transport barriers.(19,27,28) Alternatively, the flux of a molecule such as mannitol or lucifer yellow, which are only able to pass through the paracellular route may be used to assess tight junction formation. A significant reduction in flux, compared to the support material alone, indicates functional

tight junction formation; however, the extent of the reduction is highly variable across different cell lines. In addition, immunofluorescence microscopy can be used to localize the tight junction protein ZO-1 or occludin in order to visually assess tight junction formation.

Cell Culture Types

The mammary epithelium is composed of three main cell types: the luminal epithelium, which produces the milk; the myoepithelium, responsible for milk ejection; and the basal epithelium, which is responsible for regeneration following cessation of lactation. Luminal and myoepithelial cells are terminally differentiated and express low molecular weight cytokeratins and smooth muscle actin. Basal epithelial cells and *in vitro* human primary mammary epithelial cells (HMECs) and MCF10A cells express high molecular weight cytokeratins.(29) Therefore, HMECs and MCF10As have some similarity to the less-differentiated basal mammary epithelium.(29)

Two main types of cell culture systems are commonly used for drug transport studies, primary cell lines and continuous cell lines. Primary cultures are cells which have been freshly isolated from human or other tissues. They typically consist of a heterogeneous population of cells. Selection of one cell population from primary cell cultures may be accomplished through specific isolation procedures and culture conditions. The major advantage of primary cells over continuous cell lines is that their differentiation state is more representative of *in vivo* conditions. However, the cells slowly lose their differentiated states with passage *in vitro*, which can lead to a high variability in measured cell properties. Culture of primary epithelial cells is also more difficult than culture of continuous cell lines requiring complex media supplemented with

serum and other undefined components. Some primary cell lines are commercially available, including human mammary epithelial cells (HMECs).

The other main types of cell cultures are continuous or immortalized cultures which are able to multiply for extended periods of time *in vitro*. Immortalization refers to a process by which cells become capable of an infinite number of divisions through a loss of cell cycle checkpoints.(29) Continuous cell lines are more homogeneous and stable, which makes them more reproducible than primary cell cultures. However, these cell lines retain much less of the phenotypic differentiation of the *in vivo* tissue and thus may not accurately represent *in vivo* cellular functions.

A third type of cell line which is commonly used are cells obtained from malignant tumors. These cells are immortalized, as well as having undergone genetic mutation which resulted in the cells displaying a growth advantage. These advantages may include the absence of growth factor requirements for growth or removal of other environmental constraints on cell growth.(29) A diagram showing the relationship of the mammary epithelial cells used in these studies to the different cell types and their proliferation characteristics is shown in Figure 1.1

Primary epithelial cells may be further classified into pre-stasis and post-selection cells. Stasis is cell senescence in response to environmental stress. All primary cells cultured *in vitro* are, by definition, subject to environmental stress. Therefore, pre-stasis cells are normal cells which have been immediately removed from the organ or tissue. Post-selection cells are primary cells grown in culture which have a finite lifespan, yet have bypassed stasis or stress-associated senescence. Cultured primary HMECs are post-

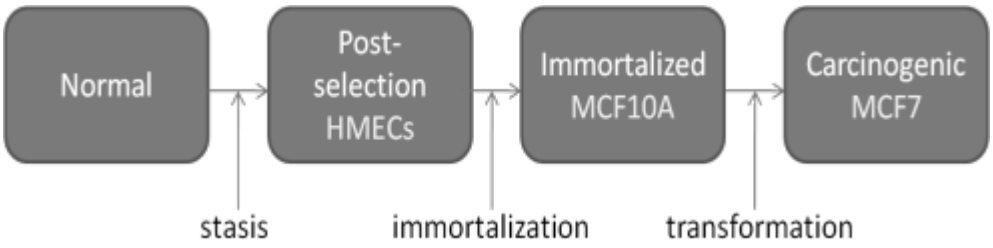

Figure 1.1 Proliferative state of selected mammary epithelial cell lines. Normal refers to the *in vivo* tissue. Stasis is the stress-associated senescence in response to stresses such as *in vitro* culture. Primary cells which have a finite lifespan but have bypassed stasis are "post-selection cells". Immortalization is the process by which cells become capable of multiplying for an extended time *in vitro*. Transformation refers to the process by which cells become carcinogenic or cells which are immortalized and have a growth advantage. The corresponding type of human mammary epithelial cells are shown below each culture type; HMECs are primary mammary cells, MCF10A, are immortalized cells and MCF7 are carcinogenic cells.

selection cells, MCF10A cells are immortalized cells, while MCF7 cells are carcinogenic (Figure 1.1).

Genetic changes and changes in protein expression are seen between primary cells, immortalized cells and carcinogenic cells. Changes in gene expression can occur between all stages of cell growth regulation. *In vivo* (pre-stasis cells) mammary epithelial cells predominately express extracellular matrix (ECM) attachment genes.(30) HMECs have increased expression of cell proliferation and cell cycle genes compared to *in vivo* cells, and further increases in proliferation-associated genes are seen with immortalized cell lines such as MCF10A cells.(30) Immortalized cell lines have reduced ECM and actin cytoskeleton regulations genes, as well.(30) Most of the genetic changes associated with immortalized cells are not expected to have a large impact on transporter expression specifically, although transporter expression is related to differentiation state and therefore may be somewhat affected. The associated genetic changes involving cellular attachment to the ECM would be expected to have a significant impact on monolayer barrier properties and cell polarity.

One major disadvantage of primary HMECs over MCF10A cells, or other immortalized MECs, is the significant morphological and functional changes which occur during cell aging. Cell deterioration results in a loss of differentiation markers within two weeks and cell senescence within three to four weeks.(31) Changes occurring during the aging process include a restructuring of attachment to the ECM, an increase in cell size and a cessation of cellular division. Young HMECs and MCF7 cells express the adhesion markers CD24, integrin β1 (CD29), and CD44 as well as the proteins mucin-1 (muc-1) and matrix metalloprotease-7 (MMP-7).(32) In senescent HMECs, a decrease in

CD24, CD44, muc-1 and MMP-7 expression has been observed.(32) Thus, changes in cell adhesion, decreased differentiation and protein expression occur as passage number increases. These changes often lead to significant variability in measured barrier or drug transport properties during the lifespan of the cells.

While cell cultures systems have many advantages over other drug transport assessment techniques, the formation of barrier properties *in vitro* can vary widely with the cell line and culture conditions. Barrier and transport properties may be different between primary cultures, serially passaged cell lines or transformed cell lines, and can also depend on passage number, presence of multiple cell types, ability of the cells to differentiate, the seeding density, stage of confluency and differentiation, and the presence of nutrients, growth factors and hormones in the growth medium.(8)

Mammary Epithelial Cell Growth Requirements

Serum present in mammary epithelial cell growth media is composed of a complex mixture of hormones and growth factors. Because the serum components are not specifically defined, studies in serum supplemented media may be highly variable and may depend upon the serum supplier and lot used.(33) In addition to hormones, and growth factors such as epidermal growth factor (EGF), which promotes cell division, serum contains attachment factors which affect cell differentiation and proliferation. Fibronectin is the most abundant attachment factor found in serum, and it is also a major component of the ECM.(34) Therefore, serum facilitates cell attachment *in vitro*. Coating of the *in vitro* growth surface with ECM can also replace growth factors in promoting cell proliferation.(33)

Numerous investigators have confirmed the importance of growth factors on mammary epithelial cell growth and their importance depends upon the proliferative stage of the cell.(29,35,36) Cell growth is triggered by binding of EGF to epidermal growth factor receptors (EGFR) on the basolateral surface of polarized epithelial cells.(36) The location of the EGFRs on the basolateral surface, while apical tight junctions limit the transport of proteins from the apical to basolateral surface, which means the signal for cell growth must come from the basolateral side as well. Other nutrient and signaling transporters and receptors are located only on the basolateral surface, indicating the importance of the basal surface in cell culture systems.

Carrier-Mediated Drug Transport in the Mammary Epithelium

As an alternative to passive diffusion, molecules may cross cell membranes by interacting with facilitative carriers or active transporters. Facilitative diffusion is the transport of a molecule across a cell membrane using a carrier or channel which does not require the expenditure of energy. Transport occurs in the direction of the electrochemical concentration gradient. Active transport, on the other hand, uses energy to transport its substrate molecules across a cell membrane and can result in transport against a concentration gradient. There are two main types of active transport: primary and secondary. Primary active transport uses the direct hydrolysis of ATP to supply the energy. Secondary active transport also uses energy to transport a molecule against a concentration gradient; however, energy for these processes is derived from the coupling of transport to the transport of another molecule such as Na^+ or H^+ down its electrochemical gradient. One such transporter, PEPT2, is a co-transporter of H^+ and oligopeptides, where the electrochemical gradient for H^+ is generated from primary active

transport.(37) Co-transporters may be symporters which transport two substrates in the same direction, or antiporters which transport each substrate in an opposite direction across the cell membrane.

Active transport mechanisms are saturable and substrate-specific.(38) For an active transport process, the permeability coefficients differ in the apical-to-basal and basal-to-apical directions due to the directional transport of the molecule by the transporter, and the permeability is observed to be saturable as substrate concentration increases because of the presence of a finite number and capacity of transporters. The kinetics of active transporters can be described by the Michaelis-Menten equation similar to that for enzyme kinetics. The Michaelis-Menten equation (Equation 1.3) describes the impact of the affinity of the transporter for its substrate (K_m) and the transport velocity (V_{max}) on total transport or flux. Flux across a cell membrane may be composed of both passive and active (transporter) components. Passive flux across a barrier is described by Fick's First Law (Equation 1.4).

$$J = \frac{[C]J_{max}}{K_m + [C]} \qquad \text{Equation 1.3}$$

Where
J = initial transport velocity (flux) (mol/min/mg protein)
[C] = substrate concentration (M)
K_m = affinity constant (M)
J_{max} = maximum transport velocity (mol/min/mg protein)

$$J = \frac{dQ}{A * dt} = P_{app} * C \text{ and}$$

$$P_{app} = \frac{D * K}{h}$$

Equation 1.4

Where
J = flux (ng/cm^{2}min)
dQ/dt = change in the cumulative amount of drug in the receiver chamber over time (slope of cumulative amount vs. time plot) (ng/min)
A = surface area of the monolayer (1.13 cm^2)
P_{app} = apparent permeability (cm/min)
C = initial concentration in the donor chamber (ng/ml)
D = diffusion coefficient (cm^2/min)
K = partition coefficient
h = membrane thickness (cm)

Transport Inhibition

Transport inhibitors may be one of three types: competitive, uncompetitive or non-competitive. Competitive inhibitors are often other transport substrates. Since they compete with the substrate for the active site, they affect the K_m of the transporter. Uncompetitive inhibitors slow the maximum transport velocity (V_{max}) but do not affect K_m since they bind after the substrate; therefore, strength of inhibition is independent of substrate concentration. Non-competitive inhibitors affect both K_m and V_{max}. One common type of noncompetitive inhibition is transporter inactivation, and since less transport is available both the K_m and V_{max} are affected.(39)

Active transporters have an ATPase function as well as a substrate transport function.(40) Since these transporters have two functions which are both essential for transport, inhibitors may affect either or both functions to impact transport velocity. Molecules which inhibit the synthesis or hydrolysis of ATP will inhibit both primary and secondary active transport processes. One such inhibitor is 2,4-dinitrophenol (2,4-DNP), a hydrophobic weak acid which can easy cross cell membranes. 2,4-DNP acts by

transporting protons across the inner mitochondrial membrane, thereby dissipating the proton gradient used to synthesize ATP. In the absence of ATP, all ATP-dependent processes, including active transport, are inhibited.(41)

Drug Transporters in the Mammary Epithelium

Carrier-mediated drug transport leads to an over or under prediction of M/P ratios calculated based on passive diffusion. Drug transport into the milk by these transporters depends upon their localization in the cell membrane and in which direction they transport their substrates. Efflux transporters such as BCRP and MDR1 present on the apical plasma membrane lead to drug accumulation in the milk, while uptake transporters on the apical membrane, such as PEPT2, remove drugs from the milk. Drugs may be substrates for multiple transporters, such as mitoxantrone which is a known substrate of BCRP, MDR1 and MRP1 and shows active uptake which may be due to an organic cation uptake transporter such as OCT1.(42)

ATP-Binding Cassette Transporters

The mammary epithelium has been shown to contain multidrug resistance transporters associated with drug efflux, as well as numerous organic anion and cation transporters and other solute transporters.(1) The physiologic function of these transporters is to aid in the secretion of various nutrients into the milk. *In vivo* observations of higher than expected milk concentrations for drugs such as nitrofurantoin, cimetidine and acyclovir, suggests a role for active transporters in drug transport in the mammary epithelium, and in the accumulation or removal of drugs in breast milk.(43,44) The milk accumulation of nitrofurantoin and cimetidine(9,45) by the Breast Cancer Resistance Protein or BCRP (ABCG2) (10) (discussed previously) is an example of the

effect transporters may have on drug concentrations in the milk. A table of the major transporters reported to be involved in drug transport in the mammary epithelium is shown in Table 1.1. and their relative mRNA expression levels in lactating and non-lactating mammary epithelia are summarized in Table 1.2.(46) ATP-dependent transporters involved in multidrug resistance (MDR), including P-glycoprotein (or multidrug resistance transporter, MDR1 (ABCB1), human multidrug resistance associated proteins such as MRP1, MRP2, and MRP5 (ABCC1.2. and 5), and BCRP have been shown to be expressed in the mammary epithelium.(46,47) MDR1 transcript levels are very low in lactating mammary epithelial cells, and therefore this transporter may not play a major role in drug accumulation in the milk.(46) Typical MDR1 substrates, such as methotrexate, indinavir, and daunorubicin are hydrophobic, neutral or positively charged molecules.

MRP1 and MRP2 substrates are amphipathic, anionic compounds and include glutathione, sulfate and glucuronide drug conjugates. MRP5 substrates include nucleoside analogs used in cancer chemotherapy.(1) MRPs, predominately MRP1 transcripts, are present in higher levels in lactating MECs than MDR1, however, their expression is lower during lactation than in non-lactating MECs.(46) BCRP substrates include a wide range of drug molecules, including mitoxantrone, nitrofurantoin and cimetidine.(10) BCRP is known to be present in lactating mammary epithelial cells (MECs) at clinically significant levels because of the observation that some of its substrates, such as nitrofurantoin and cimetidine, accumulate in the milk.

Table 1.1. Transporters of interest in the mammary epithelium

Transporter	Type	Endogenous Substrates	Xenobiotic Substrates	Misc
BCRP	ATP-dependent efflux transporter	Estrone-3-sulfate	Daunorubicin, Etoposide, Methotrexate, Rhodamine-123, Mitoxantrone, Nitrofurantoin, Cimetidine	Half-transporter, apical membrane
PEPT2	H+/peptide symporter	Di- and tri-peptides	Cephalexin, Cefadroxil, Bestatin, Valacyclovir, Zidovudine	apical membrane, high affinity, low capacity
MDR1	ATP-dependent efflux transporter		Vincristine, daunorubicin, Etoposide, Methotrexate, Paclitaxel, Digoxin, Indinavir, Grepafloxacin, Fexofenadine, Cyclosporin A, Cimetidine, Quinidine, Rhodamine-123	P-gp, Down-regulated in MEC during lactation, most substrates are also CYP3A4 substrates
MRP1	ATP-dependent efflux transporter		Vincristine, Daunorubicin, Etoposide, Methotrexate, Grepafloxacin, Rhodamine-123, Doxorubicin, Amphipathic anionic compounds and glutathione and other conjugates	Basolateral membrane
MRP2	ATP-dependent efflux transporter	Glutathione and bilirubin glucuronides	Vincristine, Etoposide, Cisplatin, Indinavir, Grepafloxacin, organic anions including glutathione and glucuronide conjugates	Apical membrane
MRP5	ATP-dependent efflux transporter		6-mercaptopurine, thioguanine, 9-(2-phosphonylmethoxyethyl)adenine, other nucleotide analogs	Basolateral membrane
OCT1	Organic cation transporter	Prostaglandin E2, prostaglandin F2	Tetraethylammonium, 1-methyl-4-phenylpyridinium, Tributylmethylammonium, N-methylquinine, N-methylquidine, Acyclovir, Ganciclovir	Potential-sensitive, pH and Na^+-independent
OCTN1	Organic cation/carnitine transporter	L-carnitine	Tetraethylammonium, Quindine, Pyrilamine, Verapamil	H^+/OC antiporter
OCTN2	Organic cation/carnitine transporter	Acetyl-L-carnitine, L-carnitine, D-carnitine	Same as OCTN1	Na^+-dependent carnitine transport and Na^+-independent OC transport

Table 1.1–continued

OATP-A	Organic anion transporting polypeptide	Bile salts, DHEA, T3, T4, bilirubin, steroids, prostaglandins	Fexofenadine, Ouabain, Digoxin, Lovastatin	Na^+-independent transport
CNT3	Concentrative Na+/nucleoside co-transporter	Purine and pyrimidine nucleosides		Na^+-coupled concentrative nucleoside transport
ENT3	Equilibrative nucleoside transporter	Purine and pyrimidine nucleosides		

Sources: (1,46,48-54)

Table 1.2. RNA expression in lactating and non-lactating mammary epithelial cells (MECs)

Transporter	Lactating MEC	Nonlactating MEC	Relative Difference	Liver	Kidney	Gene
MDR1	0.0258	1.33	-51.6	0.157	2.81	ABCB1
MRP1	0.355	0.917	-2.6	0.429	0.427	ABCC1
MRP2	0.0506	0.0586	-1.2	0.261	0.214	ABCC2
MRP3	BLD	BLD	NA	BLD	BLD	ABCC3
MRP4	BLD	BLD	NA	BLD	BLD	ABCC4
MRP5	0.067	0.0388	1.7	0.0345	0.0722	ABCC5
PEPT1	0.054	0.159	-3	3.42	5.22	SLC15A1
PEPT2	1.59	BLD	NA	BLD	E	SLC15A2
OCT1	3.5	0.451	7.8	4870	4.54	SLC22A1
OCT2	BLD	BLD	NA	BLD	10.3	SLC22A2
OCT3	0.163	0.476	-2.9	1.72	0.25	SLC22A3
OCTN1	0.336	BLD	NA	BLD	0.388	SLC22A4
OCTN2	0.622	2.51	-4	0.185	6.26	SLC22A5
OATPA	0.0833	0.0525	1.6	BLD	0.00488	SLC21A3
OATPB	0.945	0.641	1.5	16.6	1.206	SLC21A9
OATPD	3.64	6.63	-1.8	0.787	2.04	SLC21A11
OATPE	0.137	0.371	2.7	0.062	0.121	SLC21A12
CNT3	0.334	0.048	7	BLD	BLD	SLC28A3
BCRP	?	?	NA	?	?	ABCG2

Source: (46)

RNA expression levels of each transporter gene normalized to β-actin

BLD = below level of detection

Solute Transporters

Transporters from the solute carrier family also play an important role in transport across the mammary epithelium. Peptide transporters which transport di- and tri-peptides, and PEPT2 in particular, are present in relatively high levels in lactating mammary epithelial cells.(46) The mammary epithelium also contains some organic cation transporters including OCT1, OCT3, and the organic cation/carnitine transporters OCTN1 and OCTN2. Both OCT1 and OCTN1 show four times greater RNA expression in lactating MECs than in non-lactating MECs.(46) The mammary epithelium also contains solute carrier transporters for organic anions, organic anion transporting polypeptides and organic anion/prostaglandin transporters (OATP-A, OATP-B, OATP-D, and OATP-E). OATPs transport various endogenous compounds such as bile salts, conjugated metabolites of steroid hormones, thyroid hormones, anionic oligopeptides and drugs.(48) High levels of purine and pyrimidine nucleoside transporters are also seen in lactating mammary epithelium. CNT3, a concentrative nucleoside transporter, is one such example.(1)

Flow Cytometry

Flow cytometry measures light scattering and fluorescence of individual cells or particles. Suspended cells are hydrodynamically focused in a moving stream of fluid via an optical detection system. Light scattering and fluorescence are measured from a laser excitation passed through the stream of suspended cells and captured on a detector. Flow cytometry takes scattered and emitted light from cells and particles and converts that light to electrical pulses (usually with a photomultiplier tube, PMT) in the optical detectors. The light is sent to different detectors using an optical filter. The most commonly used type of optical filter is a bandpass filter (bp) which transmits a specific band of

wavelengths to the detector. In the PMT the light signal is converted into a voltage pulse. A voltage pulse arises from the change in intensity of the light as the cell or particle passes through the laser beam. As the cells passes through the laser, more light is scattered (or emitted), until the cell is in the center of the laser. As the cell leaves the laser, less and less light is scattered resulting in a voltage pulse.(49-51) The size of the voltage pulse may be quantified by the peak height, width or area. Therefore, for scattered light, the peak width reflects the amount of time the cell took to pass through the laser, the peak height reflects the intensity of the scattered light and the peak area is reflective of both. A detector measuring the forward scattered light (FSC) is in parallel with the laser and measures light scattering from the cell or particle surface. Thus FSC correlates with cell size since larger particles block and scatter more of the laser light. The side scattered light (SSC) detector and fluorescence detectors are at right angles to the laser source. SSC reflects the intracellular components such as the number of cytoplasmic granules or the roughness of the membrane. FSC and SSC are used to determine the cell population to be analyzed for their fluorescence intensity. These light scattering properties can be used to eliminate aggregates and cellular debris from analysis and enable the selection of one cell type from a mixture of different cells.

Fluorescence can be used to measure cellular properties such as transporter or other protein expression levels through immunolabeling or uptake of a fluorescent molecule. Fluorescence detection by flow cytometry is more sensitive than immunohistochemical methods.(52) Thus, uptake of fluorescent drug molecules can be used to study active transport mechanisms using this technique. However, flow cytometry is limited to the study of transporters with substrates which are fluorescent.

Multidrug resistance transporters such as MDR1 and BCRP have numerous substrates which are fluorescent, making their study by flow cytometry relatively straightforward. Fluorescent substrates are more difficult to find for other transporters, such as the peptide transporters PEPT1 and PEPT2.

Linear Mixed Effects Models

In general, models provide a method to quantitatively describe complex processes and enable predictions or comparisons to be made. Since the flow cytometry experiments performed on different days were quite variable, the assumption of independent measures required for statistical analyses such as the Student's t-test and analysis of variance data modeling methods was not met since the day on which the experiment was performed affected the fluorescence intensity reading. Instead, linear mixed effects models were used; a general form for such models is shown in Equation 1.5. These models include terms for fixed (experimentally-controlled) effects as well as terms for random effects, accounting for biological and instrumental variability.(53,54) The fixed effects parameters used in these models are the known experimental variables and are similar to those used in standard linear regression models. The random effects incorporated into the linear mixed effects model are undefined random variables which account for systematic variability in the data.(54)

$$y_{ij}=\mu+\alpha_i+\beta_j+\alpha\beta_{ij}+\varepsilon_{ij} \qquad \text{Equation 1.5}$$

Where
y_{ij} = response variable
μ = unknown overall mean
α_i = fixed effects corresponding to ith factor level
β_j = random effects corresponding to the jth factor level
$\alpha\beta_{ij}$ = interaction terms
ε_{ij} = residual variability

For mitoxantrone uptake flow cytometry data, linear mixed effects models were used to separate the fixed treatment effects which are the drug and inhibitor concentration in this case, from random effects, such as inter-day and replication (rep) variability. In the specific linear mixed effects model used fixed effects terms included drug concentration, drug concentration squared, inhibitor concentration and the product of drug and inhibitor concentrations (drug*inhibitor). The $[drug]^2$ term is needed to account for the leveling off of the fluorescence intensity at high drug concentrations which occurs with saturation of the transport system (Equation 1.6). Interaction terms between the fixed and random effects were not included in the specific model since the goal was to account for the inter-day variability, which could be accomplished without these additional terms. The drug*inhibitor term is an interaction term between the two fixed effects, drug and inhibitor. This term was necessary for some of the data sets where increased spread in the intensity values occurs at high drug and inhibitor concentrations.

$$y = \mu+(\alpha_1 x)+(\alpha_2 x^2)+(\alpha_3 I)+(\alpha_4 xI)+(\beta_1 z)+(\beta_2 z)+\varepsilon \qquad \text{Equation 1.6}$$

Linear Mixed Effects Model:
y = fluorescence sample reading
μ = population mean (y-intercept)
α_1 = drug parameter estimate
α_2 = $[drug]^2$ parameter estimate
α_3 = inhibitor parameter estimate
α_4 = drug*inhibitor parameter estimate
x = drug concentration (may be polynomial as needed)
I = inhibitor concentration
β_1 = inter-day variability parameter estimate
β_2 = inter-replication variability parameter estimate
z = random variables
ε = residual variability

The final liner mixed effects model for each data set was chosen by selecting the model with the fewest number of parameters and minimizing the Akaike Information

Criterion (AIC). The AIC is a measure of the goodness of fit of a model, which is judged by how close the model's fitted values are to the true values. The AIC minimizes the residual sum of squares, and contains a parameter which effectively penalizes the model for having too many parameters in an effort to identify the model that best describes the data with the fewest parameters.(54)

Polymerase Chain Reaction (PCR)

PCR is a process which amplifies DNA for improved detection and quantification. In PCR, double-stranded DNA (dsDNA) is heated to separate the strands, then the reaction is cooled and specific primers are added for the target gene of interest. A DNA polymerase (with 5' to 3' activity) and nucleotides are added to replicate the separated strands. This cycle is repeated to amplify the DNA, allowing sensitive detection of a specific DNA sequence. PCR requires the DNA target gene, specific primers, a thermostable DNA polymerase (Taq), nucleotides, and fluorescent detection dyes. Reporter dyes may be a fluorescently labeled polymerase combined with a fluorescence quencher or a non-specific DNA binding dye such as SYBR green with an instrument reference dye such as ROX.(55,56) PCR may also be used to detect specific mRNA sequences using a technique known as RT-PCR (reverse transcription-PCR) when an RNA strand is first reverse transcribed into its DNA complement (cDNA) which is then measured using real-time PCR.

RNA Quality Control Analysis

Since SYBR green non-specifically binds to all dsDNA, quality control analysis of the starting mRNA material is important to prevent non-specific product amplification. The isolated RNA for RT-PCR is monitored for the presence of protein and other contaminants, the concentration of RNA is determined, and the ribosomal RNA integrity

is assayed. The RNA samples are treated with DNase to degrade the genomic DNA during the isolation and purification steps. Contamination with proteins and genomic DNA is monitored by the ratio of the UV absorbance at 260 nm and 280 nm (A260/A280). The A260/A280 should be greater than 2.0 indicating the RNA sample is free of proteins such as RNases. Contamination by other substances such as extraction buffer components is monitored by the ratio of the absorbance at 260 nm and 230 nm (A260/A230). The A260/A230 ratio should be greater than 1.7. The absorbance at 260 nm is also used to determine the concentration of the RNA, which should be above 4 µg/ml. The ribosomal band integrity monitored electrophoretically for 18S and 28S ribosomal RNA (rRNA) is also used to determine the quality of the RNA samples. The 18S and 28S rRNA bands should be sharp, show minimal smearing, and other bands should be minimal.

Real-time PCR

Real-time PCR (also called quantitative PCR or qPCR) involves data collection throughout the PCR amplification process rather than at the end, thereby allowing PCR reactions to be monitored in real time.(57) Real-time PCR reactions are characterized by the time point during cycling when amplification of a target is first detected rather than measuring the amount of target after a fixed number of reaction cycles. Therefore, the higher the starting copy number of the target, the sooner a significant increase in the fluorescent signal is detected.(58) The fluorescent target signal is quantified as an R_n number which is the reporter signal (SYBR green) normalized to the internal standard fluorescence (ROX). The R_n numbers are monitored for each cycle number. A fixed fluorescence threshold is set significantly above the baseline fluorescence level but

within the exponential growth region of the amplification curve. This is then used to determine the threshold cycle (C_T) value which is the cycle number at which the fluorescence emission exceeds the fixed threshold level.

Drug Transporter Expression Levels

The C_T values are inversely proportional to the expression level of the target gene and can be converted to expression level (L) according to Equation 1.7. The expression level for the gene target can be normalized to the expression level of an endogenous control gene or housekeeping gene. Housekeeping genes are genes which are commonly expressed in most cell types and are present at consistent levels which can be used to normalize target cDNA across experiments and cell types.

$$L=2^{-C_T} \qquad \text{Equation 1.7}$$

Where
L = Target gene expression level
C_T = cycle number at which the number of gene replicates crosses the threshold value

Using the real-time PCR technique, mRNA transcripts for numerous drug transporters can be quantified in the mammary epithelium using a PCR array containing the primers for many of the important drug transporters (PCR array from SABiosciences). The expression level of these transporters is first normalized to the expression level of the housekeeping gene, β-actin, for each array,(59) allowing the expression level of the transporters to be compared across different mammary epithelial cell lines (MCF10A, HMECs, and MCF7s) and to the *in vivo* lactating and non-lactating mammary epithelium.

CHAPTER 2

OBJECTIVES

Despite the well known benefits to breast feeding, women may choose not to nurse because of the largely unknown risk of infant drug exposure through the breast milk. Development of a human cell culture model which includes the active drug transport process present in the human mammary epithelium would contribute valuable information about drug accumulation in the breast milk, as well as provide a tool for a more mechanistic investigation of drug transporter functions in this tissue.

Objective 1: Development of a Human Mammary Epithelial Cell Drug Transport Model

Specific Aim 1.1: To select a useful cell culture model of the human mammary epithelium from commercially available mammary epithelial cells. Mammary epithelial cells investigated included MCF7 cells (ATCC), primary human mammary epithelial cells (HMECs, Clonetics and Gibco), and MCF10A cells (ATCC). A cell culture model capable of forming a polarized monolayer was desired in order to conduct bi-directional drug flux studies to characterize specific drug influx and efflux transporters.

Specific Aim 1.2: To characterize and compare transporter expression among cell models. Expression of specific drug transporters was examined in MCF10A cells and HMECs using DNA microarrays developed to probe human drug transporter expression (SABiosciences). The expression results were compared to previously reported levels of transporters in primary human mammary epithelial cells.

Objective 2: Analysis of Characteristics of Selected Transporters

Since none of the cell culture models successfully formed a polarized monolayer suitable for bi-directional flux studies, flow cytometry was investigated as a method to measure uptake of drug into mammary epithelial cells.

Specific Aim 2.1: Demonstrate that flow cytometry can be used to quantify intracellular drug concentrations following incubation of MCF10A cell monolayers. The fluorescent chemotherapeutic agent mitoxantrone was used to demonstrate that a quantitative relationship existed between the drug concentration in the incubating medium and the resulting intracellular mitoxantrone concentration.

Specific Aim 2.2: Characterize the activity of BCRP and MDR1, ABC-family efflux transporters, in MCF10A cells. These transporter's activities were studied by including verapamil and fumitremorgin C (FTC), inhibitors of MDR1 and BCRP, respectively, in the incubation medium.

Specific Aim 2.3: Characterize the activity of PEPT1 and PEPT2, apically-located dipeptide uptake transporters. A fluorescently labeled dipeptide substrate was synthesized and used to evaluate PEPT1 and PEPT2 activity. Competition studies using cefadroxil and Gly-Gln were also conducted to demonstrate the ability to modulate di-peptide transport across the mammary epithelium.

These functional transporter studies, combined with transporter expression levels, were used to show that MCF10A cells provide a useful model for the investigation of active drug transport in the human mammary gland using flow cytometry. The major limitation to the generalized use of these techniques, however, is the requirement of a fluorescent substrate for quantification using flow cytometry.

CHAPTER 3

GROWTH OF A POLARIZED MONOLAYER OF MAMMARY EPITHELIAL CELLS

Introduction

Every drug that a nursing mother takes will appear, to some extent, in the breast milk. Because of the risk of infant drug exposure through the milk, knowledge of drug transport characteristics in the mammary epithelium is of crucial importance. Current methods of studying mammary drug transport and their limitations, including pH-partitioning models, *in vivo* human and animal studies and animal cell culture models, were discussed in the previous chapter. Because there is still a lack of understanding based on current models, a human mammary epithelial cell culture model would fill in some of the knowledge gaps in this area.

Use of a cell culture model for transcellular flux studies of drug transport first requires growth of the cells in polarized monolayers on porous membranes. Polarization of a cell monolayer requires cell attachment on the basal surface and tight junction formation near the apical surface of the cells.(15) Cells which are not polarized do not form a paracellular barrier to solute flux and allow membrane proteins to diffuse within the cell membrane.(22) Both of these functions are necessary for vectoral flux, which is flux that is greater in either the apical-to-basal or basal-to-apical directions. Polarization is especially important in the mammary epithelium since lactation induces an increase in polarization with very tight junctions and virtually no paracellular transport.(17,18,60)

Because of the importance of polarized monolayers for mammary drug transport studies, cell growth and polarization were measured through a number of different methods including transepithelial electrical resistance (TEER), transport of the

paracellular pathway marker compound lucifer yellow, and localization of the tight junction protein ZO-1 by immunofluorescence microscopy and vectoral flux of the MDR transporter substrate nitrofurantoin. TEER measures the resistance to ion flow across a cell layer. Since the ions are charged, they may only pass through the paracellular spaces or through ion channels or transporters embedded in the plasma membrane. Therefore, a higher resistance to ion flow indicates significant tight junction formation and closure of the paracellular route to ion flow. A similar technique utilizes the measurement of lucifer yellow transport across the cell layer since this small, hydrophobic compound can only pass through the paracellular spaces. Limited transport of lucifer yellow indicates that the paracellular pathways are tightly closed.

Since reports of TEER measurements are highly variable, localization of the tight junction protein, ZO-1 was also used to assess tight junction formation. ZO-1 is a cytosolic protein which is recruited to the tight junctions to form polarized cell layers.(16,28) Therefore, ZO-1 localization at the site of the tight junctions (and absence from the cytoplasm) is another indicator of cell polarity.

Vectoral transport of a compound which is a known substrate for a transporter present in the cell system can also be used to assess tight junction formation. These studies are the only method described which directly measures polarity since vectoral transport relies on both tight junction formation and proper transporter localization. The drug nitrofurantoin, which is a known substrate of the ABC transporter BCRP (ABCG2), is known to be present in the mammary epithelium (10) as well as in MCF10A cells and therefore is useful for vectoral transport studies in mammary epithelia.

Polarized monolayer formation in MCF10A cells was monitored in response to changes in cell cultures conditions and attachment surface and compared to different cell types including primary mammary epithelial cells, a carcinogenic mammary cell line (MCF7) and MCF10A cells transfected with the tight junction protein Crumbs3 (CRB-MCF10A).(28) These modifications and comparisons were done to determine the suitability and optimize the growth conditions for drug transport studies.

Materials and Methods

Growing Cells from Frozen Samples

MCF10A cells (ATCC, CRL-10317, Lot #7690599), and Crumbs3 transfected MCF10A cells (CRB-MCF10A) and vector transfection control cells (PNG-MCF10A) (gifts from Dr. Mark Marjolis, University of Michigan) and human mammary epithelial cells (HMECs) from Clonetics (Walkersville, MD, Lot #1203061) and Gibco (Carlsbad, CA, Lot #440212) were received frozen in 1 ml vials shipped on dry ice. Frozen cells were stored in liquid nitrogen until use. The vials were thawed by gentle agitation in a 37°C water bath (Isotemp 115, Fisher Scientific, Pittsburg, PA) and removed immediately upon thawing. Prior to addition of the cells, 10 ml growth medium in a T75 flask was warmed in a 37°C, 5% CO_2/95%O_2 incubator (Hera Cell, Thermo Scientific) for 15 minutes allowing it to reach a pH of 7.0 to 7.6. The cells were transferred from the vials to the T75 flask containing pre-warmed growth media (described below) and grown at 37°C with 5% CO_2/95% O_2. Media was replaced with fresh media after the first 24 hours and then changed every 1-2 days.

Growth Medium

MCF10A cells were grown in DMEM/F12 (+ L-glutamine, 2.438 g/L sodium bicarbonate) media (Gibco) supplemented with 5% horse serum (Hyclone, Thermo Scientific, Waltham, MA), 20 ng/ml epidermal growth factor (Sigma, St. Louis, MO) 0.5 µg/ml hydrocortisone (Sigma), 10 µg/ml insulin (Sigma), 100 ng/ml cholera toxin (Sigma), 100 units/ml penicillin, and 100 µg/ml streptomycin (Gibco) and maintained in a 5% CO_2/95% O_2 humidified incubator at 37°C.(14) Epidermal growth factor (100 µg/ml) and cholera toxin (1 mg/ml) were dissolved in dd$H_2$0, hydrocortisone was dissolved in 200-proof ethanol at 1 mg/ml. Epidermal growth factor, hydrocortisone, and penicillin/streptomycin were stored at -20°C and insulin solution and cholera toxin were stored at 4°C.

Clonetics HMECs were grown with the MEGM® Bullet Kit® (Clonetics) containing Mammary Epithelial Cell Basal Medium® and the following growth supplements: bovine pituitary extract, 2 ml; human epidermal factor, 0.5 ml; hydrocortisone, 0.5 ml; gentamicin-1000, 0.5 ml; insulin, 0.5 ml. Gibco HMECs were grown in HuMEC® medium (Gibco).

Subculturing

Upon reaching approximately 80% confluency, the cells were subcultured at a ratio of 1 flask into 3 flasks (1:3) or 1:4. Cells were detached from the flasks by treatment with 5 ml of 0.05% trypsin with 0.53 mM EDTA (Gibco) for approximately 15 minutes at 37°C (cell detachment was monitored every 2-3 minutes). Trypsin was neutralized by addition of an equal volume of serum-containing growth media. The cells were collected in 15 or 50 ml centrifuge tubes (Sarstedt, Newton, NC) and centrifuged at

300 x g for 5 minutes (Eppendorf 5810 R centrifuge). The trypsin and media were removed and the cell pellet was resuspended in fresh media and split into additional T75 flasks or 6 or 12 well Snapwell®/Transwell® cell culture inserts and placed in the 5% CO_2/95% O_2 incubator. Media was changed the following day after subculturing and then every 1-2 days.

Snapwell and Transwell Cell Cultures

Snapwell inserts consist of a polyester membrane with a 12 mm diameter, 0.4 μm pore size and a cross-sectional area of 1.13 cm^2. Snapwell inserts were coated with various extracellular matrix materials in an attempt to improve cell growth on the inserts. Coating materials included collagen type IV, laminin, and extracellular matrix (ECM) gel from Engelbreth-Holm-Swarm murine sarcoma which contains laminin V, collagen IV, heparin sulfate proteoglycan and enactin (all obtained from Sigma).

Transwell plates with 6 or 12 wells, polyester (clear) membranes and 0.4 μm pores were also used for MCF10A cell growth. Media was added to the upper and lower chambers and changed every 1-2 days for both Snapwell and Transwell cultures. Cells were added at a density (based on average counts using a hemocytometer) of approximately 10^5 cells/cm^2.

Collagen IV Coating

Collagen type IV was reconstituted to a concentration of 1.0 mg/ml in 0.25% acetic acid in ddH_2O at 2-8 °C for several hours with occasional swirling. The 6 well Snapwell plates were coated with 400 μl/well of the collagen solution and dried overnight at 2-8°C. The plates were sterilized overnight by exposure to UV light in a sterile culture hood.

Laminin Coating

Frozen laminin solution (1 mg/ml) was thawed at 2-8°C and then diluted in sterile Hank's Balanced Salt Solution (HBSS, Gibco) (1:1000). The surface of the Snapwell insert was coated with ~400 µl of dilute laminin and the plates were incubated at 37°C for 2 hours to dry, then the plates were washed 3 times with PBS (pH 7.4) and the cells were plated.

ECM Gel Coating

The frozen ECM gel was thawed overnight at 2-8°C. The gel was dispensed onto pre-cooled (2-8°C) Snapwell inserts (400 µl/well) and the gels formed over a 5 minute incubation at 20°C (the gel layer was ~0.5 mm thick). Cells were then plated onto the coated inserts.

Freezing Cell Cultures

Cells were periodically frozen to maintain a stock of the cell line for future use. Cells were trypsinized and centrifuged as described above. Cells were then slowly frozen in complete growth media supplemented with 7.5% (v/v) DMSO (Sigma) as a cryoprotectant in1 ml cryovials (Sarstedt) and stored in liquid nitrogen. Cells for western blotting were trypsinized and centrifuged as described above, washed 2 times in PBS containing protease inhibitors (1:100 dilution, Sigma) and stored at -80°C until use (Pierce Mem-PER® kit instructions).

Western Blotting

Membrane Protein Sample Preparation

Membrane protein samples from MCF10A cells were isolated using the Mem-PER Eukaryotic Membrane Protein Extraction Reagent Kit (Pierce, Rockford, IL). Isolation of approximately 5 x 10^6 cells (one T75 flask) was performed by centrifuging

trypsinized cell suspensions at 850 x g for 2 minutes. Cell pellets were resuspended and washed in phosphate buffered saline (PBS) and centrifuged at 850 x g for 2 minutes. The supernatant was removed, and 150 µl of a detergent (Reagent A) was added to the pellet to lyse the cells. The cell suspension was pipetted up and down repeatedly until a homogenous sample was obtained. The samples were incubated for 10 minutes at room temperature, then transferred to an ice bath. A second detergent was added to solubilize the membrane protein fraction (Reagent B diluted 1:3 with Reagent C) with 450 µl added to each tube of lysed cells. Samples were incubated on ice for 30 minutes with vortexing every 5 minutes. Following incubation, the tubes were centrifuged at 10,000 x g for 3 minutes at 4°C (Savant µSpeedFuge SFA13K Microcentrifuge). The supernatant was transferred to a new tube and incubated for 10 minutes at 37°C to separate the hydrophobic proteins from the hydrophilic proteins through phase partitioning. The tubes were centrifuged at room temperature for 2 minutes at 10,000 x g (Eppendorf 5415 D Centrifuge). The hydrophilic layer (top) was removed with a pipette and the hydrophobic layer (bottom) containing the majority of the membrane proteins was stored on ice until analysis.

Gel Electrophoresis

Membrane protein samples were separated by sodium dodecyl sulfate-polyacrylamide gel electrophoresis (SDS-PAGE). Membrane protein samples prepared as described above were boiled for 5 minutes in sample buffer (0.03M TrisHCl, 5% SDS, 50% glycerol, 0.5% (w/v) bromophenol blue, dithiothreitol, pH adjusted to 6.8). BioRad Ready Gels (7.5% TrisHCl 50 µl wells, 10 well comb) were assembled in a BioRad Mini-PROTEAN 3 Electrophoresis Module Assembly (BioRad). The inner chamber was filled

with ~125 ml of running buffer (2.5 mM Tris base, 19.2 mM glycine, 0.1% SDS) until the level reached approximately halfway between the tops of the taller and shorter plates of the gel cassettes. The lower buffer chamber was filled with ~200 ml of running buffer. Samples were loaded into each well using pipette gel loading tips. SeeBluePlus2® (Invitrogen, Carlsbad, CA, 10 µl) and MagicMarkXP® (Invitrogen, 10 µl) were added as molecular weight markers and 35 µl (~25-50 µg) of each sample was loaded onto the gel. The run time was 35 minutes at 200 V. After electrophoresis was completed, the gels were removed from the assembly and incubated in transfer buffer (48 mM Tris base, 39 mM glycine, 0.1% SDS, 20% methanol) for 15 minutes.

Protein Transfer to Nitrocellulose Membrane

SDS-PAGE gels were transferred to nitrocellulose membranes (Bio-Rad) by electrophoretic transfer using the BioRad Mini Trans-Blot Electrophoretic Transfer Cell. The gel sandwich consisting of a fiber pad, filter paper, SDS-PAGE gel, nitrocellulose membrane, filter paper, and fiber pad was prepared and loaded into the transfer assembly with the gel on the side of the negative electrode and the membrane on the side of the positive electrode. Protein transfer was done at 100 V, 350 mA for 1 hour at 4°C with stirring for transfer.

Chemiluminescent Protein Detection

Nitrocellulose membranes were removed from the transfer assembly, washed with 10 ml aliquots of wash buffer (10 mM Tris base, 100 mM NaCl, 0.1% Tween 20) and incubated in blocking buffer (5% non-fat milk in wash buffer) for 1 hour at room temperature with gentle shaking to block non-specific binding sites. Primary and secondary antibody solutions for BCRP or ZO-1 (Table 3.1) were prepared in blocking buffer.

Table 3.1. Western blot primary antibodies

Protein	MW	Species	Conc. Dilution	Type	Source
BCRP (BXP-21)	70 kDa	Mouse Anti-Human	250 µg/ml 1:1000	monoclonal	Sigma
ZO-1	225 kDa	Mouse Anti-Human	0.5 mg/ml 1:500-1:1000	monoclonal	Invitrogen

Sources: (61-64)

Nitrocellulose membranes were incubated in 20 ml of primary antibody solutions for one hour at room temperature with gentle shaking. The membranes were washed three times for five minutes with 10 ml of wash buffer and incubated for one hour at room temperature in 20 ml of the secondary antibody solutions. A goat anti-mouse peroxidase conjugated IgG (Sigma) secondary antibody was used at a dilution of 1:25,000.

Membranes were washed four times for five minutes in 10 ml each of wash buffer. Chemiluminescence detection was used to specifically detect the proteins of interest. The nitrocellulose membranes were treated with 5 ml each of Luminol/Enhancer Solution and Peroxide Solution (West Pico Chemiluminescent Substrate, Pierce, Rockford, IL) and incubated for 5 minutes. Chemiluminescence detection uses light produced by the peroxidase catalyzed reaction of luminol with hydrogen peroxide. Light at 425 nm is emitted as the reaction product, 3-aminophthalate, decays to its ground state. Treated membranes were exposed to X-ray film (CL-X Posure Film, 8 x 10 inches, Pierce) for 1-5 minutes in darkness to detect the light emitted by the reaction. The presence of the protein of interest was determined by the appearance of a band at the appropriate molecular weight when compared to the MagicMark MW standards.

Immunofluorescence Microscopy

MCF10A cells grown to confluency on Snapwell or Transwell cell culture inserts (Corning, Corning, NY) and were fixed in 10% zinc formalin solution (UI Central Microscopy Research Facility, UI CMRF) for 24 hours. Following fixation the membranes were washed 3 times for 5 minutes each with PBS (pH 7.4). The membranes were placed in blocking solution (10% normal goat serum, 0.1% saponin in PBS) for 1

hour. The membranes were then treated with primary antibody solution (IgG primary antibodies for ZO-1 or BCRP in blocking solution as shown in Table 3.1) at 4°C overnight. Membranes were washed with PBS with 0.1% saponin 3 times for 5 minutes and treated with secondary antibody solution (Goat anti-mouse IgG conjugated to Alexa 568 in blocking solution, 1:200 dilution, obtained from UI CMRF) for 1 hour in darkness. Membranes were washed 4 times for 5 minutes in PBS. The polyester membrane was cut from the polystyrene holder and placed on a microscope slide, 2 drops of Vecta-Shield with DAPI mountant (Vector Labs, obtained from UI CMRF) was added and the inserts were covered with a glass coverslip. Microscope slides were examined using an Olympus BX-1 Light Microscope and a BioRad MRC-1024 Confocal Microscope using a red diode laser (633 nm) and a 670 nm emission filter.

Drug Transport Studies

Transport of nitrofurantoin, a substrate for the active efflux transporter BCRP, across MCF10A cells grown on Snapwell cell culture inserts was investigated. Snapwell® inserts were placed in standard vertical diffusion chambers (Harvard Apparatus) with either the apical cell surface facing the donor chamber to measure apical-to-basolateral transport or the basal surface facing the donor chamber to measure basolateral-to-apical transport. The temperature was maintained at 37°C with a circulating water bath. All studies were performed using Krebs Ringers Bicarbonate Buffer (KRB) (0.49 mM $MgCl_26H_2O$, 4.56 mM KCl, 120 mM NaCl, 0.70 mM $NaHPO_4$, 1.50 mM $NaH_2PO_4H_2O$, 10 mM dextrose, 2.52 mM $CaCl_22H_2O$, 15 mM $NaHCO_3$ and bubbled with 95% O_2/5% CO_2 for 10 minutes, pH adjusted to 7.4 for donor solution and to 7.0 for receiver solution).(61) A pH of 7.0 was maintained in the receiver

compartment to reflect the pH of the milk (~7.0) which is lower than that of the blood (7.4). The cell monolayers were equilibrated with 6 ml KRB in the donor and receiver compartments for 30 minutes prior to initiating the diffusion studies. The cells were aerated with 95% O_2/5% CO_2 at a rate of 3-5 bubbles per second during the transport studies.

After equilibration, the KRB in the donor compartment was replaced with 6 ml of nitrofurantoin solution in KRB at varying concentrations (1-200 μM) and the receiver chamber was replaced with 6 ml of fresh KRB. Nitrofurantoin concentrations which were above and below the K_m for nitrofurantoin flux (33.5 μM) were used.(62) Sample aliquots of 300 μl were taken from the receiver compartment every 30 minutes for 180 minutes. Fresh KRB (300 μl) at 37°C was used to replace the samples withdrawn and the total amount of drug transported was corrected for the loss of the withdrawn samples in the data analysis. The samples were analyzed for nitrofurantoin concentration by HPLC. Flux and permeability values were calculated using Fick's First Law (Equation 1.4). Bi-directional flux studies comparing the apical-to-basal and basal-to-apical flux are performed to detect polarized transport processes.

Nitrofurantoin HPLC Analysis

HPLC analysis of nitrofurantoin was performed according to the method described by Kari et al.(44) The HPLC system consisted of a Spectra Chrom 200 spectrophotometric detector (Spectrum Chromatography), SP8800 ternary HPLC pump (Spectra Physics), 712 WISP autosampler (Waters), and data was processed with PC1000 software. A Luna®, 250 x 4.6 mm, 5 μM, C-18 column (Phenomenex) was used with a mobile phase consisting of 1% acetic acid in H_20:methanol (80:20) with pH adjusted to

5.0 with NaOH. A flow rate of 1.0 ml/min and UV absorbance wavelength of 365 nm were used.

Transepithelial Electrical Resistance Measurements

The TEER was monitored for each Snapwell and Transwell insert using an EVOM® Epithelial Voltohmmeter with "chopstick" electrodes (World Precision Instruments, Sarasota, FL). TEER measurements for Transwell cultures were taken prior to media changes and in the diffusion chambers prior to flux studies for the Snapwell inserts. TEER (Ωcm^2) was calculated by multiplying the resistance value (Ω) by the surface area of the cell monolayer (12-well Transwell: 1.12cm^2, 6-well Transwell: 4.67 cm^2, and 6-well Snapwell: 1.13 cm^2).(38)

Lucifer Yellow Transport

Lucifer yellow stock solutions of 10 μg/ml were prepared in KRB and warmed to 37°C. Lucifer yellow solutions were placed in the donor chamber (5 ml) and fresh KRB in the receiver chamber (5 ml) with aeration with 95% O_2/5% CO_2 at a rate of 3-5 bubbles per second at 37°C following the completion of the nitrofurantoin transport studies. Lucifer yellow transport studies were run for 1 hour. After completion, the lucifer yellow and KRB solutions from the donor and receiver chambers were removed. Lucifer yellow concentration in the receiver chambers was measured using fluorescence (excitation: 485 nm, emission: 538 nm, Kontron SFM 25 A spectrophotometer). The concentration of lucifer yellow in the receiver chamber was determined using a standard curve for lucifer yellow fluorescence and the percent of the initial lucifer yellow which was transported into the receiver chamber was determined. The percent lucifer yellow transported was used to determine the extent of tight junction barrier formation since

lucifer yellow is only transported through the paracellular spaces. Lucifer yellow flux should be between 0.3-2% for an intact cell monolayer (BD Biosciences lucifer yellow protocol) and since the mammary epithelium forms very tight junctions, the lucifer yellow flux should be in the lower region of the listed range.

Results

MCF10A Monolayer Growth and Characterization

The MCF10A cells were grown to confluence on polyester membranes (Figure 3.1). The MCF10A cells were irregularly shaped and formed multilayers around 2-3 cells thick, which created some imaging difficulties (Figure 3.2).

Tight Junction Formation

Although the cells completely covered the membrane surface, the transepithelial electrical resistance (TEER) was below 200 Ωcm^2 which is indicative of a non-polarized monolayer. The resistance measured was not significantly different from the value for the membrane alone (Figure 3.3). Lucifer yellow flux through the polyester membrane after one hour was around 2.5% of the initially applied concentration; this decreased to 1.5% for the membrane with MCF10A cells (Figure 3.4). Although the lucifer yellow flux decreased in the presence of cells, the reduction was likely only due to a reduction in the available membrane pore surface area. A reduction to ~0.3% would be expected with completely functional tight junctions.

Immunofluorescence microscopy was used to localize the tight junction protein ZO-1 in MCF10A cell cultures. Formation of tight junctions involves the localization of ZO-1 from the cytoplasm to the lateral plasma membrane on the apical side of the cell. Western blotting confirmed that ZO-1 was present in MCF10A cells (Figure 3.5). ZO-1 is known to be present in MCF10A cells; however, localization to the apical plasma

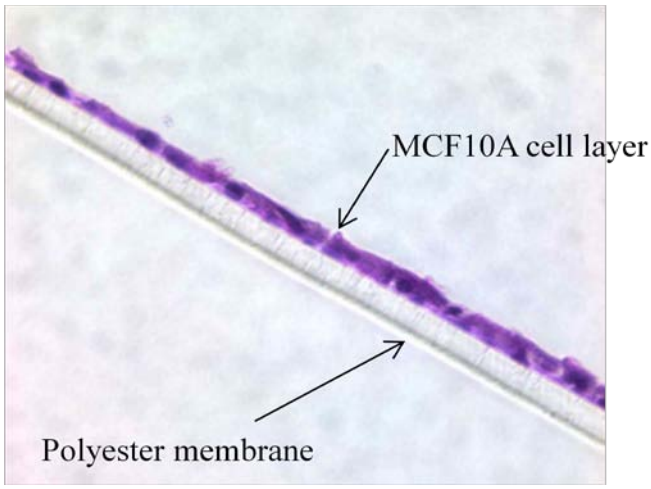

Figure 3.1. Cross-section of MCF10A cells grown on a porous polycarbonate membrane. Cells were stained with hematoxalin and eosin and visualized by light microscopy (60X magnification).

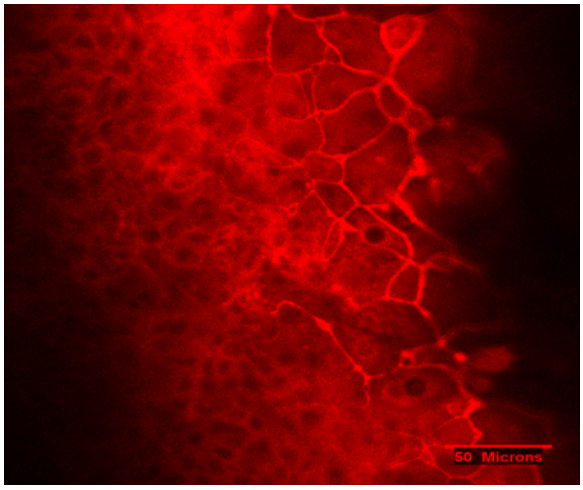

Figure 3.2. Confocal microcopy image of MCF10A cells stained for localization of the tight junction protein ZO-1. Apical cells are shown on the right and are larger than the underlying basal cells. Tight junction formation occurred between the most apical cells in each layer. ZO-1 was incompletely localized to the tight junctions in MCF10A cells.

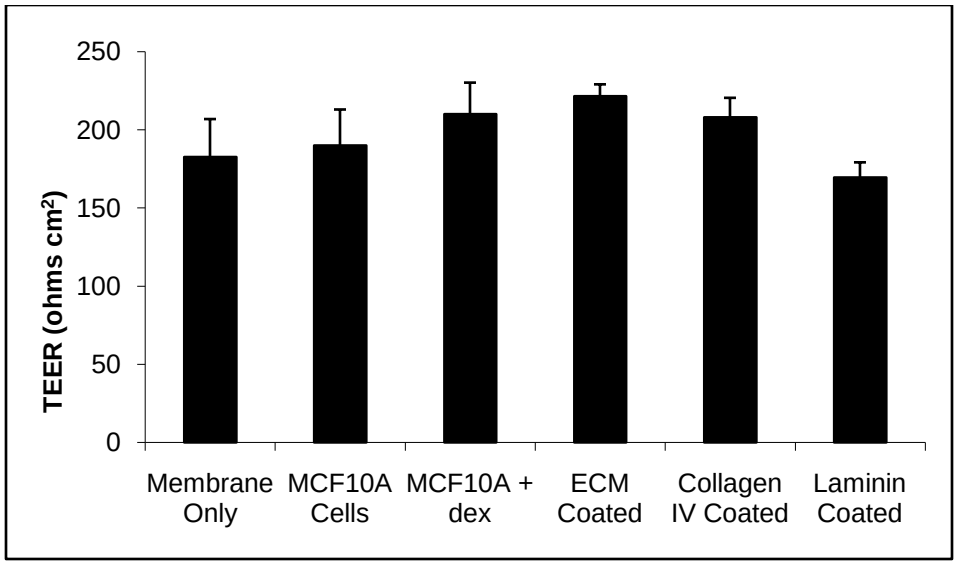

Figure 3.3. Transepithelial electrical resistance measurements of MCF10A cells under different growth conditions. Membrane only refers to the TEER of the polyester membrane alone. The remaining bars refer to MCF10A cells under different growth conditions. MCF10A cells were grown to confluency, MCF10A + dex were grown in the presence of 1 µM dexamethasone, ECM gel, collagen IV or laminin V were used as membrane coatings prior to cell seeding.

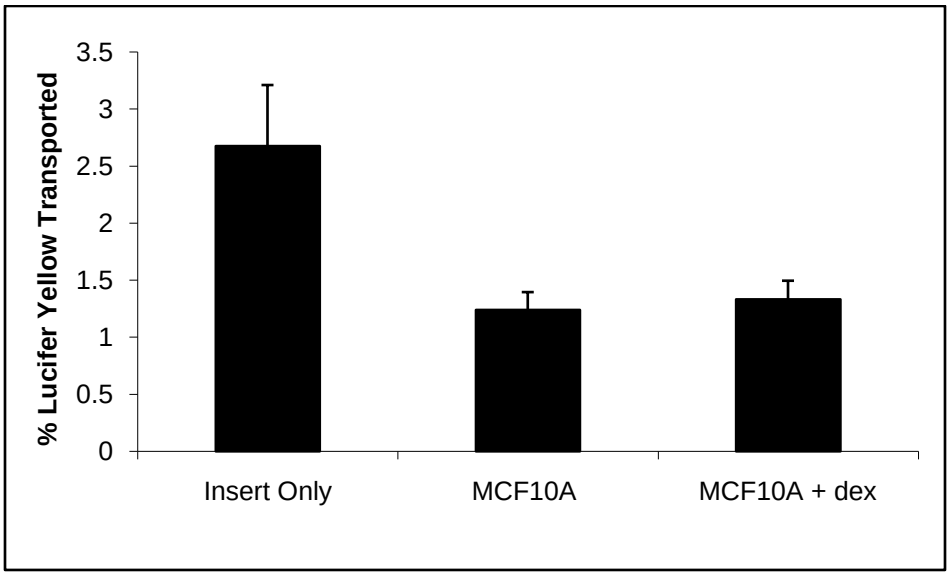

Figure 3.4. Percent transport of the paracellular marker compound lucifer yellow (10 µg/ml) after 1 hour through polycarbonate membranes after one hour, membranes with MCF10A cells and MCF10A cells grown in the presence of dexamethasone.

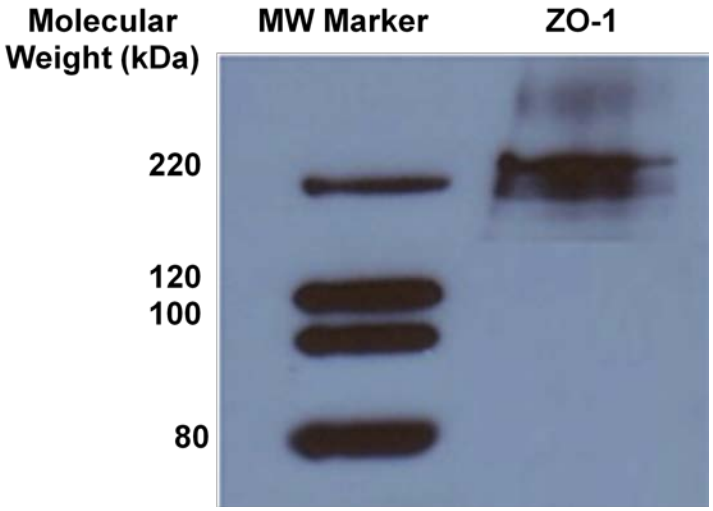

Figure 3.5. Western blot of ZO-1 in MCF10A cells. A mouse anti-(human) ZO-1 primary antibody was used for specific detection of the 225 kDa ZO-1 protein. A goat anti-mouse-HRP secondary antibody with chemiluminescence detection was used.

membrane is also vital to proper tight junction formation. ZO-1, when it is localized to the plasma membrane, appears as bright continuous bands around the cells (example shown in Figure 3.6.a). Unlocalized ZO-1 present in the cytoplasm appears as diffuse color spread throughout the cells (Figure 3.6.b). Although ZO-1 is present, it is not fully localized to the tight junctions in the apical plasma membrane. ZO-1 immunofluorescence microscopy results are consistent with the incomplete tight junction formation indicated by the low TEER and relatively high lucifer yellow flux results.

Modification of Culture Conditions to Enhance Tight Junction Formation

Since MCF10A cells showed insufficient tight junction formation, changes to the cell culture conditions were investigated to improve tight junction formation. Modifications included replacement of hydrocortisone in the media with a stronger glucocorticoid, dexamethasone, coating the polyester membranes with extracellular matrix materials and removal of cholera toxin from the media.

Glucocorticoid hormones trigger lactogenesis *in vivo* and tight junction closure both *in vivo* and *in vitro.*(18,19,27,60) MCF10A normal growth medium contains the glucocorticoid, hydrocortisone. Since dexamethasone (dex) is known to be a stronger inducer of tight junction closure in cell culture, hydrocortisone was replaced with dex (0.5 μg/ml) in MCF10A differentiation media(19,27) Addition of dex did not have a significant effect on the polarization of MCF10A cells as evidenced by no significant increase in the TEER (Figure 3.3). Lucifer yellow transport also showed no significant decrease when dex was used in the culture medium (Figure 3.4).

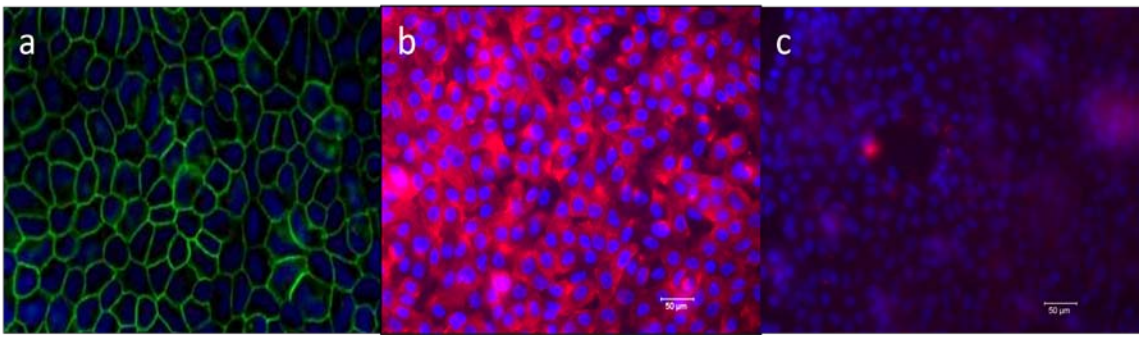

Figure 3.6. Immunofluorescence microscopy localization of the tight junction protein ZO-1

a. Example of ZO-1 localization in MDCKII cells. ZO-1 (green) staining is visible in a narrow, continuous band surrounding the cell periphery. Image taken from Invitrogen ZO-1 primary antibody technical information.
b. Localization of ZO-1 (red) in MCF10A cells. Cell nuclei are stained with DAPI (blue). Diffuse spreading of ZO-1 in MCF10A cells indicates a lack of proper tight junction formation in these cells.
c. Negative (isotype) control with a mouse IgG and a goat anti-mouse-Alexa 568 secondary antibody (red). Nuclei were stained with DAPI (blue).

Membrane Coating

Coating materials, collagen type IV, laminin V and extracellular matrix (ECM) gel, were used on the membranes in an attempt to promote cell polarization. Basement membrane coating materials are known to promote apical-basolateral polarity and formation of cell junctions in *in vitro* three dimensional cultures.(26,63) Collagen IV and laminin V are each components of the basement membrane *in vivo* and ECM gel is representative of the entire matrix.

Cells on collagen IV grew with areas of monolayer structure interspersed with clumps of multilayers, similar to the cells on the polyester membranes alone (Figure 3.7). The TEER values, around 200 Ωcm^2 (uncorrected for the blank membrane) were also similar between cells grown on collagen IV and on the polyester membranes (Figure 3.3). Laminin V is known to be important in the generation of polarity in the mammary epithelium (26,63). However, MCF10A cell grown on laminin V surfaces had a lower TEER (Figure 3.3) and formed only a very thin cell layer (Figure 3.8). These unexpected results may have occurred because cell attachment to laminin V may only be able to occur when other basement membrane components are present. Cell binding sites on pure laminin V may not have been readily available, thereby impeding cell attachment and subsequent membrane polarization. Basement membrane gel coatings are commonly used in three dimensional cultures of mammary epithelial cells.(14,23) MCF10A cells grown on ECM gel formed multilayers of cells throughout the ECM structure (Figure 3.9) but did not show a significant increase in TEER over the MCF10A cells grown on polyester membranes.

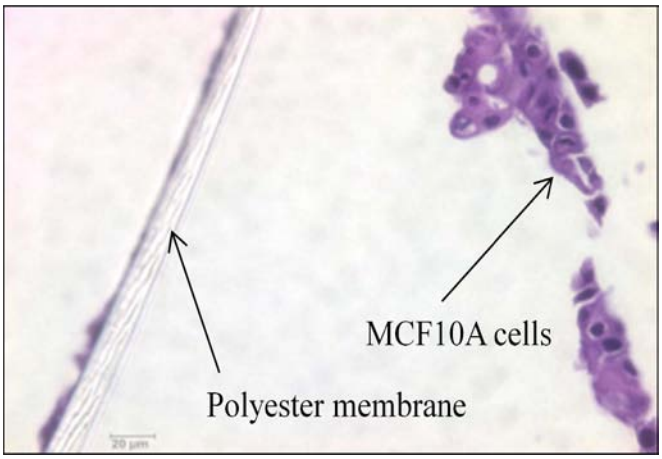

Figure 3.7. Collagen type IV coated polycarbonate membranes for MCF10A cell growth. MCF10A cells were stained with hematoxalin and eosin (60X magnification).

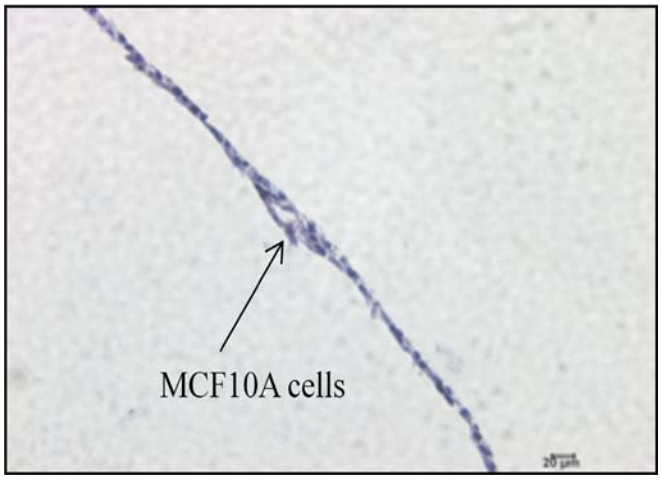

Figure 3.8. Laminin V coated polycarbonate membranes for MCF10A cell growth. MCF10A cells were stained with hematoxalin and eosin (40X magnification).

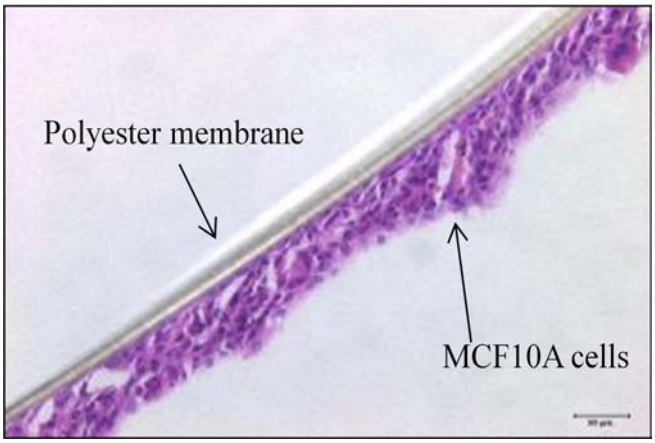

Figure 3.9. ECM gel coated polycarbonate membranes for MCF10A cell growth. MCF10A cells were stained with hematoxalin and eosin (40X magnification).

Polarized Transport Studies

Bi-directional flux studies with nitrofurantoin through the MCF10A cells were performed to study cell polarization. Nitrofurantoin is a substrate for the efflux transporter BCRP. This transporter is known to be present in the mammary epithelium and its presence was confirmed in MCF10A cells by immunoblotting (Figure 3.10). Basal-to-apical flux of nitrofurantoin was expected to be significantly greater than the apical-to-basal flux. However, bi-directional flux studies of nitrofurantoin in MCF10A cells showed no difference in apical-to-basal and basal-to-apical flux (Figure 3.11). The lack of observable transporter effect is likely due to the lack of polarization and the leaky tight junctions observed with these cells.

Removal of Cholera Toxin from MCF10A Media

MCF10A cells were grown on Transwell polyester membranes with (+ ctx) and without cholera toxin (- ctx) present in the growth media. A recent paper by Marshall et al. suggested that MCF10A cells form tight junctions when grown in the absence of cholera toxin.(20) MCF10A cells were grown on Transwell membranes with the media in the upper and lower chambers replaced daily. TEER and immunofluorescence microscopy was used to monitor tight junction formation in the absence of cholera toxin (Figure 3.12). TEER values after correction for the resistance of the polycarbonate membranes and normalizing for the area of the 6 well Transwells (4.67 cm^2) were 80 ± 58 Ωcm^2 for MCF10A cells grown with cholera toxin compared to 137 ± 62 Ωcm^2 for MCF10A cells without cholera toxin and 156 ± 61 Ωcm^2 for CRB-MCF10A cells without cholera toxin (cells grown for 30 days). The TEER values were highly variable from one day to the next, therefore, the effect of removing cholera toxin from the media

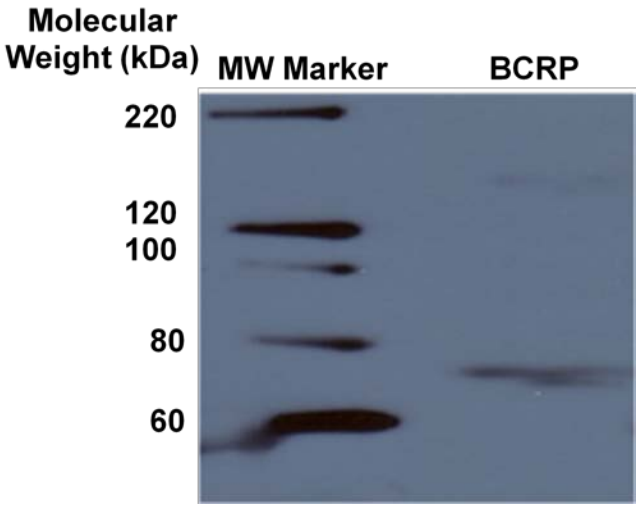

Figure 3.10. Western blot of ABCG2 in MCF10A cells. A mouse anti-ABCG2 primary antibody was used for specific detection of the 70 kDa ABCG2. A goat-anti-mouse-HRP secondary antibody with chemiluminescence detection was used.

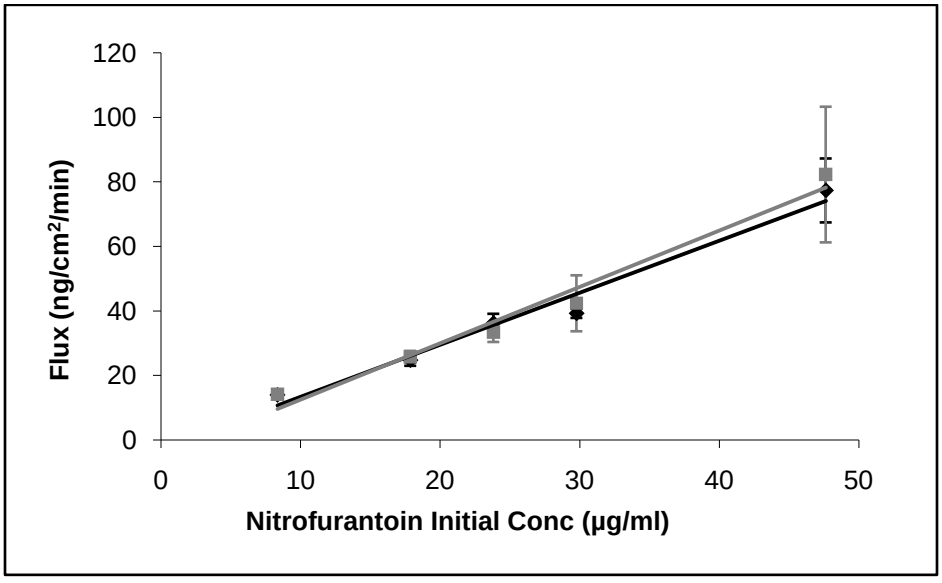

Figure 3.11. Flux of nitrofurantoin through MCF10A cells on polycarbonate membranes. Apical to basal flux (milk to plasma) (black,♦) and basal to apical (plasma to milk) (gray,■). No significant directional flux was observed.

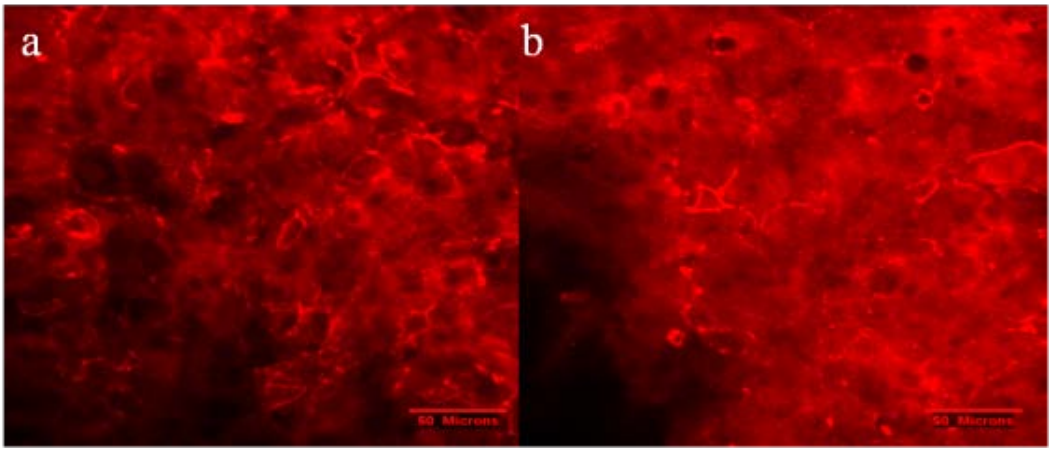

Figure 3.12. Confocal microscopy images of ZO-1 localization in MCF10A cells grown with and without cholera toxin.

a. Confocal microscopy image of ZO-1 (red) localization in MCF10A cells. ZO-1 was stained with immunofluorescence (mouse anti-(human) ZO-1 primary antibody and goat anti-mouse Alexa 568 secondary antibody).
b. Confocal microscopy image of ZO-1 (red) localization in MCF10A cells grown without cholera toxin. ZO-1 was stained with immunofluorescence (mouse anti-(human) ZO-1 primary antibody and goat anti-mouse Alexa 568 secondary antibody).

could not be demonstrated to be statistically significant. TEER measurements for MCF10A cells without cholera toxin were still well below acceptable values for polarized monolayer formation. Cells treated with and without cholera toxin showed similar tight junction localization. In both samples there were some localized areas of tight junction formation, but ZO-1 remained mostly diffusely spread throughout the cells. Crumbs3 Transfected MCF10A Cells

The epithelial tight junction protein, Crumbs3, is part of a protein complex essential for the generation of cell polarity (64). MCF10A cells express very little of this essential protein, which may explain their inability to form tight junctions under standard cell culture conditions.(28) MCF10A cells transfected with Crumbs3 (CRB3) have been shown by Fogg et al. to form tight junctions in culture.(28) Crumbs3 transfected cells were grown as described in Fogg et al.(28) These cells showed improved tight junction formation through increased TEER (Figure 3.13) and increased localization of ZO-1 to the plasma membrane (Figure 3.14), however the improvements in cell polarity were less than those reported by Fogg.(28) In their report, TEER values for CRB3 transfected MCF10A cells reached over 800 Ωcm^2 after 24 days in culture, compared to a TEER of only ~100 Ωcm^2 with the CRB-MCF10A transfected cells and ~150 Ωcm^2 for CRB-MCF10A cells without cholera toxin. The improvements in cell polarity, while statistically significant, were still not sufficient for proper barrier function for use of these cells as a drug transport model. This was confirmed by the minimal decrease in lucifer yellow transport in these monolayers (Figure 3.14). CRB-MCF10A cells were monitored for their barrier properties at 1 week and 30 days following seeding. Growing the Crumbs3 transfected cells for 30 days appeared to increase the amount of ZO-1 localized

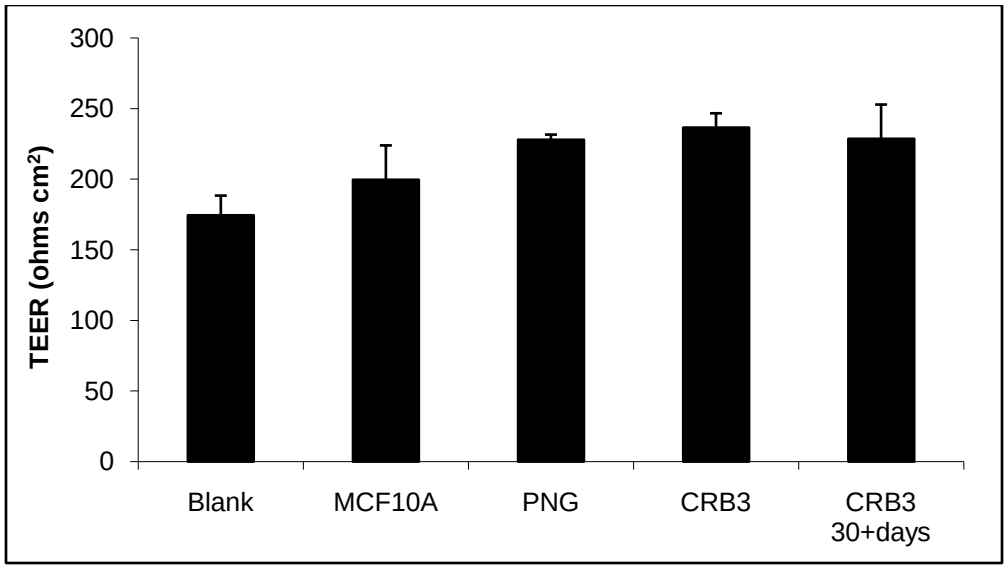

Figure 3.13. Transepithelial electrical resistance measurements of polyester membranes (blank), MCF10A cells, PNG-vector transfection control MCF10A cells, CRB3 transfected MCF10A cells grown for 7 days, and CRB3 transfected MCF10A cells grown for 30+ days. Error bars represent standard deviations of TEER measurements ($n \geq 15$ for all cell types).

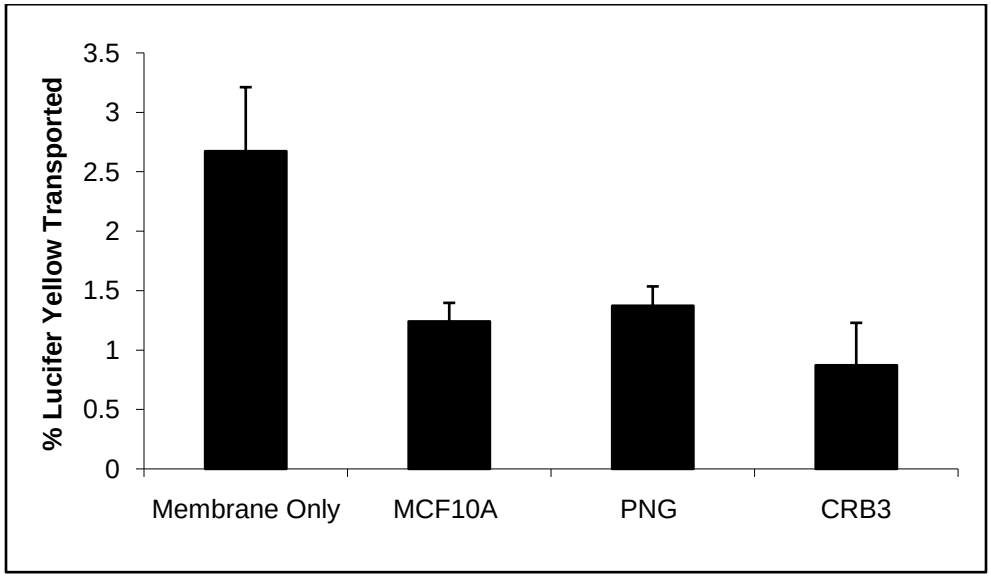

Figure 3.14. Flux of the paracellular marker compound, lucifer yellow, through polyester membranes, MCF10A cells, PNG-vector transfection control MCF10A cells and CRB3-PNG-vector transfected MCF10A cells. Error bars represent standard deviations of lucifer yellow flux (n=5).

to the tight junction over the cells grown for only 1 week (Figures 3.15 and 3.16). No significant increase was seen in TEER of the 30 day cells over Crumbs3 cells grown for one week, however (Figure 3.13). Lack of polarization of CRB-MCF10A cells was confirmed by the same lack directional flux of nitrofurantoin (Figure 3.17) as seen with the untransfected MCF10A cells.

MCF7 and HMEC Growth and Characterization

Because MCF10A cells formed monolayers with barrier properties ill-suited for drug transport, barrier properties of MCF7 cells were examined. Since MCF7 cells are a carcinogenic cell line, they are not expected to be a good model for drug transport in the normal mammary epithelium. While protein expression is known to be lower in carcinogenic cells, their abnormal growth properties could have advantages for *in vitro* barrier formation similar to that observed with the Caco 2 cell line utilized as a model for the intestinal epithelium.(41) In contrast, transporter expression, especially expression of multidrug resistance transporters such as MDR1 and BCRP, may be increased in MCF7 cells similar to other carcinogenic cell lines which over-express numerous transporter proteins.(65) MCF7 cells had a fairly low TEER values (139 Ωcm^2, Figure 3.18 and Table 2.2) and unexpectedly grew much more slowly than the MCF10A cells in culture. Therefore, this cell line was not pursued further as a drug transport model.

Primary human mammary epithelial cells were grown on 6 well polyester Snapwell inserts for bi-directional flux studies, immunofluorescence microscopy studies and TEER measurements, and on 6 well polyester Transwell inserts for immunofluorescence microscopy and TEER measurements. Primary HMECs were obtained from two different sources, Clonetics and Gibco. Clonetics cells were grown on

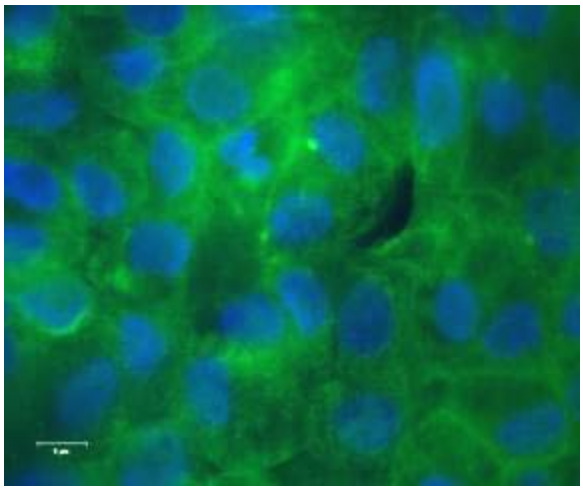

Figure 3.15. ZO-1 immunofluorescence microcopy localization in CRB3-MCF10A cells (cultured for 7 days). ZO-1 (green) stained with immunofluorescence (mouse anti-(human) ZO-1 primary antibody and goat anti-mouse FITC secondary antibody) and nuclei (blue) labeled with DAPI. ZO-1 showed slightly improved localization to the tight junctions (bottom right corner), however, it remained mostly diffusely localized throughout the cells.

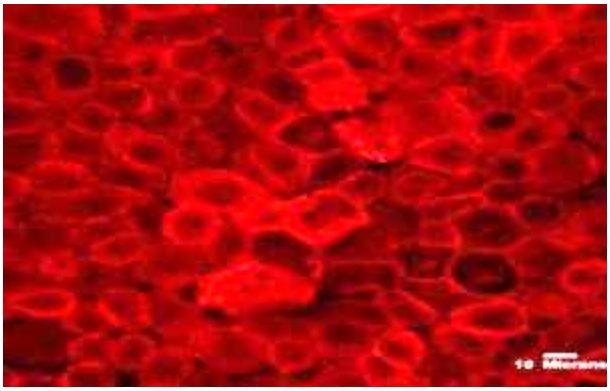

Figure 3.16. Confocal microscopy ZO-1 (red) localization in CRB3 transfected MCF10A cells cultured for 30 days. ZO-1 was stained with immunofluorescence (mouse anti-(human) ZO-1 primary antibody and goat anti-mouse Alexa 568 secondary antibody). ZO-1 localization to the tight junctions is improved over the CRB-MCF10A cells grown for 1 week and untransfected MCF10A cells.

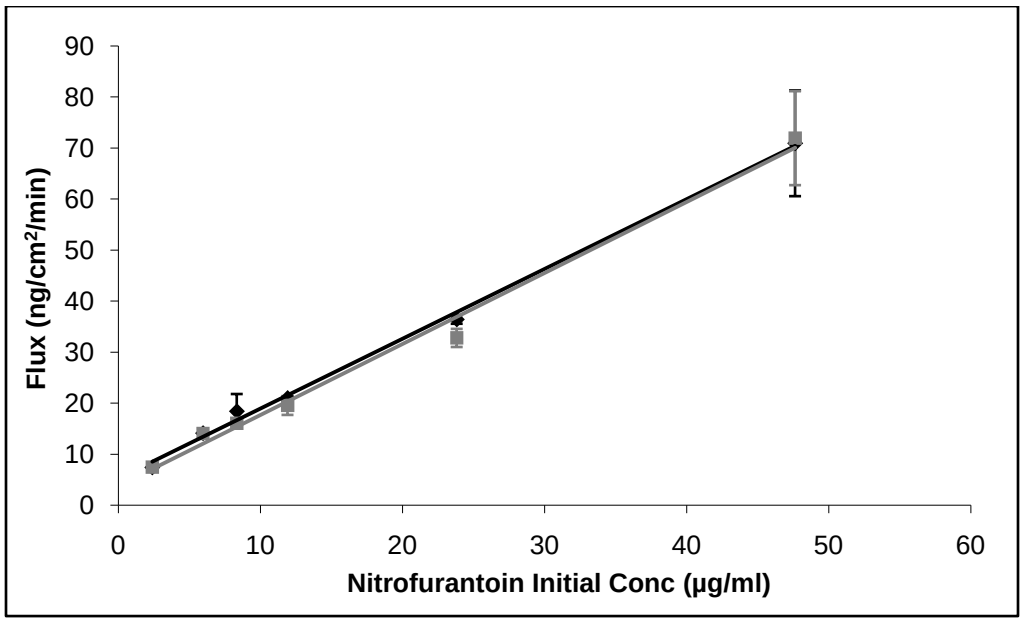

Figure 3.17. Flux of nitrofurantoin through CRB3 transfected MCF10A cells. Apical to basal (milk to plasma) flux (black, ♦) and basal to apical (plasma to milk) flux (gray, ■). Error bars represent standard deviations (n=5).

the Snapwell inserts and Gibco cells were grown on Transwells. Snapwell and Transwells inserts are identical except for the surface area available for cell growth (Snapwell 1 cm^2, Transwell 4.67 cm^2). Clonetics HMECs had a TEER of 185 ± 28 Ωcm^2 on Snapwell inserts, while Gibco cells had a TEER of 125 ± 47 Ωcm^2. In comparison, MCF10A cells had a TEER of 55 ± 17 Ωcm^2 on Snapwell inserts and a TEER of 80 ± 58 Ωcm^2 on Transwell inserts (TEER of all cell types shown in Table 3.2 and Figure 3.18).

Immunofluorescent labeling of the tight junction protein ZO-1 was used to determine if it was localized to the tight junctions in the lateral plasma membranes in HMECs. ZO-1 localization in the Clonetics HMECs (Figure 3.19.a) showed very diffuse ZO-1 with some tight junction localization. Tight junction formation is much more apparent at higher magnification (Figure 3.19.b). ZO-1 localization in Gibco HMECs (Figure 3.20) shows an increase in tight junction formation over the Clonetics HMECs, however, there is still a significant amount of cytoplasmic ZO-1 and tight junctions were absent from a significant portion of the culture insert. ZO-1 localization in HMECs was similar to the localization pattern in MCF10A cells (Figure 3.21) and primary HMECs formed multilayers similar in appearance to the MCF10A cells.

Bi-directional flux of the BCRP substrate, nitrofurantoin, was examined in the Clonetics primary mammary epithelial cells (Figure 3.22). As mentioned previously, since nitrofurantoin is a known BCRP substrate and BCRP is known to be present in the mammary epithelium,(10) a significant difference in the bi-directional flux is expected. However, no difference in flux was observed in HMECs from the apical-to-basal or basal-to-apical direction, thus suggesting incomplete polarization of these epithelial cells which is consistent with the TEER and immunohistochemistry results.

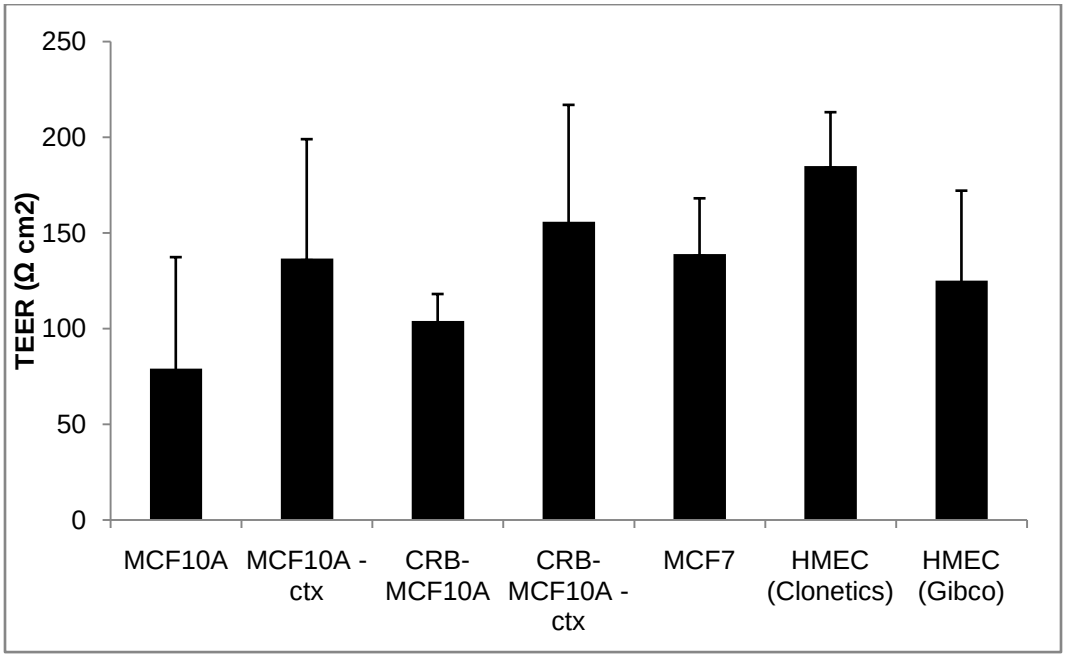

Figure 3.18. Transepithelial electrical resistance measurements of MCF10A cells grown in cholera toxin containing media (MCF10A), MCF10A cells grown in the absence of cholera toxin (MCF10 – ctx), CRB-MCF10A cells with cholera toxin containing media (CRB-MCF10A), CRB-MCF10A cells without cholera toxin containing media (CRB-MCF10A –ctx), MCF7 cells, and Gibco and Clonetics primary mammary epithelial cells (HMECs). TEER values were corrected for the resistance of the blank polyester membranes. Error bars represent the standard deviation ($n \geq 6$ for all cell types).

Table 3.2. Transepithelial electrical resistance measurements of MCF10A cells, MCF7 cells, and primary human mammary epithelial cells (HMEC) on Snapwell and Transwell polyester membranes

Cell Type	Membrane Type	TEER (Ωcm^2)
MCF10A	Snapwell	55 ± 17
MCF10A	Transwell	80 ± 58
MCF10 - ctx	Transwell	137 ±62
MCF7	Snapwell	139 ± 29
HMEC (Clonetics)	Snapwell	185 ± 28
HMEC (Gibco)	Transwell	125 ± 47
CRB-MCF10A	Snapwell	104 ± 14
CRB-MCF10A -ctx	Transwell	156 ± 61

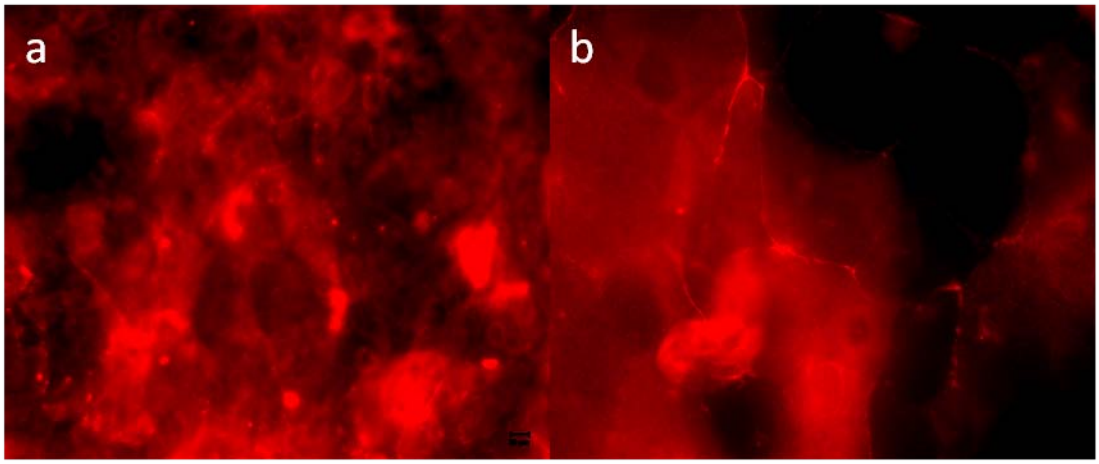

Figure 3.19. ZO-1 localization in Clonetics primary human mammary epithelial cells.

a. ZO-1 (red) localization in Clonetics primary human mammary epithelial cells (40X magnification). ZO-1 was stained with immunofluorescence (mouse anti-(human) ZO-1 primary antibody and goat anti-mouse Alexa 568 secondary antibody).
b. ZO-1 (red) localization in Clonetics primary mammary epithelial cells (100X magnification). ZO-1 was stained with immunofluorescence (mouse anti-(human) ZO-1 primary antibody and goat anti-mouse Alexa 568 secondary antibody).

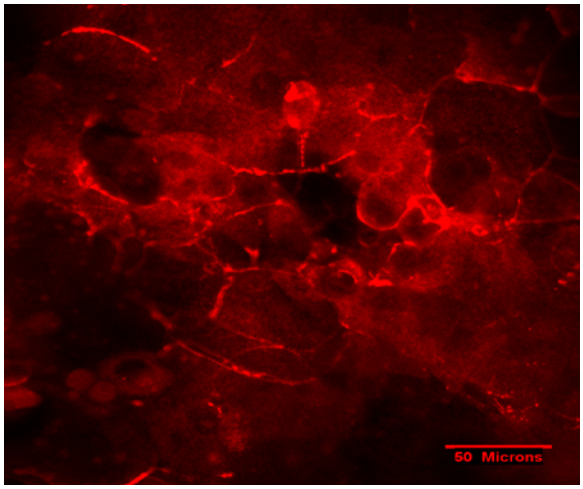

Figure 3.20. ZO-1 (red) localization in Gibco primary mammary epithelial cells (60X magnification). ZO-1 was stained with immunofluorescence (mouse anti-(human) ZO-1 primary antibody and goat anti-mouse Alexa 568 secondary antibody).

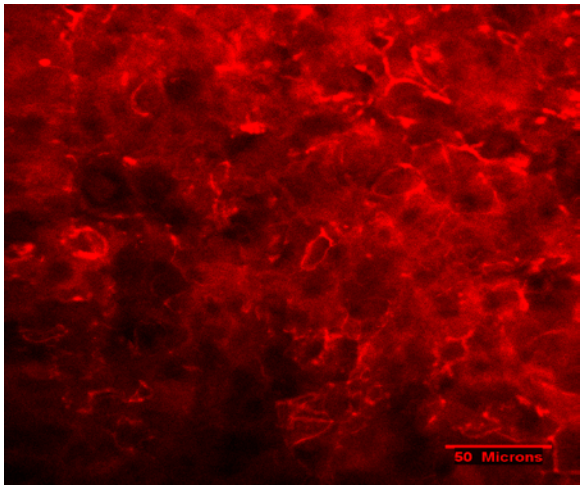

Figure 3.21. ZO-1 (red) localization in MCF10A cells (40X magnification). ZO-1 was stained with immunofluorescence (mouse anti-(human) ZO-1 primary antibody and goat anti-mouse Alexa 568 secondary antibody).

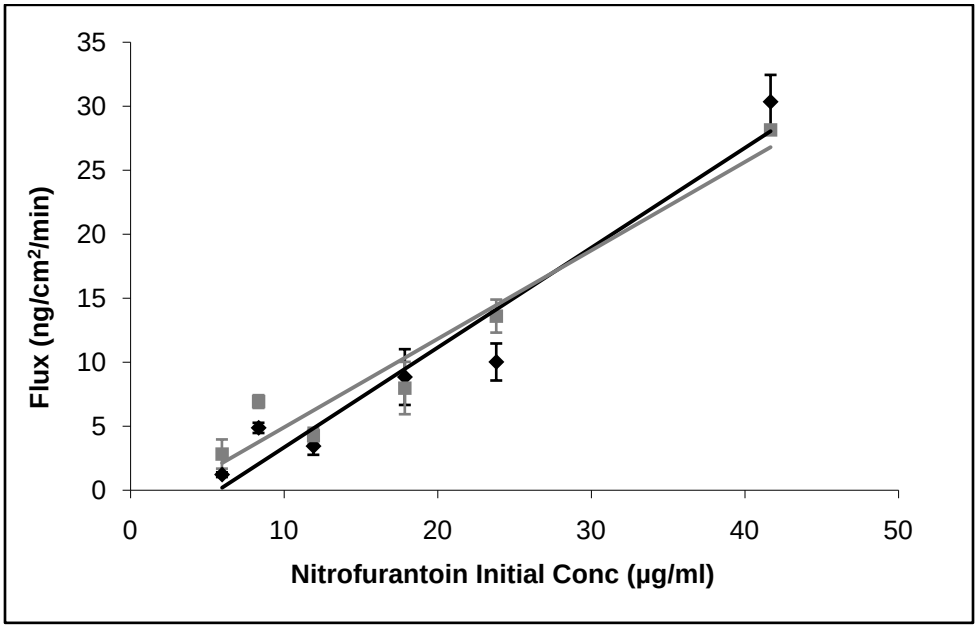

Figure 3.22. Flux of nitrofurantoin through primary mammary epithelial cells (Clonetics HMECs). Apical to basal (milk to plasma) flux is shown in red, basal to apical (plasma to milk) flux is shown in blue. Error bars represent standard deviations (n=5).

Discussion

Polarized cell monolayers are essential for proper epithelial cell function. Any cellular model used to measure epithelial drug transport, therefore, requires the accomplishment of cell polarization along with maintenance of adequate barrier properties. Both of these characteristics are highly dependent upon tight junction formation, and due to the importance of the tight junctions for this model system, emphasis was placed on the measurement of these properties when developing the cell culture system utilizing MCF10A cells.

The TEER measurements varied slightly among identical types grown on Snapwell and Transwell membranes which both contain porous, polyester membranes. The Snapwells have a growth area of 1.13 cm^2, while the Transwells have a growth area of 4.67 cm^2. Since the TEER measurements are normalized for the total resistance of the membrane surface, this should have a minimal effect on the difference in the measurements. The difference between the Snapwell and Transwell measurements was likely caused by the difference in electrode placement for the measurements. For the Snapwell membranes, the TEER is measured in the diffusion chambers with one electrode placed on either side of the vertical membrane. TEER in the Transwells is measured with the membrane placed horizontally and one electrode placed in the inner chamber and one in the outer chamber.

Barrier function was evaluated by TEER measurements, lucifer yellow transport and localization of the tight junction protein ZO-1 by fluorescence microscopy. Bi-directional flux studies were used to assess cell polarization. Measurement of these properties showed low levels of tight junction formation and a lack of polarization which makes the MCF10A and CRB3-MCF10A monolayers unsuitable models for studying

drug transport by traditional transcellular flux studies. A number of methods to improve MCF10A cell barrier properties and polarization were undertaken, including treatment with the glucocorticoid dexamethasone, using growth-promoting membrane coatings, and removal of cholera toxin from the media. Each of these methods was unsuccessful in increasing barrier properties and cell polarity to the extent required for a transcellular model of drug transport.

Cell attachment to the basement membrane is known to be important in the generation of cell polarity. It is thought that polarity is established through environmental signals, with attachment to the basement membrane playing an important role, leading to cell membrane asymmetry between the basal and apical surfaces.(22) When Snapwell inserts were coated with ECM components to simulate the *in vivo* surface to which the cells are attached, little improvement in cell polarity was observed. Collagen IV and laminin V, both components of the ECM, failed to increase MCF10A cell polarity and laminin V actually diminished cell growth compared to cells grown on uncoated Snapwells. Laminin V has been shown by many researchers to be necessary for epithelial cell polarity,(26,63) therefore, the MCF10A results were surprising. However, laminin *in vivo* is one component of a three-dimensional, multi-protein polymerized structure, and certain isoforms of laminin are unable to polymerize on their own.(26,63) Thus either laminin or collagen without other ECM components would not be expected to be a good representation of the *in vivo* ECM structure on cell culture membranes. As expected, the reconstituted ECM gel had the greatest effect on cell growth. As mentioned previously, reconstituted ECM is commonly used for three-dimensional cell cultures, but its use in monolayer cultures for drug transport studies is limited due to the increased

formation of the multiple cell layers. Multilayer cell growth creates some minor complications for transport flux measurements because the assumption is that the cells exist in monolayers, therefore, the increased thickness of the diffusional barrier to flux would have to be accounted for, as well as transporter expression patterns in the various cell layers. Also, tight junction formation occurs only in the most apical layer of cells; therefore, barrier formation is incomplete in areas where multiple cell layers are established.

MCF10A cells have been reported to have abnormal ZO-1 localization to the tight junctions due to their low endogenous expression of Crumbs3. In our studies, Crumbs3 transfection of MCF10A cells failed to improve tight junction formation adequately for use as a drug transport model. The reason for our inability to reproduce the results of Fogg et al.(28) is likely due to unspecified differences in cell culture conditions, cell growth environment or experimental technique. The importance of numerous experimental parameters was described by Marshall et al. who reported other aspects of the cellular environment, such as the frequency of media changing and the quality of the horse serum used are important for cell growth and tight junction formation.(20)

Elimination of cholera toxin from the MCF10A growth medium has been shown to produce cells which form tight junctions.(20) MCF10A cells grown without cholera toxin in these studies did not exhibit the desired barrier properties. The reason for this discrepancy is unknown, but may also be related to any of a number of small differences in the media, the frequency the media was changed, or differences in cell culture conditions. Very small differences in cell culture conditions may cause large differences in assay results.(66-69), and even after controlling for a number of these culture

conditions during the growth of MCF10A cells, polarized monolayer formation with these cells, as demonstrated by other researchers, was not able to be replicated.

Use of Transwell culture inserts was also reported to be very important for MCF10A cell differentiation by Marshall et al.(20) MCF10A cells grown on cell culture plastic and cells grown on Transwell cultures expressed different growth and differentiation genes.(20) The difference in cell growth between monolayers and Transwells indicates the importance of the basal cell surface interactions with media components. Uptake of cell nutrients *in vivo* takes place through the basal (or blood-facing) surface; therefore it is logical that nutrient exposure on this surface would be important *in vitro*. In fact, Marshall and coworkers noted that changing only the basal media in Transwell cultures maintains the TEER of MCF10A cells.(20) All of these studies underscore the importance of the cell growth conditions *in vitro* for a proper model of drug transport *in vivo*.

HMECs

The TEER values for the Clonetics and Gibco HMECs were highly variable, as were the values for MCF10A cells. This variability is greater than the differences in TEER values between the cell types. Overall, the resistance values for the HMECs were similar to the resistance values for MCF10A and MCF7 cells. As mentioned previously, some of the variability in the measurements is due to the necessary difference in method used to measure the resistance on the Snapwell and Transwell inserts.

The passage number of the HMECs may have also affected the TEER results, since aging in primary cells is expected to have a dramatic effect on cellular morphological and functional characteristics. The Gibco HMECs were used at passage

seven while no starting passage number was listed for the Clonetics HMECs. These cells were used for TEER measurements three passages after they were received. Gibco HMECs are sent at passage six which is claimed to be two passages earlier than their competitors (Gibco website), therefore, Clonetics cells may have started around passage seven and were measured at passage ten. A difference in passage number from seven to ten may be significant in terms of their functional properties, in this case their barrier properties. The MCF10A cells measured on the 6 well Transwell inserts were also a fairly low passage number (passage 6) which may partially explain their higher TEER compared to MCF10As on Snapwells (passage 10- passage 60). Although passage number is expected to have much less of an effect on immortalized cell lines such as MCF10A, it appears there may be some small changes in the functional properties of these cells with aging.

The primary HMECs also showed similar ZO-1 localization to the tight junctions as MCF10A cells (Figures 3.19, 3.20 and 3.21). The immunofluorescence microscopy results are consistent with the TEER results and indicate there was some tight junction formation, but it was far from complete. Therefore, although the TEER values increased from below 100 Ωcm^2 for MCF10A cells to 125 to 185 Ωcm^2 for the HMECs, this increase was not sufficient to indicate the formation of polarized cells with fully functional tight junctions (~1000 Ωcm^2).

Bi-directional flux studies with nitrofurantoin confirmed that the tight junction formation was still incomplete in all of the cell systems studied. The difference in directional flux expected from a polarized, functional barrier of mammary epithelium was not observed experimentally. Since tight junction formation affects both barrier function

and cell polarity, the lack of observable directional flux may be have been caused by either of these consequences of incomplete tight junction formation. If the barrier function is incomplete, the drug may diffuse freely in either direction between the cells through the low resistance paracellular route. Also, if cell polarization is incomplete, transporter expression will not be organized. Thus, transporters which are meant to be on the apical side of the membrane may diffuse within the membrane to the basal side. When the transporters are located at random points around the cell, no net directional flux will be observed for their substrates. Both of these consequences of proper tight junction formation are therefore necessary for a cellular drug transport model, and both are incomplete in the primary mammary epithelial cells.

In summary, MCF10A cells grown using "typical" cell culture conditions (14) did not possess adequate barrier properties or demonstrate sufficient polarization to enable them to be used as an *in vitro* model of drug transport in the mammary epithelium. A variety of methods were attempted to increase tight junction barrier formation, and while some were successful in increasing tight junction formation, such as CRB3 transfection, the extent of the improvement was still insufficient to use this cell line in traditional monolayer-type transcellular drug transport studies. HMECs had similar limitations. Due to the increased variability and cost the of primary cell lines compared to immortalized cell lines, primary mammary epithelial cells do not appear to have any significant advantages over MCF10A cells as models for use in drug transport studies. MCF7 cells grew slowly in culture and also did not show any significant advantages in barrier formation over the other cells types. MCF10A cells do grow well in culture and

do express important drug transporters. Therefore, they may still be useful for assessing drug transport using methods other than monolayer flux measurements.

CHAPTER 4

DEVELOPMENT OF A QUANTITATIVE MODEL OF DRUG TRANSPORT IN MCF10A CELLS USING FLOW CYTOMETRY

Introduction

Flow cytometry is a technique which has been used to assess drug resistance resulting from the activity of the multidrug resistance transporters (MDR1, BCRP, and MRP1) and has primarily been used to identify substrates and inhibitors for chemotherapeutic drugs. Since this technique measures light scattering and fluorescence from suspended cells it can be used to monitor drug uptake and efflux of fluorescent drug molecules, without the concerns of monolayer polarity development. The limitations of this technique are that transcellular flux cannot be measured and that transporter substrates must be fluorescent to be detected. However, flow cytometry does allow quantitative measurements of fluorescent drug accumulation within a cell to be measured, allowing the effects of substrate and transport inhibitor compounds to be measured.

Flow cytometry can be used to study both drug uptake and efflux; however, measurements for efflux studies are less accurate. For efflux studies, the cells must be preloaded with the drug and, therefore, measurement complications arise from intracellular drug binding limiting intracellular concentrations available for efflux and a much smaller net difference between the varying drug concentrations.(42)

Flow Cytometry Assays of MDR Transport

Flow cytometry has been used for monitoring drug resistance by multidrug resistance (MDR) transporters, and along with antibody staining of the transporters, has been used to functionally assess transport within cells.(70) These assays can be used to compare different cell lines, examine substrate and inhibitor transport specificity, or

compare cells expressing mutated transporters and cells which over-express transporters.(42,70-74) Flow cytometry studies have provided valuable information on substrate and inhibitor affinity and specificity of the MDR transporters, specifically MDR1 and BCRP. The MDR transporters are complex systems possessing multiple substrate binding sites, overlapping substrate and inhibitor specificities and affinities, up- or down-regulation of expression levels, and differing substrate affinity due to mutations in the substrate binding site.(70,71,73-75) The extent and level of drug resistance depends upon the transporter expression level, mutations affecting substrate specificity and transport velocity, reversal efficiency of inhibitors and substrate affinity.(70)

In general, these are all comparative studies of transporter function, and very few quantitative studies of drug transport have been done using flow cytometry.(72,73) One quantitative analysis method which has been used is the relative increase in mean fluorescence intensity (MFI), however, this technique is only accurate for homogenous cell populations with narrow fluorescence distributions and large differences between fluorescence intensity measurements (little or no overlap of fluorescence histograms). A widely applicable, quantitative flow cytometry drug transport assay would provide valuable information on transporter function.

Numerous studies have demonstrated that mitoxantrone (MXR) is an excellent substrate for flow cytometry assays of BCRP function, and MXR has also been shown to be a substrate for MDR1 (and MRP1 to a lesser extent).(70,71,74) Although some studies on inhibition of MXR efflux have been reported,(70,71,74) quantitative studies on inhibitor effects examining both BCRP and MDR1 have not.

Flow cytometry was used to determine the uptake, efflux, and transport inhibition properties of the fluorescent drug, mitoxantrone, in the mammary epithelial cell line MCF10A. Flow cytometry is used to quantitatively assess the transport of mitoxantrone by the multidrug resistance transporters BCRP and MDR1. To investigate the role of each of these transporters on mitoxantrone uptake and efflux, studies were performed in the presence of specific transport inhibitors. Fumitremorgin C (FTC) was used as a BCRP antagonist and verapamil was used to inhibit MDR1 transport.(70,72,76-78) Analysis of flow cytometry results was accomplished through the utilization of a linear mixed effects model to quantify inhibitor effects.

Materials and Methods

Cell Culture

MCF10A (ATCC, CRL-10317), an immortalized human mammary epithelial cell line, was used for transport studies. MCF10A cells were grown in DMEM:F12 (1:1; Gibco) with 2 mM glutamine, containing 5% equine serum (HyClone), insulin (10 μg/ml; Sigma), hydrocortisone (0.5 μg/ml; Sigma), epithelial growth factor (20 ng/ml; Sigma), 100 ng/ml cholera toxin, 1 IU/ml penicillin, and 0.1 μg/ml streptomycin (Gibco). Cells were grown in Corning T75 (75 cm^2) cell culture flasks in a monolayer to 90-95% confluency, trypsinized and seeded into Costar 12 well cell culture clusters at a seeding density of around 10^5 cells/cm^2. Media was changed the day after seeding and then 3-4 times per week. MCF10A cells were used for flow cytometry studies 1-2 weeks after seeding.

Uptake Studies

MCF10A cells were washed with pre-warmed phosphate buffered saline (PBS, containing 0.90 mM $CaCl_2 \cdot 2H_20$, 0.49 mM $MgSO_4$, 2.68 mM KCl, 1.47 mM KH_2PO_4, 136.89 mM NaCl, and 8.10 mM Na_2HPO_4, pH 7.4) and then incubated in 1 ml of PBS per well for 30 minutes at 37°C. PBS was replaced with 1 ml of pre-warmed mitoxantrone solutions of varying concentrations (1, 2.5, 5, 10, and 20 μM in PBS) and cells were incubated at 37°C for 30 minutes (incubation times were chosen based on other drug accumulation studies using flow cytometry.(72,74) One sample of cells was treated with only PBS (untreated cells).

Efflux Studies

MCF10A cells were washed with 1 ml pre-warmed PBS per well and incubated in 1 ml PBS for 30 minutes at 37°C. PBS was replaced with 1 ml pre-warmed mitoxantrone solutions of varying concentrations (1, 2.5, 5, 10, and 20 μM in PBS) and cells were incubated at 37°C for 30 minutes. After incubation, each well was rinsed briefly with about 1 ml of PBS and 2 ml of fresh PBS was added; cells were incubated at 37°C for 30 minutes.

Inhibitor Studies

MCF10A cells for uptake studies were washed with 1 ml of PBS and incubated in 1 ml of 1 mM 2,4-dinitrophenol (2,4-DNP), 1-10 μM verapamil in or FTC for 30 minutes at 37°C. Inhibitor solutions were replaced with mitoxantrone solutions (1, 2.5, 5, 10, and 20 μM in PBS) with inhibitor and incubated at 37°C for 30 minutes. For efflux studies, MCF10A cells were treated with mitoxantrone solutions (1, 2,5, 5, 10 and 20 μM in PBS)

for 30 minutes at 37°C to load the cells with mitoxantrone. Cells were washed briefly in warm PBS and incubated in inhibitor solutions in PBS at 37°C for 30 minutes.

Flow Cytometry Analysis

Treated MCF10A cells were incubated in 0.5 ml of phenol red-free 0.05% trypsin with 1 mM EDTA (Gibco, 10X solution diluted to 1X in PBS) at 37°C until they detached from the plate. Trypsin was neutralized with an equal volume (0.5 ml) of 20% fetal bovine serum (FBS) solution in PBS. Cells were pelleted at 300 x g for 5 minutes at 4°C and then resuspended in 10% FBS solution and stored on ice until analysis (analysis was completed in 3 hours or less). Two replicates of each treatment (mitoxantrone and inhibitor for uptake or efflux studies) were performed each day, and each study was repeated on 3-5 different days. Intracellular mitoxantrone concentration was analyzed using a BD LSRII flow cytometer equipped with a 633 nm laser excitation source and a 660/20 bandpass emission filter (Becton, Dickinson and Company). Voltage pulse area and width for forward angle light scatter (FSC-A and FSC-W), voltage pulse area for side scatter light (SSC-A), and mitoxantrone fluorescence were set using untreated MCF10A cells. FSC-A, FSC-W and SSC-A voltages were set to center the main population of cells in the SSC-A vs. FSC-A and FSC-W vs. FSC-A dot plots. Gates were drawn by visual examination around the main population of single cells on SSC-A vs. FSC-A and FSC-W vs. FSC-A dot plots. These gates were used to select the populations of cells to be analyzed for mitoxantrone fluorescence (Figure 4.1). Mitoxantrone fluorescence data was collected for ~30,000 cells (Figure 4.2). The geometric mean of the fluorescence intensity for each sample is used since mitoxantrone fluorescence was measured on a log scale.

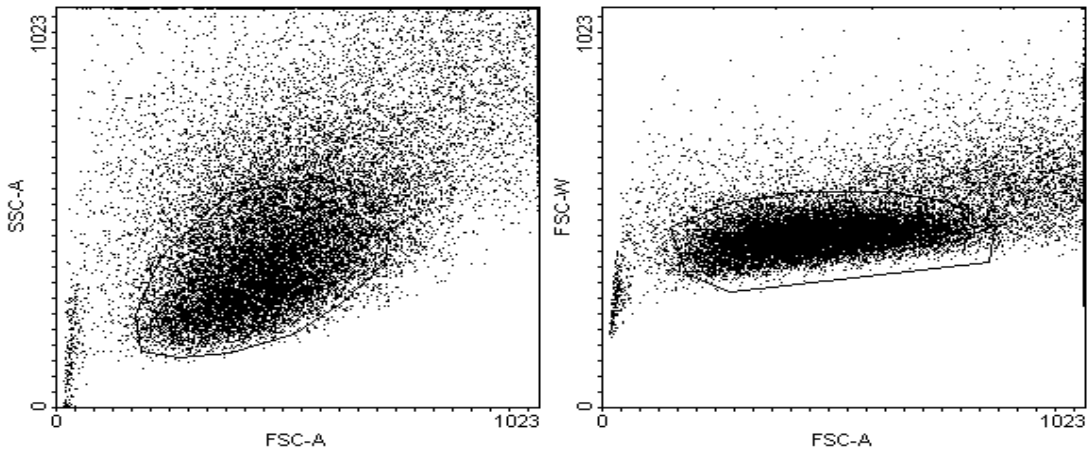

Figure 4.1. Side scattered area (SSC-A) vs. forward scattered area (FSC-A) and forward scattered width (FSC-W) vs. forward scattered area (FSC-A) dot plots. Gates were placed around the main population of cells on each dot plot to select the cell population to be used for fluorescence measurements. Each dot represents a cell or particle (1/2 of the total cells/particles are shown for clarity).

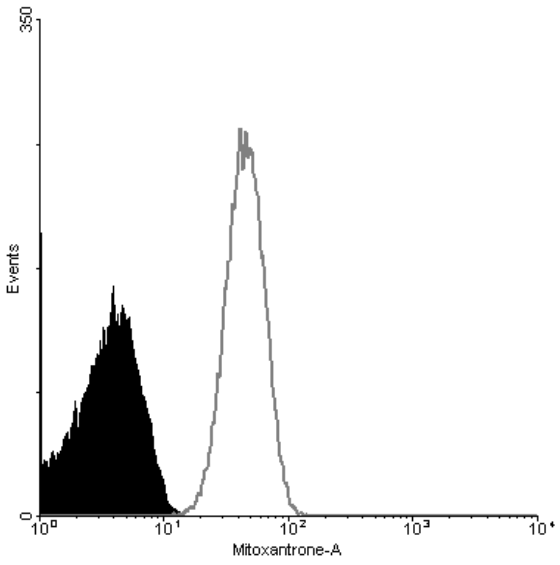

Figure 4.2. Mitoxantrone fluorescence histogram of number of cells (events) vs. log mitoxantrone fluorescence intensity. Untreated cells are shown in black and mitoxantrone treated cells (10 μM) are shown in gray.

Data Analysis

Due to the large inter-day variability in the fluorescence intensity measurements, standard data analysis methods such as t-tests, analysis of variance or linear regression could not be used to assess the effect of the inhibitors on mitoxantrone uptake and efflux. In order to accurately analyze the results, a linear mixed effects model was used for analysis of the fluorescence intensity data.(53) Statistical analysis of each data set was performed with a mixed effects model using the data analysis program SAS (SAS Institute). The geometric mean fluorescence intensity corrected for the background fluorescence intensity determined for untreated MCF10A cells was used for each sample data point. Data points were normalized by the highest fluorescence intensity measurements obtained with no inhibitor present to account for some of the variability due to cellular and instrumental effects. The data were weighted using the inverse of the square of the fluorescence measurement to account for the larger variance in the data points at the higher fluorescence intensity measurements.(60) Necessity of weighting of the data was determined from residual plots for linear mixed effects model effects and reduction in the AIC (calculated from SAS, flow cytometry data, SAS results and linear mixed effects model parameters for various models are shown in Appendix A). Data sets for each inhibitor were fit to linear mixed effects models as shown in Equation 4.1.

$$y = \mu+(\alpha_1 x)+(\alpha_2 x^2)+(\alpha_3 I)+(\alpha_4 xI)+(\beta_j z)+\varepsilon \qquad \text{Equation 4.1}$$

Linear Mixed Effects Model:
y = fluorescence sample reading
μ = population mean (y-intercept)
$\alpha_{1,2,3,4}$ = drug, $[drug]^2$, inhibitor or drug*inhibitor parameter estimate respectively
x/I = drug/inhibitor concentration (may be polynomial as needed)
$\beta_j z$ = variability estimates
ε = residual variability

MDR1 and BCRP Western Blot

The Western blotting procedure used was described in chapter 3. Specific detection of MDR1 and BCRP was accomplished using the antibodies listed in Table 4.1. A goat, anti-mouse, peroxidase-labeled secondary antibody (Sigma, 7.2 mg/ml, 1:160000 dilution) was used for detection.

Results

Western blots were inconclusive as to whether BCRP and MDR1 are present in MCF10A cells (Figure 4.3). Bands for both transporters were visible, but faint and narrow (especially for MDR1), possibly indicating low expression and were not characteristic widely-spread bands typical for glycoslyated membrane proteins.(67) Mitoxantrone was chosen as a model substrate for flow cytometry studies of multidrug resistance, and since it is a good substrate for both transporters (MDR1 and BCRP), the inhibitors FTC (BCRP inhibitor) and verapamil (MDR1 inhibitor) were used to distinguish the effect of each transporter on mitoxantrone accumulation in this cell line.(65,70,72,74)

MCF10A cells without mitoxantrone treatment gave an autofluorescence intensity value of ~2-4 (Figure 4.2). Since mitoxantrone is only very weakly fluorescent in solution (which is further decreased by dimerization), its native fluorescence intensity cannot be used to convert the measured intracellular fluorescence intensity to intracellular mitoxantrone concentration.(79) However, relative fluorescence intensity can still be used to compare mitoxantrone uptake between test conditions. Representative histogram plots of mitoxantrone intracellular fluorescence intensity for MCF10A cells treated with mitoxantrone and mitoxantrone with verapamil (Figure 4.4) or mitoxantrone with FTC (Figure 4.5) show the directional changes observed for each inhibitor; an increase in

Table 4.1. Western blot primary antibodies

Protein	MW	Species	Conc. Dilution	Type	Source
BCRP (BXP-21)	70 kDa	Mouse Anti-Human	250 µg/ml 1:1000	monoclonal	Sigma
MDR1	170 kDa	Mouse Anti-Human	7 mg/ml 1:1000	monoclonal	Sigma

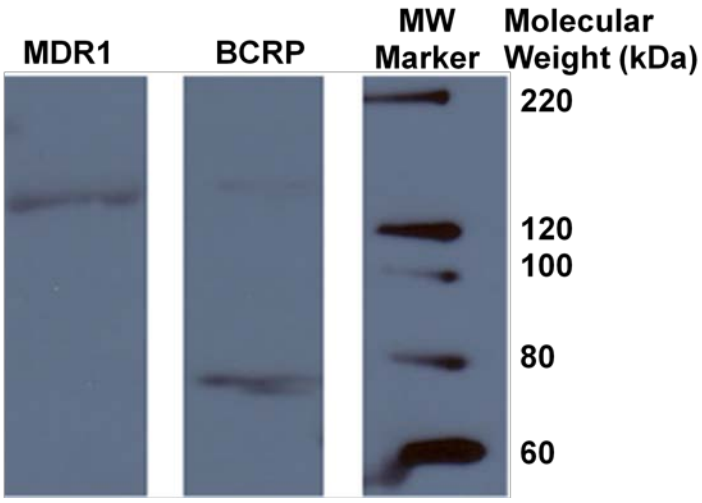

Figure 4.3. Western blot of MDR1 (MW = 170 kDa) and BCRP (MW = 70 kDa) in MCF10A cells. Both transporters are present in MCF10A cells, but expression levels are likely low as demonstrated by the faint bands on the blot.

intracellular fluorescence with verapamil indicated by a peak shift to the right and a decrease in fluorescence with FTC was observed, indicated by a peak shift to the left. The direction of change was always in the same direction for each inhibitor studied, however, the magnitude of the intensity values varied significantly between experiments.

Large inter-day variability was observed between the intensity of the mitoxantrone fluorescence values, which made inhibitor effects difficult to determine using standard statistical analysis methods. Variability in the measurements was attempted to be addressed experimentally. Changing the voltage setting for mitoxantrone fluorescence changes the signal intensity of the fluorescence values. To help control variability, the same voltage was set for mitoxantrone fluorescence and the fluorescence intensity values were normalized using the value for the highest drug concentration analyzed in each data set (example of normalization procedure shown in Appendix A). Even using these techniques, the inter-day variability was still very large and masked any significant inhibitor effects. A linear mixed effects model was evaluated to account for the inter-day variability which allowed the effects of the inhibitors to be determined.

The mixed effects models of mitoxantrone uptake and efflux transport were created using the statistical software program SAS. Geometric mean fluorescence intensity values were used to fit a linear mixed effects model which included two terms for the effect of increasing mitoxantrone concentrations (drug and drug^2 where the drug^2 term accounted for the leveling off of the fluorescence intensity seen at high mitoxantrone concentrations, typically occurring around 20 μM initial concentrations) and a term for the effect of the inhibitor. Some of the drug and inhibitor studies required an additional model term which was a drug-inhibitor interaction term (drug*inhibitor) to

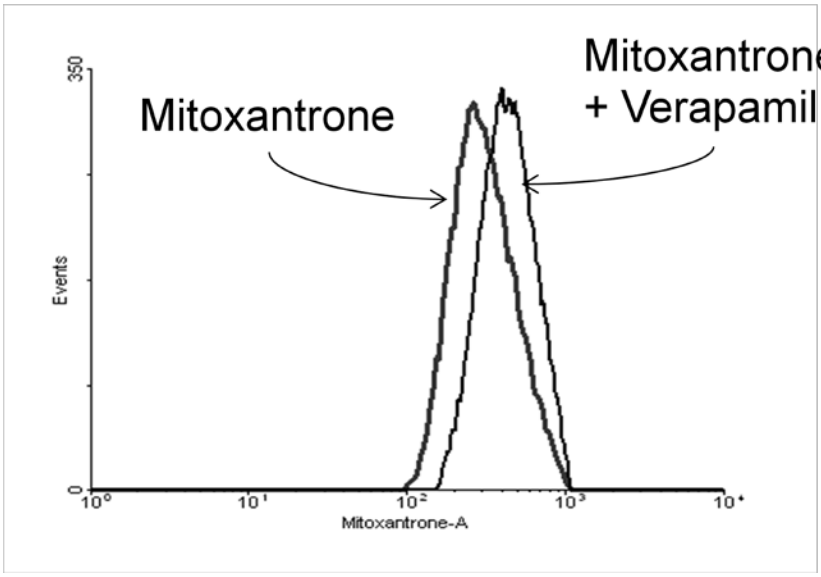

Figure 4.4. Histogram plots of mitoxantrone fluorescence for MCF10A cells treated with 10 µM mitoxantrone and 10 µM mitoxantrone and 10 µM verapamil. The MDR1 inhibitor verapamil shifts the peak to the right indicating increased intracellular uptake of mitoxantrone.

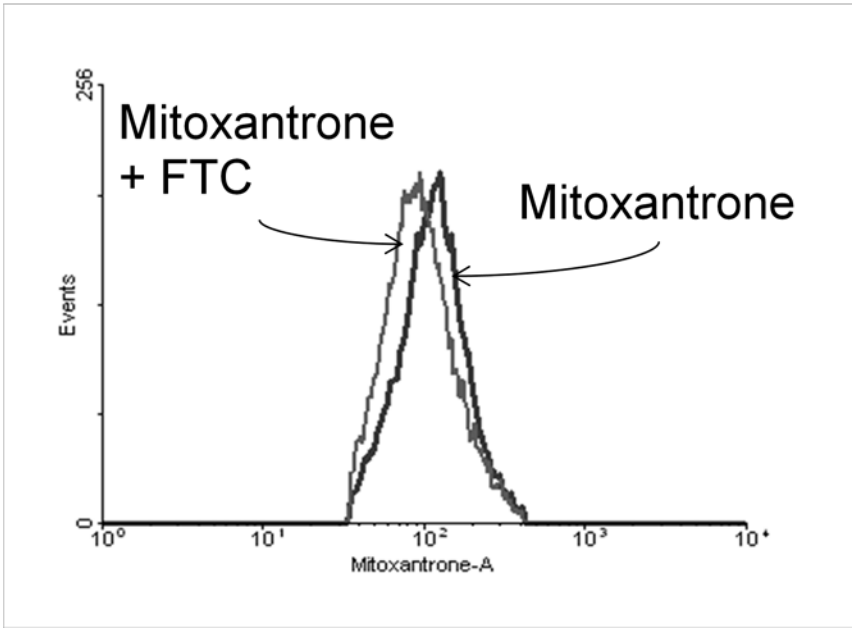

Figure 4.5. Histogram plots of mitoxantrone fluorescence for MCF10A cells treated with 10 µM mitoxantrone and 10 µM mitoxantrone and 10 µM FTC. The BCRP inhibitor FTC shifts the peak to the left indicating decreased intracellular uptake of mitoxantrone.

account for the increased spread in the values at higher concentrations. A significant drug-inhibitor interaction term was still considered as a significant inhibitor effect on mitoxantrone transport. Inclusion of model terms was determined by selecting the model with the minimum AIC fit values (as determined by SAS) from numerous models tested on each data set (all models shown in Appendix A). (53,54) The mixed effects model results for the random effects and model fitting values for each inhibitor study on mitoxantrone uptake and efflux are shown in Table 4.2.

Mitoxantrone uptake and efflux in the presence of inhibitors was used to determine if the active efflux transporters BCRP and MDR1 were functioning in MCF10A cells. The metabolic inhibitor 2,4-dinitrophenol (2,4-DNP) was used to show if any active transporters affect mitoxantrone flux in this cell culture system. Since 2,4-DNP inhibits ATP synthesis, all ATP dependent processes will be inhibited. All of the ATP-binding cassette family of transporters, including MDR1 and BCRP, couple ATP hydrolysis to substrate transport and therefore, should be affected by 2,4-DNP.(75,78,80) 2,4-DNP decreased the intracellular accumulation of mitoxantrone significantly in both uptake (Figure 4.6, Table 4.3) and efflux (Figure 4.7, Table 4.4) indicating that mitoxantrone transport has at least one ATP-dependent component. The effect of 2,4-DNP on mitoxantrone efflux required a drug*inhibitor term in the linear mixed effects model to account for the greater spread in the data values at the higher end of the mitoxantrone concentration range investigated. The decrease in intracellular mitoxantrone with 2,4-DNP inhibition suggests the presence of an active uptake transporter. Since inhibition of efflux transporters such as BCRP and MDR1 should result in increased intracellular concentrations.

Table 4.2. Mixed effects model variability parameter estimates and AIC fit statistics

Variability Parameter	2,4-DNP Uptake	2,4-DNP Efflux	Verapamil Uptake	Verapamil Efflux	FTC Uptake	FTC Efflux
Day	0.00016	0.001982	0.01471	0.02347	0.003819	0.008872
Rep (Day)	0.00023	NA	0.001311	8.03E-20	0.000103	0.000118
Residual	0.00956	0.02599	0.01358	0.02223	0.1054	0.02875
AIC	-114.4	-93.4	-336.0	-230.3	-27.9	-133.5

Mitoxantrone uptake at 37°C (Figure 4.8) and 4°C (Figure 4.9) was also used to investigate the presence of active transport. Colder temperatures inhibit active transport (but also slow passive diffusion). Some of the mitoxantrone uptake at 4°C was likely due to binding to the plasma membrane and not actual passive intracellular uptake. Mitoxantrone flux was higher and saturable around 20 μM initial concentrations at 37°C (Figure 4.8), but it showed linear concentration dependence at 4°C (Figure 4.9). Significantly higher flux at 37°C than at 4°C is consistent with the 2,4-DNP results and also suggests an active uptake transporter may dominate mitoxantrone flux in MCF10A cells. Since the flux at 4°C is representative of only the passive uptake and membrane binding processes, when the mitoxantrone flux at 4°C is subtracted from the mitoxantrone flux at 37°C, it reaches saturation between 10 and 20 μM initial mitoxantrone concentration and has an apparent K_m* of 4.50 ± 1.74 μM (Figure 4.10 and Table 4.5).(81) This K_m* value is similar to the K_m reported for a mitoxantrone active uptake transporter observed in MDCKII cells.(42)

Verapamil, an inhibitor of MDR1, was used to examine its effect on mitoxantrone transport in MCF10A cells. Inhibition of an efflux transporter such as MDR1 is expected to increase the intracellular accumulation of mitoxantrone. Verapamil showed a concentration dependent inhibition of mitoxantrone uptake and efflux as seen in Figure 4.11 and Figure 4.12. Increasing concentrations of verapamil increased the intracellular accumulation of mitoxantrone consistent with inhibition of MDR1 efflux. Linear mixed effects model fitting results for the effect of verapamil on mitoxantrone uptake and efflux had a positive and significant parameter estimate (uptake: 0.014, Table 4.6, efflux: 0.008, Table 4.7). Positive parameter estimates reflect increased mitoxantrone accumulation

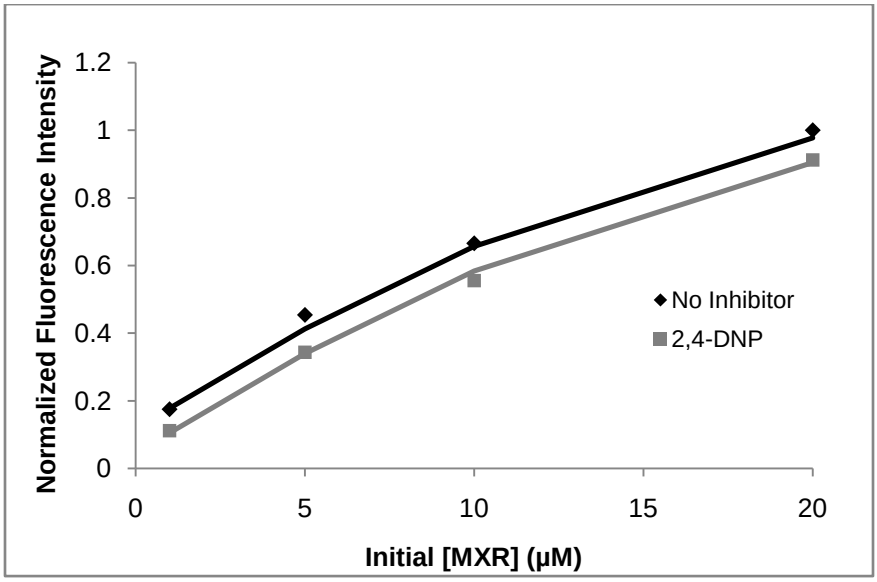

Figure 4.6. 2,4-DNP inhibition of mitoxantrone uptake in MCF10A cells. MCF10A cells were exposed to mitoxantrone (1-20μM) (black line) or mitoxantrone with the general metabolic inhibitor 1 mM 2,4-DNP (gray line). Data points are the geometric mean fluorescence intensity values (n=3) for each mitoxantrone and inhibitor concentration normalized by the fluorescence intensity of cells treated with 20 μM mitoxantrone. Errors bars are omitted for clarity. Curves were generated from the linear mixed effects model in SAS.

Table 4.3. Mixed effects model parameter estimates and p-values for 2,4-DNP inhibition of mitoxantrone uptake.

Effect	Estimate	Standard Error	p-value
Intercept	0.1137	0.01224	0.0114
Drug	0.06537	0.003076	<.0001
$Drug^2$	-0.00111	0.000178	<.0001
Inhibitor	-0.07302	0.007292	<.0001

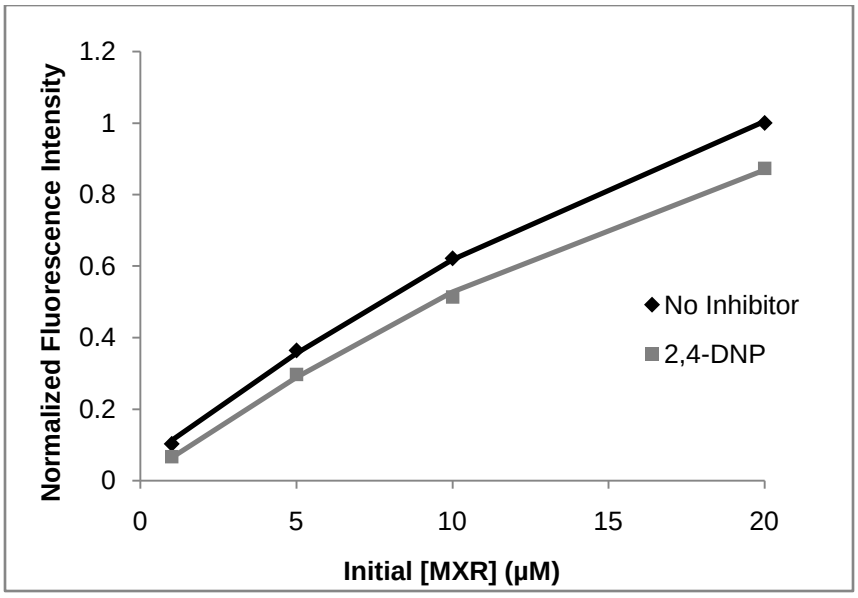

Figure 4.7. 2,4-DNP inhibition of mitoxantrone efflux in MCF10A cells. MCF10A cells were loaded with mitoxantrone (1-20μM) followed by an efflux period into PBS (black line) or 1mM 2,4-DNP (gray line). Data points are the geometric mean fluorescence intensity values (n=3) for each mitoxantrone and inhibitor concentration normalized by the fluorescence intensity of cells treated with 20 μM mitoxantrone. Errors bars are omitted for clarity. Curves were generated from the linear mixed effects model in SAS.

Table 4.4. Mixed effects model parameter estimates and p-values for 2,4-DNP inhibition of mitoxantrone efflux

Effect	Estimate	Standard Error	p-value
Intercept	0.04737	0.03555	0.3143
Drug	0.06628	0.004353	<.0001
Drug*Drug	-0.00092	0.000189	<.0001
Inhibitor	-0.04298	0.02352	0.0755
Drug*Inhibitor	-0.00465	0.002051	0.0292

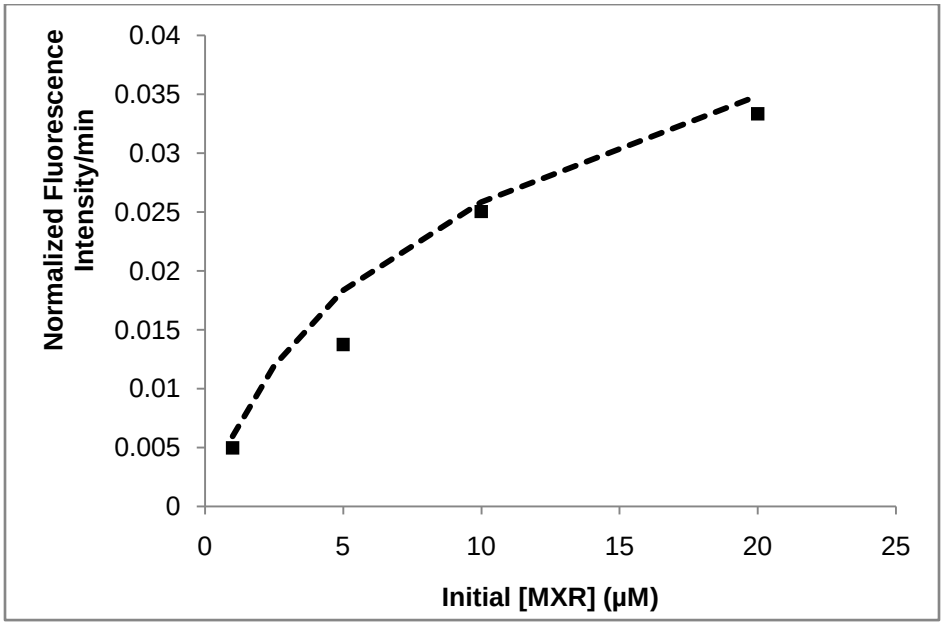

Figure 4.8. Mitoxantrone uptake was measured by flow cytometry at 37°C (n=3). Curve represents the Michaelis-Menten equation plus a passive diffusion term fit to the mean data values (Equations 1.3 and 1.4). Values were normalized to the fluorescence intensity of 20 μM uptake at 37°C.

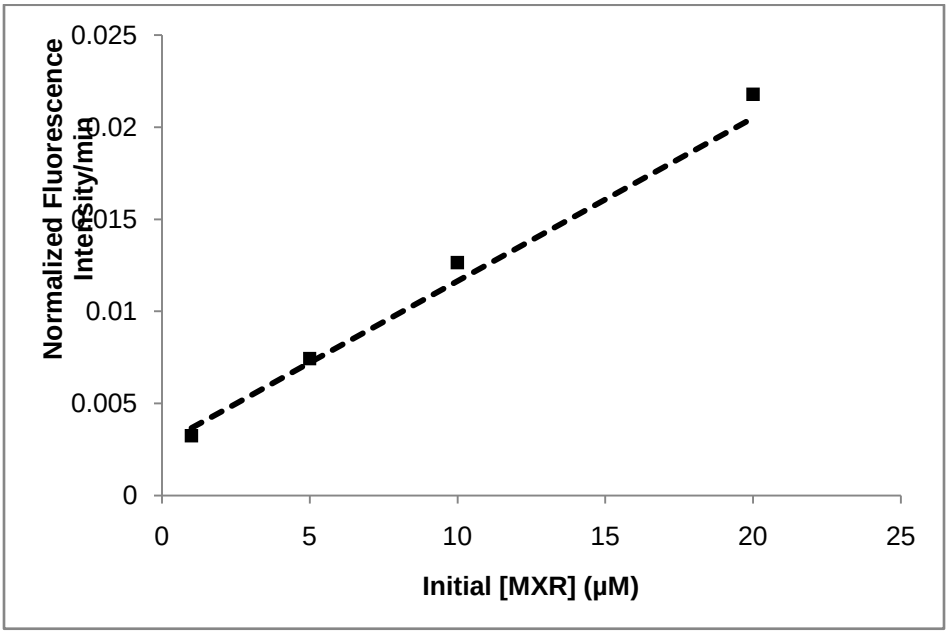

Figure 4.9. Linear uptake of mitoxantrone at 4 °C (n=3). Values were normalized to the fluorescence intensity of 20 μM uptake at 37°C.

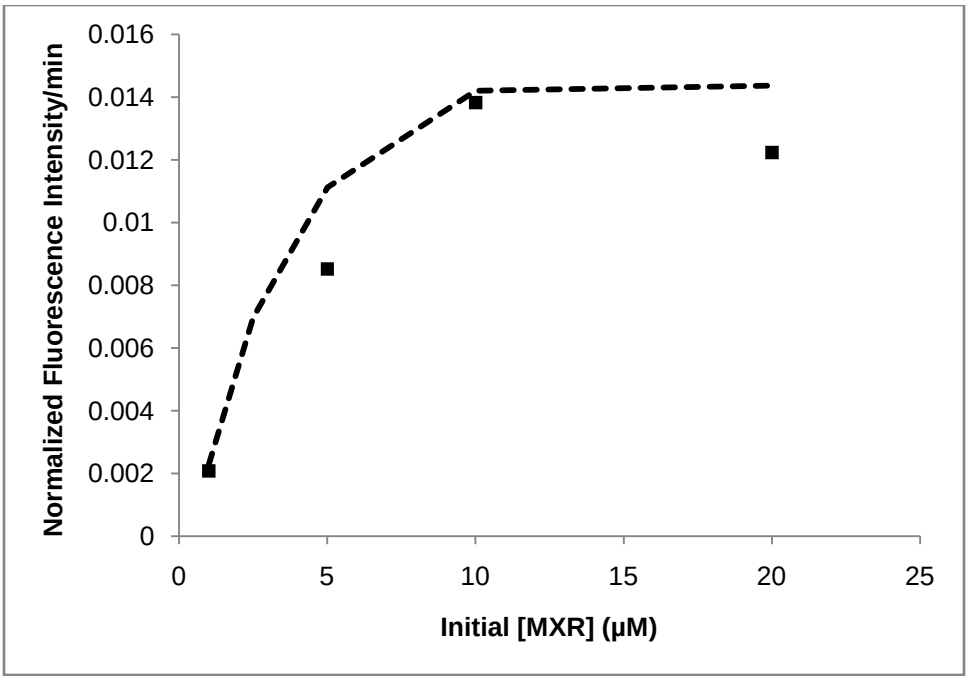

Figure 4.10. Michaelis-Menten kinetics of mitoxantrone uptake in MCF10A cells. Data points are the difference between 37°C and 4°C results. Data was fit using nonlinear regression to Michaelis-Menten equation (Equation 1.3).

Table 4.5. Michaelis-Menten SAS regression parameters. K_m* and V_{max} parameters were determined through non-linear regression analysis using SAS from flow cytometry data from the 37°C samples and P_{app} and intercept were determined from flow cytometry data from the 4°C samples (data shown in Appendix A).

Parameter	Estimate
K_m*	4.5151
V_{max}	0.89681
P_{app}	0.0266
Intercept	0.08307

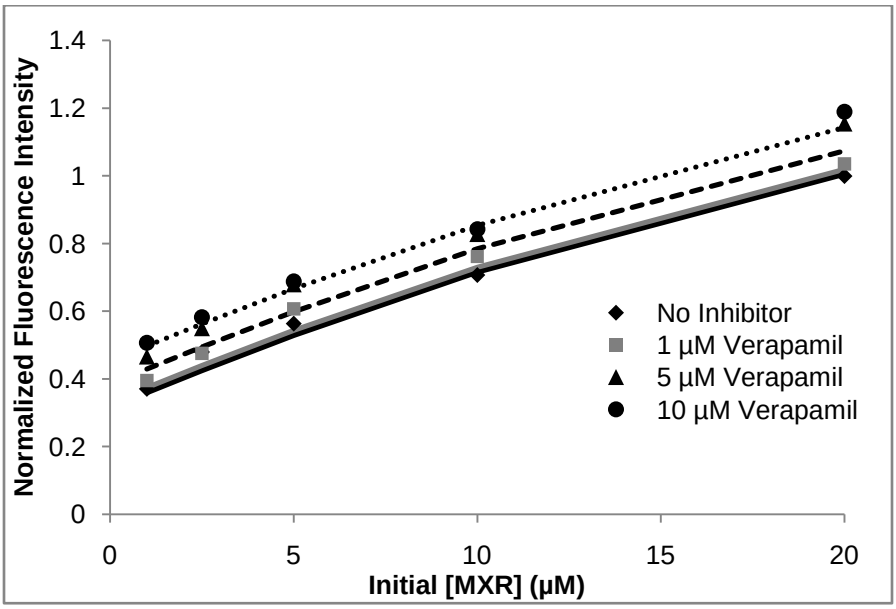

Figure 4.11. Verapamil inhibition of mitoxantrone uptake. MCF10A cells were exposed to mitoxantrone (1-20μM) (solid black line) or mitoxantrone with increasing concentrations of the MDR1 inhibitor verapamil; 1 μM (gray line), 5 μM (dashed line), and 10 μM (dotted line). Data points are the mean fluorescence intensity values (n=5) for each mitoxantrone and inhibitor concentration and normalized by the fluorescence intensity of cells treated with 20 μM mitoxantrone. Curves were generated from the linear mixed effects model in SAS. Errors bars are omitted for clarity. Verapamil showed a concentration dependent inhibition of intracellular mitoxantrone accumulation.

Table 4.6. Mixed effects model parameter estimates and p-values for verapamil inhibition of mitoxantrone uptake

Effect	Estimate	Standard Error	p-value
Intercept	0.3156	0.04312	0.0003
Drug	0.04588	0.00439	<.0001
$Drug^2$	-0.00056	0.00020	0.0054
Inhibitor	0.01383	0.00174	<.0001

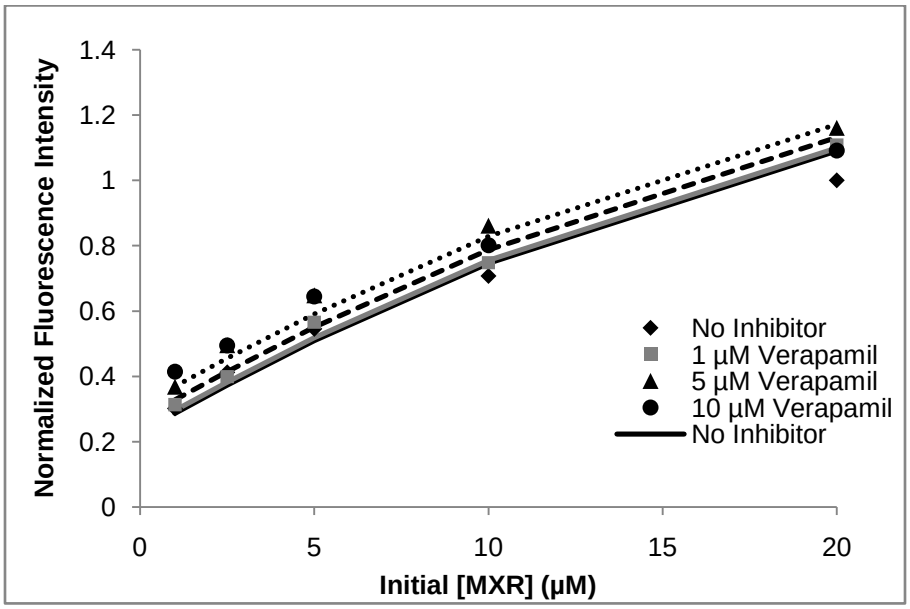

Figure 4.12. Verapamil inhibition of mitoxantrone efflux. MCF10A cells were loaded with mitoxantrone (1-20μM) followed by an efflux period in PBS (black line), 1μM verapamil (gray line), 5 μM verapamil (dashed line) or 10 μM verapamil (dotted line). Data points are the mean fluorescence intensity values (n=5) for each mitoxantrone and inhibitor concentration normalized by the fluorescence intensity of cells treated with 20 μM mitoxantrone. Curves were generated from the linear mixed effects model in SAS. Curves were generated from the linear mixed effects model in SAS. Errors bars are omitted for clarity. Verapamil showed a concentration dependent inhibition of mitoxantrone efflux.

Table 4.7. Mixed effects model parameter estimates and p-values for verapamil inhibition of mitoxantrone efflux

Effect	Estimate	Standard Error	p-value
Intercept	0.2277	0.06374	0.0375
Drug	0.06897	0.00422	<.0001
$Drug^2$	-0.00139	0.00022	<.0001
Inhibitor	0.003952	0.001264	0.0022

due to an increase in uptake due to verapamil inhibition. Effects on mitoxantrone uptake were greater than on efflux, which is expected since the driving intracellular concentrations for efflux was likely far smaller than the verapamil concentrations in the bathing solution which gave a slightly higher driving force for uptake.

FTC, an inhibitor of BCRP, was used to examine mitoxantrone transport in MCF10A cells. As shown in Figure 4.13, FTC decreased mitoxantrone intracellular accumulation with a negative drug*inhibitor effect of -0.00116 (Table 4.8). Negative parameter estimates for FTC effects indicates that FTC caused a decrease in mitoxantrone fluorescence accumulation. The inhibitor parameter estimate alone for the effect of FTC on uptake was not statistically significant; however, the drug*inhibitor term was significant. This indicates that FTC did effect mitoxantrone accumulation; however, its effect on transport is not as straightforward as the effect of verapamil. FTC did not have a significant effect on mitoxantrone efflux, although, in general, it did appear to decrease intracellular mitoxantrone accumulation (Figure 4.14 and Table 4.9). The observed results with the BCRP inhibitor FTC are opposite those of the MDR1 inhibitor verapamil. In addition, FTC linear mixed effects models required the addition of the drug*inhibitor interaction term.

Discussion

Flow cytometry was able to be used to quantitatively measure drug transport by accounting for the inter-day variability in the measurements using a linear mixed effects model. 2,4-Dinitrophenol, a general metabolic inhibitor, decreased mitoxantrone accumulation in MCF10A cells. This decrease in mitoxantrone intracellular accumulation with 2,4-DNP inhibition is likely due to inhibition of an active uptake

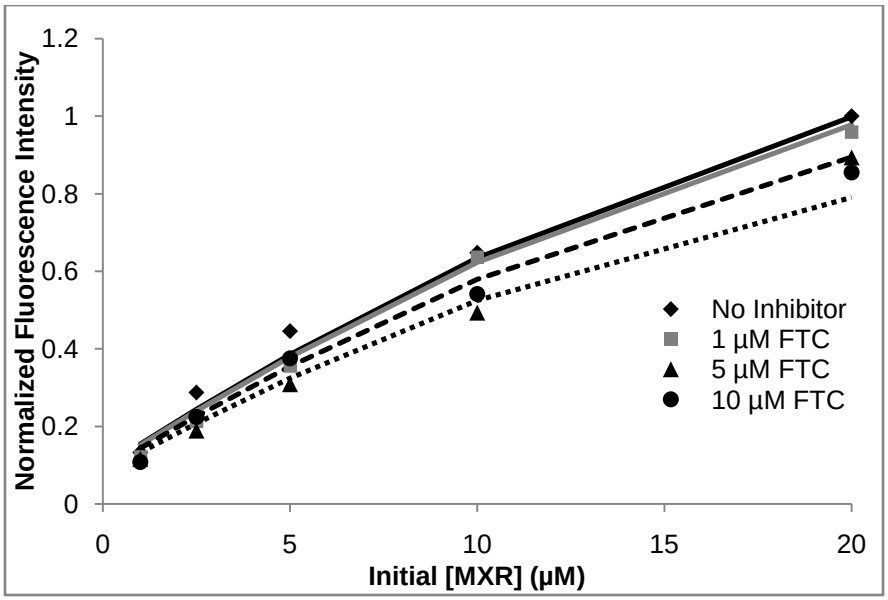

Figure 4.13. FTC inhibition of mitoxantrone uptake. MCF10A cells were exposed to mitoxantrone in the presence of the ABCG2 inhibitor FTC; no inhibitor (solid black line), 1 μM FTC (gray line), 5 μM FTC (dashed line), or 10 μM FTC (dotted line). Data points are the mean fluorescence intensity values (n=5) for each mitoxantrone and inhibitor concentration normalized by the fluorescence intensity of cells treated with 20 μM mitoxantrone. Curves were generated from the linear mixed effects model in SAS. Errors bars are omitted for clarity. FTC showed a concentration dependent decrease in intracellular mitoxantrone accumulation.

Table 4.8. Mixed effects model parameter estimates and p-values for FTC inhibition of mitoxantrone uptake.

Effect	Estimate	Standard Error	p-value
Intercept	0.09194	0.03235	0.0361
Drug	0.06312	0.00229	<.0001
$Drug^2$	-0.00089	0.00012	<.0001
Inhibitor	-0.00119	0.00071	0.0946
Drug*Inhibitor	-0.00098	0.00018	<.0001

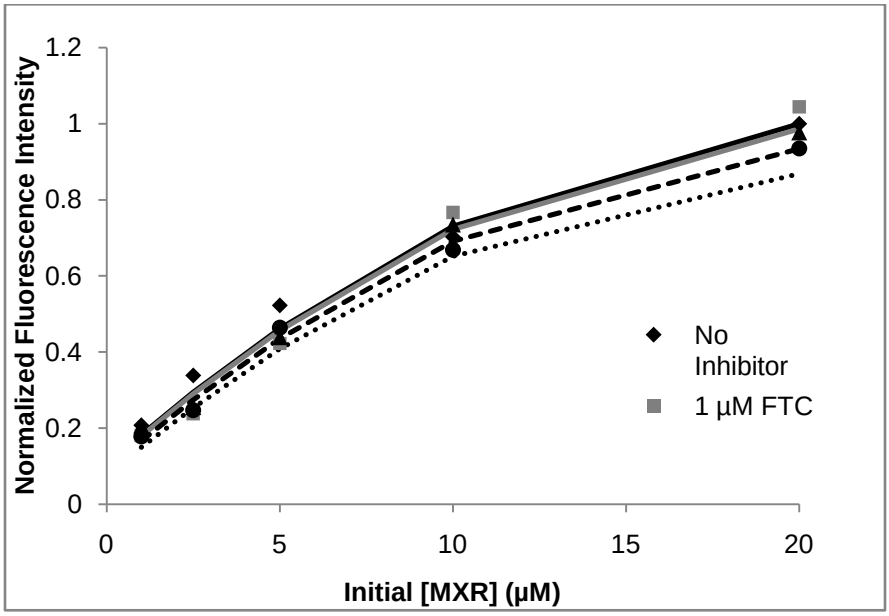

Figure 4.14. FTC inhibition of mitoxantrone efflux. MCF10A cells MCF10A cells were loaded with mitoxantrone (1-20μM) followed by an efflux period in PBS (black line), 1μM FTC (gray line), 5 μM FTC (dashed line) or 10 μM FTC (dotted line). Data points are the mean fluorescence intensity values (n=5) for each mitoxantrone and inhibitor concentration normalized by the fluorescence intensity of cells treated with 20 μM mitoxantrone. Curves were generated from the linear mixed effects model in SAS. Errors bars are omitted for clarity. FTC showed a concentration dependent decrease on mitoxantrone efflux.

Table 4.9. Mixed effects model parameter estimates and p-values for FTC inhibition of mitoxantrone efflux.

Effect	Estimate	Standard Error	p-value
Intercept	0.1039	0.05005	0.1736
Drug	0.08058	0.00543	<.0001
$Drug^2$	-0.00179	0.00027	<.0001
Inhibitor	-0.00272	0.00166	0.1043
Drug*Inhibitor	-0.00052	0.00037	0.1677

transporter for mitoxantrone. Active uptake of mitoxantrone was observed to be temperature dependent and the active component had a K_m* of ~4.5 μM. These results indicate a definite presence of active transport processes for mitoxantrone flux in MCF10A cells.

The MDR1 efflux transporter inhibitor, verapamil, increased mitoxantrone accumulation in MCF10A cells, as expected. The BCRP efflux transporter inhibitor, FTC, decreased mitoxantrone accumulation in MCF10A cells, however, which was counter to the expected result. Inhibition of BCRP was expected to increase the intracellular accumulation of mitoxantrone similar to MDR1 inhibition. These unexpected results may be due to FTC interaction with an uptake transporter, or they may be influenced by incomplete polarization of MCF10A cells. Other researchers have concluded that mitoxantrone is also a substrate for an unidentified uptake transporter.(42) This uptake transporter was demonstrated to be present on the apical plasma membrane, and it has a higher affinity for mitoxantrone than does BCRP. These studies also suggest that mitoxantrone concentrations higher than 20 μM could saturate the uptake transporter revealing efflux activity.(42) An active uptake transporter for mitoxantrone is consistent with the decrease in mitoxantrone uptake seen with 2,4-DNP inhibition. This is also supported by the necessity of including the drug*inhibitor interaction term for the effect of 2,4-DNP on efflux, and in the FTC uptake and efflux linear mixed effects models. One likely explanation for the need to include this term is the presence of multiple transporters with different K_m values for transport. Since the K_m value is reflective of the substrate affinity of the transporter, a change in affinity with increasing concentration could indicate activity of another (lower affinity) transporter. Since this shift occurs

around initial mitoxantrone concentrations of 20 μM, this is also consistent with the reported data on a, as of yet unidentified, uptake transporter determined by Pan et al.(42) This uptake transporter may be one of the organic cation transporters (OCT) or organic cation/zwitterions transporters (OCTNs) since mitoxantrone has a positive charge at physiologic pH.

The steady-state accumulation of mitoxantrone represents the net effect of both uptake and efflux transport. While there may be some active efflux of mitoxantrone in MCF10A cells, it is dominated by the effects of an active uptake transporter. The quantification of the efflux transport is made more difficult due to lower intracellular concentrations of mitoxantrone, due to incomplete loading of the cells, compared to the extracellular concentrations used in the uptake studies. This results in a lower substrate concentration for efflux transport compared to uptake transport. The intracellular concentration of mitoxantrone may also have been further reduced by intracellular binding since mitoxantrone is known to bind to DNA.(79,82) These effects result in only small changes in fluorescence intensity due to efflux compared to the total mitoxantrone fluorescence.

Since there may be little or no expression of BCRP and MDR1 transporters in MCF10A cells, the small amount of efflux observed may be due to another transporter such as MRP1 which has some substrate overlap with MDR1 and BCRP. Although mitoxantrone is not a known substrate for this transporter and verapamil and FTC are reported to be specific transport inhibitors, there may be a small amount of overlap with MRP1 substrate specificity. These results indicate that multidrug resistance transport in

MCF10A cells is a complicated process potentially involving numerous uptake and efflux transporters.

Reports on the quantitative analysis of flow cytometry data on drug uptake by active transporters are scarce, and no data analysis methods using linear mixed effects modeling to quantify flow cytometry data were found in the literature. This novel method of analyzing flow cytometry transport data allowed significant determination of efflux transport even though the transporters studied may be only lowly expressed in the cell line used, and efflux effects were likely masked by uptake transport. This data analysis method can also be applied to other actively transported molecules and transport inhibitors since it is not specific to any transporter or substrate molecule.

CHAPTER 5

ANALYSIS OF PEPTIDE TRANSPORT IN MCF10A CELLS BY FLOW CYTOMETRY

Introduction

Of the mammalian peptide transporters, two of the most important are the peptide/H+ symporters, PEPT1 and PEPT2. Both transporters have been identified in humans, rodents and rabbits,(37) and are expressed in epithelial, endothelial and nervous tissue throughout the body.(83) PEPT1 and PEPT2 differ in their capacity and affinity for substrates, but the identity of the substrates is the same. PEPT1 is a high capacity transporter with a relatively low substrate affinity (K_m values ranging from 0.2 to 10 mM, typically ~ 1 mM). This low substrate affinity and high transport capacity makes PEPT1 well suited for transport of its peptide substrates in the intestinal epithelium, where it is primarily expressed. PEPT2 has a lower capacity, yet a higher affinity (K_m values ranging from 5 to 500 µM, typically ~50 µM).(84) The high substrate affinity allows PEPT2 to be an effective peptide transporter at lower substrate concentrations such as those found in the nephron of the kidney and other epithelial tissues such as the lung, mammary gland, enteric nervous system and central nervous system.(84,85) PEPT2 has been detected in the human mammary gland and was localized to the ducts and alveoli which are the primary areas of milk secretion.(86)

Both peptide transporters are located in the apical plasma membrane of epithelial cells.(87) Peptide uptake into the cell occurs against a concentration gradient through coupling of substrate transport to proton transport down its electrochemical concentration gradient. Providing the energy for uphill transport through coupling to transport of another molecule is known as secondary active transport. These processes still require

ATP utilization to create the electrochemical gradient which serves as the driving force for transport.(88) In the case of PEPT1 and PEPT2, protons and peptides are both transported in the same direction, thus peptide accumulation in the cell and increased intracellular acidity occur concomitantly. As a result of this symporter behavior, substrate uptake depends on extracellular pH and membrane potential. The optimal pH for PEPT1/PEPT2 transport is between 4.5 and 6.5, and varies slightly with the charge of the substrate molecule.(84,89) Dipeptide transport reduces intracellular pH to a greater extent than do peptidomimetics; therefore, dipeptides have a higher rate of transport. Increased transport is likely due to the stereoselectivity of the transporters for D- and L-enantiomers (peptidomimetics often have the D-conformation such as cefadroxil).(90)

PEPT1 and PEPT2 transport all di- and tripeptides independent of their sequence and charge, as well as a variety of peptidomimetic drugs and other compounds such as β-lactam antibiotics and angiotensin-converting enzyme (ACE) inhibitors. Peptide substrates include 400 different dipeptides and 8000 possible tripeptides, as well as those containing D-enantiomers.(84) Transport efficiency is stereoselective, however, and peptides containing all L-enantiomers have a higher affinity for binding and transport than those containing D-enantiomers. Peptides with D-amino acids at the N-terminus still have high affinities, but those containing all D-enantiomers are not substrates.(91) Inclusion of D- or β-amino acids at the amino terminus of the peptide makes the molecule relatively stable to enzymatic degradation while retaining high affinity for the peptide transporters.(1,6,7,9,37,89)

Conjugation of a fluorescent molecule to a dipeptide can allow for detection of the molecule, however, the usefulness for transport studies is dependent upon the

molecule retaining its affinity for the transporters. The resulting labeled peptides are therefore useful for studying transport compared with di- and tripeptides, which are rapidly hydrolyzed by proteases into the free amino acids and cannot be readily detected within the cells.

The peptide transporters are able to transport molecules with a variety of charges, molecular weights, physiochemical characteristics and polarities. Structural features for transport affinity by these transporters include an N-terminus, preferably with a free NH_3^+ group, a planar, four carbon backbone containing a carbonyl group, and the L-enantiomer stereochemistry of the C-terminal amino acid group.

Peptide Transporter Expression in the Mammary Epithelium

Breast milk contains very few di- and tripeptides, however, it does contain numerous free amino acids. The milk contains a number of proteases which degrade proteins and peptides into small peptide fragments. These di- and tripeptides formed in the milk through proteolysis are efficiently removed from the milk most likely by PEPT2. Once within the epithelial cells, the peptides are degraded into their constituent amino acids which may then be secreted into the milk or utilized by the cells.(13) Milk pH is lower than that of plasma (7.0 versus 7.4),(5,13) therefore, a proton driving force for transport exists, aiding in peptide removal, which also helps to explain the absence of small peptides from breast milk.(86) PEPT2 is also likely quite efficient at removing other substrates from the milk such as peptidomimetic drug compounds, thereby lowering their milk concentrations.

The majority of PEPT1 and PEPT2 substrates are di- or tripeptides or peptidomimetic compounds which are not easily detected by spectrophotometric

methods. However, due to the structure-affinity characteristics of the transporters, fluorescently labeled dipeptides can retain peptide transporter affinity and can be readily detected.

Fluorescently labeled (D- or β-) Ala-Lys with 7-amino-4-methylcoumarin-3-acetic acid (D-/β-A-K-AMCA) can be detected intracellularly by epifluorescence microscopy or confocal microscopy.(37,89,90,92-95) PEPT1 and PEPT2 uptake of D-A-K-AMCA (K_m = 25 μM for PEPT2) resulted in bright blue cell fluorescence following excitation at 355 nm. Its uptake is competitively inhibited by dipeptides such as glycyl-glutamine (Gly-Gln) and peptidomimetic compounds such as cefadroxil.(89,90,92-96) D-A-K-AMCA uptake was demonstrated to reduce intracellular pH, independent from any effect of the compound itself, which is further evidence that its uptake is due to the peptide transporters. Microscopy studies with D-A-K-AMCA do not show uptake into tissues that do not express PEPT1 or PEPT2.(92,93,95) This suggests that passive uptake of D-A-K-AMCA does not occur and the fluorescent AMCA molecule was only transported across the cell membranes as part of the dipeptide conjugate.

Cefadroxil is an aminocephalosporin antibiotic which is a known substrate for PEPT1 and PEPT2. Cefadroxil has a high affinity for PEPT2 with a K_m of 3 μM.(85,96) The aminocephalosporins have also been shown to competitively inhibit dipeptide uptake by PEPT2 up to 88%.(97) Cephalosporins and ACE-inhibitors have been detected in the breast milk, but their concentrations in the milk are relatively low likely due to efficient reabsorption by PEPT2.(86) Since cefadroxil is a known peptidomimetic substrate and a competitive inhibitor of dipeptide transport by PEPT2, it, along with the dipeptide, Gly-Gln, were chosen as transport inhibitors of the peptide transporter model compound, A-

K-AMCA, to study PEPT2-mediated uptake in MCF10A cells using the flow cytometry technique described in the previous chapter.

Materials and Methods

Cell Culture

MCF10A cells were grown in 12 well plates for flow cytometry studies as described in chapter 4.

β-Ala-Lys-Amino Methyl Coumarin Synthesis

Synthesis of the fluorescently labeled dipeptide was performed with the assistance of Dr. Robert Kerns and Jon Rosen (University of Iowa) based on previously described methods with some modifications.(93,98)

Synthesis of Boc-β-Ala-L-Lys(Fmoc)-OH

H-Lys(Fmoc)-OH (1 mole equivalent, Bachem, Torrance, CA, Lot #1000598, Fmoc is the fluorenylmethyloxycarbonyl protecting group) and Boc-β-Ala-NHS (1.1 mole equivalents, Bachem, Lot #0564204, Boc is the tert-butyloxycarbonyl protecting group and NHS is an N-hydroxysuccinimide amine reactive group) were mixed in acetonitrile/aqueous sodium bicarbonate (50 mg/ml, pH 8.5) and stirred under argon for 1.5 hours. The reaction was monitored by HPLC (Schimadzu LC-10AT VP) using a Luna C18 column 5 µm particle size (Phenomenex), 5% to 95% linear concentration ramp over 35 minutes of acetonitrile/water + 0.1% trifluoroacetic acid (TFA) mobile phase, with a λ_{max} = 264 nm. H-Lys(Fmoc)-OH has a retention time of 14.9 minutes and Boc-β-Ala-Lys(Fmoc)-OH has a retention time of 20.5 minutes (Figure 5.1). The acetonitrile was removed using a rotavap leaving a milky, white liquid (pH 8-9). Dichloromethane was added to dissolve the Boc-β-Ala-Lys(Fmoc)-OH, and HCl was added to acidify the aqueous phase in order to protonate the carboxyl group on the

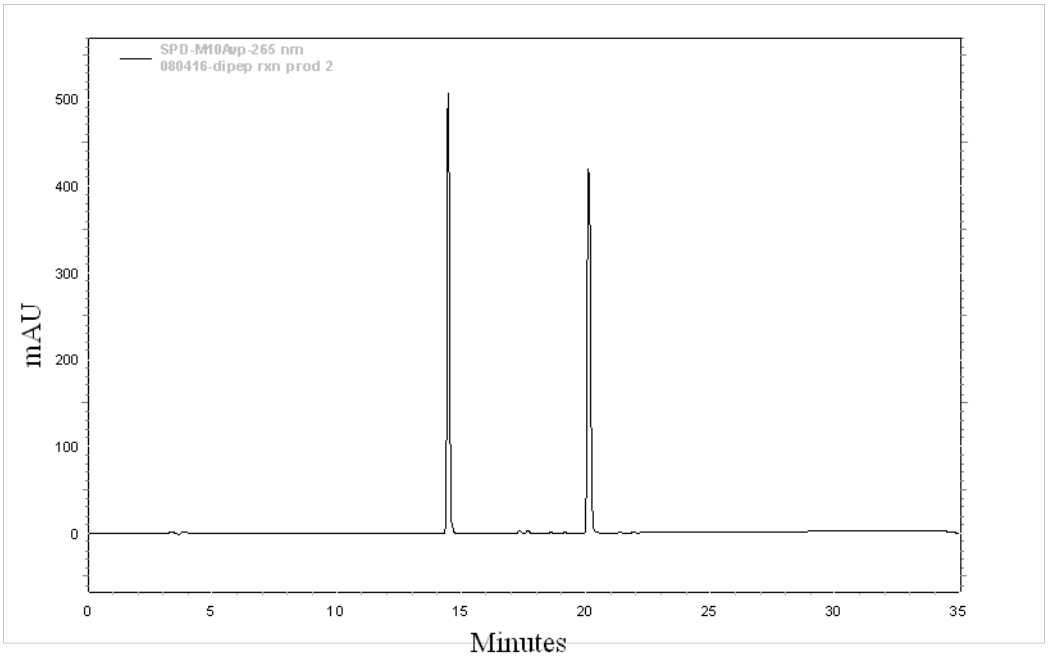

Figure 5.1. HPLC chromatogram of H-Lys(Fmoc)-OH reaction with Boc-β-Ala-NHS. Fmoc fluorescence (excitation: 264 nm, emission: 313 nm) was used for detection. H-Lys(Fmoc)-OH eluted at 14.9 minutes and the product Boc-β-Ala-Lys(Fmoc)-OH eluted at 20.5 minutes. The Boc-β-Ala-NHS starting material was not detectable.

dipeptide and drive it into the organic dichloromethane. Saturated sodium chloride solution was added to break up the emulsion formed between the aqueous and organic phases during the separation. The organic phase was removed and retained. The remaining aqueous phase was washed with dichloromethane. The organic phases were combined and were washed with water and transferred to a rotavap. The dichloromethane was removed by evaporation leaving a white solid. The product was placed under vacuum overnight at room temperature to dry. The reaction yield was ~87%.

Fmoc Deprotection

Removal of the Fmoc protecting group on the N_{ε} amino group of the lysine residue was performed by addition of neat piperidine to the Boc-β-Ala-Lys(Fmoc)-OH product. The reaction continued for 30 minutes and was monitored for completion by HPLC as described above. Ice cold water was added to the completed reaction and the solid product formed was filtered and placed in a rotavap. Water was removed and the product was placed under vacuum to dry.

AMCA Conjugation

Boc-β-Ala-Lys-OH from the previous step was dissolved in 0.05M sodium borate buffer (1.914 g/100 ml H_2O, pH 9.25). The NHS-AMCA (succinimidyl-7-amino-4-methylcoumarin-3-acetate, Prochem, Rockford, IL) was dissolved (10 mg/ml) in dimethylformamide (DMF, Acros). The reaction was run overnight with stirring and analyzed by HPLC as described above. The retention time for NHS-AMCA was 14 minutes and the retention time for Boc-β-Ala-Lys-AMCA was 13.5 minutes (Figure 5.2).

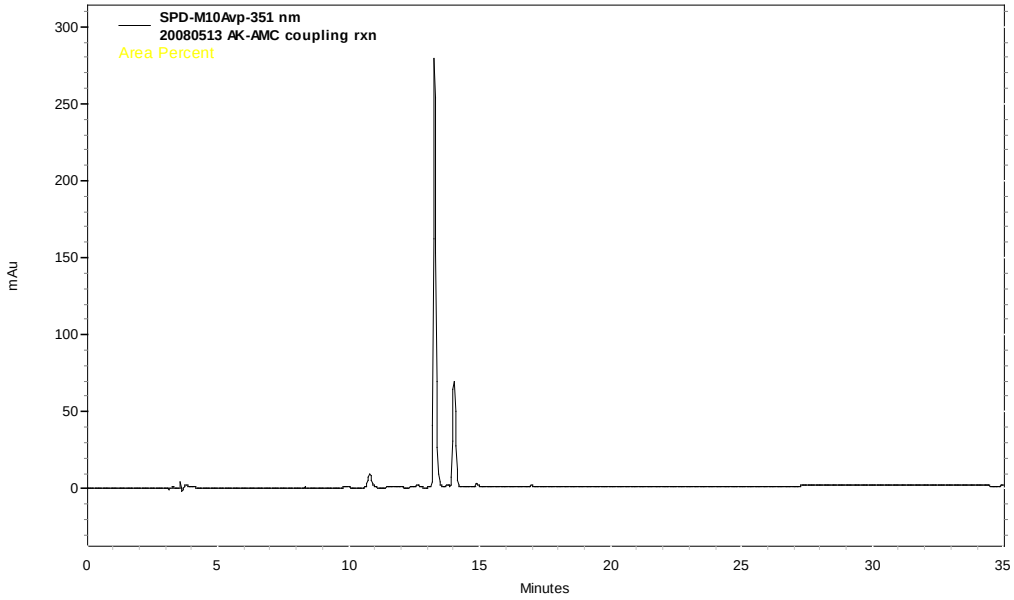

Figure 5.2. HPLC chromatogram of Boc-β-Ala-Lys-OH and AMCA-NHS conjugation reaction. AMCA fluorescence (excitation: 345-350 nm, emission: 440-460 nm) was used for detection. AMCA-NHS eluted around 14 minutes and the reaction product Boc-β-Ala-Lys-AMCA eluted at 13.5 minutes.

Boc Deprotection

Concentrated HCl (12.1 N, ~10 drops) was added to remove the Boc protecting group from the alanine residue. The reaction was run overnight with stirring and analyzed by HPLC as described above. The retention time for Boc-β-Ala-Lys-AMCA was 13.5 minutes and the retention time for β-Ala-Lys-AMCA (A-K-AMCA) was 9 minutes.

Prep HPLC

β-Ala-Lys-AMCA was purified by prep HPLC (Schimadzu LC-10AT VP, diode array detector, Luna C18 10 µm 250 x 21.2 mm column). Mobile phase was acetonitrile/water + 0.1% TFA with a 5% to 95% linear gradient run over 1 hour with a ramp up over 40 minutes, hold for 10 minutes and then returned to the initial conditions. The flow rate was 7 ml/min, and the injection volume was 2.5 ml. The peak corresponding to the product (retention time 19.5 minutes) was collected in glass vials, frozen, and lyophilized overnight (-55 °C condenser temperature and vacuum pressure of 25 mTorr, Lyo-Centre, VirTis, (Figure 5.3). Confirmation of the desired product was performed by electrospray ionionization-mass spectrometry (ESI-MS) (Figure 5.4, University of Iowa, Department of Chemistry, Mass Spectrometry Facility). A schematic diagram of the complete synthesis is shown in Figure 5.5.

Uptake Studies

MCF10A cells grown for 1 to 2 weeks in 12-well plates as described in chapter 4 were washed in phosphate buffered saline (PBS, pH 7.4) with ~1 ml/well followed by incubation in 0.5 ml phenol red-free trypsin with EDTA (Gibco) at 37°C until they detached from the plate. Trypsin was neutralized with an equal volume of 20% fetal bovine serum (FBS, Gibco) solution in PBS. Cells were transferred to 5 ml polystyrene

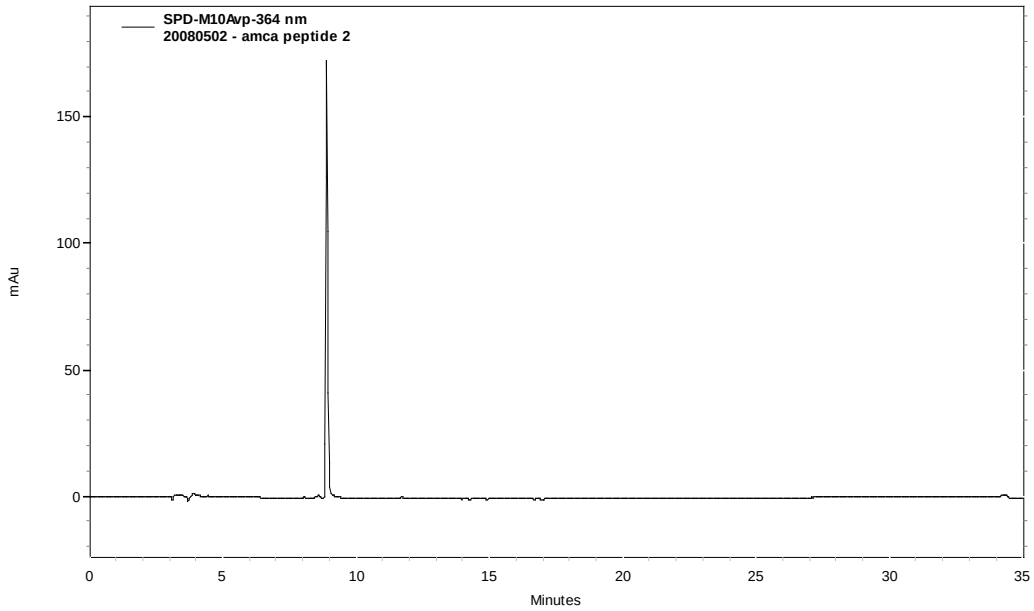

Figure 5.3. HPLC chromatogram of final reaction product of β-Ala-Lys-AMCA synthesis following Boc group removal and purification. AMCA fluorescence was used for detection (excitation: 345-350 nm, emission: 440-460 nm).

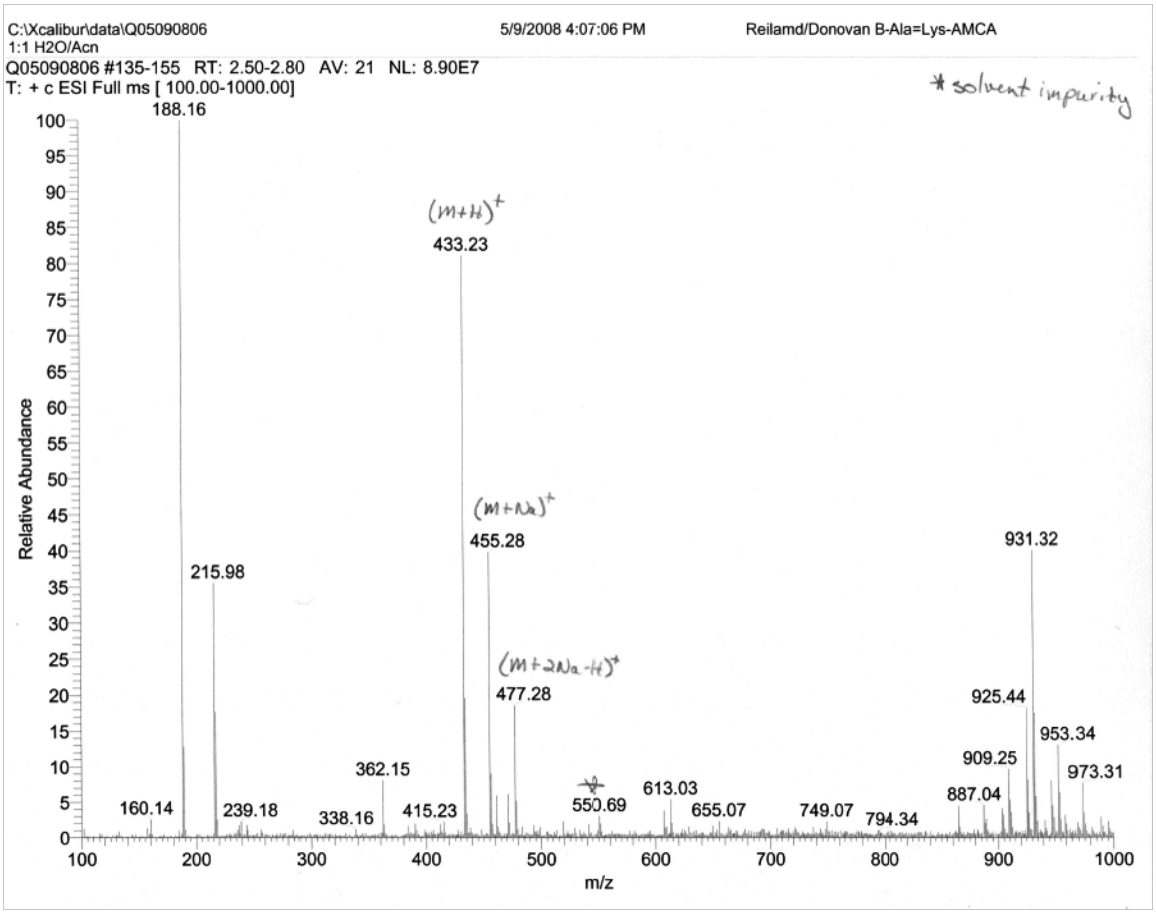

Figure 5.4. ESI-Mass Spectroscopy Analysis of β-Ala-Lys-AMCA Synthesis Product. A-K-AMCA has a molecular weight of 432.47 with an expected m/z of 432.2. The peak at 433.23 m/z corresponds to the $(m+H)^+$ peak of the product.

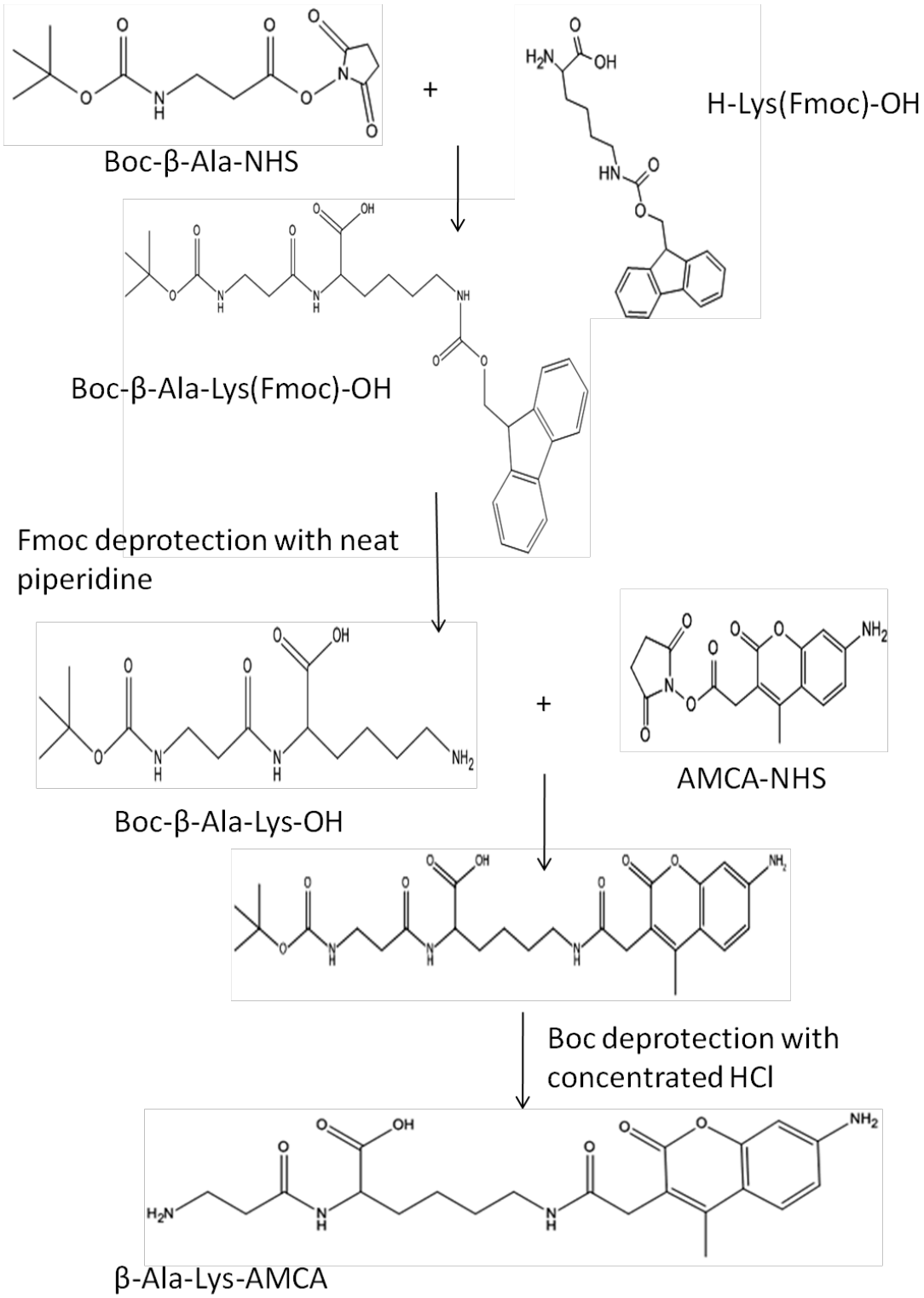

Figure 5.5. β-Ala-Lys-AMCA synthetic scheme

test tubes and pelleted by centrifugation at 300 x g for 5 minutes (Eppendorf 5810 R centrifuge). MCF10A cell pellets were washed with ~1 ml pre-warmed D-PBS (Dulbecco's PBS with 1000 mg/l D-glucose and 36 mg/l sodium pyruvate, Gibco) and resuspended and incubated in 1 ml D-PBS (pH 8.0) for 30 minutes at 37°C. D-PBS was replaced with 1 ml pre-warmed A-K-AMCA solutions of varying concentrations (0.1-1 mM) in D-PBS (pH 6.0) or D-PBS alone (untreated cells), and cells were incubated at 37°C for 30 minutes (incubation times were chosen based on other drug accumulation studies using flow cytometry).(72,74) The cells were incubated at pH 8.0 and uptake studies were performed at pH 6.0 to establish a proton gradient driving force for substrate uptake since the pH optimum for PEPT2 transport is between 4.5 and 6.5, depending on the substrate charge.(84,89,90,97,99) One sample of cells was treated with only PBS (untreated cells).

Efflux Studies

Efflux studies were performed by loading the MCF10A cells with varying concentrations of A-K-AMCA (0.1-1 mM) as described in the uptake studies. After incubation, each sample was rinsed briefly with D-PBS and 2 ml of fresh D-PBS (pH 6.0) was added and cells were incubated at 37°C for 30 minutes.

Inhibitor Studies

MCF10A cell pellets were washed with ~1 ml PBS (pH 8.0) and resuspended and incubated in 1 ml 1 mM 2,4-dinitrophenol (2,4-DNP), 1-10 mM glycyl-glutamine (Gly-Gln) or 0.5-5 mM cefadroxil for 30 minutes at 37°C. Inhibitor solutions were replaced with 1 ml of A-K-AMCA solutions (0.1-1 mM) containing inhibitor and incubated at 37°C for 30 minutes. A-K-AMCA solutions were removed and each well was rinsed

briefly with PBS (pH 6.0). For inhibitor efflux studies, cells were then incubated for an additional 30 minutes in inhibitor solution.

Flow Cytometry Analysis

Intracellular A-K-AMCA concentration was analyzed using a BD LSRII flow cytometer equipped with a UV (355 nm) laser excitation source and a 440/40 bandpass emission filter. Forward and side-scattered light were used to select the cells and the background fluorescence was set as described in chapter 4. Side scattered light (SSC) vs. forward angle light scatter area (FSC-A) and forward scattered width (FSC-W) vs. FSC-A dot plots were used to select the population of cells to be analyzed as shown in Figure 5.6. Background fluorescence intensity was determined from untreated cells and A-K-AMCA fluorescence data was collected for ~30,000 cells (Figure 5.7).

Data Analysis

Statistical analysis of each data set was performed with a mixed effects model using SAS utilizing the procedure outlined in chapter 4. A linear mixed effects model was fit to geometric mean fluorescence intensity values. The model included two terms for the effect of increasing A-K-AMCA concentrations (drug and drug^2 where the drug^2 term accounted for saturation at high A-K-AMCA concentrations) and a term for the effect of the inhibitor.

PEPT1 and PEPT2 Immunoblot

PEPT1 and PEPT2 immunoblots were performed as described in chapter 3. The transporters were detected with goat polyclonal anti-PEPT1 antibody (1:2000 dilution, Santa Cruz Biotechnology) or goat polyclonal anti-PEPT2 (1:2000 dilution, Santa Cruz

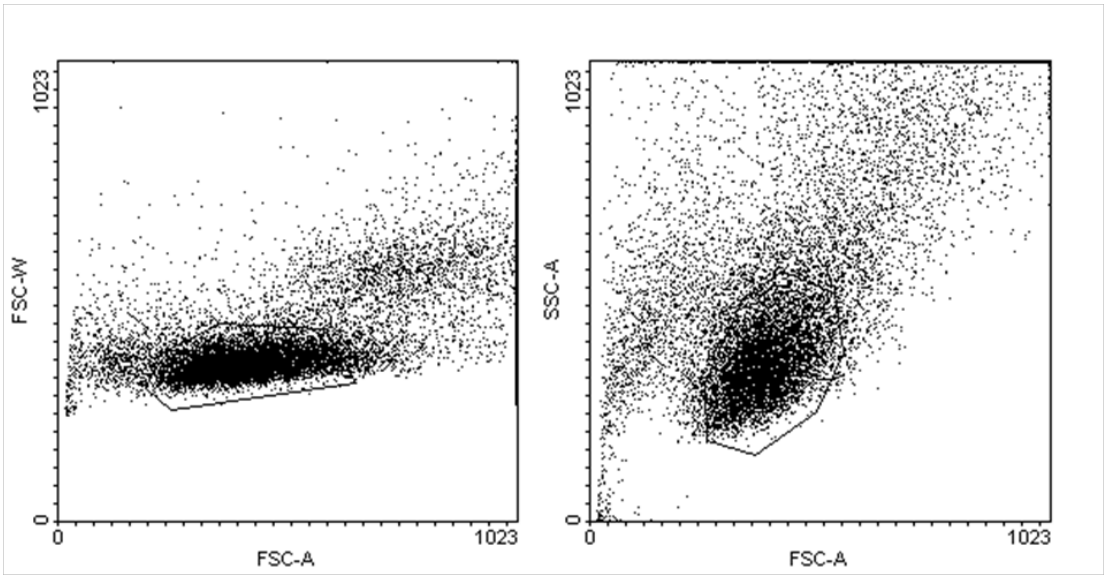

Figure 5.6. Gating of FSC and SSC of MCF10A cells following A-K-AMCA uptake. Side scattered area vs. forward scattered area and forward scattered width vs. forward scattered area dot plots. Gates are placed around the main population of cells on each dot plot to select the single cells to be used for fluorescence measurements.

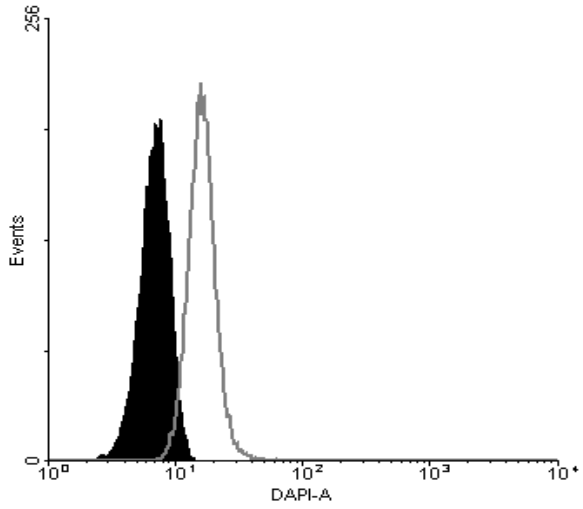

Figure 5.7. A-K-AMCA fluorescence histogram of number of cells vs. log A-K-AMCA fluorescence intensity (axis labeled DAPI-A for instrument settings used for measurements). Untreated cells are shown in black and A-K-AMCA treated cells (1 mM) are shown in gray.

Biotechnology) and donkey anti-goat IgG-Peroxidase (HRP) secondary antibody (1:200 dilution, Santa Cruz Biotechnology).

Results

The first step in analyzing PEPT2 transport in MCF10A cells was to verify that the transporter was expressed in these cells. PEPT2 expression was determined by western blotting which showed a band at ~85 kDa which corresponds to the reported molecular weight of PEPT2 (Figure 5.8).(83,89) PEPT1 (also has a molecular weight of ~85 kDa, similar to PEPT2) (83,94) was also detected in MCF10A cells, although much lower levels were observed as indicated by a visibly fainter band (Figure 5.8). Lower expression of PEPT1 relative to PEPT2 was expected because PEPT2 is the high capacity peptide transporter capable of operating at lower substrate concentrations, such as those found in the breast milk, and PEPT1 mRNA has been shown to have lower expression in the lactating mammary gland compared to PEPT2.(46)

MCF10A cells had a background fluorescence intensity of 4 - 6 when measured using flow cytometry (UV laser, excitation 355 nm, emission 440/20 bp filter). Uptake of A-K-AMCA increased the fluorescence intensity. Inhibitors were used to determine if A-K-AMCA uptake was due to active uptake by PEPT2. Inhibitors included the general metabolic inhibitor 2,4-DNP, and the peptide transporter specific inhibitors Gly-Gln and cefadroxil. Gly-Gln and cefadroxil are inhibitors of both PEPT1 and PEPT2, however, PEPT1 expression in MCF10A cells is significantly lower than that of PEPT2; therefore, PEPT1 was not expected to have an observable effect on transport, especially in the range of substrate concentrations chosen for these investigations.

The inhibitors, 2,4-DNP and Gly-Gln, shifted the fluorescence intensity peak to the left, indicating a decrease in A-K-AMCA uptake as expected (Figures 5.9 and 5.10).

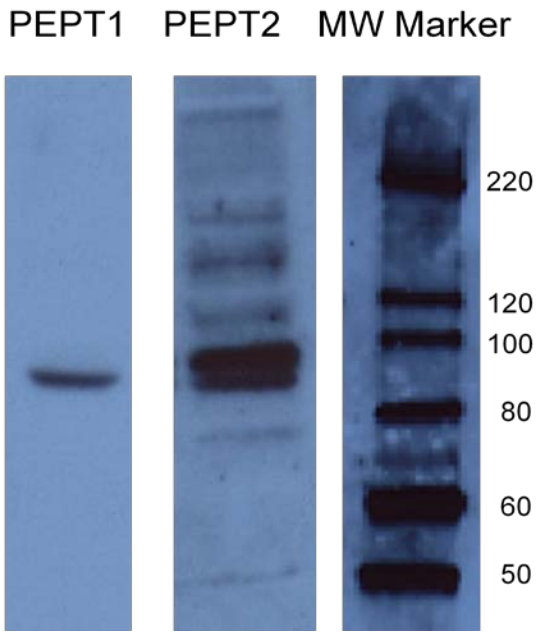

Figure 5.8. Western blot of PEPT1 and PEPT2 in MCF10A cells. PEPT1 and PEPT2 have a molecular weight of 85 kDa.(83,94,100) Detection was performed with goat polyclonal anti-PEPT1 and PEPT2 primary antibodies and a donkey anti-goat IgG-Peroxidase labeled secondary antibody.

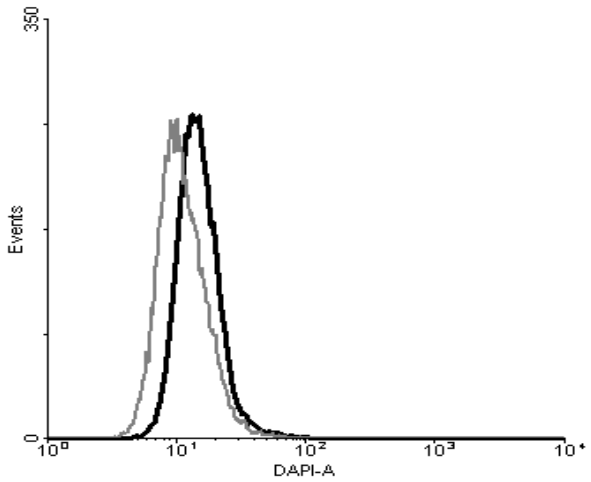

Figure 5.9. Histograms for A-K-AMCA fluorescence (labeled as DAPI-A due to instrument settings) for MCF10A cells treated with 1 mM A-K-AMCA (black line) and 1 mM A-K-AMCA and 1 mM 2,4-DNP (gray line). Addition of 2,4-DNP shifted the A-K-AMCA peak to the left indicating decreased accumulation.

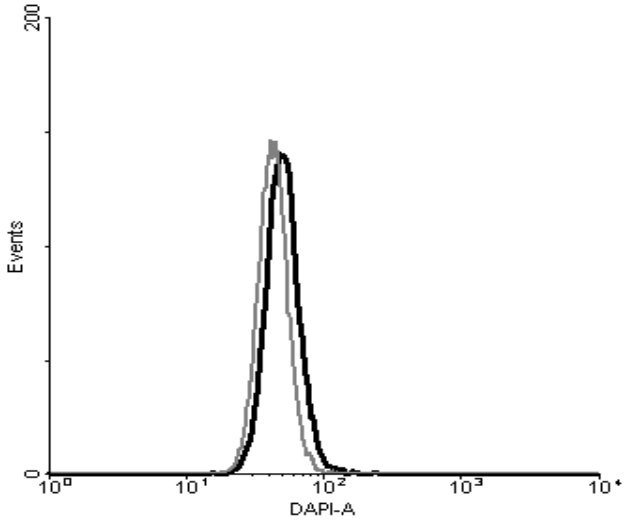

Figure 5.10. Histograms for A-K-AMCA fluorescence (labeled as DAPI-A due to instrument settings) for MCF10A cells treated with 0.5 mM A-K-AMCA (black line) and 0.5 mM A-K-AMCA and 10 mM Gly-Gln (gray line). Addition of Gly-Gln shifted the A-K-AMCA peak to the left indicating decreased accumulation.

However, cefadroxil shifted the fluorescence intensity to the right (Figure 5.11) indicating increased intracellular fluorescence. This was not expected since cefadroxil is a known inhibitor of PEPT2 and it shows no fluorescence in solution. However, the degradation products of cefadroxil are fluorescent,(101) therefore, even though the cefadroxil solutions were freshly prepared prior to each experiment, some enzymatic degradation of cefadroxil may have occurred within the cells, resulting in a slight increase in fluorescence detectable by flow cytometry. Due to the very high sensitivity of flow cytometry compared to spectrophotometers, even though cefadroxil fluorescence is not readily detectable in solution, it may have a slight fluorescence detectable by flow cytometry.(74)

The statistical analysis of the inhibitor studies required the inclusion of a drug-inhibitor interaction term (drug*inhibitor) to account for the increased spread in the fluorescence values at higher intracellular substrate concentrations. A significant drug-inhibitor interaction term was still considered as a significant inhibitor effect on A-K-AMCA transport. Inclusion of model terms was determined by selecting the model with the minimum AIC fit values (as determined by SAS) from numerous models tested on each data set.(53,54) The mixed effects model results for the random effects and model fitting AIC values for each inhibitor study on A-K-AMCA uptake are shown in Table 5.1. The data and model-generated curves are shown in Tables 5.2-5.4 and Figures 5.12-5.16.

A-K-AMCA uptake in the presence of inhibitors was used to determine if the active uptake transporter, PEPT2, was functioning in MCF10A cells. The metabolic inhibitor, 2,4-dinitrophenol (2,4-DNP), was used to determine if there was any type of active transport of A-K-AMCA present in the cells. Since 2,4-DNP inhibits ATP

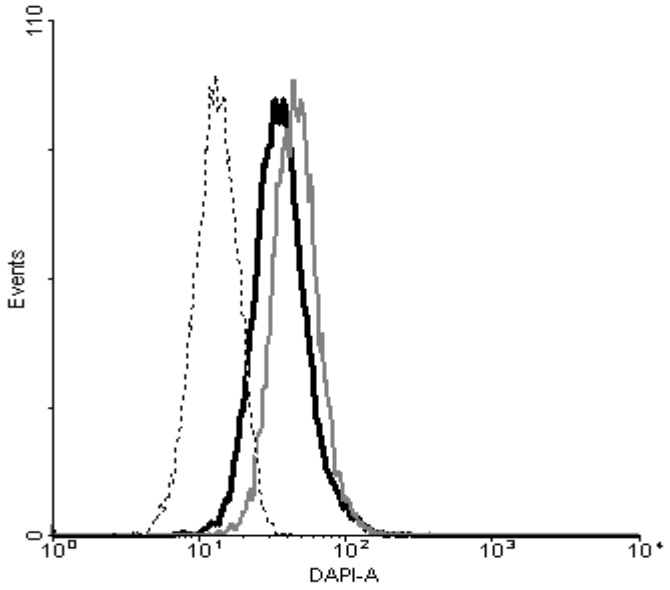

Figure 5.11. Histograms for A-K-AMCA fluorescence (labeled as DAPI-A due to instrument settings) for MCF10A cells treated with 0.4 mM A-K-AMCA (black line), 0.4 mM A-K-AMCA and 5 mM cefadroxil (gray line) and 5 mM cefadroxil (dashed line). The observed slight fluorescence of cefadroxil may mask any inhibition effects of cefadroxil on A-K-AMCA uptake.

Table 5.1. Mixed effects model variability parameter estimates and AIC fit statistics

Variability Parameter	2,4-DNP	Gly-Gln	Cefadroxil
Inter-day	0.000436	NA	NA
Rep (Day)	0.000043	1.53E-06	2.79E-06
Residual	0.07158	0.03613	0.02829
AIC	-158.8	-506.1	-336.6

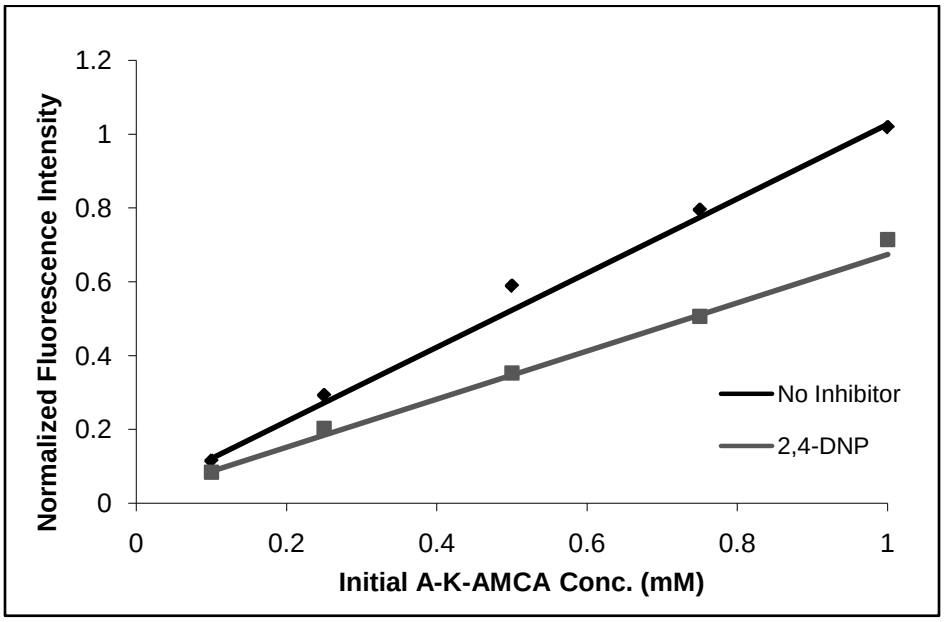

Figure 5.12. 2,4-DNP inhibition of A-K-AMCA uptake in MCF10A cells. MCF10A cells were treated with 0.1 to 1 mM A-K-AMCA (♦) and A-K-AMCA with 1 mM 2,4-DNP (■). Data points represent the geometric mean fluorescence intensity values (n=3) for each A-K-AMCA and inhibitor concentration normalized by the fluorescence intensity values of cells treated with 1 mM A-K-AMCA. Curves were generated from the linear mixed effects model in SAS. Error bars were omitted for clarity.

Table 5.2. Mixed effects model parameter estimates and p-values for 2,4-DNP inhibition of A-K-AMCA uptake.

Effect	Estimate	Standard Error	Probability
Intercept	0.02068	0.01374	0.2294
Drug	1.004	0.08765	<0.0001
Drug*Drug	0.00214	0.09596	0.9823
Inhibitor	-0.02529	0.005134	<0.0001
Drug*Inhibitor	-0.3524	0.06803	<0.0001

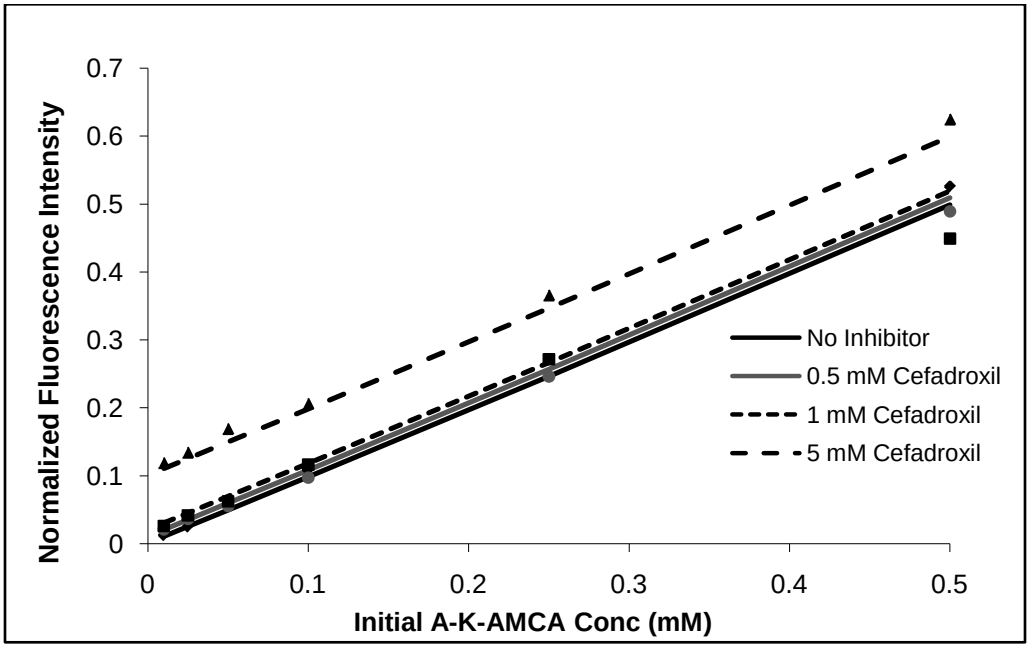

Figure 5.13. Cefadroxil inhibition of A-K-AMCA uptake. MCF10A cells were exposed to A-K-AMCA (0.01-0.5 mM) or A-K-AMCA with increasing concentrations of the peptidomimetic cefadroxil (0.5-5 mM). Data points are geometric mean fluorescence intensity values (n=4) for each A-K-AMCA and inhibitor concentration and are normalized by the fluorescence intensity value of cells treated with 1 mM A-K-AMCA. Curves were generated from the linear mixed effects model in SAS. Error bars were omitted for clarity.

Table 5.3. Mixed effects model parameter estimates and p-values for cefadroxil inhibition of A-K-AMCA uptake.

Effect	Estimate	Standard Error	p-value
Intercept	0.001275	0.001138	0.3789
Drug	0.9678	0.04266	<0.0001
Drug*Drug	0.05508	0.08652	0.5266
Inhibitor	0.02002	0.001283	<0.0001

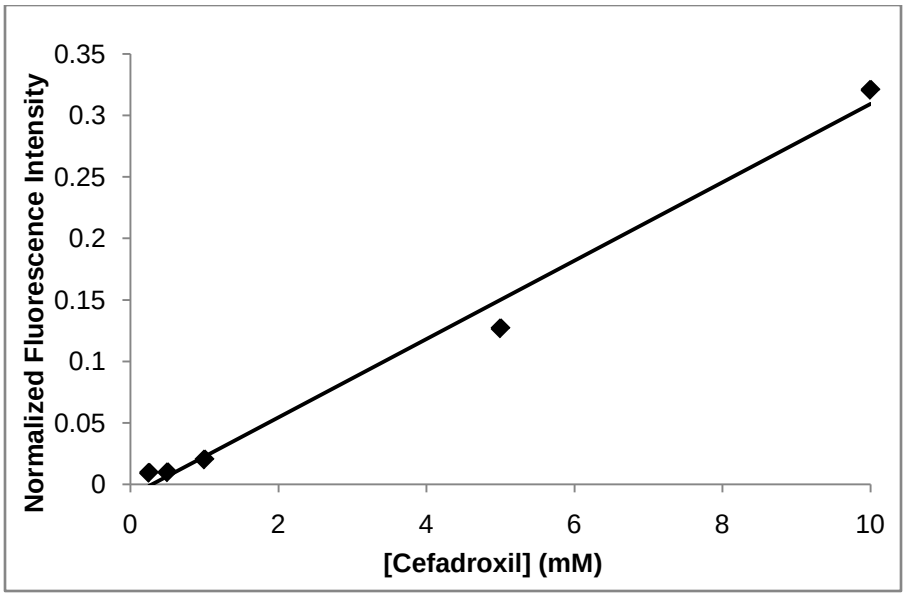

Figure 5.14. Cefadroxil fluorescence in MCF10A cells measured by flow cytometry. MCF10A cells were exposed to cefadroxil (0.25-10 mM). Data points are geometric mean fluorescence intensity values normalized for A-K-AMCA mean fluorescence intensity at 1 mM (n=3). Curve is a linear regression line fit to the data points.

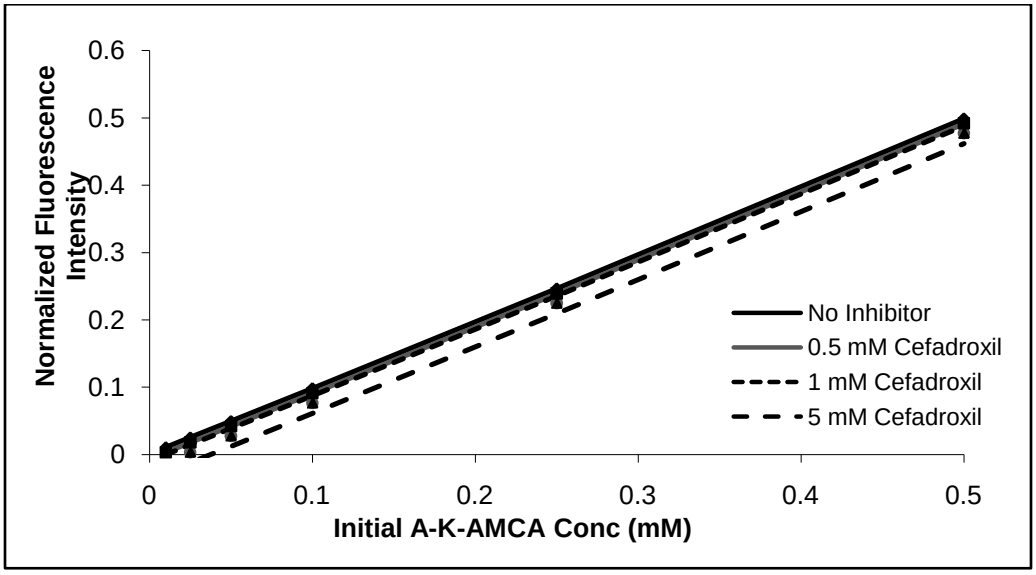

Figure 5.15. Inhibition of A-K-AMCA uptake in MCF10A cells by cefadroxil corrected for cefadroxil fluorescence. Data points (n=4) are geometric mean fluorescence intensity values for MCF10A cells treated with cefadroxil only subtracted from mean fluorescence intensity values for cells treated with A-K-AMCA and cefadroxil. Curves were generated from the linear mixed effects model in SAS. Error bars were omitted for clarity. Correction for cefadroxil fluorescence showed inhibition of A-K-AMCA uptake.

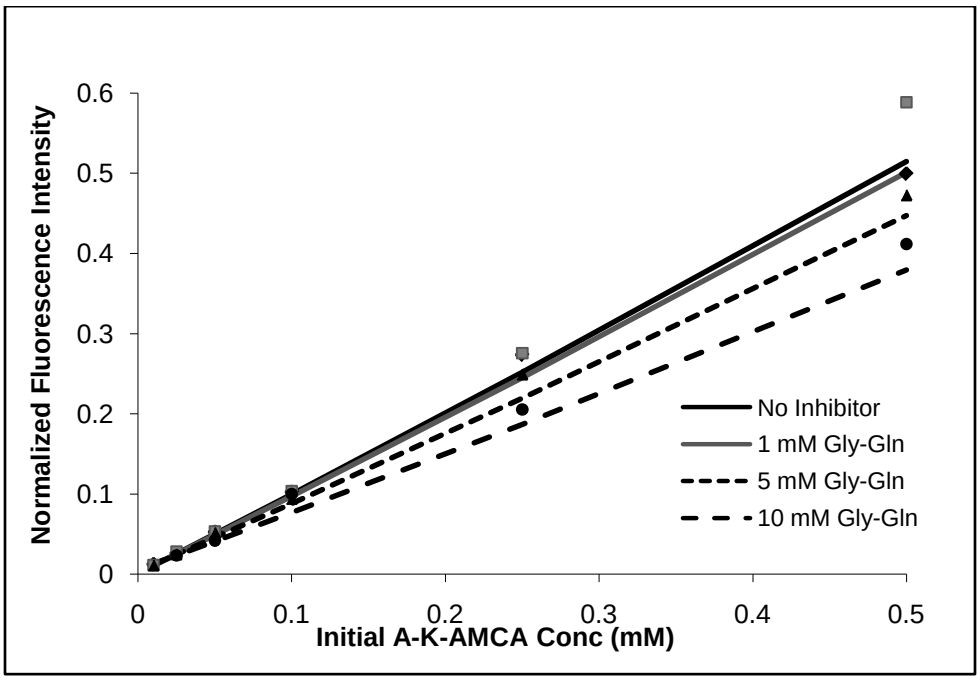

Figure 5.16. Gly-Gln inhibition of A-K-AMCA uptake. MCF10A cells were exposed to A-K-AMCA (0.01-0.5 mM) or A-K-AMCA with increasing concentrations of the dipeptide Gly-Gln (1-10 mM). Data points are mean fluorescence intensity values (n=4) for each A-K-AMCA and inhibitor concentration and are normalized by the fluorescence intensity value of cells treated with 1 mM A-K-AMCA. Curves were generated from the linear mixed effects model in SAS. Error bars were omitted for clarity.

Table 5.4. Mixed effects model parameter estimates and p-values for Gly-Gln inhibition of A-K-AMCA uptake

Effect	Estimate	Standard Error	p-value
Intercept	0.000501	0.001106	0.6814
Drug	0.9794	0.0341	<0.0001
Drug*Drug	0.09866	0.05589	0.0802
Inhibitor	0.00052	0.000188	0.0066
Drug*Inhibitor	-0.0281	0.004556	<0.0001

synthesis, all ATP dependent processes, including secondary active transport processes will be inhibited. 2,4-DNP decreased the intracellular accumulation of A-K-AMCA significantly (Figure 5.12 and Table 5.2) indicating that A-K-AMCA transport has at least one active component. The decrease in intracellular A-K-AMCA with 2,4-DNP inhibition was likely due to inhibition of the uptake transporter PEPT2.

As mentioned previously, a slight increase in intracellular fluorescence intensity was observed in the cefadroxil inhibition studies (Figure 5.13 and Table 5.3). This increase could be accounted for by correcting for the fluorescence of cefadroxil alone determined from flow cytometry uptake studies in MCF10A cells (Figure 5.14). When the cefadroxil fluorescence was subtracted from the total observed fluorescence intensity flow cytometry values, slight inhibition of A-K-AMCA uptake by cefadroxil was observed (Figure 5.15). Cefadroxil is also a substrate of PEPT2 and therefore is expected to be a competitive inhibitor of A-K-AMCA uptake.(85) Difficulties arose performing the statistical calculations using the small fluorescence values obtained after correcting for cefadroxil fluorescence; therefore, another inhibitor with no fluorescence, the dipeptide Gly-Gln, was investigated.

Glycyl-glutamine (Gly-Gln), a competitive inhibitor of PETP1 and PEPT2, was used to examine the effect of PEPT2 on A-K-AMCA transport in MCF10A cells. Inhibition of an uptake transporter such as PEPT2 is expected to decrease the intracellular accumulation of A-K-AMCA. Inhibition of A-K-AMCA uptake by Gly-Gln caused a decrease in accumulation measured through a decrease in the mean fluorescence intensity with increasing Gly-Gln concentration (Figure 5.16 and Table 5.4). Although the inhibitor effect in the model is positive, which reflects an increase in fluorescence

intensity with increasing concentrations of inhibitor, the drug*inhibitor term is a significantly larger and negative, indicating inhibition of uptake as evidenced by the decreasing slope of the lines in Figure 5.16 with increasing Gly-Gln concentration. The inhibition pattern shown is consistent with competitive inhibition as expected for dipeptide inhibition of peptide transporters.

Discussion

Results showed that both PEPT1 and PEPT2 were present in MCF10A cells, although PEPT2 appeared to be more highly expressed than PEPT1. This is consistent with PEPT1 being a low-affinity, high-capacity intestinal transporter, while PEPT2 is the high-affinity, low capacity transporter necessary for peptide transport in other tissues (including the mammary epithelium) were the peptide concentrations are much lower than those in the intestine.(86,90,94)

Flow cytometry was shown to be a highly sensitive technique for measuring intracellular fluorescence, allowing functional assays of transport to be performed even with low transporter expression levels as seen with the MDR1 results discussed in chapter 4. Therefore, low A-K-AMCA concentration ranges were used (< 1 mM) to avoid overlap with transport by PEPT1 as much as possible. However, use of a low concentration range made analysis of the fluorescence intensity complicated since AMCA fluorescence uses a UV excitation source which produces high autofluorescence levels in the cells since many endogenous compounds are also fluorescent near the wavelengths used. The combination of low concentrations and high background made changes in fluorescence with changes in concentration of A-K-AMCA very small.

The small changes in fluorescence intensity also confounded the measurement of inhibitor effects. Therefore, use of the linear mixed effects models developed for

mitoxantrone transport described previously were also important for analysis of A-K-AMCA transport. Also, the high end of inhibitor concentrations were likely in the range for PEPT1 inhibition. Although PEPT2 is much more highly expressed than PEPT1, some overlap of transport likely occurred at the high end of the substrate and inhibitor concentration ranges. This is further supported by the necessary inclusion of the drug*inhibitor term for 2,4-DNP and Gly-Gln results in the linear mixed effects models. As discussed in chapter 4, this term likely indicates transport by more than one transporter. In this case the two transporters are likely PEPT1 and PEPT2, with PEPT1 activity increasing at higher A-K-AMCA concentrations since it is a lower affinity peptide transporter than PEPT2.

The inhibitor Gly-Gln showed the expected concentration dependent inhibition of uptake for a competitive inhibitor. Since inhibition primarily affected the slope of the plots of fluorescence intensity vs. initial A-K-AMCA concentration, inhibition primarily affected the K_m of transport, consistent with competitive inhibition.

Both Gly-Gln and cefadroxil are high affinity PEPT2 transport inhibitors with K_i values in the low micromolar range (K_i = 15 μM for cefadroxil and K_i = 30 μM for Gly-Gln).(89,90,102) Both are also strong inhibitors of peptide transport, with Gly-Gln reducing transport to around 1% of the control and cefadroxil reducing transport to around 7% of the control.(90) Cefadroxil was not an ideal inhibitor for use in flow cytometry studies, due to its observed intracellular fluorescence. Both the dipeptide Gly-Gln and the peptidomimetic cefadroxil did affect transport of A-K-AMCA, therefore, PEPT1 and PEPT2 are very likely both active on transport in MCF10A cells.

Based on these results and the reported results on PEPT2 expression in the lactating mammary epithelium,(86) PEPT2 appears to play an important role in peptide and peptidomimetic transport relevant to drug levels in the milk. Since PEPT2 is located on the apical (milk facing) membrane of the mammary epithelium and functions as an uptake transporter, it will likely decrease the milk accumulation of its substrates. PEPT2 substrates such as some cephalosporin antibiotics have lower than expected milk accumulations than those predicted based on passive diffusion. At least some of the cephalosporin antibiotics including cefadroxil and cephalexin have M/P ratios which are significantly lower than predicted. Cefadroxil has a predicted M/P ratio based on its physicochemical properties of 0.5 which is significantly higher than the observed value of 0.009-0.02, and cephalexin shows a similar disparity of observed and predicted M/P with a predicted value of 1.5 compared to an observed 0.008-0.14.(4,5,103) MCF10A cells, since they do express PEPT2, appear to be a good model of peptide and peptidomimetic transport in the human mammary epithelium.

CHAPTER 6

COMPARISON OF TRANSPORTER EXPRESSION LEVELS IN MCF10A CELLS WITH IN VIVO HUMAN MAMMARY EPITHELIUM

Introduction

Uptake and efflux drug transport studies are currently limited to well-characterized transporters, and are complicated by substrate and inhibitor overlap between the various transporters. There are many transporters which are expressed in the lactating mammary epithelium that will impact drug transport into the breast milk.(1) Initially the focus of this work was placed on the transporter, BCRP, due its demonstrated effect on drug accumulation in the milk in mice.(10) MDR1 transport was also studied since the fluorescent substrate chosen for flow cytometry studies of BCRP, mitoxantrone, is also a known substrate of MDR1. MDR1 transport was not expected to be significant, however, due to down-regulation of this transporter during lactation.(46) Peptides transported by PEPT2 were also selected for investigation by flow cytometry because this transporter was shown to be up-regulated in the lactating mammary epithelium.(46,86) Flow cytometry and western blotting allow detailed information about transport of several substrates to be determined, such as kinetic parameters, substrate specificity and transporter inhibition. Although flow cytometry provided valuable insight into drug transport processes in the human mammary epithelium, only uptake and efflux (instead of transcellular flux) could be measured, the studies were limited by the necessity of using fluorescent substrates for detection and confined to specific transporters.

Comparison of transporter gene expression *in vivo* in lactating and non-lactating human mammary epithelial cells has been performed by Alcorn et al. for certain transporters using PCR.(46) The lactating mammary epithelium showed higher levels of

transporter expression for some transporters including OCT1, OCTN1, PEPT2, CNT1, CNT3 and ENT3 compared with the non-lactating mammary epithelium. While expression levels of OCTN2 and MDR1 were lower in the lactating mammary epithelium. The transporter BCRP was not included in this study. Transporter expression levels in lactating mammary epithelial cells were also compared to levels in the liver, kidney and placenta. OCT1, OCT3, OATP-B and CNT1 were more highly expressed in the liver and OCTN2 and MDR1 were more highly expressed in the kidney than in the mammary epithelium. While expression levels of CNT3, PEPT2 and OATP-A were higher in the mammary epithelium relative to at least one of the other tissues. Expression levels in the placenta were similar to the mammary epithelium except for MDR1, PEPT1 and ENT3 which had significantly higher expression in the placenta.(46) Ideally, MCF10A and HMEC mammary epithelial cells should show similar relative expression levels to these studies.

Knowledge about the relative expression levels of the transporters already functionally studied, as well as other drug transporters which may be clinically relevant, in the lactating mammary gland was desired. Analysis of drug transporter expression in the mammary epithelium can aid in extending the limited functional studies on transport and contribute to future study design. Polymerase chain reaction (PCR) assays of drug transporter mRNA expression levels in MCF10A cells and primary human mammary epithelial cells (HMECs) were compared and used to identify additional important transporters for drugs in the mammary epithelium.

RT-PCR (reverse transcription-PCR) was used to first convert the mRNA isolated from the cells into the complementary DNA (cDNA), and then the expression of the drug

transporters was analyzed by real-time PCR. Real-time PCR allowed mRNA transcripts for numerous drug transporters to be quantified in the mammary epithelium through a PCR array containing the primers for many of the important drug transporters (RT^2 Profiler PCR Array System from SABiosciences). The expression level of these transporters was normalized to the expression level of the endogenous control gene, β-actin, for each array, allowing the expression level of the transporter to be compared across different mammary epithelial cell lines (MCF10A and HMECs) and to expression reported previously for the *in vivo* lactating and non-lactating mammary epithelium.

Materials and Methods

RNA Isolation

RNA isolation was performed using the Manual PerfectPure RNA Cell & Tissue kit from 5 Prime (Fisher Scientific, Pittsburg, PA) according to the kit instructions (kit contains lysis solution, Tris (2-carboxyethyl) phosphine (TCEP), wash 1 solution, wash 2 solution, elution solution, purification columns, collection tubes, lyophilized DNase, DNase buffer, DNase wash solution. Media was removed from MCF10A cells grown in T75 cell culture flasks and 5 ml of 0.05% trypsin with EDTA (Gibco) was added to each flask and incubated at 37ºC until cells detached. Trypsin was neutralized with 5 ml of media and the contents of the flask were transferred to a 15 ml centrifuge tube. Cells were pelleted by centrifugation (Eppendorf 5810 R Centrifuge) at 1,000 x g for 2 minutes and the supernatant was removed.

Lysis of the resulting cell pellet was done in 400 µl lysis solution with 4 µl TCEP. Tubes were vortexed vigorously for a minimum of 2 minutes to resuspend the pellets, and homogenous samples were obtained. The lysate was placed on ice until further use.

RNA was purified from the lysed cells by placing the 400 µl lysate onto a purification column followed by centrifugation at 15,000 x g for 1 minute (Eppendorf 5415 D Centrifuge). The purification column was transferred to a new collection tube and 400 µl of Wash 1 Solution was added to the purification column and was centrifuged at 15,000 x g for 1 minute. The purification column was transferred to a new tube. The DNase Enzyme was reconstituted in 2.6 ml DNase Buffer and stored on ice. DNase Solution (50 µl) was added to the purification column and incubated at room temperature for 15 minutes; followed by addition of 200 µl of DNase Wash Solution to the column, and the column was centrifuged at 15,000 x g for 1 minute. Another 200 µl of DNase Wash Solution was added to the column and the column was centrifuged at 15,000 x g for 2 minutes. The purification column was transferred to a new tube and 200 µl of Wash 2 solution was added to the column and the column was centrifuged at 15,000 x g for 1 minute. Another 200 µl of Wash 2 solution was added to the column and the column was centrifuged at 15,000 x g for 2 minutes. The purification column was transferred to a new tube and purified RNA was eluted with 100 µl of Elution Solution with centrifugation at 15,000 x g for 1 minute. The purification column was discarded. Purified RNA was stored on ice or at -80ºC overnight.

RNA Quality Control

RNA concentration and purity was determined by absorbance spectroscopy using a Nanodrop spectrophotometer (Thermo Scientific). Concentration was measured by absorbance at 260 nm. Purity was determined by A260/A280 and A260/A230 ratios. Nucleic acids (DNA and RNA) absorb at 260 nm while proteins typically absorb at 280 nm. An A260/A280 ratio of greater than 2.0 indicates that there is little protein

contamination of the sample. The A260/A230 ratio is an indicator of other contaminates in the sample; an A260/A230 ratio greater the 1.7 indicates that there is little contamination. RNA quality was determined by ribosomal RNA band integrity using an Agilent 2100 BioAnalyzer (by the UI DNA Facility) and verifying that there was a sharp distinction at the small side of both the 18S and 28S ribosomal RNA peaks. Any smearing or shoulder to the rRNA peaks indicates that degradation of the RNA samples has occurred.

Reverse Transcription of RNA Samples

The SABiosciences RT^2 First Strand Kit was used to reverse transcribe the RNA samples into cDNA. Genomic DNA was eliminated from the RNA samples by incubation of 1 µg (1-3 µl) of the RNA sample with 2 µl GE (5X gDNA Elimination Buffer) and 5-7 µl RNase-free H_20 (total of 10 µl) at 42ºC for 5 minutes. The sample was then chilled on ice for 1 minute. The RT Cocktail consisting of 4 µl BC3 (5X RT Buffer 3), 1 µl P2 (Primer & External Control Mix), 2 µl RE3 (RT Enzyme Mix), and 3 µl RNase-free H_20 was added to the 10 µl RNA sample. The resulting mixture was mixed gently by pipetting and incubated at 42ºC for 15 minutes. The reaction was immediately stopped by heating the sample at 95ºC for 5 minutes. The cDNA sample (20 µl) was diluted with 91 µl of ddH_20 and was stored on ice.

PCR

The experimental cocktail containing 1275 µl 2X SABiosciences RT^2 qPCR Master Mix, 102 µl diluted First Strand cDNA Synthesis Reaction, and 1173 µl ddH_20 was mixed in a 5 ml tube and transferred to a multi-channel pipette reservoir. The Experimental Cocktail (25 µl) was added to each well of the PCR plate with an eight

channel pipettor. The wells were sealed with the included optical thin-wall 8-cap strips. The plate was placed on ice until PCR analysis. A two-step cycling program on an Applied Biosystems Model 7000 sequence detection system was used with one 10 minute cycle at 95ºC followed by 40 cycles of 15 seconds at 95ºC and 1 minute at 60ºC. The cycle number at which the target copy number (R_n) reached the set threshold value (C_T) was calculated for each well using the Sequence Detection System Analysis Software v. 1.7 (Applied Biosystems). A dissociation (melting) curve was run immediately after the cycling program.

Data Analysis

The relative expression level (L) for each gene was calculated from the C_T values using Equation 1.7 ($L=2^{-C_T}$). Normalization of expression level of transporter genes to endogenous control (housekeeping) genes in the sample is performed by dividing the expression levels of the gene of interest by the expression level of the housekeeping gene. Housekeeping genes included on the array are beta-2-microglobulin, hypoxanthine phosphoribosyltransferase 1, ribosomal protein L13a, glyceraldehydes-3-phosphate dehydrogenase and β-actin. β-actin was chosen as the housekeeping gene for normalization since it has been used for normalization of transporters in the mammary epithelium in previously published results.(46)

Quality control measures included running a dissociation (melting) curve, a genomic DNA control, a reverse transcription control, and a positive PCR control. Melting curves were run immediately after the cycling program and first derivative dissociation curves were generated for each well. Wells in which more than one peak appeared above 80°C were thrown out. A genomic DNA control, reverse transcription

control and positive PCR control were included in the PCR array. Genomic DNA control (GDC) was used to verify that the level of genomic DNA contamination was too low to affect gene expression results as determined by a C_T value greater than 35. The reverse transcription control (RTC) is used to detect any impurities in the RNA sample that affect reverse transcription and the positive PCR control (PPC) is used to detect any impurities in the RNA sample that affect PCR amplification. The average C_T^{PPC} should be 20 ± 2 and should not vary by more than two cycles between arrays being compared. Impurities affecting reverse transcription were determined by calculating ΔC_T = AVG C_T^{RTC} – AVG C_T^{PPC}. Values for ΔC_T of less than 5 indicate no apparent inhibition. An undetermined value indicates the sample did not meet the threshold value and is therefore considered as >38.

Results

PCR quality control measures met the standards for the MCF10A cells (Table 6.1 and Figure 6.1). Each MCF10A plate had a HGDC C_T value of greater than 35, therefore there was no contaminating genomic DNA. The PPC C_T values were all within 20 ± 2, therefore there was adequate amplification of the samples. Also, the C_T values were within 2 cycles between all PCR plates indicating consistent amplification between each plate. The calculated RTC controls were less than 5 indicating no apparent inhibition. The melting temperatures for each well were consistent and contained only one peak. One plate was removed from the analysis because it did not pass the quality control analysis ($\Delta C_T > 5$, with low expression of housekeeping genes).

PCR quality control measures for HMEC plates had some minor issues with contamination, but were still acceptable for analysis (Table 6.2 and Figure 6.2). The genomic DNA control for two of the three HMEC PCR arrays were slightly lower than

35, indicating some genomic DNA contamination of the samples. Since the values were still fairly low (C_T ~33), these plates were still used for the analysis but there is slightly less confidence in the results for these plates for samples with C_T values greater than 33 (instead of greater than 35). The PPC control was within 20 ± 2 at 18.54, therefore there was adequate amplification of the samples. The C_T values were all within 2 across the 3 plates showing consistent amplification. The calculated RTC control was less than 5 indicating no apparent inhibition.

Expression of endogenous controls, or housekeeping genes, are used to both assess the PCR results for sample loading efficiency and proper function of all the process steps, as well as to normalize target gene expression levels across experiments. Of these 5 housekeeping genes, β-actin had the highest expression level and was therefore used for normalization of the target gene expression levels. Expression level and C_T values for MCF10A and HMEC housekeeping genes are shown in Table 6.3 and Table 6.4. Expression levels and C_T values for MCF10A cells and HMECs are shown in Appendix B along with a brief description of all the transporters and housekeeping genes included in the array. Expression levels for ABC-type transporters in MCF10A cells (Figure 6.3 and Table 6.5) and HMECs (Figure 6.4 and Table 6.5) were fairly similar, although in HMECs, ABC transporter expression levels were generally lower than in MCF10A cells. Expression of the multidrug resistance transporters examined in the mitoxantrone flow cytometry studies described in chapter 4, MDR1 (ABCB1) and BCRP (ABCG2), were very low. Since 40 cycles were run, a C_T value greater than 35 indicates that there was virtually zero expression of that target gene. The C_T values for ABCB1 were 34.31 in MCF10A cells and 33.42 in HMECs which are at the detection limit. The

Table 6.1. Human drug transporters PCR array quality controls in MCF10A cells. Genomic DNA control (HGDC), reverse transcription control (RTC) and positive PCR control (PPC) average C_T values (n=3) are shown. RTC and PPC were run in triplicate and average values are shown.

Position	Symbol	Average C_T
H6	**HGDC**	**36.51**
H7	RTC	21.21
H8	RTC	21.31
H9	RTC	21.19
Average	**RTC**	**21.24**
H10	PPC	18.85
H11	PPC	18.78
H12	PPC	18.87
Average	**PPC**	**18.84**

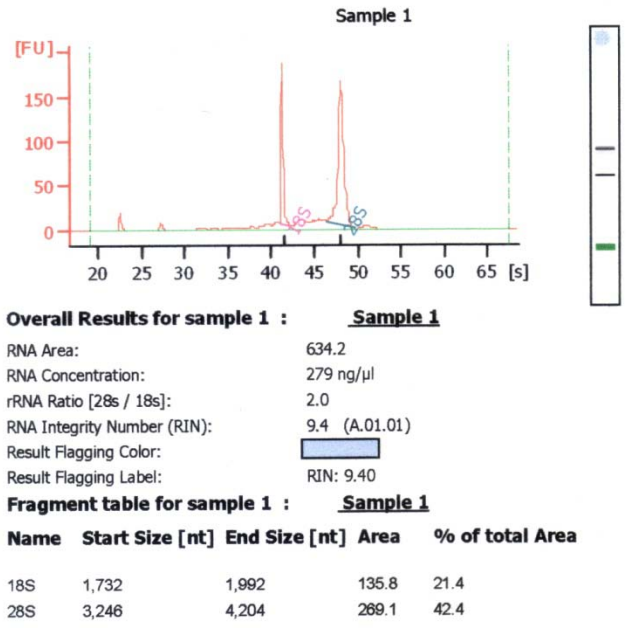

Figure 6.1. Ribosomal RNA band integrity analysis of RNA samples from MCF10A cells. Both the 18S and 28S rRNA peaks are sharp indicative of good RNA quality.

Table 6.2. Human drug transporters PCR array controls in HMECs. Genomic DNA control (HGDC), reverse transcription control (RTC) and positive PCR control (PPC) average C_T values (n=3) are shown. RTC and PPC were run in triplicate and average values are shown.

Position	Symbol	Average C_T
H6	**HGDC**	**34.24**
H7	RTC	22.93
H8	RTC	22.74
H9	RTC	22.92
Average	**RTC**	**22.82**
H10	PPC	18.40
H11	PPC	18.49
H12	PPC	18.45
Average	**PPC**	**18.45**

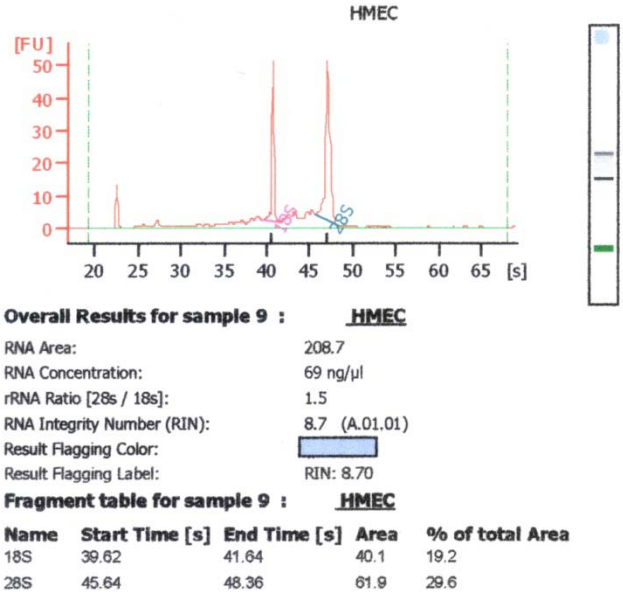

Figure 6.2. Ribosomal RNA band integrity analysis of RNA samples from HMECs. Both the 18S and 28S rRNA peaks are sharp indicative of good RNA quality.

Table 6.3 Human drug transporters PCR array housekeeping genes C_T and expression levels in MCF10A cells

Position	Symbol	C_T 1	C_T 2	C_T 3	Average C_T	Expression Level
H1	B2M	19.67	19.61	27.03	22.10	2.22E-07
H2	HPRT	22.33	BLD	24.79	23.56	8.08E-08
H3	RPL13A	17.90	17.19	18.04	17.71	4.66E-06
H4	GAPDH	16.46	15.44	15.38	15.76	1.80E-05
H5	ACTB	15.41	15.04	14.56	15.00	3.04E-05

Table 6.4 Human drug transporters PCR array housekeeping genes C_T and expression levels in HMECs

Position	Symbol	C_T 1	C_T 2	C_T 3	Average C_T	Expression Level
H1	B2M	19.98	19.93	18.7	19.54	1.32E-06
H2	HPRT1	23.36	23.80	22.13	23.10	1.12E-07
H3	RPL13A	19.02	19.47	17.39	18.63	2.47E-06
H4	GAPDH	17.78	17.94	15.47	17.06	7.30E-06
H5	ACTB	16.9	17.51	14.7	16.37	1.18E-05

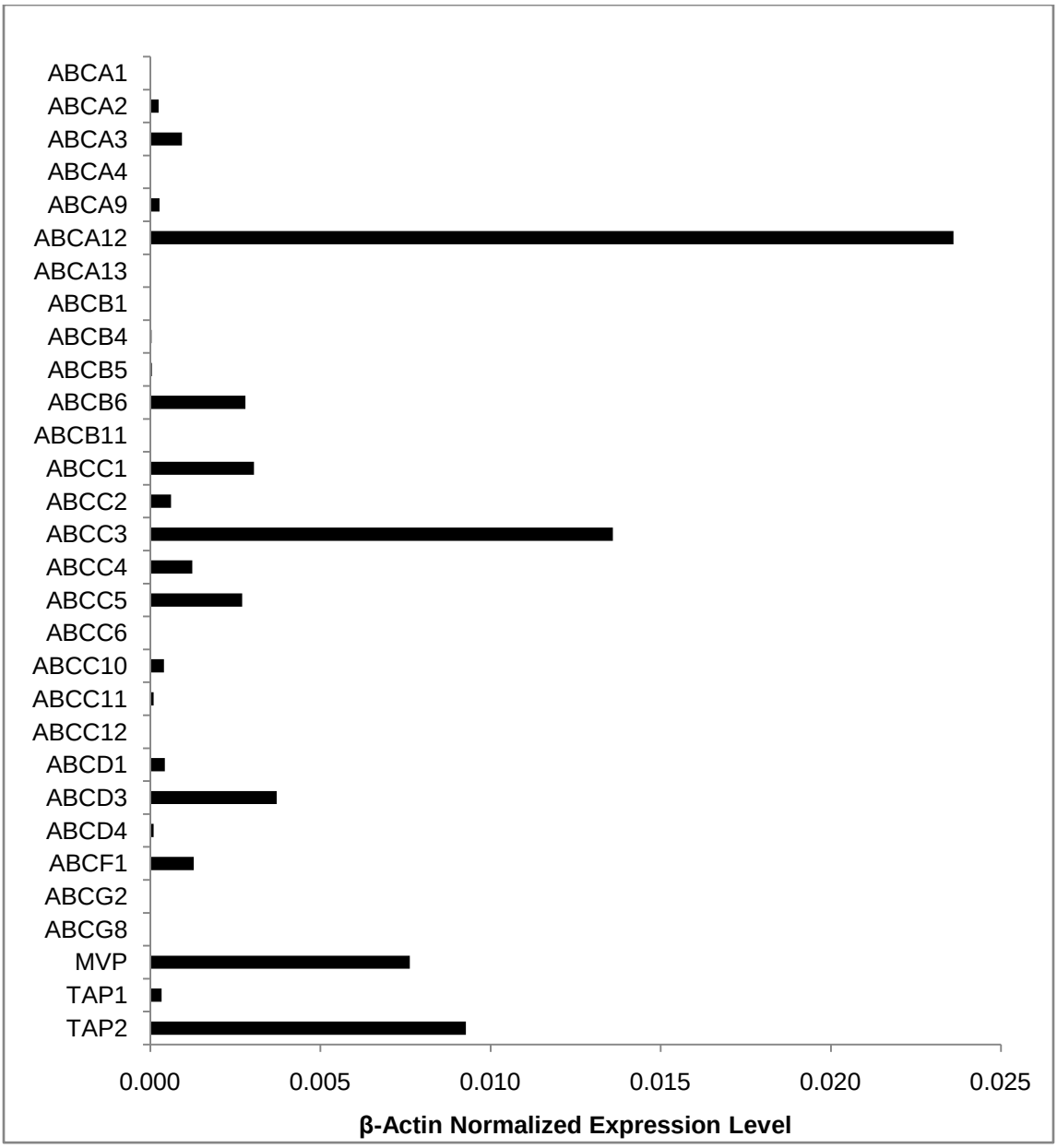

Figure 6.3. Normalized expression level of ABC transporters in MCF10A cells (data from SABiosciences RT^2 Profiler PCR Arrays). Expression levels were normalized by expression level of the housekeeping gene β-actin.

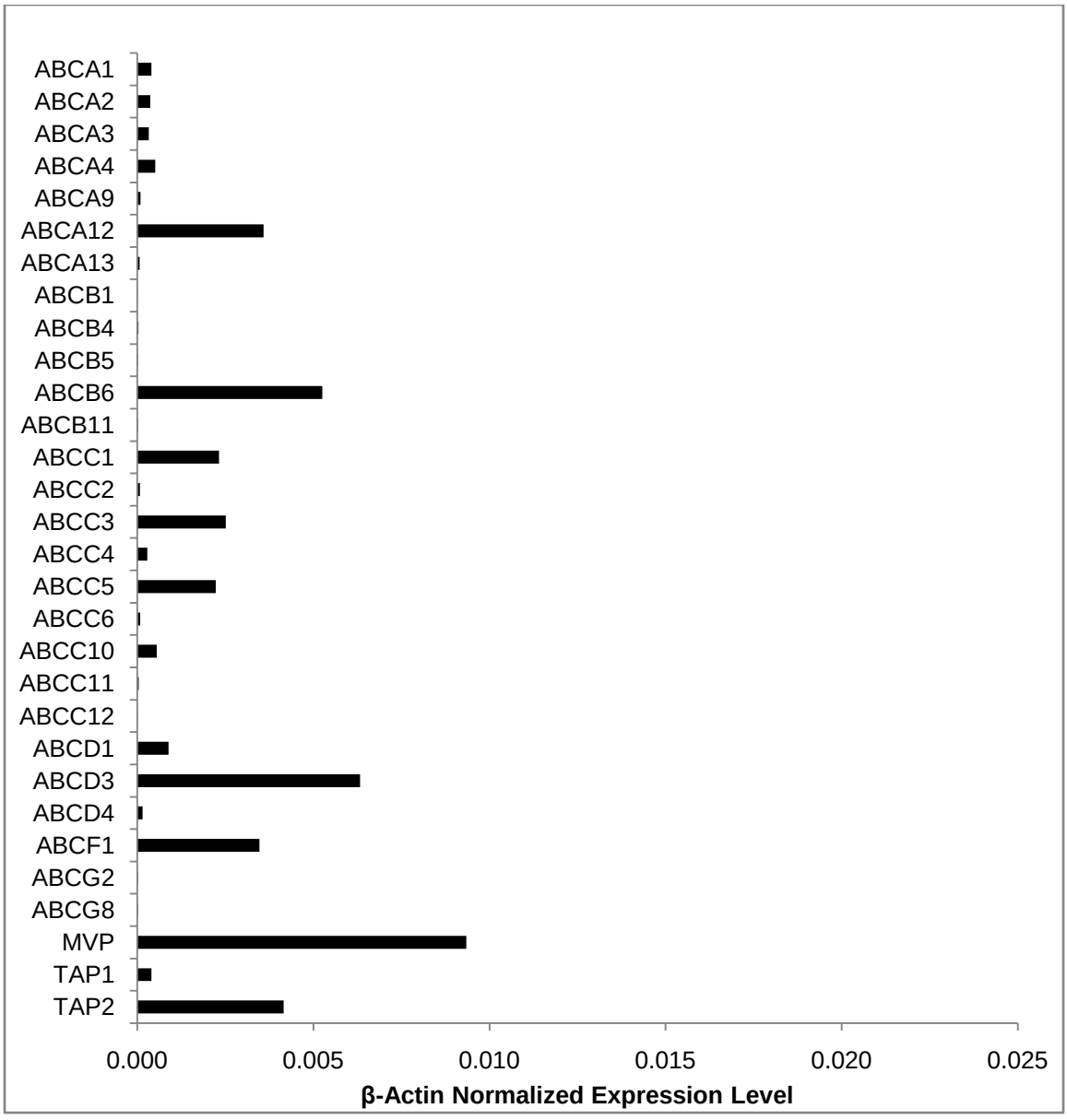

Figure 6.4. Normalized expression level of ABC transporters in primary human mammary epithelial cells (data from SABiosciences RT^2 Profiler PCR Arrays). Expression levels were normalized by expression level of the housekeeping gene β-actin.

Table 6.5. Expression levels of ABC transporters in MCF10A cells and HMECs

Symbol	MCF10A Expression Level	HMEC Expression Level
ABCA1	7.48E-07	4.01E-04
ABCA2	0.000241	3.67E-04
ABCA3	0.000929	3.27E-04
ABCA4	2.49E-05	5.09E-04
ABCA9	0.000272	9.21E-05
ABCA12	0.0236	3.59E-03
ABCA13	2.61E-05	6.92E-05
ABCB1	1.54E-06	5.19E-06
ABCB4	3.8E-05	3.42E-05
ABCB5	4.43E-05	1.96E-05
ABCB6	0.00279	5.26E-03
ABCB11	3.44E-07	1.31E-05
ABCC1	0.003048	2.32E-03
ABCC2	0.00061	7.76E-05
ABCC3	0.013594	2.52E-03
ABCC4	0.001235	2.83E-04
ABCC5	0.002693	2.23E-03
ABCC6	3.52E-06	8.43E-05
ABCC10	0.0004	5.54E-04
ABCC11	9.45E-05	4.27E-05
ABCC12	6.39E-06	5.37E-06
ABCD1	0.000426	8.88E-04
ABCD3	0.003712	6.32E-03
ABCD4	9.3E-05	1.50E-04
ABCF1	0.001277	3.47E-03
ABCG2	2.82E-06	1.56E-05
ABCG8	3.97E-06	1.77E-05
MVP	0.007629	9.34E-03
TAP1	0.000331	4.01E-04
TAP2	0.009274	4.15E-03

C_T values were also near the detection limit for ABCG2, 33.44 in MCF10A cells and 33.05 in HMECs, respectively. These C_T values correspond to a normalized expression level of around $4x10^{-6}$. Expression for some ABC transporters was slightly higher, such as ABCA12, many of the ABCCs (MRPs), MVP, TAP1 and TAP2.

Expression of many of the solute transporters (SLC) for MCF10A cells is shown in Figure 6.5 and Table 6.6 and for HMECs in Figure 6.6 and Table 6.6. Expression levels for a few transporters were significantly higher in MCF10A cells than in HMECs (RFC3, CNT2 and OATPE). HMECs had a somewhat higher expression level than MCF10A cells for PEPT1 & 2, OCT3, citrin, ENT2, NBAT2, OATPA and OATPC. However, the relative expression levels of SLC transporters were quite similar between the cell lines.

The expression levels of the transporters PEPT1 and PEPT2 were of interest for comparison to the flow cytometry studies discussed in chapter 5. The HMECs had a higher expression level of both transporters (expression level of $1.79\text{-}3.74x10^{-4}$, C_T values of around 28-29), while PEPT1 expression in MCF10A cells was at the detection limit (expression level of $1.23x10^{-6}$, C_T values of 34.63) and PEPT2 was slightly higher with a normalized expression level of $1.31x10^{-5}$ (C_T values of 31.22).

The organic cation transporter (OCT) and organic anion transporter (OAT) transport subfamilies are important for drug transport. OCTs showed moderate expression in HMECs but little or no expression in MCF10A cells. The OATs had little or no expression in both cell lines. Some of the OATPs (organic anion transporting peptides), especially OATP-D showed significant expression in both cell lines and OATP-A, OATP-C and OATP-E were highly expressed in at least one of the cell lines.

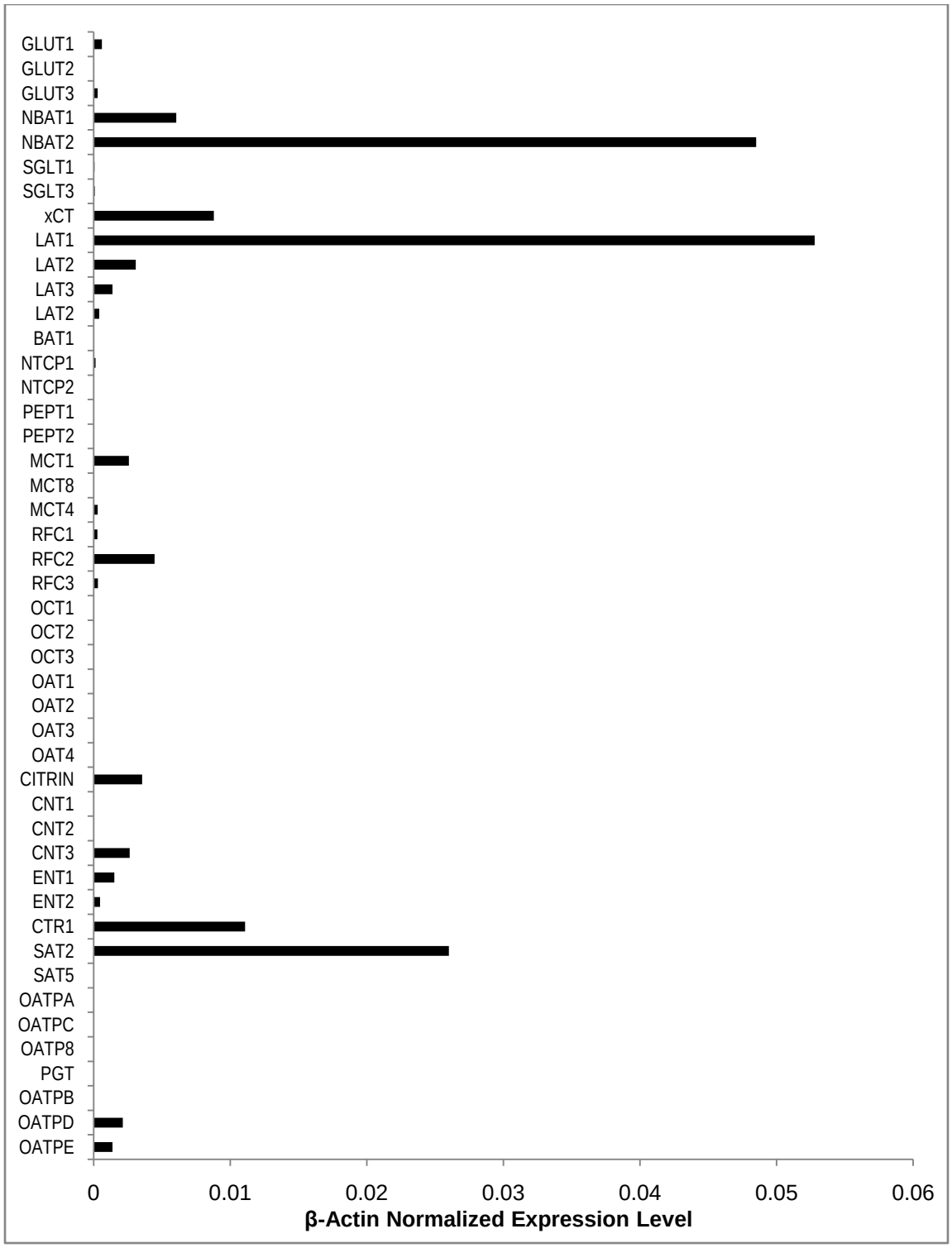

Figure 6.5. Normalized expression level of solute transporters in MCF10A cells (data from SABiosciences RT^2 Profiler PCR Arrays). Expression levels were normalized by expression level of the housekeeping gene β-actin.

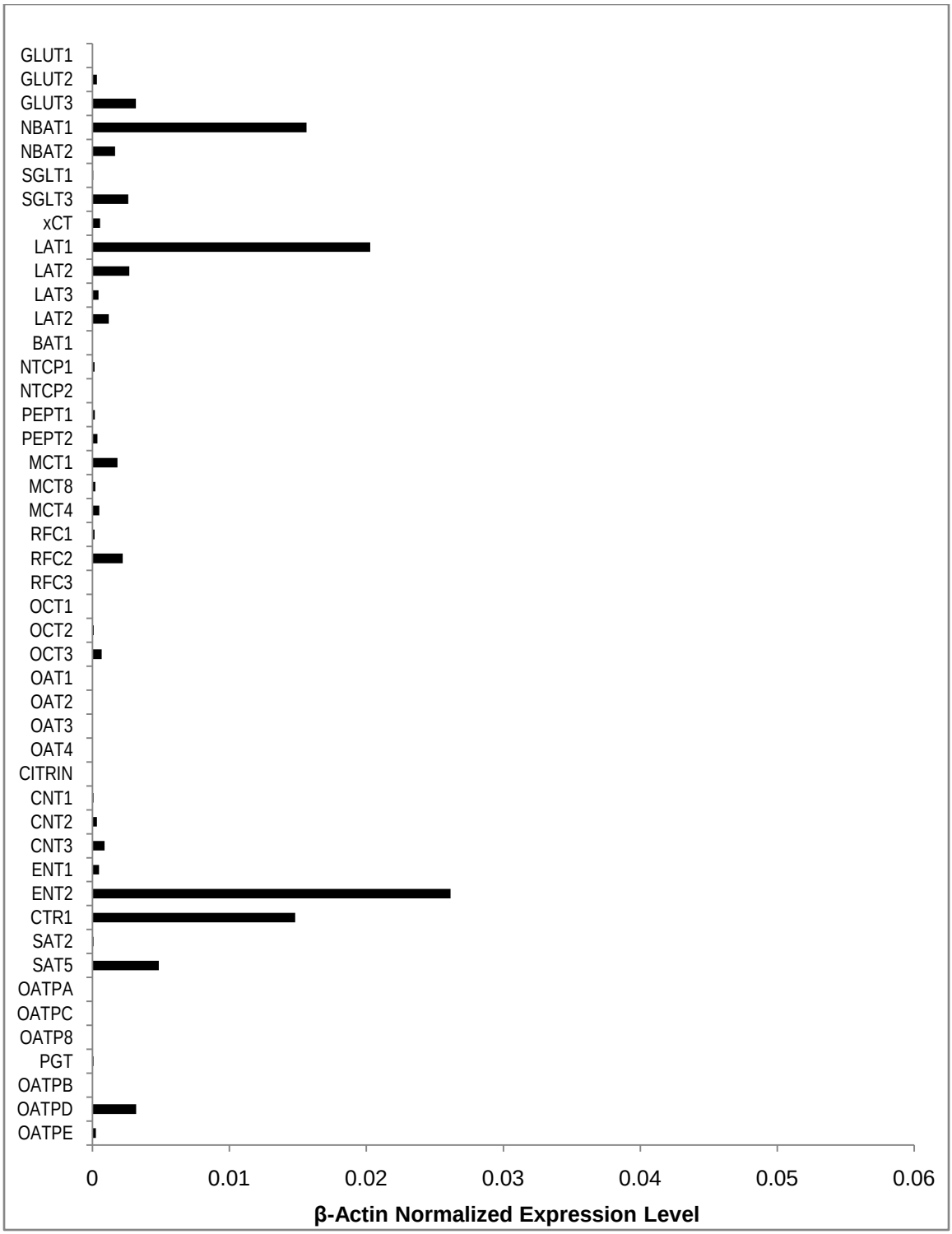

Figure 6.6. Normalized expression level of solute transporters in primary human mammary epithelial cells (data from SABiosciences RT^2 Profiler PCR Arrays). Expression levels were normalized by expression level of the housekeeping gene β-actin.

Table 6.6. Expression levels of solute carriers (SLC) in MCF10A cells and HMECs

Symbol	Common Name	MCF10A Expression Level	HMEC Expression Level
SLC2A1	GLUT1	0.0006	1.53E-05
SLC2A2	GLUT2	8.36E-06	3.20E-04
SLC2A3	GLUT3	0.000296	3.18E-03
SLC3A1	NBAT1	0.006047	1.56E-02
SLC3A2	NBAT2	0.048508	1.65E-03
SLC5A1	SGLT1	6.27E-05	5.56E-05
SLC5A4	SGLT3	7.45E-05	2.61E-03
SLC7A11	xCT	0.008806	5.60E-04
SLC7A5	LAT1	0.052783	2.03E-02
SLC7A6	LAT2	0.003088	2.69E-03
SLC7A7	LAT3	0.001368	4.51E-04
SLC7A8	LAT2	0.000414	1.20E-03
SLC7A9	BAT1	6.74E-06	8.99E-06
SLC10A1	NTCP1	0.00013	1.51E-04
SLC10A2	NTCP2	4.46E-06	1.16E-05
SLC15A1	PEPT1	1.23E-06	1.79E-04
SLC15A2	PEPT2	1.31E-05	3.74E-04
SLC16A1	MCT1	0.002584	1.82E-03
SLC16A2	MCT8	3.17E-05	2.10E-04
SLC16A3	MCT4	0.0003	4.96E-04
SLC19A1	RFC1	0.000277	1.58E-04
SLC19A2	RFC2	0.004453	2.21E-03
SLC19A3	RFC3	0.000311	2.54E-05
SLC22A1	OCT1	4.56E-05	4.20E-05
SLC22A2	OCT2	4.3E-05	1.03E-04
SLC22A3	OCT3	1.81E-05	6.67E-04
SLC22A6	OAT1	2.92E-06	7.04E-06
SLC22A7	OAT2	2.08E-07	7.22E-07
SLC22A8	OAT3	1.98E-07	1.44E-05
SLC22A9	OAT4	8.53E-06	1.91E-05
SLC25A13	CITRIN	0.003546	2.87E-05
SLC28A1	CNT1	6.14E-07	7.17E-05
SLC28A2	CNT2	1.52E-05	3.31E-04
SLC28A3	CNT3	0.002631	8.81E-04
SLC29A1	ENT1	0.001518	4.77E-04
SLC29A2	ENT2	0.000469	2.61E-02
SLC31A1	CTR1	0.011091	1.48E-02
SLC38A2	SAT2	0.026006	8.64E-05
SLC38A5	SAT5	2.16E-05	4.84E-03

Table 6.6–continued

SLC1A2	OATPA	1.16E-07	7.73E-06
SLCO1B1	OATPC	1.26E-06	2.62E-05
SLCO1B3	OATP8	1.24E-05	2.30E-05
SLCO2A1	PGT	2.57E-05	6.98E-05
SLCO2B1	OATPB	1.95E-05	4.13E-05
SLCO3A1	OATPD	0.002122	3.19E-03
SLCO4A1	OATPE	0.001371	2.59E-04

Both cell lines also expressed some of the concentrative and equilibrative nucleoside transporters (CNTs and ENTs).

A comparison of a few selected transporters in MCF10A and HMECs is shown in Figure 6.7. Expression levels for the transporters were similar, with the exception of ABCA12 and ABCC3 (MRP3) which showed significantly higher expression in MCF10A cells.

Transporter expression levels determined from PCR drug transporter arrays in MCF10A cells were also compared to reports of drug transporter expression levels in non-lactating and lactating mammary epithelial cells (Figure 6.8 and Table 6.7.).(46) Following normalization to β-actin expression in both studies, expression levels were significantly lower in the MCF10A cells. When comparing the relative expression levels, MCF10A cells expressed higher relative levels of the MRPs compared to other transporters in both lactating and non-lactation mammary epithelial cells. Another important difference between the three cells types studied were the higher expression of PEPT2 during lactation and the down-regulation of MDR1. Expression levels were similar for OATP-E, MRP1, CNT3, and ENT1 between all the cell types. Absolute expression levels were different between the two studies likely due to a difference in the way expression levels were determined. Expression levels in the study by Alcorn were determined from a standard curve of serial dilutions of the target genes.(46) Expression levels in these studies were generated from Equation 1.7. Therefore, although both are normalized to β-actin expression, the manner in which they were determined was significantly different and only relative expression levels can be compared between the two studies.

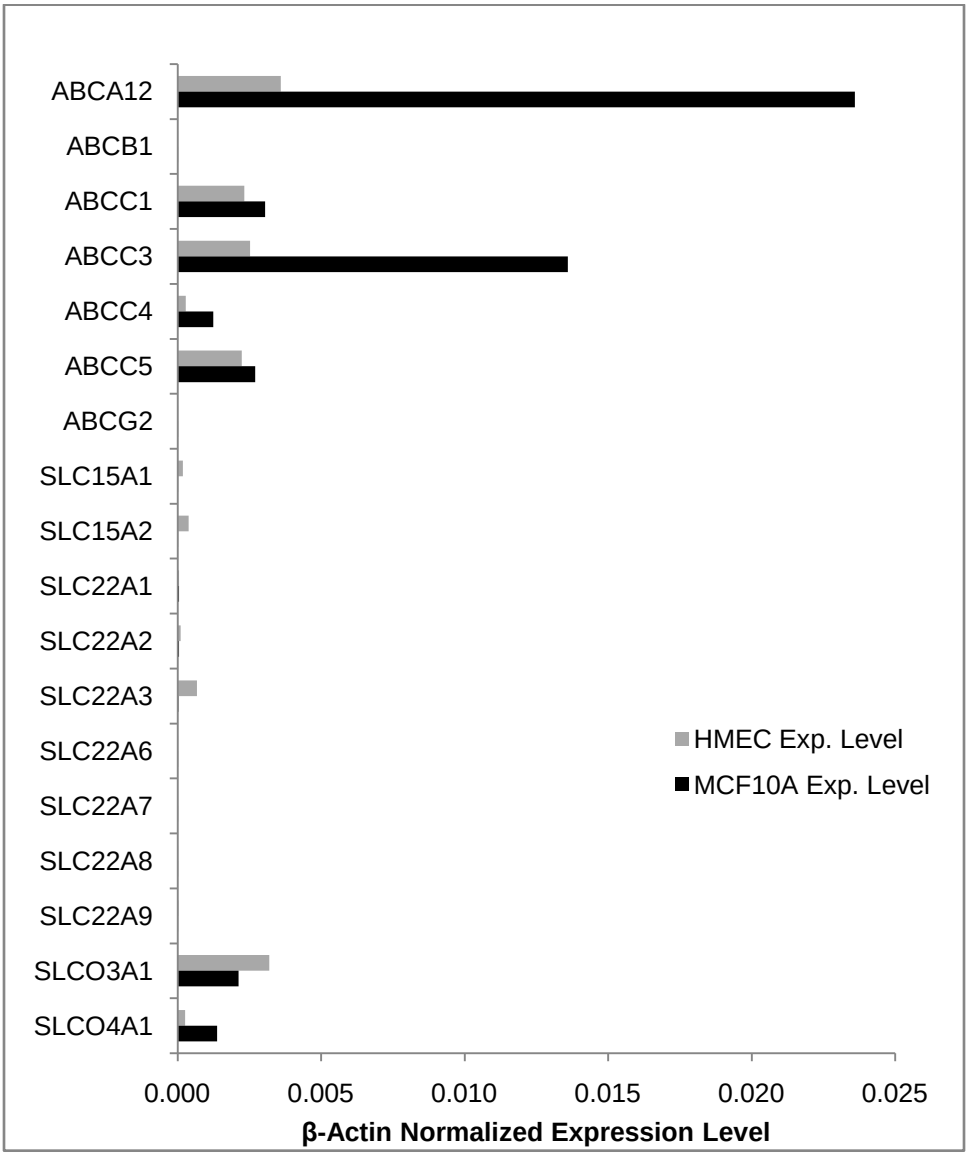

Figure 6.7. Comparison of normalized transporter expression levels in MCF10A and HMECs for selected transporters. Expression levels were normalized by β-actin expression levels. Expression levels in MCF10A cells are shown in black and expression levels in HMECs are shown in gray.

Table 6.7. Comparison of transporter gene expression levels between MCF10A cells, HMECs, and lactating and non-lactating mammary epithelial cells (MECs) and liver, kidney and placental tissue.

Transporter Gene	Gene Symbol	Lactating MECs	Non-Lactating MECs	MCF10A	HMECs	Liver	Kidney	Placenta
OCT1	SLC22A1	3.5	0.451	4.56E-05	4.20E-05	4870	4.54	1.44
OCT2	SLC22A2	BLD	BLD	4.30E-05	1.03E-04	BLD	10.3	BLD
OCT3	SLC22A3	0.163	0.476	1.81E-05	6.67E-04	1.72	0.25	1.17
OCTN1	SLC22A4	0.336	BLD	NA	NA	BLD	0.388	0.0517
OCTN2	SLC22A5	0.622	2.51	NA	NA	0.185	6.26	2.64
OAT1	SLC22A6	BLD	BLD	2.92E-06	7.04E-06	BLD	54.1	BLD
OAT2	SLC22A7	BLD	BLD	2.08E-07	7.22E-07	39.3	2.76	BLD
OAT3	SLC22A8	BLD	BLD	1.98E-07	1.44E-05	BLD	124	BLD
OAT4	SLC22A9	BLD	BLD	8.53E-06	1.91E-05	0.174	48.6	17.7
OATPA	SLCO1A2	0.0833	0.0525	1.16E-07	7.73E-06	BLD	0.00488	0.0111
OATPB	SLCO2B1	0.945	0.641	1.95E-05	4.13E-05	16.6	1.206	5.04
OATPC	SLCO1B1	BLD	BLD	1.26E-06	2.62E-05	18.9	BLD	BLD
OATPD	SLCO3A1	3.64	6.63	2.12E-03	3.19E-03	0.787	2.04	1.07
OATPE	SLCO4A1	0.137	0.371	1.37E-03	2.59E-04	0.062	0.121	0.179
MDR1	ABCB1	0.0258	1.33	1.54E-06	5.19E-06	0.157	2.81	6.3
MRP1	ABCC1	0.355	0.917	3.05E-03	2.32E-03	0.429	0.427	1.09
MRP2	ABCC2	0.0506	0.0586	6.10E-04	7.76E-05	0.261	0.214	0.0733
MRP3	ABCC3	BLD	BLD	1.36E-02	2.52E-03	BLD	BLD	BLD
MRP4	ABCC4	BLD	BLD	1.24E-03	2.83E-04	BLD	BLD	BLD
MRP5	ABCC5	0.067	0.0388	2.69E-03	2.23E-03	0.035	0.0722	0.244
PEPT1	SLC15A1	0.054	0.159	1.23E-06	1.79E-04	3.42	5.22	0.876
PEPT2	SLC15A2	1.59	BLD	1.31E-05	3.74E-04	BLD	E	E
CNT1	SLC28A1	0.176	BLD	6.14E-07	7.17E-05	ACR	BLD	BLD
CNT2	SLC28A2	BLD	BLD	1.52E-05	3.31E-04	BLD	E	E
CNT3	SLC28A3	0.334	0.048	2.63E-03	8.81E-04	BLD	BLD	BLD
ENT1	SLC29A1	0.49	0.658	1.52E-03	4.77E-04	2.74	0.707	0.462
ENT2	SLC29A2	BLD	BLD	4.69E-04	2.61E-02	BLD	E	E
ENT3	SLC29A3	0.0782	BLD	NA	NA	0.127	0.101	41
NCBT1	SLC23A1	0.961	0.44	NA	NA	6.24	1.14	0.476
NCBT2	SLC23A2	BLD	BLD	NA	NA	E	ACR	BLD
BCRP	ABCG2	NA	NA	2.82E-06	1.56E-05	NA	NA	NA

Note: Expression levels for lactating and non-lactating MECs, liver, kidney and placenta are from the study by Alcorn.(46) MCF10A and HMEC expression levels were determined from RT^2 Profiler Drug Transporter PCR Arrays (SABiosciences).

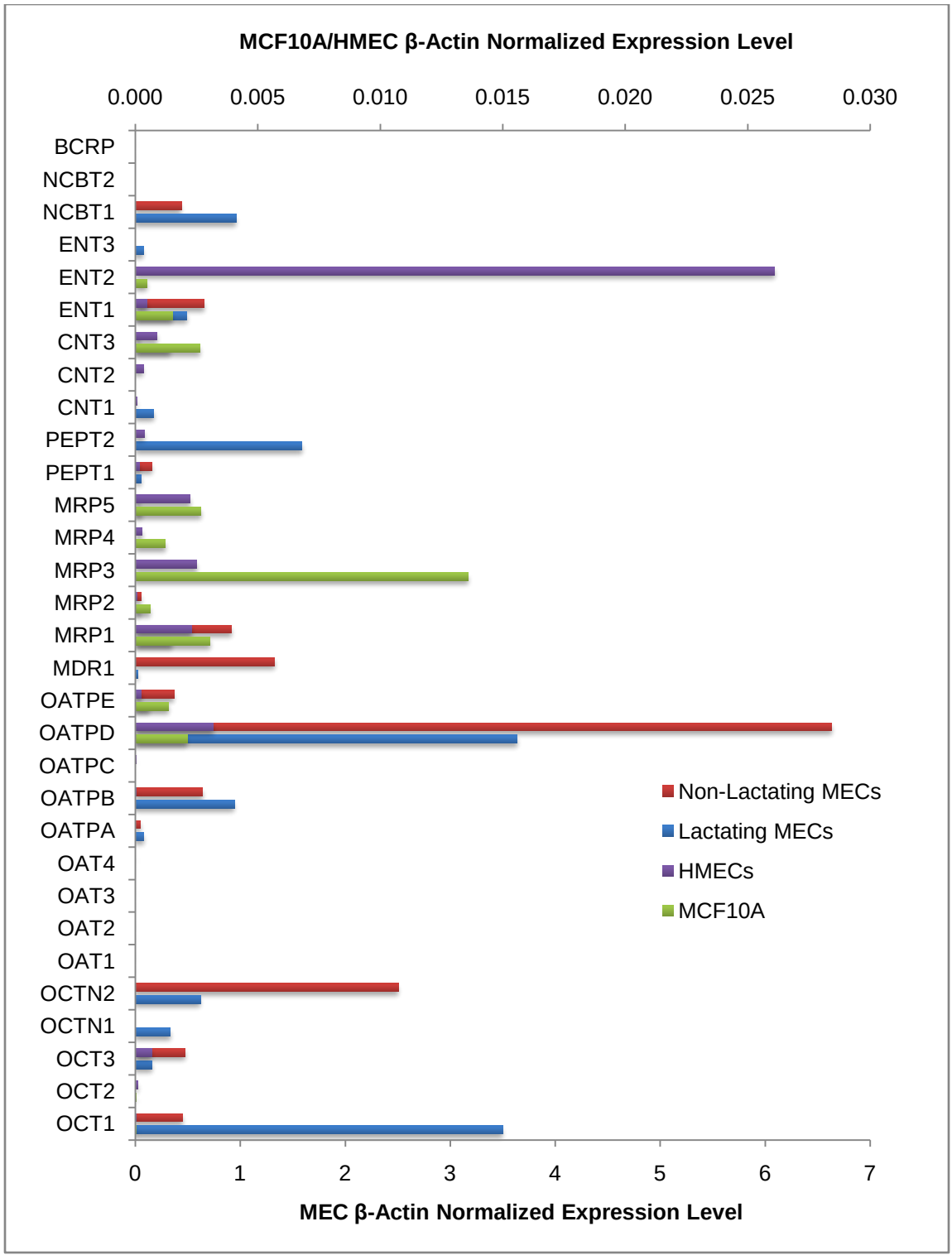

Figure 6.8. Comparison of transporter gene expression levels between MCF10A Cells and *in vivo* lactating and non-lactating mammary epithelial cells.(46)

Discussion

The flow cytometry method described in chapter 4 was able to detect functional transport by MDR1 even at very low expression levels which suggests possible drug-induced up-regulation of this transporter in MCF10A cells. The results also demonstrate that the flow cytometry assay is sufficiently sensitive to detect transport function even at low levels of transporter. Up-regulation in response to a cytotoxic compound has been known to occur for other multidrug resistance transporters.(65) Although, this is less likely under the experimental conditions used since the cells were only exposed to mitoxantrone for 30 minutes during the studies. Relatively high expression of the ABC transporter, ABCA12, was seen in MCF10A cells. The exact function of ABCA12 is unknown; however, it is thought to function as a lipid transporter. Relatively high expression of this transporter in the mammary epithelium is not surprising due to the relatively high lipid concentration in the milk relative to the plasma.(2,4) The MRP sub-family of transporters is also relatively highly expressed in the mammary cell lines studied. Some of these transporters are known to play a role in multidrug resistance. Given the low expression of the other major drug resistance transporters, MDR1 and BCRP, the high expression of MRP1 and the other MRP transporters may play an important role in drug distribution into milk.

Expression of PEPT1 and PEPT2 was somewhat higher in HMECs than in MCF10A cells as described above. However, the expression levels of the two transporters in HMECs were very similar ($1.79x10^{-4}$ vs. $3.74x10^{-4}$) in HMECs while there was a significant difference between the expression levels of the two transporters in MCF10A cells. Since PEPT2 is known to be expressed at higher levels than PEPT1 in peripheral tissues, including the mammary epithelium, the higher expression levels of

both transporters in HMECs may not be beneficial enough to outweigh the very small difference between their expression levels in that cell line, especially since the flow cytometry techniques developed for PEPT1/PEPT2 transport are relatively sensitive assays and can handle low transporter expression levels as discussed for the multidrug resistance transporters. Cells which have a lower expression of PEPT2, but a greater difference in PEPT1 and PEPT2 expression levels are therefore preferable for physiologically relevant drug transport studies.

Expression levels in HMECs and MCF10A were very similar for most transporters. The increased cost associated with HMECs compared to MCF10A cells limits the usefulness of this cell line as a model for drug transporters since they did not show any benefits over MCF10A cells. MCF10A cells show a relatively higher expression of the MRP multiple drug resistance transporters compared to the primary lactating and non-lactating mammary epithelial cells in the Alcorn study.

Since transporter expression levels were relatively similar in MCF10A cells and the *in vivo* lactating mammary epithelium for OATP-E, MRP1, MRP2, CNT3, and ENT1, MCF10A cells may provide an excellent *in vitro* model for functional transport studies for their substrates. MCF10A cells do not fully represent the lactating mammary epithelium; therefore, caution must be used in interpreting drug transport studies performed with these cells since some transporters may be over or under represented in *in vivo* drug transport studies. Relatively similar expression levels in all cell types seen for the drug transporter MRP1 and its function as an efflux transporter, this transporter may play an important role in drug accumulation in the milk and MCF10A cells are a useful model for further study of this transporter.

CHAPTER 7

CONCLUSIONS

Development of a model system for the analysis of drug transport in the human mammary epithelium initially focused on the formation of a polarized cellular barrier to drug transport. A variety of cell culture conditions for the growth of MCF10A and HMEC human mammary epithelial cells were investigated in order to develop a polarized monolayer of cells which could be used for transcellular flux studies. Tight junction formation in MCF10A cells was inadequate for polarized monolayer formation despite multiple attempts at improvement including treatment with the glucocorticoid dexamethasone, extracellular matrix coating on the cell growth surfaces, removal of cholera toxin from the growth media, and transfection with the tight junction protein Crumbs3. Primary human mammary epithelial cells (HMECs) were also investigated as a model system for drug transport studies. HMECs did not have a significant advantage over MCF10A cells in polarized monolayer formation, and had the additional disadvantage of having a more variable response than the MCF10A cells.

MCF10A cells showed little or no expression of the ABC transporters MDR1 and BCRP and low expression of the solute transporters PEPT1 and PEPT2. A quantitative assessment of the function of these transporters was performed using flow cytometry measurements of uptake and efflux along with investigations of the effects of specific transporter inhibitors.

Investigation of MDR1 and BCRP transport activity was performed using mitoxantrone and the transporter specific inhibitors verapamil (MDR1) and FTC (BCRP). Verapamil clearly inhibited mitoxantrone uptake and efflux; however, FTC appeared to

decrease intracellular accumulation. Combined with the results for the general metabolic inhibitor, 2,4-DNP which inhibited mitoxantrone uptake, these results suggest the presence of an active uptake transporter for mitoxantrone. Further transport studies with additional transport inhibitors for uptake transporters known to be expressed in MCF10A cells would be needed to determine the identity of the specific transporter(s) involved. Since mitoxantrone is positively charged at physiologic pH, it may be a substrate for one of the organic cation transporters, although these showed relatively low expression levels in the MCF10A cells. Further studies into the ability of mitoxantrone or other multidrug resistance transporter substrates to induce expression of MDR1, BCRP or other MDR transporters would aid in the understanding of the flow cytometry data collected for these transporters.

A linear mixed effects model was required for analysis of the transport data due to the high inter-day variability in the flow cytometry fluorescence measurements. This statistical modeling technique allowed for the sensitive detection of transporter function even at low transporter expression levels. The linear mixed effects model developed from the mitoxantrone flow cytometry data was applied in a similar manner to describe flow cytometry results for other transporter systems. This model was used to analyze flow cytometry data for the uptake of a fluorescently labeled dipeptide by the peptide transporters PEPT1 and PEPT2. Transport by PEPT2 at low substrate concentrations and possible PEPT1 transport at the high end of the substrate concentration range is demonstrated from the flow cytometry data. Both Gly-Gln and cefadroxil (PEPT1 and PEPT2 inhibitors) showed concentration dependent effects on substrate transport, therefore, PEPT2 (and possibly PEPT1 as well) likely decrease the milk accumulation of

peptidomimetic drug compounds due to their localization to the apical plasma membrane of the mammary epithelium.

MCF10A cells and lactating mammary epithelial cells showed relatively similar transporter expression levels for a few transporters including MRP1, OATP-E, CNT3 and ENT1. MCF10A cells would be a valuable model for studying MRP1 transport and its role in drug accumulation in the milk. Other members of the MRP sub-family (especially MRP3 and MRP5) are over-expressed in MCF10A cells, therefore, care should be taken when evaluating transport data for this sub-family of transporters since an over-estimation of milk accumulation may be predicted. Another potential sub-family of transporters which may not be well-described by MCF10A cells are the OCTs since virtually no expression of these transporters was seen in MCF10A cells, but OCT1 and OCT3 are expressed in the lactating mammary epithelium. However, both of these differences favor over-estimation of milk expression which is preferable for safety reasons. MCF10A cells may also be a good cell culture model for identifying substrates of the lipid transporter ABCA12 which is highly expressed in this cell line. While MCF10A cells are not a perfect model for drug transport in the lactating mammary epithelium, they can add significant understanding to drug transport processes in this tissue.

APPENDIX A

FLOW CYTOMETRY DATA

Normalization Procedure Example

Flow cytometry fluorescence intensity values were first normalized by the concentration of the 20 μM mitoxantrone or 1 mM A-K-AMCA fluorescence intensity values. For example, the fluorescence intensity values in Table A.3 were normalized by dividing the fluorescence intensity by the mean of the two 20 μM mitoxantrone, 0 μM inhibitor fluorescence intensity values (360.96). Therefore, for the first value in the table (2,5 μM mitoxantrone, 0 μM verapamil) the normalized fluorescence intensity of 0.246 was obtained by dividing the fluorescence intensity for that sample (88.83) by 360.96.

Example SAS Program

```
proc import datafile="\\H:\\ jreiland\My SAS Files\9.1\AMCA SAS Data.xls"
out=datafile;
sheet='Cef';
   getnames=yes;
run;

proc print data=datafile;
run;

data datafile;
set datafile;
wt = 1/(fluorescence**2);
run;

  ods html;
  ods graphics on;
proc mixed data=datafile ;
class day rep;
model fluorescence = drug drug*drug inhibitor drug*inhibitor / solution residual;
random day rep(day);
weight wt;
run;
  ods graphics off;
  ods html close;
```

Flow Cytometry Fluorescence Intensity Data and Linear Mixed Effects Models SAS Output

Table A.1. Flow cytometry data for 2,4-DNP inhibition of mitoxantrone uptake

Drug Conc. (μM)	Inhibitor Conc. (μM)	Day	Rep	Fluorescence Intensity
1	0	32808	1	0.141
5	0	32808	1	0.475
10	0	32808	1	0.704
20	0	32808	1	0.947
1	0	32808	2	0.153
5	0	32808	2	0.459
10	0	32808	2	0.716
20	0	32808	2	1.053
1	1	32808	1	0.085
5	1	32808	1	0.349
10	1	32808	1	0.584
20	1	32808	1	0.952
1	1	32808	2	0.087
5	1	32808	2	0.361
10	1	32808	2	0.490
20	1	32808	2	0.806
1	0	4408	1	0.204
5	0	4408	1	0.421
10	0	4408	1	0.727
20	0	4408	1	1.037
1	0	4408	2	0.198
5	0	4408	2	0.513
10	0	4408	2	0.599
20	0	4408	2	0.963
1	1	4408	1	0.169
5	1	4408	1	0.337
10	1	4408	1	0.614
20	1	4408	1	0.907
1	1	4408	2	0.094
5	1	4408	2	0.348
10	1	4408	2	0.500
20	1	4408	2	0.956
1	0	4908	1	0.171
5	0	4908	1	0.426
10	0	4908	1	0.614
20	0	4908	1	0.953
1	0	4908	2	0.181
5	0	4908	2	0.427
10	0	4908	2	0.633

Table A.1–continued

20	0	4908	2	1.047
1	1	4908	1	0.127
5	1	4908	1	0.359
10	1	4908	1	0.624
20	1	4908	1	0.965
1	1	4908	2	0.106
5	1	4908	2	0.307
10	1	4908	2	0.518
20	1	4908	2	0.890

Figure A.1. SAS Data: 2,4-DNP inhibition of mitoxantrone uptake in MCF10A cells (page 87, Figure 4.6, Table 4.3, data set: Table A.1).

The SAS System

The Mixed Procedure

Model Information

Data Set	WORK.DATAFILE
Dependent Variable	Fluorescence
Weight Variable	wt
Covariance Structure	Variance Components
Estimation Method	REML
Residual Variance Method	Profile
Fixed Effects SE Method	Model-Based
Degrees of Freedom Method	Containment

Class Level Information

Class	Levels	Values
Day	3	4408 4908 32808
Rep	2	1 2

Dimensions

Covariance Parameters	3
Columns in X	4
Columns in Z	9
Subjects	1
Max Obs Per Subject	48

Number of Observations

Number of Observations Read	48
Number of Observations Used	48
Number of Observations Not Used	0

Iteration History

Iteration	Evaluations	-2 Res Log Like	Criterion
0	1	-111.28165342	
1	2	-119.65716666	0.00438545
2	1	-120.21563950	0.00157554
3	1	-120.40927057	0.00032923
4	1	-120.44707683	0.00002154
5	1	-120.44934542	0.00000012
6	1	-120.44935726	0.00000000

Convergence criteria met.

Figure A.1–continued

The SAS System

The Mixed Procedure

Covariance Parameter Estimates

Cov Parm	Estimate
Day	0.000159
Rep(Day)	0.000233
Residual	0.009562

Fit Statistics

-2 Res Log Likelihood	-120.4
AIC (smaller is better)	-114.4
AICC (smaller is better)	-113.8
BIC (smaller is better)	-117.2

Solution for Fixed Effects

Effect	Estimate	Standard Error	DF	t Value	Pr > |t|
Intercept	0.1137	0.01224	2	9.29	0.0114
Drug	0.06537	0.003076	39	21.25	<.0001
Drug*Drug	-0.00111	0.000178	39	-6.23	<.0001
Inhibitor	-0.07302	0.007292	39	-10.01	<.0001

Type 3 Tests of Fixed Effects

Effect	Num DF	Den DF	F Value	Pr > F
Drug	1	39	451.74	<.0001
Drug*Drug	1	39	38.87	<.0001
Inhibitor	1	39	100.28	<.0001

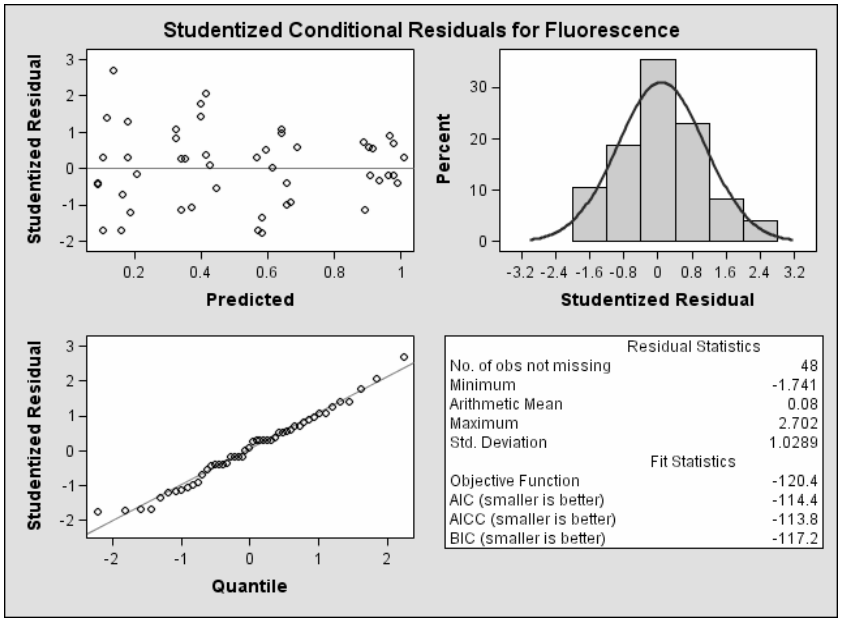

Table A.2. Flow cytometry data for 2,4-DNP inhibition of mitoxantrone efflux

Drug Conc. (μM)	Inhibitor Conc. (μM)	Day	Rep	Fluorescence Intensity
1	0	32808	1	0.087
5	0	32808	1	0.339
10	0	32808	1	0.635
20	0	32808	1	0.991
1	0	32808	2	0.100
5	0	32808	2	0.385
10	0	32808	2	0.691
20	0	32808	2	1.009
1	1	32808	1	0.075
5	1	32808	1	0.341
10	1	32808	1	0.589
20	1	32808	1	1.003
1	1	32808	2	0.059
5	1	32808	2	0.296
10	1	32808	2	0.497
20	1	32808	2	0.874
1	0	4408	1	0.029
5	0	4408	1	0.317
10	0	4408	1	0.433
20	0	4408	1	0.993
1	0	4408	2	0.035
5	0	4408	2	0.297
10	0	4408	2	0.548
20	0	4408	2	1.007
1	1	4408	1	0.031
5	1	4408	1	0.268
10	1	4408	1	0.458
20	1	4408	1	0.908
1	1	4408	2	0.026
5	1	4408	2	0.206
10	1	4408	2	0.424
20	1	4408	2	0.766
1	0	4908	1	0.182
5	0	4908	1	0.412
10	0	4908	1	0.742
20	0	4908	1	0.955
1	0	4908	2	0.189
5	0	4908	2	0.437
10	0	4908	2	0.683
20	0	4908	2	1.045
1	1	4908	1	0.129
5	1	4908	1	0.369
10	1	4908	1	0.602
20	1	4908	1	0.855
1	1	4908	2	0.083

Table A.2–continued

5	1	4908	2	0.301
10	1	4908	2	0.511
20	1	4908	2	0.833

Figure A.2. SAS Data: 2,4-DNP inhibition of mitoxantrone efflux in MCF10A cells (page 88, Figure 4.7, Table 4.4, data set: Table A.2)

The SAS System

The Mixed Procedure

Model Information

Data Set	WORK.DATAFILE
Dependent Variable	Fluorescence
Covariance Structure	Variance Components
Estimation Method	REML
Residual Variance Method	Profile
Fixed Effects SE Method	Model-Based
Degrees of Freedom Method	Containment

Class Level Information

Class	Levels	Values
Day	3	4408 4908 32808
Rep	2	1 2

Dimensions

Covariance Parameters	3
Columns in X	5
Columns in Z	9
Subjects	1
Max Obs Per Subject	48

Number of Observations

Number of Observations Read	48
Number of Observations Used	48
Number of Observations Not Used	0

Iteration History

Iteration	Evaluations	-2 Res Log Like	Criterion
0	1	-79.30310676	
1	2	-97.37357489	0.00000000

Convergence criteria met.

Figure A.2–continued

The SAS System

The Mixed Procedure

Covariance Parameter Estimates

Cov Parm	Estimate
Day	0.002521
Rep(Day)	0
Residual	0.002550

Fit Statistics

-2 Res Log Likelihood	-97.4
AIC (smaller is better)	-93.4
AICC (smaller is better)	-93.1
BIC (smaller is better)	-95.2

Solution for Fixed Effects

Effect	Estimate	Standard Error	DF	t Value	Pr > |t|
Intercept	0.04737	0.03555	2	1.33	0.3143
Drug	0.06628	0.004353	38	15.23	<.0001
Drug*Drug	-0.00092	0.000189	38	-4.89	<.0001
Inhibitor	-0.04298	0.02352	38	-1.83	0.0755
Drug*Inhibitor	-0.00465	0.002051	38	-2.27	0.0292

Type 3 Tests of Fixed Effects

Effect	Num DF	Den DF	F Value	Pr > F
Drug	1	38	231.84	<.0001
Drug*Drug	1	38	23.91	<.0001
Inhibitor	1	38	3.34	0.0755
Drug*Inhibitor	1	38	5.14	0.0292

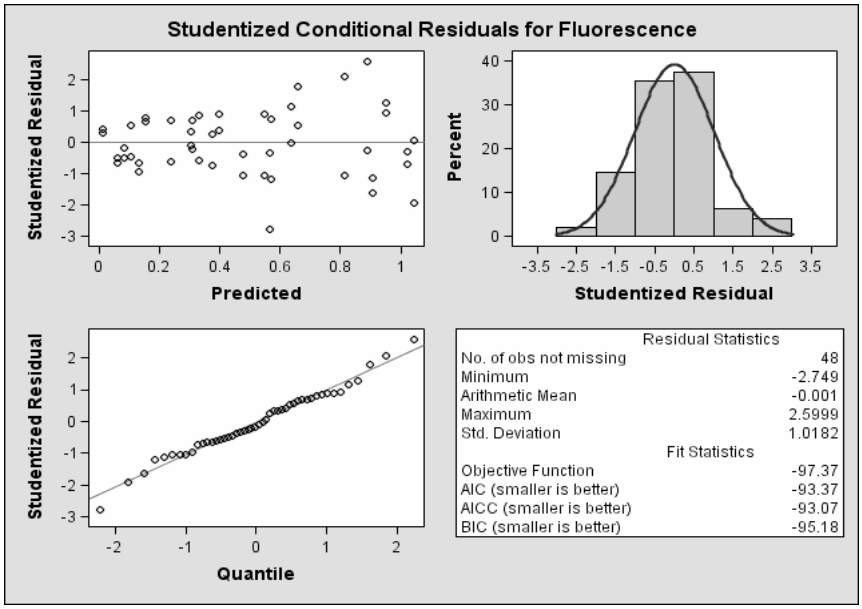

Table A.3. Flow cytometry data for verapamil inhibition of mitoxantrone uptake

Drug Conc. (μM)	Inhibitor Conc. (μM)	Day	Rep	Fluorescence Intensity
2.5	0	80207	1	0.246
5	0	80207	1	0.409
10	0	80207	1	0.676
20	0	80207	1	1.030
2.5	0	82907	1	0.246
5	0	82907	1	0.424
10	0	82907	1	0.676
20	0	82907	1	0.972
2.5	10	82907	1	0.231
5	10	82907	1	0.327
10	10	82907	1	0.785
20	10	82907	1	0.891
2.5	0	82907	2	0.240
5	0	82907	2	0.366
10	0	82907	2	0.729
20	0	82907	2	1.175
2.5	10	82907	2	0.272
5	10	82907	2	0.461
10	10	82907	2	0.831
20	10	82907	2	1.147
1	0	121107	1	0.232
2.5	0	121107	1	0.427
5	0	121107	1	0.566
10	0	121107	1	0.776
20	0	121107	1	1.084
1	1	121107	1	0.259
2.5	1	121107	1	0.368
5	1	121107	1	0.485
10	1	121107	1	0.754
20	1	121107	1	1.021
1	5	121107	1	0.315
2.5	5	121107	1	0.425
5	5	121107	1	0.562
10	5	121107	1	0.817
20	5	121107	1	1.261
1	10	121107	1	0.328
2.5	10	121107	1	0.508
5	10	121107	1	0.689
10	10	121107	1	0.822
20	10	121107	1	1.111
1	0	121107	2	0.239
2.5	0	121107	2	0.396
5	0	121107	2	0.496
10	0	121107	2	0.659
20	0	121107	2	0.916
1	1	121107	2	0.262

Table A.3–continued

2.5	1	121107	2	0.380
5	1	121107	2	0.472
10	1	121107	2	0.747
20	1	121107	2	1.003
1	5	121107	2	0.301
2.5	5	121107	2	0.502
5	5	121107	2	0.652
10	5	121107	2	0.684
20	5	121107	2	1.082
1	10	121107	2	0.272
2.5	10	121107	2	0.393
5	10	121107	2	0.524
10	10	121107	2	0.779
20	10	121107	2	1.111
1	0	121307	1	0.226
2.5	0	121307	1	0.438
5	0	121307	1	0.457
10	0	121307	1	0.851
20	0	121307	1	1.074
1	1	121307	1	0.229
2.5	1	121307	1	0.413
5	1	121307	1	0.503
10	1	121307	1	0.872
20	1	121307	1	1.335
1	5	121307	1	0.315
2.5	5	121307	1	0.578
5	5	121307	1	0.595
10	5	121307	1	0.860
20	5	121307	1	1.513
1	10	121307	1	0.415
2.5	10	121307	1	0.702
5	10	121307	1	0.749
10	10	121307	1	1.113
20	10	121307	1	1.584
1	0	121307	2	0.168
2.5	0	121307	2	0.368
5	0	121307	2	0.433
10	0	121307	2	0.736
20	0	121307	2	0.926
1	1	121307	2	0.250
2.5	1	121307	2	0.429
5	1	121307	2	0.489
10	1	121307	2	0.865
20	1	121307	2	1.225
1	5	121307	2	0.333
2.5	5	121307	2	0.549
5	5	121307	2	0.556
10	5	121307	2	0.817

Table A.3–continued

20	5	121307	2	1.245
1	10	121307	2	0.404
2.5	10	121307	2	0.644
5	10	121307	2	0.761
10	10	121307	2	1.089
20	10	121307	2	1.453
1	0	122607	1	0.649
2.5	0	122607	1	0.704
5	0	122607	1	0.666
10	0	122607	1	0.691
20	0	122607	1	1.005
1	1	122607	1	0.735
2.5	1	122607	1	0.671
5	1	122607	1	0.822
10	1	122607	1	0.816
20	1	122607	1	1.002
1	5	122607	1	0.725
2.5	5	122607	1	0.711
5	5	122607	1	0.792
10	5	122607	1	0.912
20	5	122607	1	1.215
1	10	122607	1	0.904
2.5	10	122607	1	0.813
5	10	122607	1	0.825
10	10	122607	1	0.993
20	10	122607	1	1.245
1	0	122607	2	0.591
2.5	0	122607	2	0.914
5	0	122607	2	0.644
10	0	122607	2	0.732
20	0	122607	2	0.995
1	1	122607	2	0.717
2.5	1	122607	2	0.569
5	1	122607	2	0.732
10	1	122607	2	0.897
20	1	122607	2	1.077
1	5	122607	2	0.739
2.5	5	122607	2	0.774
5	5	122607	2	0.779
10	5	122607	2	0.907
20	5	122607	2	0.992
1	10	122607	2	0.734
2.5	10	122607	2	0.712
5	10	122607	2	0.775
10	10	122607	2	0.847
20	10	122607	2	1.109
1	0	122707	1	0.737
2.5	0	122707	1	0.682

Table A.3–continued

5	0	122707	1	0.851
10	0	122707	1	0.847
20	0	122707	1	1.006
1	1	122707	1	0.614
2.5	1	122707	1	0.656
5	1	122707	1	0.769
10	1	122707	1	0.801
20	1	122707	1	0.930
1	5	122707	1	0.813
2.5	5	122707	1	0.590
5	5	122707	1	0.801
10	5	122707	1	0.897
20	5	122707	1	1.140
1	10	122707	1	0.869
2.5	10	122707	1	0.927
5	10	122707	1	0.845
10	10	122707	1	0.928
20	10	122707	1	1.225
1	0	122707	2	0.604
2.5	0	122707	2	0.675
5	0	122707	2	0.706
10	0	122707	2	0.738
20	0	122707	2	0.994
1	1	122707	2	0.556
2.5	1	122707	2	0.731
5	1	122707	2	0.781
10	1	122707	2	0.693
20	1	122707	2	0.921
1	5	122707	2	0.756
2.5	5	122707	2	0.663
5	5	122707	2	0.792
10	5	122707	2	0.957
20	5	122707	2	0.939
1	10	122707	2	0.903
2.5	10	122707	2	0.850
5	10	122707	2	0.959
10	10	122707	2	1.053
20	10	122707	2	1.157
1	0	122807	1	0.301
2.5	0	122807	1	0.461
5	0	122807	1	0.601
10	0	122807	1	0.642
20	0	122807	1	1.097
1	1	122807	1	0.315
2.5	1	122807	1	0.460
5	1	122807	1	0.675
10	1	122807	1	0.663
20	1	122807	1	0.998

Table A.3–continued

1	5	122807	1	0.427
2.5	5	122807	1	0.591
5	5	122807	1	0.822
10	5	122807	1	0.914
20	5	122807	1	1.230
1	10	122807	1	0.343
2.5	10	122807	1	0.568
5	10	122807	1	0.754
10	10	122807	1	0.738
20	10	122807	1	1.069
1	0	122807	2	0.244
2.5	0	122807	2	0.423
5	0	122807	2	0.598
10	0	122807	2	0.625
20	0	122807	2	0.903
1	1	122807	2	0.313
2.5	1	122807	2	0.401
5	1	122807	2	0.638
10	1	122807	2	0.670
20	1	122807	2	0.958
1	5	122807	2	0.400
2.5	5	122807	2	0.605
5	5	122807	2	0.750
10	5	122807	2	0.826
20	5	122807	2	1.305
1	10	122807	2	0.381
2.5	10	122807	2	0.588
5	10	122807	2	0.838
10	10	122807	2	0.805
20	10	122807	2	1.221
1	0	10908	1	0.495
2.5	0	10908	1	0.556
5	0	10908	1	0.772
10	0	10908	1	0.820
20	0	10908	1	1.000
1	1	10908	1	0.533
2.5	1	10908	1	0.581
5	1	10908	1	0.687
10	1	10908	1	0.877
20	1	10908	1	0.983
1	5	10908	1	0.513
2.5	5	10908	1	0.556
5	5	10908	1	0.792
10	5	10908	1	0.877
20	5	10908	1	1.128
1	10	10908	1	0.634
2.5	10	10908	1	0.659
5	10	10908	1	0.732

Table A.3–continued

10	10	10908	1	0.815
20	10	10908	1	1.270
1	0	11008	1	0.264
2.5	0	11008	1	0.340
5	0	11008	1	0.577
10	0	11008	1	0.658
20	0	11008	1	1.000
1	1	11008	1	0.278
2.5	1	11008	1	0.363
5	1	11008	1	0.520
10	1	11008	1	0.636
20	1	11008	1	0.958
1	5	11008	1	0.326
2.5	5	11008	1	0.405
5	5	11008	1	0.647
10	5	11008	1	0.750
20	5	11008	1	1.010
1	10	11008	1	0.316
2.5	10	11008	1	0.444
5	10	11008	1	0.681
10	10	11008	1	0.721
20	10	11008	1	1.184
1	0	11608	1	0.090
2.5	0	11608	1	0.219
5	0	11608	1	0.391
10	0	11608	1	0.609
20	0	11608	1	1.000
1	1	11608	1	0.091
2.5	1	11608	1	0.179
5	1	11608	1	0.332
10	1	11608	1	0.625
20	1	11608	1	1.051
1	5	11608	1	0.104
2.5	5	11608	1	0.206
5	5	11608	1	0.301
10	5	11608	1	0.554
20	5	11608	1	0.961
1	10	11608	1	0.105
2.5	10	11608	1	0.199
5	10	11608	1	0.346
10	10	11608	1	0.603
20	10	11608	1	0.950

Figure A.3. SAS Data: Verapamil inhibition of mitoxantrone uptake in MCF10A cells (page 92, Figure 4.11, Table 4.6, data set: Table A.3)

The SAS System

The Mixed Procedure

Model Information

Data Set	WORK.DATAFILE
Dependent Variable	Fluorescence
Covariance Structure	Variance Components
Estimation Method	REML
Residual Variance Method	Profile
Fixed Effects SE Method	Model-Based
Degrees of Freedom Method	Containment

Class Level Information

Class	Levels	Values
Day	10	10908 11008 11608 80207 82907 121107 121307 122607 122707 122807
Rep	2	1 2

Dimensions

Covariance Parameters	3
Columns in X	4
Columns in Z	26
Subjects	1
Max Obs Per Subject	280

Number of Observations

Number of Observations Read	280
Number of Observations Used	280
Number of Observations Not Used	0

Iteration History

Iteration	Evaluations	-2 Res Log Like	Criterion
0	1	-179.08572197	
1	3	-330.48102691	0.00238025
2	2	-330.97360298	0.00032127
3	1	-331.12654923	0.00001980
4	1	-331.13523822	0.00000011
5	1	-331.13528592	0.00000000

Convergence criteria met.

Figure A.3–continued

The SAS System

The Mixed Procedure

Covariance Parameter Estimates

Cov Parm	Estimate
Day	0.01471
Rep(Day)	0.001311
Residual	0.01358

Fit Statistics

-2 Res Log Likelihood	-331.1
AIC (smaller is better)	-325.1
AICC (smaller is better)	-325.0
BIC (smaller is better)	-324.2

Solution for Fixed Effects

Effect	Estimate	Standard Error	DF	t Value	Pr > |t|
Intercept	0.3146	0.04352	6	7.23	0.0004
Drug	0.04588	0.004411	261	10.40	<.0001
Drug*Drug	-0.00056	0.000200	261	-2.82	0.0052
Inhibitor	0.01383	0.001749	261	7.91	<.0001

Type 3 Tests of Fixed Effects

Effect	Num DF	Den DF	F Value	Pr > F
Drug	1	261	108.22	<.0001
Drug*Drug	1	261	7.96	0.0052
Inhibitor	1	261	62.52	<.0001

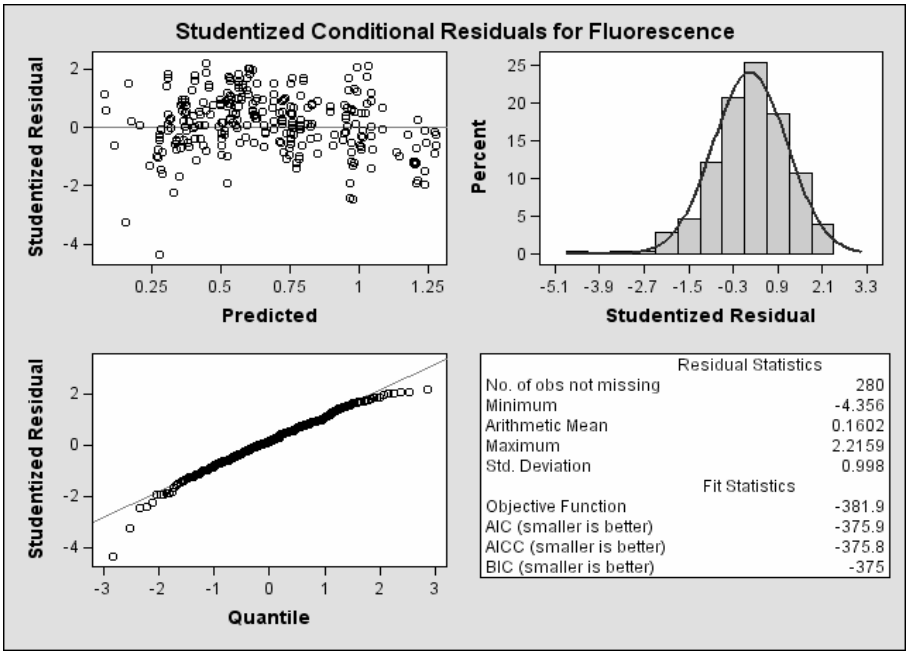

Table A.4. Flow cytometry data for verapamil inhibition of mitoxantrone efflux

Drug Conc. (μM)	Inhibitor Conc. (μM)	Day	Rep	Fluorescence Intensity
2.5	0	82907	1	0.407
5	0	82907	1	0.398
10	0	82907	1	0.712
20	0	82907	1	1.008
2.5	10	82907	1	0.482
5	10	82907	1	0.507
10	10	82907	1	0.738
20	10	82907	1	1.241
2.5	0	82907	2	0.388
5	0	82907	2	0.435
10	0	82907	2	0.650
20	0	82907	2	0.992
2.5	10	82907	2	0.504
5	10	82907	2	0.457
10	10	82907	2	0.747
20	10	82907	2	1.170
1.25	0	80207	1	0.201
2.5	0	80207	1	0.253
5	0	80207	1	0.436
10	0	80207	1	0.696
20	0	80207	1	1.000
1.25	1	80207	1	0.217
2.5	1	80207	1	0.267
5	1	80207	1	0.452
10	1	80207	1	0.680
20	1	80207	1	1.003
1.25	5	80207	1	0.280
2.5	5	80207	1	0.298
5	5	80207	1	0.559
10	5	80207	1	0.831
20	5	80207	1	1.101
1.25	10	80207	1	0.165
2.5	10	80207	1	0.237
5	10	80207	1	0.336
10	10	80207	1	0.808
20	10	80207	1	0.917
1.25	1	80207	2	0.176
2.5	1	80207	2	0.257
5	1	80207	2	0.376
10	1	80207	2	0.750
20	1	80207	2	1.209
1.25	5	80207	2	0.278
2.5	5	80207	2	0.280
5	5	80207	2	0.474
10	5	80207	2	0.855
20	5	80207	2	1.180

Table A.4–continued

1	0	10308	1	0.338
2.5	0	10308	1	0.507
5	0	10308	1	0.661
10	0	10308	1	0.696
20	0	10308	1	1.060
1	1	10308	1	0.471
2.5	1	10308	1	0.533
5	1	10308	1	0.657
10	1	10308	1	0.727
20	1	10308	1	1.028
1	5	10308	1	0.443
2.5	5	10308	1	0.693
5	5	10308	1	0.696
10	5	10308	1	0.774
20	5	10308	1	1.090
1	10	10308	1	0.508
2.5	10	10308	1	0.638
5	10	10308	1	0.816
10	10	10308	1	0.814
20	10	10308	1	1.168
1	0	10308	2	0.262
2.5	0	10308	2	0.506
5	0	10308	2	0.652
10	0	10308	2	0.692
20	0	10308	2	0.940
1	1	10308	2	0.397
2.5	1	10308	2	0.530
5	1	10308	2	0.685
10	1	10308	2	0.767
20	1	10308	2	1.056
1	5	10308	2	0.436
2.5	5	10308	2	0.671
5	5	10308	2	0.727
10	5	10308	2	0.820
20	5	10308	2	1.123
1	10	10308	2	0.481
2.5	10	10308	2	0.583
5	10	10308	2	0.785
10	10	10308	2	0.802
20	10	10308	2	1.025
1	0	10908	1	0.553
2.5	0	10908	1	0.532
5	0	10908	1	0.742
10	0	10908	1	0.879
20	0	10908	1	1.000
1	1	10908	1	0.540
2.5	1	10908	1	0.646
5	1	10908	1	0.814

Table A.4–continued

10	1	10908	1	0.882
20	1	10908	1	1.185
1	5	10908	1	0.653
2.5	5	10908	1	0.799
5	5	10908	1	0.998
10	5	10908	1	1.148
20	5	10908	1	1.286
1	10	10908	1	0.798
2.5	10	10908	1	0.794
5	10	10908	1	1.038
10	10	10908	1	1.029
20	10	10908	1	1.169
1	0	11008	1	0.330
2.5	0	11008	1	0.435
5	0	11008	1	0.605
10	0	11008	1	0.707
20	0	11008	1	1.000
1	1	11008	1	0.283
2.5	1	11008	1	0.345
5	1	11008	1	0.613
10	1	11008	1	0.761
20	1	11008	1	1.151
1	5	11008	1	0.363
2.5	5	11008	1	0.474
5	5	11008	1	0.683
10	5	11008	1	0.867
20	5	11008	1	1.155
1	10	11008	1	0.395
2.5	10	11008	1	0.436
5	10	11008	1	0.686
10	10	11008	1	0.760
20	10	11008	1	1.167
1	0	11608	1	0.126
2.5	0	11608	1	0.270
5	0	11608	1	0.431
10	0	11608	1	0.625
20	0	11608	1	1.000
1	1	11608	1	0.107
2.5	1	11608	1	0.215
5	1	11608	1	0.360
10	1	11608	1	0.666
20	1	11608	1	1.122
1	5	11608	1	0.123
2.5	5	11608	1	0.250
5	5	11608	1	0.398
10	5	11608	1	0.735
20	5	11608	1	1.194
1	10	11608	1	0.136

Table A.4–continued

2.5	10	11608	1	0.265
5	10	11608	1	0.392
10	10	11608	1	0.646
20	10	11608	1	1.025

Figure A.4. SAS Data: Verapamil inhibition of mitoxantrone efflux in MCF10A cells (page 93, Figure 4.12, Table 4.7, data set: Table A.4)

The SAS System

The Mixed Procedure

Model Information

Data Set	WORK.DATAFILE
Dependent Variable	Fluorescence
Weight Variable	wt
Covariance Structure	Variance Components
Estimation Method	REML
Residual Variance Method	Profile
Fixed Effects SE Method	Model-Based
Degrees of Freedom Method	Containment

Class Level Information

Class	Levels	Values
Day	6	10308 10908 11008 11608 80207 82907
Rep	2	1 2

Dimensions

Covariance Parameters	3
Columns in X	4
Columns in Z	15
Subjects	1
Max Obs Per Subject	146

Number of Observations

Number of Observations Read	146
Number of Observations Used	146
Number of Observations Not Used	0

Iteration History

Iteration	Evaluations	-2 Res Log Like	Criterion
0	1	-48.14912409	
1	4	-232.03999604	0.00459528
2	1	-233.49588157	0.00193152
3	1	-234.09296895	0.00055977
4	1	-234.25748527	0.00007432
5	1	-234.27759542	0.00000183
6	1	-234.27805687	0.00000000

Figure A.4–continued

The SAS System

The Mixed Procedure

Convergence criteria met.

Covariance Parameter Estimates

Cov Parm	Estimate
Day	0.02347
Rep(Day)	1.26E-19
Residual	0.02223

Fit Statistics

-2 Res Log Likelihood	-234.3
AIC (smaller is better)	-230.3
AICC (smaller is better)	-230.2
BIC (smaller is better)	-230.7

Solution for Fixed Effects

Effect	Estimate	Standard Error	DF	t Value	Pr > |t|
Intercept	0.2277	0.06374	3	3.57	0.0375
Drug	0.06897	0.004218	134	16.35	<.0001
Drug*Drug	-0.00139	0.000222	134	-6.24	<.0001
Inhibitor	0.003952	0.001264	134	3.13	0.0022

Type 3 Tests of Fixed Effects

Effect	Num DF	Den DF	F Value	Pr > F
Drug	1	134	267.34	<.0001
Drug*Drug	1	134	38.92	<.0001
Inhibitor	1	134	9.77	0.0022

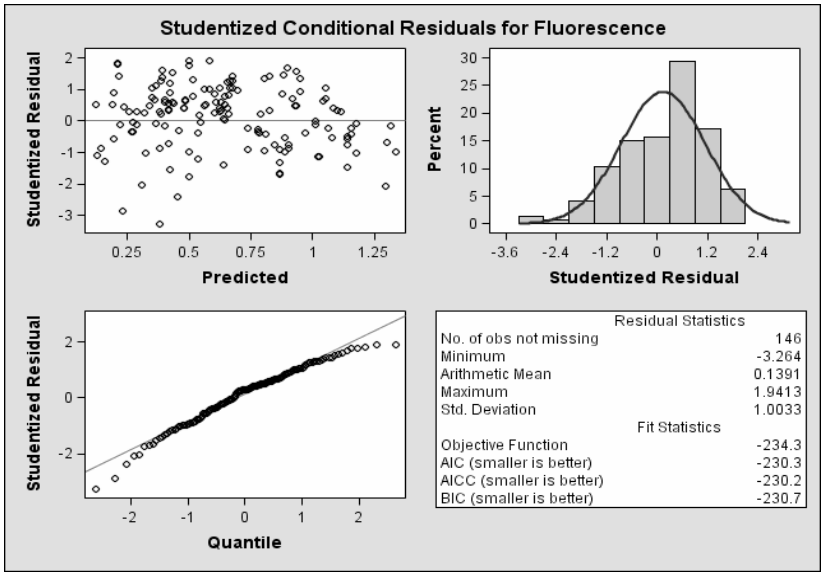

Table A.5. Flow cytometry data for FTC inhibition of mitoxantrone uptake

Drug Conc. (μM)	Inhibitor Conc. (μM)	Day	Rep	Fluorescence Intensity
2.5	0	71507	1	0.214
5	0	71507	1	0.324
10	0	71507	1	0.580
20	0	71507	1	1.000
2.5	5	71507	1	0.214
5	5	71507	1	0.245
10	5	71507	1	0.435
20	5	71507	1	0.957
2.5	10	71507	1	0.170
5	10	71507	1	0.260
10	10	71507	1	0.441
20	10	71507	1	0.689
2.5	0	72607	1	0.160
5	0	72607	1	0.287
10	0	72607	1	0.494
20	0	72607	1	1.000
2.5	5	72607	1	0.121
5	5	72607	1	0.215
10	5	72607	1	0.473
20	5	72607	1	0.733
2.5	10	72607	1	0.129
5	10	72607	1	0.218
10	10	72607	1	0.340
20	10	72607	1	0.663
2.5	0	91107	1	0.435
5	0	91107	1	0.619
10	0	91107	1	0.790
20	0	91107	1	0.967
2.5	10	91107	1	0.314
5	10	91107	1	0.515
10	10	91107	1	0.533
20	10	91107	1	0.776
2.5	0	91107	2	0.522
5	0	91107	2	0.657
10	0	91107	2	0.758
20	0	91107	2	1.033
2.5	10	91107	2	0.357
5	10	91107	2	0.433
10	10	91107	2	0.582
20	10	91107	2	0.807
2.5	0	91307	1	0.306
5	0	91307	1	0.472
10	0	91307	1	0.689
20	0	91307	1	0.988
2.5	10	91307	1	0.300
5	10	91307	1	0.518

Table A.5–continued

10	10	91307	1	0.692
20	10	91307	1	1.108
2.5	0	91307	2	0.308
5	0	91307	2	0.515
10	0	91307	2	0.653
20	0	91307	2	1.012
2.5	10	91307	2	0.315
5	10	91307	2	0.491
10	10	91307	2	0.735
20	10	91307	2	1.090
1	0	12308	1	0.130
2.5	0	12308	1	0.220
5	0	12308	1	0.404
10	0	12308	1	0.554
20	0	12308	1	1.081
1	1	12308	1	0.128
2.5	1	12308	1	0.193
5	1	12308	1	0.356
10	1	12308	1	0.579
20	1	12308	1	0.946
1	5	12308	1	0.131
2.5	5	12308	1	0.203
5	5	12308	1	0.388
10	5	12308	1	0.551
20	5	12308	1	0.985
1	10	12308	1	0.101
2.5	10	12308	1	0.184
5	10	12308	1	0.372
10	10	12308	1	0.468
20	10	12308	1	0.887
1	0	12308	2	0.110
2.5	0	12308	2	0.209
5	0	12308	2	0.355
10	0	12308	2	0.562
20	0	12308	2	0.919
1	1	12308	2	0.107
2.5	1	12308	2	0.177
5	1	12308	2	0.332
10	1	12308	2	0.639
20	1	12308	2	0.877
1	5	12308	2	0.103
2.5	5	12308	2	0.162
5	5	12308	2	0.322
10	5	12308	2	0.451
20	5	12308	2	0.932
1	10	12308	2	0.082
2.5	10	12308	2	0.139
5	10	12308	2	0.269

Table A.5–continued

10	10	12308	2	0.439
20	10	12308	2	0.796
1	0	12208	1	0.160
2.5	0	12208	1	0.289
5	0	12208	1	0.432
10	0	12208	1	0.665
20	0	12208	1	1.060
1	1	12208	1	0.148
2.5	1	12208	1	0.252
5	1	12208	1	0.438
10	1	12208	1	0.621
20	1	12208	1	0.977
1	5	12208	1	0.116
2.5	5	12208	1	0.220
5	5	12208	1	0.385
10	5	12208	1	0.607
20	5	12208	1	0.907
1	10	12208	1	0.128
2.5	10	12208	1	0.238
5	10	12208	1	0.416
10	10	12208	1	0.657
20	10	12208	1	0.892
1	0	12208	2	0.140
2.5	0	12208	2	0.259
5	0	12208	2	0.436
10	0	12208	2	0.632
20	0	12208	2	0.940
1	1	12208	2	0.095
2.5	1	12208	2	0.205
5	1	12208	2	0.332
10	1	12208	2	0.562
20	1	12208	2	0.985
1	5	12208	2	0.135
2.5	5	12208	2	0.179
5	5	12208	2	0.300
10	5	12208	2	0.476
20	5	12208	2	0.735
1	10	12208	2	0.098
2.5	10	12208	2	0.182
5	10	12208	2	0.282
10	10	12208	2	0.458
20	10	12208	2	0.704
1	0	11708	1	0.146
2.5	0	11708	1	0.320
5	0	11708	1	0.465
10	0	11708	1	0.785
20	0	11708	1	1.019
1	1	11708	1	0.124

Table A.5–continued

2.5	1	11708	1	0.240
5	1	11708	1	0.400
10	1	11708	1	0.675
20	1	11708	1	1.004
1	5	11708	1	0.095
2.5	5	11708	1	0.215
5	5	11708	1	0.301
10	5	11708	1	0.509
20	5	11708	1	0.883
1	10	11708	1	0.117
2.5	10	11708	1	0.164
5	10	11708	1	0.397
10	10	11708	1	0.590
20	10	11708	1	0.995
1	0	11708	2	0.109
2.5	0	11708	2	0.205
5	0	11708	2	0.379
10	0	11708	2	0.607
20	0	11708	2	0.981
1	1	11708	2	0.123
2.5	1	11708	2	0.209
5	1	11708	2	0.273
10	1	11708	2	0.741
20	1	11708	2	0.964
1	5	11708	2	0.116
2.5	5	11708	2	0.198
5	5	11708	2	0.315
10	5	11708	2	0.447
20	5	11708	2	1.021
1	10	11708	2	0.121
2.5	10	11708	2	0.204
5	10	11708	2	0.333
10	10	11708	2	0.556
20	10	11708	2	0.850

Figure A.5. SAS Data: FTC inhibition of mitoxantrone uptake in MCF10A cells (page 94, Figure 4.13, Table 4.8)

The SAS System

The Mixed Procedure

Model Information

Data Set	WORK.DATAFILE
Dependent Variable	Fluorescence
Weight Variable	wt
Covariance Structure	Variance Components
Estimation Method	REML
Residual Variance Method	Profile
Fixed Effects SE Method	Model-Based
Degrees of Freedom Method	Containment

Class Level Information

Class	Levels	Values
Day	7	11708 12208 12308 71507 72607 91107 91307
Rep	2	1 2

Dimensions

Covariance Parameters	3
Columns in X	5
Columns in Z	19
Subjects	1
Max Obs Per Subject	176

Number of Observations

Number of Observations Read	176
Number of Observations Used	176
Number of Observations Not Used	0

Iteration History

Iteration	Evaluations	-2 Res Log Like	Criterion
0	1	-342.46607603	
1	2	-436.37582883	0.03399258
2	1	-453.32261672	0.02110399
3	1	-464.04071885	0.01265385
4	1	-470.52341973	0.00717297
5	1	-474.19867603	0.00368870
6	1	-476.07091618	0.00158692
7	1	-476.85759089	0.00048166
8	1	-477.08518408	0.00007057
9	1	-477.11594930	0.00000215

Figure A.5–continued

The SAS System

The Mixed Procedure

Iteration History

Iteration	Evaluations	-2 Res Log Like	Criterion
10	1	-477.11681813	0.00000000

Convergence criteria met.

Covariance Parameter Estimates

Cov Parm	Estimate
Day	0.006809
Rep(Day)	0.000264
Residual	0.01556

Fit Statistics

-2 Res Log Likelihood	-477.1
AIC (smaller is better)	-471.1
AICC (smaller is better)	-471.0
BIC (smaller is better)	-471.3

Solution for Fixed Effects

Effect	Estimate	Standard Error	DF	t Value	Pr > |t|
Intercept	0.09194	0.03235	5	2.84	0.0361
Drug	0.06312	0.002286	160	27.62	<.0001
Drug*Drug	-0.00089	0.000119	160	-7.50	<.0001
Inhibitor	-0.00119	0.000705	160	-1.68	0.0946
Drug*Inhibitor	-0.00098	0.000180	160	-5.46	<.0001

Type 3 Tests of Fixed Effects

Effect	Num DF	Den DF	F Value	Pr > F
Drug	1	160	762.75	<.0001
Drug*Drug	1	160	56.27	<.0001
Inhibitor	1	160	2.83	0.0946
Drug*Inhibitor	1	160	29.83	<.0001

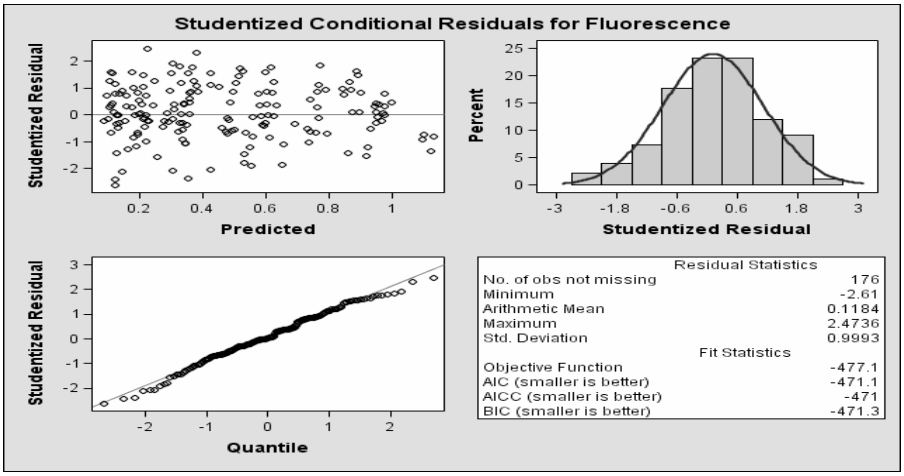

Table A.6. Flow cytometry data for FTC inhibition of mitoxantrone efflux

Drug Conc. (μM)	Inhibitor Conc. (μM)	Day	Rep	Fluorescence Intensity
1	0	61807	1	0.297
2	0	61807	1	0.375
5	0	61807	1	0.498
10	0	61807	1	0.783
20	0	61807	1	1.000
1	1	61807	1	0.265
2	1	61807	1	0.345
5	1	61807	1	0.543
10	1	61807	1	1.044
20	1	61807	1	1.181
1	5	61807	1	0.330
2	5	61807	1	0.351
5	5	61807	1	0.653
10	5	61807	1	1.212
20	5	61807	1	1.288
1	10	61807	1	0.306
2	10	61807	1	0.345
5	10	61807	1	0.689
10	10	61807	1	1.056
20	10	61807	1	1.235
2.5	0	71507	1	0.215
5	0	71507	1	0.349
10	0	71507	1	0.545
20	0	71507	1	1.000
2.5	1	71507	1	0.209
5	1	71507	1	0.282
10	1	71507	1	0.464
20	1	71507	1	1.081
2.5	5	71507	1	0.206
5	5	71507	1	0.316
10	5	71507	1	0.532
20	5	71507	1	0.746
2.5	10	71507	1	0.203
5	10	71507	1	0.319
10	10	71507	1	0.457
20	10	71507	1	0.861
2.5	0	72607	1	0.237
5	0	72607	1	0.371
10	0	72607	1	0.680
20	0	72607	1	1.000
2.5	1	72607	1	0.191
5	1	72607	1	0.315
10	1	72607	1	0.735
20	1	72607	1	0.979
2.5	5	72607	1	0.215
5	5	72607	1	0.362

Table A.6–continued

10	5	72607	1	0.507
20	5	72607	1	0.876
2.5	10	72607	1	0.217
5	10	72607	1	0.310
10	10	72607	1	0.585
20	10	72607	1	0.931
2.5	0	91107	1	0.610
5	0	91107	1	0.813
10	0	91107	1	0.814
20	0	91107	1	1.047
2.5	10	91107	1	0.252
5	10	91107	1	0.511
10	10	91107	1	0.611
20	10	91107	1	0.840
2.5	0	91107	2	0.576
5	0	91107	2	0.841
10	0	91107	2	0.776
20	0	91107	2	0.953
2.5	10	91107	2	0.219
5	10	91107	2	0.409
10	10	91107	2	0.539
20	10	91107	2	0.732
2.5	0	91307	1	0.277
5	0	91307	1	0.394
10	0	91307	1	0.637
20	0	91307	1	1.012
2.5	10	91307	1	0.264
5	10	91307	1	0.500
10	10	91307	1	0.706
20	10	91307	1	0.921
2.5	0	91307	2	0.270
5	0	91307	2	0.430
10	0	91307	2	0.662
20	0	91307	2	0.988
2.5	10	91307	2	0.265
5	10	91307	2	0.473
10	10	91307	2	0.706
20	10	91307	2	1.031
1	0	12407	1	0.163
2.5	0	12407	1	0.251
5	0	12407	1	0.492
10	0	12407	1	0.762
20	0	12407	1	1.034
1	1	12407	1	0.134
2.5	1	12407	1	0.214
5	1	12407	1	0.459
10	1	12407	1	0.747
20	1	12407	1	1.006

Table A.6–continued

1	5	12407	1	0.172
2.5	5	12407	1	0.266
5	5	12407	1	0.440
10	5	12407	1	0.727
20	5	12407	1	0.982
1	10	12407	1	0.130
2.5	10	12407	1	0.265
5	10	12407	1	0.529
10	10	12407	1	0.680
20	10	12407	1	0.963
1	0	12407	2	0.164
2.5	0	12407	2	0.240
5	0	12407	2	0.520
10	0	12407	2	0.667
20	0	12407	2	0.966
1	1	12407	2	0.144
2.5	1	12407	2	0.229
5	1	12407	2	0.514
10	1	12407	2	0.844
20	1	12407	2	0.974
1	5	12407	2	0.120
2.5	5	12407	2	0.240
5	5	12407	2	0.425
10	5	12407	2	0.698
20	5	12407	2	0.994
1	10	12407	2	0.099
2.5	10	12407	2	0.197
5	10	12407	2	0.437
10	10	12407	2	0.678
20	10	12407	2	0.901

Figure A.6. SAS Data: FTC inhibition of mitoxantrone efflux in MCF10A cells (page 95, Figure 4.14, Table 4.9, data set: Table A.6)

The SAS System

The Mixed Procedure

Model Information

Data Set	WORK.DATAFILE
Dependent Variable	Fluorescence
Weight Variable	wt
Covariance Structure	Variance Components
Estimation Method	REML
Residual Variance Method	Profile
Fixed Effects SE Method	Model-Based
Degrees of Freedom Method	Containment

Class Level Information

Class	Levels	Values
Day	4	12407 61807 71507 91107
Rep	2	1 2

Dimensions

Covariance Parameters	3
Columns in X	5
Columns in Z	10
Subjects	1
Max Obs Per Subject	92

Number of Observations

Number of Observations Read	92
Number of Observations Used	92
Number of Observations Not Used	0

Iteration History

Iteration	Evaluations	-2 Res Log Like	Criterion
0	1	-79.71265594	
1	3	-137.90763734	0.03340041
2	2	-138.08232176	0.00475059
3	2	-138.96581243	0.00199686
4	1	-139.33790854	0.00056505
5	1	-139.43821010	0.00007475
6	1	-139.45044104	0.00000186
7	1	-139.45072472	0.00000000

Figure A.6–continued

The SAS System

The Mixed Procedure

Convergence criteria met.

Covariance Parameter Estimates

Cov Parm	Estimate
Day	0.008872
Rep(Day)	0.000118
Residual	0.02875

Fit Statistics

-2 Res Log Likelihood	-139.5
AIC (smaller is better)	-133.5
AICC (smaller is better)	-133.2
BIC (smaller is better)	-135.3

Solution for Fixed Effects

Effect	Estimate	Standard Error	DF	t Value	Pr > |t|
Intercept	0.1039	0.05005	2	2.08	0.1736
Drug	0.08058	0.005428	82	14.85	<.0001
Drug*Drug	-0.00179	0.000271	82	-6.63	<.0001
Inhibitor	-0.00272	0.001657	82	-1.64	0.1043
Drug*Inhibitor	-0.00052	0.000374	82	-1.39	0.1677

Type 3 Tests of Fixed Effects

Effect	Num DF	Den DF	F Value	Pr > F
Drug	1	82	220.39	<.0001
Drug*Drug	1	82	44.01	<.0001
Inhibitor	1	82	2.70	0.1043
Drug*Inhibitor	1	82	1.94	0.1677

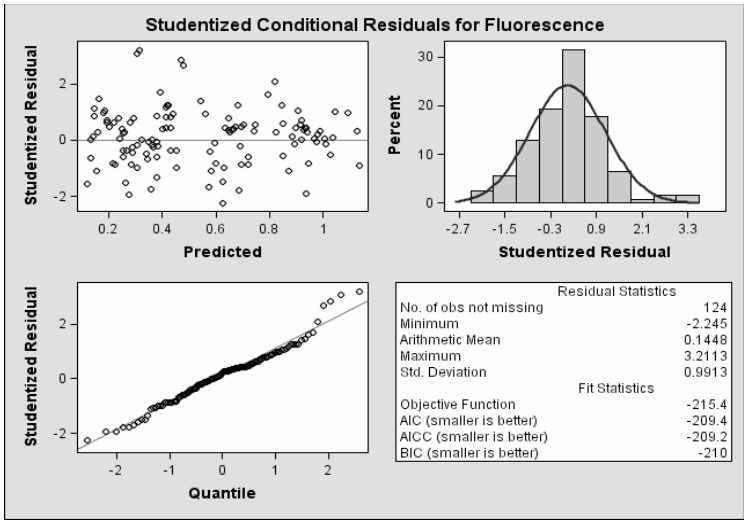

Table A.7. Flow cytometry data for 2,4-DNP inhibition of A-K-AMCA uptake

Drug Conc. (mM)	Inhibitor Conc. (mM)	Day	Rep	Fluorescence Intensity
0.025	0	90408	1	0.030
0.05	0	90408	1	0.045
0.1	0	90408	1	0.086
0.25	0	90408	1	0.334
0.5	0	90408	1	0.513
0.025	0	90408	2	0.023
0.05	0	90408	2	0.033
0.1	0	90408	2	0.098
0.25	0	90408	2	0.213
0.5	0	90408	2	0.465
0.025	1	90408	1	-0.012
0.05	1	90408	1	-0.010
0.1	1	90408	1	0.056
0.25	1	90408	1	0.185
0.5	1	90408	1	0.341
0.025	1	90408	2	-0.009
0.05	1	90408	2	0.006
0.1	1	90408	2	0.075
0.25	1	90408	2	0.268
0.5	1	90408	2	0.414
0.1	0	82808	1	0.145
0.25	0	82808	1	0.286
0.5	0	82808	1	0.719
0.75	0	82808	1	0.716
1	0	82808	1	0.997
0.1	0	82808	2	0.139
0.25	0	82808	2	0.268
0.5	0	82808	2	0.633
0.75	0	82808	2	0.770
1	0	82808	2	1.128
0.1	1	82808	1	0.081
0.25	1	82808	1	0.129
0.5	1	82808	1	0.344
1	1	82808	1	0.907
0.1	1	82808	2	0.049
0.25	1	82808	2	0.108
0.1	0	82708	1	0.084
0.25	0	82708	1	0.276
0.5	0	82708	1	0.561
0.75	0	82708	1	0.805
1	0	82708	1	0.879
0.1	0	82708	2	0.147
0.25	0	82708	2	0.309
0.5	0	82708	2	0.618
0.75	0	82708	2	0.786
1	0	82708	2	1.159

Table A.7–continued

0.1	1	82708	1	0.129
0.25	1	82708	1	0.209
0.5	1	82708	1	0.394
0.75	1	82708	1	0.585
1	1	82708	1	0.671
0.1	1	82708	2	0.122
0.25	1	82708	2	0.259
0.5	1	82708	2	0.377
0.75	1	82708	2	0.633
1	1	82708	2	0.782
0.1	0	82608	1	0.194
0.25	0	82608	1	0.352
0.5	0	82608	1	0.591
0.75	0	82608	1	0.692
1	0	82608	1	0.944
0.1	0	82608	2	0.000
0.25	0	82608	2	0.328
0.5	0	82608	2	0.651
0.75	0	82608	2	0.826
1	0	82608	2	1.154
0.1	1	82608	1	0.062
0.25	1	82608	1	0.193
0.5	1	82608	1	0.339
0.75	1	82608	1	0.408
1	1	82608	1	0.543
0.1	1	82608	2	0.093
0.25	1	82608	2	0.313
0.5	1	82608	2	0.280
0.75	1	82608	2	0.391
1	1	82608	2	0.555

Figure A.7. SAS Data: 2,4-DNP inhibition of A-K-AMCA uptake in MCF10A cells (page 119, Figure 5.12, Table 5.2, data set: Table A.7)

The SAS System

The Mixed Procedure

Model Information

Data Set	WORK.DATAFILE
Dependent Variable	Fluorescence
Weight Variable	wt
Covariance Structure	Variance Components
Estimation Method	REML
Residual Variance Method	Profile
Fixed Effects SE Method	Model-Based
Degrees of Freedom Method	Containment

Class Level Information

Class	Levels	Values
Day	4	82608 82708 82808 90408
Rep	2	1 2

Dimensions

Covariance Parameters	3
Columns in X	5
Columns in Z	12
Subjects	1
Max Obs Per Subject	76

Number of Observations

Number of Observations Read	76
Number of Observations Used	75
Number of Observations Not Used	1

Iteration History

Iteration	Evaluations	-2 Res Log Like	Criterion
0	1	-148.88692829	
1	3	-164.75580701	0.00008502
2	1	-164.77032326	0.00000833
3	1	-164.77163226	0.00000011
4	1	-164.77164904	0.00000000

Convergence criteria met.

Figure A.7–continued

The SAS System

The Mixed Procedure

Covariance Parameter Estimates

Cov Parm	Estimate
Day	0.000436
Rep(Day)	0.000043
Residual	0.07158

Fit Statistics

-2 Res Log Likelihood	-164.8
AIC (smaller is better)	-158.8
AICC (smaller is better)	-158.4
BIC (smaller is better)	-160.6

Solution for Fixed Effects

Effect	Estimate	Standard Error	DF	t Value	Pr > |t|
Intercept	0.02068	0.01374	3	1.50	0.2294
Drug	1.0040	0.08765	63	11.46	<.0001
Drug*Drug	0.002140	0.09596	63	0.02	0.9823
Inhibitor	-0.02529	0.005134	63	-4.93	<.0001
Drug*Inhibitor	-0.3524	0.06803	63	-5.18	<.0001

Type 3 Tests of Fixed Effects

Effect	Num DF	Den DF	F Value	Pr > F
Drug	1	63	131.22	<.0001
Drug*Drug	1	63	0.00	0.9823
Inhibitor	1	63	24.27	<.0001
Drug*Inhibitor	1	63	26.83	<.0001

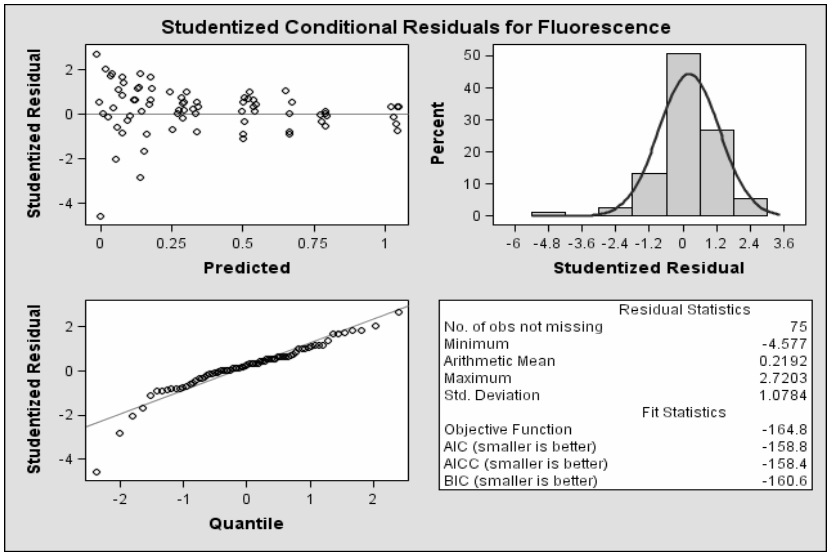

Table A.8. Flow cytometry data for cefadroxil inhibition of A-K-AMCA uptake

Drug Conc. (mM)	Inhibitor Conc. (mM)	Day	Rep	Fluorescence Intensity
0.1	0	82908	1	0.111
0.25	0	82908	1	0.256
0.5	0	82908	1	0.553
0.75	0	82908	1	0.666
1	0	82908	1	1.048
0.1	0	82908	2	0.097
0.25	0	82908	2	0.211
0.5	0	82908	2	0.499
0.75	0	82908	2	0.826
1	0	82908	2	0.918
0.1	0.5	82908	1	0.106
0.25	0.5	82908	1	0.256
0.5	0.5	82908	1	0.489
0.75	0.5	82908	1	0.839
1	0.5	82908	1	1.180
0.1	1	82908	1	0.116
0.25	1	82908	1	0.263
0.5	1	82908	1	0.449
0.75	1	82908	1	1.005
1	1	82908	1	1.132
0.1	5	82908	1	0.180
0.25	5	82908	1	0.332
0.5	5	82908	1	0.625
0.75	5	82908	1	0.828
1	5	82908	1	1.024
0.01	0	90308	1	0.011
0.025	0	90308	1	0.027
0.05	0	90308	1	0.069
0.1	0	90308	1	0.120
0.25	0	90308	1	0.250
0.01	0.025	90308	1	0.011
0.025	0.025	90308	1	0.036
0.05	0.025	90308	1	0.082
0.1	0.025	90308	1	0.137
0.25	0.025	90308	1	0.315
0.01	1	90308	1	0.027
0.025	1	90308	1	0.048
0.05	1	90308	1	0.077
0.1	1	90308	1	0.133
0.25	1	90308	1	0.323
0.01	5	90308	1	0.119
0.025	5	90308	1	0.134
0.05	5	90308	1	0.169
0.1	5	90308	1	0.233
0.25	5	90308	1	0.399
0.01	0	90208	1	0.014

Table A.8–continued

0.025	0	90208	1	0.025
0.05	0	90208	1	0.050
0.1	0	90208	1	0.105
0.25	0	90208	1	0.250
0.01	0.25	90208	1	0.017
0.025	0.25	90208	1	0.035
0.05	0.25	90208	1	0.054
0.1	0.25	90208	1	0.092
0.25	0.25	90208	1	0.244
0.01	0.5	90208	1	0.021
0.025	0.5	90208	1	0.037
0.05	0.5	90208	1	0.055
0.1	0.5	90208	1	0.089
0.25	0.5	90208	1	0.236
0.01	1	90208	1	0.026
0.025	1	90208	1	0.036
0.05	1	90208	1	0.048
0.1	1	90208	1	0.101
0.25	1	90208	1	0.230
0.025	0	90408	1	0.030
0.05	0	90408	1	0.045
0.1	0	90408	1	0.086
0.25	0	90408	1	0.334
0.5	0	90408	1	0.513
0.025	0	90408	2	0.023
0.05	0	90408	2	0.033
0.1	0	90408	2	0.098
0.25	0	90408	2	0.213
0.5	0	90408	2	0.465
0.025	10	90408	1	0.008
0.05	10	90408	1	0.008
0.1	10	90408	1	0.008
0.25	10	90408	1	0.008
0.5	10	90408	1	0.008
0.025	10	90408	2	0.017
0.05	10	90408	2	0.017
0.1	10	90408	2	0.017
0.25	10	90408	2	0.017
0.5	10	90408	2	0.017
0.025	5	90408	1	0.008
0.05	5	90408	1	0.008
0.1	5	90408	1	0.008
0.25	5	90408	1	0.008
0.5	5	90408	1	0.008
0.025	5	90408	2	0.017
0.05	5	90408	2	0.017
0.1	5	90408	2	0.017
0.25	5	90408	2	0.017

Table A.8–continued

0.5	5	90408	2	0.017
0	0.25	90808	1	0.014
0	0.5	90808	1	0.012
0	1	90808	1	0.018
0	5	90808	1	0.133
0	10	90808	1	0.321
0	0.25	90808	2	0.005
0	0.5	90808	2	0.008
0	1	90808	2	0.022
0	5	90808	2	0.121
0	10	90808	2	0.284
0.1	0	90808	1	0.089
0.25	0	90808	1	0.296
0.5	0	90808	1	0.489
0.75	0	90808	1	0.601
1	0	90808	1	1.143
0.1	0	90808	2	0.098
0.25	0	90808	2	0.346
0.5	0	90808	2	0.531
0.75	0	90808	2	0.810
1	0	90808	2	0.969
0.1	5	90808	1	0.237
0.25	5	90808	1	0.401
0.5	5	90808	1	0.586
0.75	5	90808	1	0.873
1	5	90808	1	1.262
0.1	5	90808	2	0.240
0.25	5	90808	2	0.428
0.5	5	90808	2	0.506
0.75	5	90808	2	0.812
1	5	90808	2	1.265
0.1	10	90808	1	0.426
0.25	10	90808	1	0.563
0.5	10	90808	1	0.886
0.75	10	90808	1	1.082
1	10	90808	1	1.748
0.1	10	90808	2	0.375
0.25	10	90808	2	0.587
0.5	10	90808	2	0.803
0.75	10	90808	2	0.923
1	10	90808	2	1.251
2	0	90808	1	2.243
0.05	0	92308	1	0.048
0.1	0	92308	1	0.229
0.25	0	92308	1	0.266
0.4	0	92308	1	0.417
0.5	0	92308	1	0.529
0.05	0	92308	2	0.053

Table A.8–continued

0.1	0	92308	2	0.095
0.25	0	92308	2	0.571
0.4	0	92308	2	0.459
0.5	0	92308	2	0.589
0.05	0	92308	3	0.048
0.1	0	92308	3	0.137
0.25	0	92308	3	0.309
0.4	0	92308	3	0.477
0.5	0	92308	3	0.680
0.05	1	92308	1	0.067
0.1	1	92308	1	0.127
0.25	1	92308	1	0.237
0.4	1	92308	1	0.370
0.5	1	92308	1	0.541
0.05	1	92308	2	0.063
0.1	1	92308	2	0.146
0.25	1	92308	2	0.306
0.4	1	92308	2	0.729
0.5	1	92308	2	0.542
0.05	5	92308	1	0.158
0.1	5	92308	1	0.214
0.25	5	92308	1	0.447
0.4	5	92308	1	0.562
0.5	5	92308	1	0.789
0.05	5	92308	2	0.150
0.1	5	92308	2	0.226
0.25	5	92308	2	0.403
0.4	5	92308	2	0.600
0.5	5	92308	2	0.839
0.05	10	92308	1	0.268
0.1	10	92308	1	0.316
0.25	10	92308	1	0.452
0.4	10	92308	1	0.697
0.5	10	92308	1	0.985
0.05	10	92308	2	0.258
0.1	10	92308	2	0.362
0.25	10	92308	2	0.471
0.4	10	92308	2	0.681
0.5	10	92308	2	0.844
0.05	0.5	92308	1	0.066
0.1	0.5	92308	1	0.125
0.25	0.5	92308	1	0.293
0.4	0.5	92308	1	0.513
0.5	0.5	92308	1	0.599
0.05	0.5	92308	2	0.065
0.1	0.5	92308	2	0.138
0.25	0.5	92308	2	0.317
0.5	0.5	92308	2	0.580

Figure A.8. SAS Data: Cefadroxil inhibition of A-K-AMCA uptake in MCF10A cells (page 120, Figure 5.13, Table 5.3, data set: Table A.8)

The SAS System

The Mixed Procedure

Model Information

Data Set	WORK.DATAFILE
Dependent Variable	Fluorescence
Weight Variable	wt
Covariance Structure	Variance Components
Estimation Method	REML
Residual Variance Method	Profile
Fixed Effects SE Method	Model-Based
Degrees of Freedom Method	Containment

Class Level Information

Class	Levels	Values
Day	4	82908 90208 90308 90808
Rep	2	1 2

Dimensions

Covariance Parameters	3
Columns in X	4
Columns in Z	10
Subjects	1
Max Obs Per Subject	75

Number of Observations

Number of Observations Read	75
Number of Observations Used	75
Number of Observations Not Used	0

Iteration History

Iteration	Evaluations	-2 Res Log Like	Criterion
0	1	-336.48760506	
1	3	-340.38383140	0.00141777
2	2	-340.51610059	0.00013974
3	1	-340.55359408	0.00000886
4	1	-340.55577531	0.00000004
5	1	-340.55578590	0.00000000

Convergence criteria met.

Figure A.8–continued

The SAS System

The Mixed Procedure

Covariance Parameter Estimates

Cov Parm	Estimate
Day	0
Rep(Day)	2.792E-6
Residual	0.02829

Fit Statistics

-2 Res Log Likelihood	-340.6
AIC (smaller is better)	-336.6
AICC (smaller is better)	-336.4
BIC (smaller is better)	-337.8

Solution for Fixed Effects

Effect	Estimate	Standard Error	DF	t Value	Pr > |t|
Intercept	0.001275	0.001138	2	1.12	0.3789
Drug	0.9678	0.04266	66	22.69	<.0001
Drug*Drug	0.05508	0.08652	66	0.64	0.5266
Inhibitor	0.02002	0.001283	66	15.60	<.0001

Type 3 Tests of Fixed Effects

Effect	Num DF	Den DF	F Value	Pr > F
Drug	1	66	514.71	<.0001
Drug*Drug	1	66	0.41	0.5266
Inhibitor	1	66	243.37	<.0001

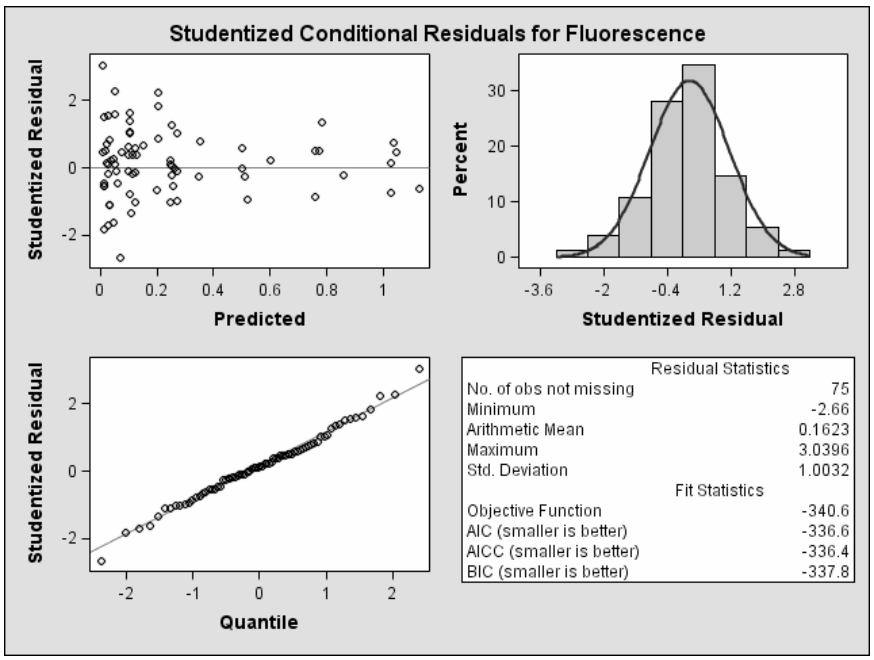

Table A.9. Flow cytometry data for Gly-Gln inhibition of A-K-AMCA uptake

Drug Conc. (mM)	Inhibitor Conc. (mM)	Day	Rep	Fluorescence Intensity
0.1	0	82908	1	0.111
0.25	0	82908	1	0.256
0.5	0	82908	1	0.553
0.75	0	82908	1	0.666
1	0	82908	1	1.048
0.1	0	82908	2	0.097
0.25	0	82908	2	0.211
0.5	0	82908	2	0.499
0.75	0	82908	2	0.826
1	0	82908	2	0.918
0.1	0.5	82908	1	0.097
0.25	0.5	82908	1	0.245
0.5	0.5	82908	1	0.534
0.75	0.5	82908	1	0.813
1	0.5	82908	1	1.231
0.1	1	82908	1	0.108
0.25	1	82908	1	0.250
0.5	1	82908	1	0.589
0.75	1	82908	1	0.776
1	1	82908	1	1.165
0.1	5	82908	1	0.088
0.25	5	82908	1	0.230
0.5	5	82908	1	0.503
0.75	5	82908	1	0.845
1	5	82908	1	1.316
0.01	0	90308	1	0.011
0.025	0	90308	1	0.027
0.05	0	90308	1	0.069
0.1	0	90308	1	0.120
0.25	0	90308	1	0.250
0.01	0.025	90308	1	0.014
0.025	0.025	90308	1	0.033
0.05	0.025	90308	1	0.082
0.1	0.025	90308	1	0.127
0.25	0.025	90308	1	0.289
0.01	1	90308	1	0.011
0.025	1	90308	1	0.031
0.05	1	90308	1	0.059
0.1	1	90308	1	0.114
0.25	1	90308	1	0.356
0.01	5	90308	1	0.010
0.025	5	90308	1	0.032
0.05	5	90308	1	0.063
0.1	5	90308	1	0.112
0.25	5	90308	1	0.286
0.01	0	90208	1	0.014

Table A.9–continued

0.025	0	90208	1	0.025
0.05	0	90208	1	0.050
0.1	0	90208	1	0.105
0.25	0	90208	1	0.250
0.01	0.25	90208	1	0.010
0.025	0.25	90208	1	0.027
0.05	0.25	90208	1	0.046
0.1	0.25	90208	1	0.096
0.25	0.25	90208	1	0.226
0.01	0.5	90208	1	0.012
0.025	0.5	90208	1	0.020
0.05	0.5	90208	1	0.043
0.1	0.5	90208	1	0.079
0.25	0.5	90208	1	0.233
0.01	1	90208	1	0.011
0.025	1	90208	1	0.025
0.05	1	90208	1	0.047
0.1	1	90208	1	0.089
0.25	1	90208	1	0.221
0.025	0	90408	1	0.030
0.05	0	90408	1	0.045
0.1	0	90408	1	0.086
0.25	0	90408	1	0.334
0.5	0	90408	1	0.513
0.025	0	90408	2	0.023
0.05	0	90408	2	0.033
0.1	0	90408	2	0.098
0.25	0	90408	2	0.213
0.5	0	90408	2	0.465
0.025	10	90408	1	0.029
0.05	10	90408	1	0.042
0.1	10	90408	1	0.081
0.25	10	90408	1	0.098
0.5	10	90408	1	0.499
0.025	10	90408	2	0.018
0.05	10	90408	2	0.042
0.1	10	90408	2	0.112
0.25	10	90408	2	0.214
0.5	10	90408	2	0.241
0.025	5	90408	1	0.022
0.05	5	90408	1	0.051
0.1	5	90408	1	0.103
0.25	5	90408	1	0.190
0.5	5	90408	1	0.524
0.025	5	90408	2	0.021
0.05	5	90408	2	0.045
0.1	5	90408	2	0.093
0.25	5	90408	2	0.253

Table A.9–continued

0.5	5	90408	2	0.380
0	5	90808	1	0.003
0	10	90808	1	0.007
0.1	0	90808	1	0.089
0.25	0	90808	1	0.296
0.5	0	90808	1	0.489
0.75	0	90808	1	0.601
1	0	90808	1	1.143
0.1	0	90808	2	0.098
0.25	0	90808	2	0.346
0.5	0	90808	2	0.531
0.75	0	90808	2	0.810
1	0	90808	2	0.969
0.1	5	90808	1	0.089
0.25	5	90808	1	0.341
0.5	5	90808	1	0.447
0.75	5	90808	1	0.701
1	5	90808	1	0.892
0.1	5	90808	2	0.097
0.25	5	90808	2	0.211
0.5	5	90808	2	0.481
0.75	5	90808	2	0.754
1	5	90808	2	0.916
0.1	10	90808	1	0.119
0.25	10	90808	1	0.265
0.5	10	90808	1	0.440
0.75	10	90808	1	0.703
1	10	90808	1	0.821
0.1	10	90808	2	0.088
0.25	10	90808	2	0.246
0.5	10	90808	2	0.466
0.75	10	90808	2	0.838
1	10	90808	2	1.093
2	0	90808	1	2.243

Figure A.9. SAS data: Gly-Gln Inhibition of A-K-AMCA uptake in MCF10A cells (page 122, Figure 5.16, Table 5.4, data set: Table A.9)

The SAS System

The Mixed Procedure

Model Information

Data Set	WORK.DATAFILE
Dependent Variable	Fluorescence
Weight Variable	wt
Covariance Structure	Variance Components
Estimation Method	REML
Residual Variance Method	Profile
Fixed Effects SE Method	Model-Based
Degrees of Freedom Method	Containment

Class Level Information

Class	Levels	Values
Day	5	82908 90208 90308 90408 90808
Rep	2	1 2

Dimensions

Covariance Parameters	3
Columns in X	5
Columns in Z	13
Subjects	1
Max Obs Per Subject	128

Number of Observations

Number of Observations Read	128
Number of Observations Used	128
Number of Observations Not Used	0

Iteration History

Iteration	Evaluations	-2 Res Log Like	Criterion
0	1	-509.69742561	
1	3	-510.14872514	0.00000008
2	1	-510.14875514	0.00000000

Convergence criteria met.

Figure A.9–continued

The SAS System

The Mixed Procedure

Covariance Parameter Estimates

Cov Parm	Estimate
Day	0
Rep(Day)	1.527E-6
Residual	0.03613

Fit Statistics

-2 Res Log Likelihood	-510.1
AIC (smaller is better)	-506.1
AICC (smaller is better)	-506.0
BIC (smaller is better)	-506.9

Solution for Fixed Effects

Effect	Estimate	Standard Error	DF	t Value	Pr > |t|
Intercept	0.000501	0.001106	3	0.45	0.6814
Drug	0.9794	0.03410	116	28.72	<.0001
Drug*Drug	0.09866	0.05589	116	1.77	0.0802
Inhibitor	0.000520	0.000188	116	2.77	0.0066
Drug*Inhibitor	-0.02810	0.004556	116	-6.17	<.0001

Type 3 Tests of Fixed Effects

Effect	Num DF	Den DF	F Value	Pr > F
Drug	1	116	824.77	<.0001
Drug*Drug	1	116	3.12	0.0802
Inhibitor	1	116	7.66	0.0066
Drug*Inhibitor	1	116	38.04	<.0001

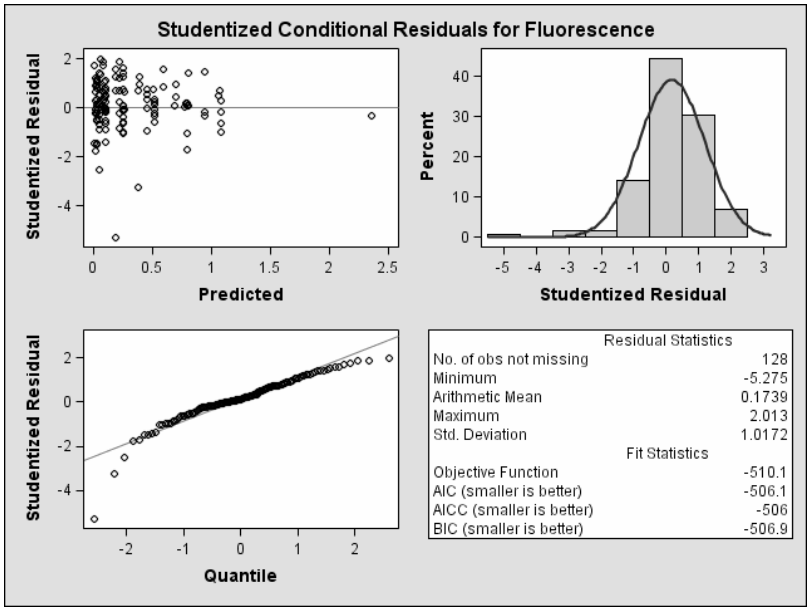

Linear Mixed Effects Models for 2,4-DNP Inhibition of Mitoxantrone Uptake

Table A.10. Linear mixed effects model parameters for 2,4-DNP inhibition of mitoxantrone uptake. Full model without weighting or normalization.

Variability Parameter	Estimate	Fixed Effect	Estimate	Standard Error	p-value
Day	2319.73	**Intercept**	6.3948	32.5354	0.8623
Rep (Day)	0.00E+00	**Drug**	15.8216	3.5731	<.0001
Residual	1718.1	**Drug^2**	-0.1855	0.1549	0.2386
AIC	484.3	**Inhibitor**	-7.2988	19.3086	0.7075
Weighting	no	**Drug*Inhibitor**	-1.2974	1.6838	0.4458
Normalization	no				

Table A.11. Linear mixed effects model parameters for 2,4-DNP inhibition of mitoxantrone uptake. Full model with weighting and without normalization.

Variability Parameter	Estimate	Fixed Effect	Estimate	Standard Error	p-value
Day	13.7026	**Intercept**	3.4506	4.2544	0.5025
Rep (Day)	0.00E+00	**Drug**	13.5671	2.1577	<.0001
Residual	0.1389	**Drug^2**	-0.2678	0.1142	0.0244
AIC	447.2	**Inhibitor**	-2.4808	3.7379	0.5109
Weighting	yes	**Drug*Inhibitor**	-1.6362	1.4352	0.2614
Normalization	no				

Table A.12. Linear mixed effects model parameters for 2,4-DNP inhibition of mitoxantrone uptake. Full model without weighting and with normalization.

Variability Parameter	Estimate	Fixed Effect	Estimate	Standard Error	p-value
Day	0	**Intercept**	0.1323	0.01886	0.0197
Rep (Day)	0.00E+00	**Drug**	0.06378	0.00399	<.0001
Residual	0.002143	**Drug^2**	-0.00101	0.000173	<.0001
AIC	-108.5	**Inhibitor**	-0.08763	0.02156	0.0002
Weighting	no	**Drug*Inhibitor**	-0.0006	0.00188	0.7524
Normalization	yes				

Table A.13. Linear mixed effects model parameters for 2,4-DNP inhibition of mitoxantrone uptake. Model without drug*inhibitor term, with weighting, and without normalization.

Variability Parameter	Estimate	Fixed Effect	Estimate	Standard Error	p-value
Day	13.7969	**Intercept**	5.0364	4.0343	0.3382
Rep (Day)	0	**Drug**	12.5077	1.954	<.0001
Residual	0.1398	**Drug^2**	-0.2625	0.1145	0.0273
AIC	451.1	**Inhibitor**	-4.9152	3.0784	0.1184
Weighting	yes	**Drug*Inhibitor**	0	0	0
Normalization	no				

Table A.14. Linear mixed effects model parameters for 2,4-DNP inhibition of mitoxantrone uptake. Model without [drug]^2 term, with weighting, and without normalization.

Variability Parameter	Estimate	Fixed Effect	Estimate	Standard Error	p-value
Day	12.4854	**Intercept**	8.1385	3.8149	0.1665
Rep (Day)	0	**Drug**	9.2346	1.1718	<.0001
Residual	0.1539	**Drug^2**	0	0	0
AIC	450	**Inhibitor**	-2.8206	3.9292	0.4771
Weighting	yes	**Drug*Inhibitor**	-1.5016	1.5095	0.326
Normalization	no				

Table A.15. Linear mixed effects model parameters for 2,4-DNP inhibition of mitoxantrone uptake. Model without [drug]^2 and drug*inhibitor term, with weighting, and without normalization.

Variability Parameter	Estimate	Fixed Effect	Estimate	Standard Error	p-value
Day	12.7359	**Intercept**	9.5157	3.5691	0.1166
Rep (Day)	0	**Drug**	8.3394	0.7503	<.0001
Residual	0.1538	**Drug^2**	0	0	0
AIC	453.6	**Inhibitor**	-5.0519	3.2256	0.1252
Weighting	yes	**Drug*Inhibitor**	0	0	0
Normalization	no				

Table A.16. Linear mixed effects model parameters for 2,4-DNP inhibition of mitoxantrone uptake. Full model with weighting and normalization.

Variability Parameter	Estimate	Fixed Effect	Estimate	Standard Error	p-value
Day	0.000155	**Intercept**	0.1087	0.01266	0.0133
Rep (Day)	2.48E-04	**Drug**	0.06763	0.003377	<.0001
Residual	0.009226	**Drug^2**	-0.00113	0.000175	<.0001
AIC	-106.3	**Inhibitor**	-0.06575	0.08607	<.0001
Weighting	yes	**Drug*Inhibitor**	-0.00332	0.002199	0.1391
Normalization	yes				

Table A.17. Linear mixed effects model parameters for 2,4-DNP inhibition of mitoxantrone uptake. Model without drug*inhibitor term, with weighting and normalization.

Variability Parameter	Estimate	Fixed Effect	Estimate	Standard Error	p-value
Day	0.000159	**Intercept**	0.1137	0.01224	0.0114
Rep (Day)	2.33E-04	**Drug**	0.06537	0.003076	<.0001
Residual	0.009562	**Drug^2**	-0.00111	0.000178	<.0001
AIC	-114.4	**Inhibitor**	-0.07302	0.007292	<.0001
Weighting	yes	**Drug*Inhibitor**	0	0	0
Normalization	yes				

Table A.18. Linear mixed effects model parameters for 2,4-DNP inhibition of mitoxantrone uptake. Model without [drug]^2 term, with weighting and normalization.

Variability Parameter	Estimate	Fixed Effect	Estimate	Standard Error	p-value
Day	0.000194	**Intercept**	0.1327	0.01416	0.0112
Rep (Day)	0	**Drug**	0.04881	0.002404	<.0001
Residual	0.01888	**Drug^2**	0	0	0
AIC	-92.8	**Inhibitor**	-0.07054	0.01226	<.0001
Weighting	yes	**Drug*Inhibitor**	-0.00214	0.003136	0.4985
Normalization	yes				

Table A.19. Linear mixed effects model parameters for 2,4-DNP inhibition of mitoxantrone uptake. Model without [drug]^2 and drug*inhibitor terms, with weighting and normalization.

Variability Parameter	Estimate	Fixed Effect	Estimate	Standard Error	p-value
Day	0.000196	**Intercept**	0.1357	0.01341	0.0096
Rep (Day)	1.60E-04	**Drug**	0.04755	0.001539	<.0001
Residual	0.01866	**Drug^2**	0	0	0
AIC	-102	**Inhibitor**	-0.07518	0.01016	<.0001
Weighting	Yes	**Drug*Inhibitor**	0	0	0
Normalization	Yes				

Linear Mixed Effects Models for 2,4-DNP Inhibition of Mitoxantrone Efflux

Table A.20. Linear mixed effects model parameters for 2,4-DNP inhibition of mitoxantrone efflux. Full model without weighting or normalization.

Variability Parameter	Estimate	Fixed Effect	Estimate	Standard Error	p-value
Day	1278.11	**Intercept**	21.166	22.3572	0.4437
Rep (Day)	0.00E+00	**Drug**	11.1501	1.8173	<.0001
Residual	444.44	**Drug^2**	-0.1874	0.07881	0.0225
AIC	427.6	**Inhibitor**	-14.9983	9.8205	0.135
Weighting	no	**Drug*Inhibitor**	-0.1854	0.8564	0.8297
Normalization	no				

Table A.21. Linear mixed effects model parameters for 2,4-DNP inhibition of mitoxantrone efflux. Full model, with weighting and without normalization.

Variability Parameter	Estimate	Fixed Effect	Estimate	Standard Error	p-value
Day	62.4996	**Intercept**	19.6296	5.5384	0.0712
Rep (Day)	0.00E+00	**Drug**	9.0561	1.2257	<.0001
Residual	0.05689	**Drug^2**	-0.141	0.0637	0.033
AIC	402.7	**Inhibitor**	-10.6921	3.2868	0.0024
Weighting	yes	**Drug*Inhibitor**	-0.1579	0.8059	0.8457
Normalization	no				

Table A.22. Linear mixed effects model parameters for 2,4-DNP inhibition of mitoxantrone efflux. Full model without weighting, and with normalization.

Variability Parameter	Estimate	Fixed Effect	Estimate	Standard Error	p-value
Day	0.02521	**Intercept**	0.04737	0.03555	0.3143
Rep (Day)	0.00E+00	**Drug**	0.06628	0.004353	<.0001
Residual	0.00255	**Drug^2**	-0.00092	0.000189	<.0001
AIC	-93.4	**Inhibitor**	-0.04298	0.02352	0.0755
Weighting	no	**Drug*Inhibitor**	-0.00465	0.002051	0.0292
Normalization	yes				

Table A.23. Linear mixed effects model parameters for 2,4-DNP inhibition of mitoxantrone efflux. Model without drug*inhibitor term, with weighting, and without normalization.

Variability Parameter	Estimate	Fixed Effect	Estimate	Standard Error	p-value
Day	62.6992	**Intercept**	19.8886	5.3734	0.0659
Rep (Day)	0	**Drug**	8.9497	1.0844	<.0001
Residual	0.05558	**Drug^2**	-0.14	0.06277	0.0315
AIC	404.1	**Inhibitor**	-11.0547	2.6875	0.0002
Weighting	yes	**Drug*Inhibitor**	0	0	0
Normalization	no				

Table A.24. Linear mixed effects model parameters for 2,4-DNP inhibition of mitoxantrone efflux. Model without [drug]^2 term, with weighting, and without normalization.

Variability Parameter	Estimate	Fixed Effect	Estimate	Standard Error	p-value
Day	58.8694	**Intercept**	22.6746	5.3173	0.0508
Rep (Day)	0	**Drug**	6.7051	0.6404	<.0001
Residual	0.06229	**Drug^2**	0	0	0
AIC	403.7	**Inhibitor**	-11.2075	3.4305	0.0023
Weighting	yes	**Drug*Inhibitor**	-0.01995	0.8407	0.9812
Normalization	no				

Table A.25. Linear mixed effects model parameters for 2,4-DNP inhibition of mitoxantrone efflux. Model without [drug]^2 and drug*inhibitor terms, with weighting, and without normalization.

Variability Parameter	Estimate	Fixed Effect	Estimate	Standard Error	p-value
Day	59.0758	**Intercept**	22.7106	5.1597	0.0479
Rep (Day)	0	**Drug**	6.6938	0.4107	<.0001
Residual	0.06084	**Drug^2**	0	0	0
AIC	405.2	**Inhibitor**	-11.2539	2.8101	0.0003
Weighting	yes	**Drug*Inhibitor**	0	0	0
Normalization	no				

Table A.26. Linear mixed effects model parameters for 2,4-DNP inhibition of mitoxantrone efflux. Full model with weighting and normalization.

Variability Parameter	Estimate	Fixed Effect	Estimate	Standard Error	p-value
Day	0.001982	**Intercept**	0.01183	0.02652	0.6992
Rep (Day)	0.00E+00	**Drug**	0.0695	0.004284	<.0001
Residual	0.02187	**Drug^2**	-0.00097	0.000237	0.0002
AIC	-91	**Inhibitor**	-0.00115	0.005371	0.8317
Weighting	yes	**Drug*Inhibitor**	-0.00889	0.002978	0.0049
Normalization	yes				

Table A.27. Linear mixed effects model parameters for 2,4-DNP inhibition of mitoxantrone efflux. Model without drug*inhibitor term, with weighting and normalization.

Variability Parameter	Estimate	Fixed Effect	Estimate	Standard Error	p-value
Day	0.001982	**Intercept**	0.0183	0.02656	0.5621
Rep (Day)	0.00E+00	**Drug**	0.06404	0.00422	<.0001
Residual	0.02599	**Drug^2**	-0.00095	0.000258	0.0007
AIC	-92.5	**Inhibitor**	-0.0118	0.00437	0.0102
Weighting	yes	**Drug*Inhibitor**	0	0	0
Normalization	yes				

Table A.28. Linear mixed effects model parameters for 2,4-DNP inhibition of mitoxantrone efflux. Model without [drug]^2 term with weighting and normalization.

Variability Parameter	Estimate	Fixed Effect	Estimate	Standard Error	p-value
Day	0.002078	**Intercept**	0.02716	0.02704	0.4209
Rep (Day)	0	**Drug**	0.05474	0.002676	<.0001
Residual	0.02996	**Drug^2**	0	0	0
AIC	-91.5	**Inhibitor**	-0.00156	0.006285	0.8047
Weighting	yes	**Drug*Inhibitor**	-0.00856	0.003485	0.0185
Normalization	yes				

Table A.29. Linear mixed effects model parameters for 2,4-DNP inhibition of mitoxantrone efflux. Model without [drug]^2 and drug*inhibitor term, with weighting and normalization.

Variability Parameter	Estimate	Fixed Effect	Estimate	Standard Error	p-value
Day	0.002077	**Intercept**	0.03312	0.02699	0.3446
Rep (Day)	0.00E+00	**Drug**	0.04975	0.001841	<.0001
Residual	0.03347	**Drug^2**	0	0	0
AIC	-95.2	**Inhibitor**	-0.01183	0.004959	0.0219
Weighting	yes	**Drug*Inhibitor**	0	0	0
Normalization	yes				

Linear Mixed Effects Models for Verapamil Inhibition of Mitoxantrone Uptake

Table A.30. Linear mixed effects model parameters for verapamil inhibition of mitoxantrone uptake. Full model without weighting or normalization.

Variability Parameter	Estimate	Fixed Effect	Estimate	Standard Error	p-value
Day	3284.96	**Intercept**	81.7659	19.0024	0.0051
Rep (Day)	1.05E-14	**Drug**	8.5308	1.2824	<.0001
Residual	1072.5	**Drug^2**	-0.07261	0.05635	0.1987
AIC	2770.6	**Inhibitor**	2.1014	0.7491	0.0054
Weighting	no	**Drug*Inhibitor**	0.1012	0.07128	0.1567
Normalization	no				

Table A.31. Linear mixed effects model parameters for verapamil inhibition of mitoxantrone uptake. Full model with weighting, and without normalization.

Variability Parameter	Estimate	Fixed Effect	Estimate	Standard Error	p-value
Day	2037.25	**Intercept**	70.6033	14.5515	0.0028
Rep (Day)	3.97E-15	**Drug**	10.7304	0.7987	<.0001
Residual	0.03694	**Drug^2**	-0.2324	0.03998	<.0001
AIC	2630	**Inhibitor**	0.831	0.3126	0.0083
Weighting	yes	**Drug*Inhibitor**	0.1167	0.0619	0.0604
Normalization	no				

Table A.32. Linear mixed effects model parameters for verapamil inhibition of mitoxantrone uptake. Full model without weighting, and with normalization.

Variability Parameter	Estimate	Fixed Effect	Estimate	Standard Error	p-value
Day	0.01528	**Intercept**	0.3272	0.04382	0.0003
Rep (Day)	0.00E+00	**Drug**	0.04427	0.004492	<.0001
Residual	0.01339	**Drug^2**	-0.00056	0.000198	0.0053
AIC	-323.4	**Inhibitor**	0.01082	0.002626	<.0001
Weighting	no	**Drug*Inhibitor**	0.000365	0.000251	0.1472
Normalization	yes				

Table A.33. Linear mixed effects model parameters for verapamil inhibition of mitoxantrone uptake. Model without drug*inhibitor term, with weighting and without normalization.

Variability Parameter	Estimate	Fixed Effect	Estimate	Standard Error	p-value
Day	2037.51	**Intercept**	9.2993	14.5385	0.0031
Rep (Day)	0	**Drug**	11.1546	0.7701	<.0001
Residual	0.03684	**Drug^2**	-0.2331	0.04017	<.0001
AIC	2629.9	**Inhibitor**	1.1884	0.2498	<.0001
Weighting	yes	**Drug*Inhibitor**	0	0	0
Normalization	no				

Table A.34. Linear mixed effects model parameters for verapamil inhibition of mitoxantrone uptake. Model without [drug]^2 term, with weighting, and without normalization.

Variability Parameter	Estimate	Fixed Effect	Estimate	Standard Error	p-value
Day	2147.97	**Intercept**	78.8691	14.8827	0.0018
Rep (Day)	0	**Drug**	6.5102	0.3522	<.0001
Residual	0.04094	**Drug^2**	0	0	0
AIC	2657.4	**Inhibitor**	0.8522	0.3311	0.0106
Weighting	yes	**Drug*Inhibitor**	0.12	0.06556	0.0683
Normalization	no				

Table A.35. Linear mixed effects model parameters for verapamil inhibition of mitoxantrone uptake. Model without [drug]^2 and drug*inhibitor terms, with weighting, and without normalization.

Variability Parameter	Estimate	Fixed Effect	Estimate	Standard Error	p-value
Day	2148.54	**Intercept**	77.5543	14.8693	0.002
Rep (Day)	0	**Drug**	6.9333	0.267	<.0001
Residual	0.0413	**Drug^2**	0	0	0
AIC	2657.1	**Inhibitor**	1.2199	0.2644	<.0001
Weighting	yes	**Drug*Inhibitor**	0	0	0
Normalization	no				

Table A.36. Linear mixed effects model parameters for verapamil inhibition of mitoxantrone uptake. Full model with weighting and normalization.

Variability Parameter	Estimate	Fixed Effect	Estimate	Standard Error	p-value
Day	0.02247	**Intercept**	0.2544	0.0487	0.002
Rep (Day)	1.10E-05	**Drug**	0.06239	0.003653	<.0001
Residual	0.02788	**Drug^2**	-0.00136	0.000184	<.0001
AIC	-364.6	**Inhibitor**	0.006075	0.001444	<.0001
Weighting	yes	**Drug*Inhibitor**	0.000502	0.00028	0.0739
Normalization	yes				

Table A.37. Linear mixed effects model parameters for verapamil inhibition of mitoxantrone uptake. Model without drug*inhibitor, with weighting and normalization.

Variability Parameter	Estimate	Fixed Effect	Estimate	Standard Error	p-value
Day	0.02249	**Intercept**	0.2491	0.04864	0.0022
Rep (Day)	8.62E-06	**Drug**	0.06407	0.003545	<.0001
Residual	0.02812	**Drug^2**	-0.00136	0.000185	<.0001
AIC	-375.9	**Inhibitor**	0.007654	0.001151	<.0001
Weighting	yes	**Drug*Inhibitor**	0	0	0
Normalization	yes				

Table A.38. Linear mixed effects model parameters for verapamil inhibition of mitoxantrone uptake. Model without [drug]^2 term, with weighting and normalization.

Variability Parameter	Estimate	Fixed Effect	Estimate	Standard Error	p-value
Day	0.0229	**Intercept**	0.302	0.04887	0.0008
Rep (Day)	0	**Drug**	0.03772	0.001654	<.0001
Residual	0.03352	**Drug^2**	0	0	0
AIC	-331.8	**Inhibitor**	0.006374	0.001583	<.0001
Weighting	yes	**Drug*Inhibitor**	0.000485	0.000306	0.115
Normalization	yes				

Table A.39. Linear mixed effects model parameters for verapamil inhibition of mitoxantrone uptake. Model without [drug]^2 and drug*inhibitor term, with weighting and normalization.

Variability Parameter	Estimate	Fixed Effect	Estimate	Standard Error	p-value
Day	0.02291	**Intercept**	0.2968	0.04878	0.0009
Rep (Day)	0.00E+00	**Drug**	0.03939	0.001273	<.0001
Residual	0.03371	**Drug^2**	0	0	0
AIC	-343.6	**Inhibitor**	0.007988	0.001259	<.0001
Weighting	yes	**Drug*Inhibitor**	0	0	0
Normalization	yes				

Linear Mixed Effects Models for Verapamil Inhibition of Mitoxantrone Efflux

Table A.40. Linear mixed effects model parameters for verapamil inhibition of mitoxantrone efflux. Full model without weighting or normalization.

Variability Parameter	Estimate	Fixed Effect	Estimate	Standard Error	p-value
Day	3061.23	**Intercept**	44.7314	24.3049	0.163
Rep (Day)	0.00E+00	**Drug**	11.9884	2.0788	<.0001
Residual	1460.87	**Drug^2**	-0.1733	0.09145	0.0602
AIC	1496.3	**Inhibitor**	1.639	1.2195	0.1813
Weighting	no	**Drug*Inhibitor**	-0.0049	0.1155	0.9663
Normalization	no				

Table A.41. Linear mixed effects model parameters for verapamil inhibition of mitoxantrone efflux. Full model with weighting, and without normalization.

Variability Parameter	Estimate	Fixed Effect	Estimate	Standard Error	p-value
Day	1407.53	**Intercept**	49.9709	15.7015	0.05
Rep (Day)	0.00E+00	**Drug**	10.6008	1.1134	<.0001
Residual	0.05437	**Drug^2**	-0.2529	0.05623	<.0001
AIC	1384.8	**Inhibitor**	0.6468	0.4284	0.1335
Weighting	yes	**Drug*Inhibitor**	0.05741	0.08402	0.4956
Normalization	no				

Table A.42. Linear mixed effects model parameters for verapamil inhibition of mitoxantrone efflux. Full model, without weighting, and with normalization.

Variability Parameter	Estimate	Fixed Effect	Estimate	Standard Error	p-value
Day	0.01701	**Intercept**	0.258	0.05774	0.0209
Rep (Day)	5.50E-06	**Drug**	0.05968	0.005175	<.0001
Residual	0.009056	**Drug^2**	-0.00099	0.000228	<.0001
AIC	-193	**Inhibitor**	0.01	0.003036	0.0013
Weighting	no	**Drug*Inhibitor**	-0.0001	0.000288	0.7161
Normalization	yes				

Table A.43. Linear mixed effects model parameters for verapamil inhibition of mitoxantrone efflux. Model without drug*inhibitor term, with weighting, and without normalization.

Variability Parameter	Estimate	Fixed Effect	Estimate	Standard Error	p-value
Day	1409.79	**Intercept**	49.378	15.6878	0.0514
Rep (Day)	0	**Drug**	10.7985	1.073	<.0001
Residual	0.05416	**Drug^2**	-0.2522	0.05611	<.0001
AIC	1382.2	**Inhibitor**	0.8248	0.3393	0.0164
Weighting	yes	**Drug*Inhibitor**	0	0	0
Normalization	no				

Table A.44. Linear mixed effects model parameters for verapamil inhibition of mitoxantrone efflux. Model without [drug]^2 term, with weighting, and without normalization.

Variability Parameter	Estimate	Fixed Effect	Estimate	Standard Error	p-value
Day	1525.35	**Intercept**	58.5113	16.2381	0.0367
Rep (Day)	0	**Drug**	6.0551	0.4978	<.0001
Residual	0.06183	**Drug^2**	0	0	0
AIC	1400	**Inhibitor**	0.7007	0.4567	0.1273
Weighting	yes	**Drug*Inhibitor**	0.05055	0.08958	0.5735
Normalization	no				

Table A.45. Linear mixed effects model parameters for verapamil inhibition of mitoxantrone efflux. Model without [drug]^2 and drug*inhibitor terms, with weighting, and without normalization.

Variability Parameter	Estimate	Fixed Effect	Estimate	Standard Error	p-value
Day	1527.28	**Intercept**	57.9689	16.2178	0.0374
Rep (Day)	0	**Drug**	6.2404	0.3731	<.0001
Residual	0.06153	**Drug^2**	0	0	0
AIC	1397.3	**Inhibitor**	0.8575	0.3616	0.0191
Weighting	yes	**Drug*Inhibitor**	0	0	0
Normalization	no				

Table A.46. Linear mixed effects model parameters for verapamil inhibition of mitoxantrone efflux. Full model with weighting and normalization.

Variability Parameter	Estimate	Fixed Effect	Estimate	Standard Error	p-value
Day	0.02347	**Intercept**	0.2307	0.06385	0.0364
Rep (Day)	1.18E-19	**Drug**	0.06799	0.004381	<.0001
Residual	0.02228	**Drug^2**	-0.00139	0.000222	<.0001
AIC	-216.8	**Inhibitor**	0.003084	0.00163	0.0607
Weighting	yes	**Drug*Inhibitor**	0.000282	0.000333	0.3998
Normalization	yes				

Table A.47. Linear mixed effects model parameters for verapamil inhibition of mitoxantrone efflux. Model without drug*inhibitor term, with weighting and normalization.

Variability Parameter	Estimate	Fixed Effect	Estimate	Standard Error	p-value
Day	0.02347	**Intercept**	0.2277	0.06374	0.0375
Rep (Day)	8.03E-20	**Drug**	0.06897	0.004218	<.0001
Residual	0.02223	**Drug^2**	-0.00139	0.000222	<.0001
AIC	-230.3	**Inhibitor**	0.003952	0.001264	0.0022
Weighting	yes	**Drug*Inhibitor**	0	0	0
Normalization	yes				

Table A.48. Linear mixed effects model parameters for verapamil inhibition of mitoxantrone efflux. Model without [drug]^2 term, with weighting and normalization.

Variability Parameter	Estimate	Fixed Effect	Estimate	Standard Error	p-value
Day	0.02393	**Intercept**	0.2768	0.06425	0.023
Rep (Day)	0	**Drug**	0.04328	0.002125	<.0001
Residual	0.02844	**Drug^2**	0	0	0
AIC	-197.2	**Inhibitor**	0.003353	0.001842	0.0709
Weighting	yes	**Drug*Inhibitor**	0.000239	0.000377	0.5265
Normalization	yes				

Table A.49. Linear mixed effects model parameters for verapamil inhibition of mitoxantrone efflux. Model without [drug]^2 and drug*inhibitor terms, with weighting and normalization.

Variability Parameter	Estimate	Fixed Effect	Estimate	Standard Error	p-value
Day	0.02393	**Intercept**	0.2741	0.06411	0.0235
Rep (Day)	3.63E-19	**Drug**	0.04417	0.001585	<.0001
Residual	0.02832	**Drug^2**	0	0	0
AIC	-210.7	**Inhibitor**	0.00409	0.001427	0.0048
Weighting	yes	**Drug*Inhibitor**	0	0	0
Normalization	yes				

Linear Mixed Effects Models for FTC Inhibition of Mitoxantrone Uptake

Table A.50. Linear mixed effects model parameters for FTC inhibition of mitoxantrone uptake. Full model without weighting or normalization.

Variability Parameter	Estimate	Fixed Effect	Estimate	Standard Error	p-value
Day	151.65	**Intercept**	18.7528	5.4763	0.0187
Rep (Day)	1.34E+01	**Drug**	9.1589	0.5808	<.0001
Residual	131.07	**Drug^2**	-0.1375	0.02541	<.0001
AIC	1380	**Inhibitor**	-0.6814	0.3257	0.038
Weighting	no	**Drug*Inhibitor**	-0.05207	0.03034	0.088
Normalization	no				

Table A.51. Linear mixed effects model parameters for FTC inhibition of mitoxantrone uptake. Full model with weighting, and without normalization.

Variability Parameter	Estimate	Fixed Effect	Estimate	Standard Error	p-value
Day	86.6359	**Intercept**	15.4458	3.7833	0.0095
Rep (Day)	5.25E+00	**Drug**	9.3349	0.3861	<.0001
Residual	0.02055	**Drug^2**	-0.1455	0.02019	<.0001
AIC	1264	**Inhibitor**	-0.2122	0.119	0.0764
Weighting	yes	**Drug*Inhibitor**	-0.1271	0.0306	<.0001
Normalization	no				

Table A.52. Linear mixed effects model parameters for FTC inhibition of mitoxantrone uptake. Full model without weighting, and with normalization.

Variability Parameter	Estimate	Fixed Effect	Estimate	Standard Error	p-value
Day	0.006458	**Intercept**	0.1065	0.03474	0.0279
Rep (Day)	0.000801	**Drug**	0.06137	0.003172	<.0001
Residual	0.003921	**Drug^2**	-0.00085	0.000138	<.0001
AIC	-381.2	**Inhibitor**	-0.00331	0.001779	0.0648
Weighting	no	**Drug*Inhibitor**	-0.00061	0.000164	0.0003
Normalization	yes				

Table A.53. Linear mixed effects model parameters for FTC inhibition of mitoxantrone uptake. Model without drug*inhibitor term, with weighting, and without normalization.

Variability Parameter	Estimate	Fixed Effect	Estimate	Standard Error	p-value
Day	84.1642	**Intercept**	16.6507	3.7436	0.0067
Rep (Day)	5.3523	**Drug**	8.7653	0.3783	<.0001
Residual	0.02264	**Drug^2**	-0.1484	0.02118	<.0001
AIC	1275.4	**Inhibitor**	-0.5207	0.09749	<.0001
Weighting	yes	**Drug*Inhibitor**	0	0	0
Normalization	no				

Table A.54. Linear mixed effects model parameters for FTC inhibition of mitoxantrone uptake. Model without [drug]^2 term, with weighting, and without normalization.

Variability Parameter	Estimate	Fixed Effect	Estimate	Standard Error	p-value
Day	99.9996	**Intercept**	20.0087	4.0141	0.0042
Rep (Day)	5.0024	**Drug**	6.962	0.23	<.0001
Residual	0.02695	**Drug^2**	0	0	0
AIC	1303.4	**Inhibitor**	-0.189	0.1362	0.1671
Weighting	yes	**Drug*Inhibitor**	-0.1346	0.03502	0.0002
Normalization	no				

Table A.55. Linear mixed effects model parameters for FTC inhibition of mitoxantrone uptake. Model without [drug]^2 and drug*inhibitor terms, with weighting, and without normalization.

Variability Parameter	Estimate	Fixed Effect	Estimate	Standard Error	p-value
Day	97.2943	**Intercept**	21.3838	3.9625	0.003
Rep (Day)	5.10E+00	**Drug**	6.3069	0.1604	<.0001
Residual	0.02925	**Drug^2**	0	0	0
AIC	1312.8	**Inhibitor**	-0.5155	0.1108	<.0001
Weighting	yes	**Drug*Inhibitor**	0	0	0
Normalization	no				

Table A.56. Linear mixed effects model parameters for FTC inhibition of mitoxantrone uptake. Full model with weighting and normalization.

Variability Parameter	Estimate	Fixed Effect	Estimate	Standard Error	p-value
Day	0.006809	**Intercept**	0.09194	0.3235	0.0361
Rep (Day)	2.64E-04	**Drug**	0.06312	0.002286	<.0001
Residual	0.01556	**Drug^2**	-0.00089	0.000119	<.0001
AIC	-471.1	**Inhibitor**	-0.00119	0.000705	0.0946
Weighting	yes	**Drug*Inhibitor**	-0.00098	0.00018	<.0001
Normalization	yes				

Table A.57. Linear mixed effects model parameters for FTC inhibition of mitoxantrone uptake. Model without drug*inhibitor term, with weighting and normalization.

Variability Parameter	Estimate	Fixed Effect	Estimate	Standard Error	p-value
Day	0.006647	**Intercept**	0.102	0.03207	0.0246
Rep (Day)	0	**Drug**	0.0586	0.002311	<.0001
Residual	0.01832	**Drug^2**	-0.00091	0.000129	<.0001
AIC	-459	**Inhibitor**	-0.00363	0.000592	<.0001
Weighting	yes	**Drug*Inhibitor**	0	0	0
Normalization	yes				

Table A.58. Linear mixed effects model parameters for FTC inhibition of mitoxantrone uptake. Model without [drug]^2 term, with weighting and normalization.

Variability Parameter	Estimate	Fixed Effect	Estimate	Standard Error	p-value
Day	0.006986	**Intercept**	0.1201	0.03268	0.0144
Rep (Day)	2.54E-04	**Drug**	0.04849	0.001375	<.0001
Residual	0.02084	**Drug^2**	0	0	0
AIC	-438.7	**Inhibitor**	-0.00106	0.000816	0.1971
Weighting	yes	**Drug*Inhibitor**	-0.00102	0.000208	<.0001
Normalization	yes				

Table A.59. Linear mixed effects model parameters for FTC inhibition of mitoxantrone uptake. Model without [drug]^2 and drug*inhibitor terms, with weighting and normalization.

Variability Parameter	Estimate	Fixed Effect	Estimate	Standard Error	p-value
Day	0.006805	**Intercept**	0.1311	0.03229	0.0097
Rep (Day)	2.58E-04	**Drug**	0.04345	0.000976	<.0001
Residual	0.02379	**Drug^2**	0	0	0
AIC	-431.2	**Inhibitor**	-0.0036	0.000674	<.0001
Weighting	yes	**Drug*Inhibitor**	0	0	0
Normalization	yes				

Linear Mixed Effects Models for FTC Inhibition of Mitoxantrone Efflux

Table A.60. Linear mixed effects model parameters for FTC inhibition of mitoxantrone efflux. Full model, without weighting or normalization.

Variability Parameter	Estimate	Fixed Effect	Estimate	Standard Error	p-value
Day	85.7764	**Intercept**	11.7988	7.5029	0.3606
Rep (Day)	0.00E+00	**Drug**	17.1451	1.2002	<.0001
Residual	253.82	**Drug^2**	-0.3993	0.05254	<.0001
AIC	644.8	**Inhibitor**	-0.1582	0.7127	0.825
Weighting	no	**Drug*Inhibitor**	-0.02493	0.06738	0.7125
Normalization	no				

Table A.61. Linear mixed effects model parameters for FTC inhibition of mitoxantrone efflux. Full model, with weighting, and without normalization.

Variability Parameter	Estimate	Fixed Effect	Estimate	Standard Error	p-value
Day	0	**Intercept**	17.1279	2.6389	0.0973
Rep (Day)	2.19E+00	**Drug**	15.0987	1.0434	<.0001
Residual	0.0257	**Drug^2**	-0.3496	0.053	<.0001
AIC	621.4	**Inhibitor**	-0.6248	0.3307	0.0631
Weighting	yes	**Drug*Inhibitor**	0.104	0.08387	0.219
Normalization	no				

Table A.62. Linear mixed effects model parameters for FTC inhibition of mitoxantrone efflux. Full model, without weighting and with normalization.

Variability Parameter	Estimate	Fixed Effect	Estimate	Standard Error	p-value
Day	0.01055	**Intercept**	0.1023	0.05011	0.1338
Rep (Day)	0.00E+00	**Drug**	0.08396	0.006033	<.0001
Residual	0.009446	**Drug^2**	-0.00191	0.000259	<.0001
AIC	-153	**Inhibitor**	-0.00386	0.003315	0.2468
Weighting	no	**Drug*Inhibitor**	-0.00021	0.0003	0.4793
Normalization	yes				

Table A.63. Linear mixed effects model parameters for FTC inhibition of mitoxantrone efflux. Model without drug*inhibitor term, with weighting and without normalization.

Variability Parameter	Estimate	Fixed Effect	Estimate	Standard Error	p-value
Day	0	**Intercept**	15.9944	2.4921	0.0984
Rep (Day)	2.2873	**Drug**	15.5518	0.9818	<.0001
Residual	0.02588	**Drug^2**	-0.3516	0.05318	<.0001
AIC	619.8	**Inhibitor**	-0.3721	0.2618	0.1597
Weighting	yes	**Drug*Inhibitor**	0	0	0
Normalization	no				

Table A.64. Linear mixed effects model parameters for FTC inhibition of mitoxantrone efflux. Model without [drug]^2 term, with weighting, and without normalization.

Variability Parameter	Estimate	Fixed Effect	Estimate	Standard Error	p-value
Day	0	**Intercept**	27.2342	2.5499	0.0594
Rep (Day)	0.41	**Drug**	8.99	0.6037	<.0001
Residual	0.04132	**Drug^2**	0	0	0
AIC	651.5	**Inhibitor**	-0.7737	0.4175	0.0681
Weighting	yes	**Drug*Inhibitor**	0.1219	0.1063	0.2554
Normalization	no				

Table A.65. Linear mixed effects model parameters for FTC inhibition of mitoxantrone efflux. Model without [drug]^2 and drug*inhibitor terms, with weighting and without normalization.

Variability Parameter	Estimate	Fixed Effect	Estimate	Standard Error	p-value
Day	0	**Intercept**	25.9831	2.3223	0.0567
Rep (Day)	0.7206	**Drug**	9.4787	0.426	<.0001
Residual	0.04143	**Drug^2**	0	0	0
AIC	650.2	**Inhibitor**	-0.4761	0.3298	0.1533
Weighting	yes	**Drug*Inhibitor**	0	0	0
Normalization	no				

Table A.66. Linear mixed effects model parameters for FTC inhibition of mitoxantrone efflux. Full model with weighting and normalization.

Variability Parameter	Estimate	Fixed Effect	Estimate	Standard Error	p-value
Day	0.006213	**Intercept**	0.09327	0.03536	0.0778
Rep (Day)	1.20E-04	**Drug**	0.07862	0.004558	<.0001
Residual	0.02439	**Drug^2**	-0.00167	0.000224	<.0001
AIC	-209.4	**Inhibitor**	-0.00234	0.00144	0.1069
Weighting	yes	**Drug*Inhibitor**	-0.00033	0.000301	0.281
Normalization	yes				

Table A.67. Linear mixed effects model parameters for FTC inhibition of mitoxantrone efflux. Model without drug*inhibitor terms, with weighting and normalization.

Variability Parameter	Estimate	Fixed Effect	Estimate	Standard Error	p-value
Day	0.006211	**Intercept**	0.09771	0.03511	0.0688
Rep (Day)	1.11E-04	**Drug**	0.07717	0.004361	<.0001
Residual	0.02444	**Drug^2**	-0.00167	0.000224	<.0001
AIC	-222.6	**Inhibitor**	-0.00335	0.0011	0.0029
Weighting	yes	**Drug*Inhibitor**	0	0	0
Normalization	yes				

Table A.68. Linear mixed effects model parameters for FTC inhibition of mitoxantrone efflux. Model without [drug]^2 term, with weighting and normalization.

Variability Parameter	Estimate	Fixed Effect	Estimate	Standard Error	p-value
Day	0.004948	**Intercept**	0.1625	0.03169	0.0144
Rep (Day)	1.01E-04	**Drug**	0.04795	0.00239	<.0001
Residual	0.03626	**Drug^2**	0	0	0
AIC	-179.2	**Inhibitor**	-0.0026	0.001754	0.1412
Weighting	yes	**Drug*Inhibitor**	-0.00035	0.000367	0.3395
Normalization	yes				

Table A.69. Linear mixed effects model parameters for FTC inhibition of mitoxantrone efflux. Model without [drug]^2 and drug*inhibitor terms, with weighting and normalization.

Variability Parameter	Estimate	Fixed Effect	Estimate	Standard Error	p-value
Day	0.004936	**Intercept**	0.1674	0.03121	0.0127
Rep (Day)	9.10E-05	**Drug**	0.04631	0.001678	<.0001
Residual	0.03626	**Drug^2**	0	0	0
AIC	-192.3	**Inhibitor**	-0.00369	0.001337	0.0067
Weighting	yes	**Drug*Inhibitor**	0	0	0
Normalization	yes				

Linear Mixed Effects Models for 2,4-DNP Inhibition of A-K-AMCA Uptake

Table A.70. Linear mixed effects model parameters for 2,4-DNP inhibition of A-K-AMCA uptake. Full model with weighting and normalization.

Variability Parameter	Estimate	Fixed Effect	Estimate	Standard Error	p-value
Day	0.000436	**Intercept**	0.02068	0.01374	0.2294
Rep (Day)	4.30E-05	**Drug**	1.004	0.08765	<.0001
Residual	0.07158	**Drug^2**	0.00214	0.09596	0.9823
AIC	-158.8	**Inhibitor**	-0.02529	0.005134	<.0001
Weighting	yes	**Drug*Inhibitor**	-0.3524	0.06803	<.0001
Normalization	yes				

Table A.71. Linear mixed effects model parameters for 2,4-DNP inhibition of A-K-AMCA uptake. Full model without weighting and with normalization.

Variability Parameter	Estimate	Fixed Effect	Estimate	Standard Error	p-value
Day	0.000211	**Intercept**	0.004238	0.02561	0.8791
Rep (Day)	7.50E-05	**Drug**	1.1904	0.1061	<.0001
Residual	0.005364	**Drug^2**	-0.1628	0.09678	0.0974
AIC	-151.9	**Inhibitor**	-0.01206	0.02732	0.6603
Weighting	no	**Drug*Inhibitor**	-0.3504	0.05162	<.0001
Normalization	yes				

Table A.72. Linear mixed effects model parameters for 2,4-DNP inhibition of A-K-AMCA uptake. Model without drug*inhibitor term with weighting and normalization.

Variability Parameter	Estimate	Fixed Effect	Estimate	Standard Error	p-value
Day	0.000463	**Intercept**	0.03291	0.01453	0.1084
Rep (Day)	0.000032	**Drug**	0.7278	0.08064	<.0001
Residual	0.09937	**Drug^2**	0.05336	0.1122	0.6359
AIC	-139.5	**Inhibitor**	-0.0421	0.004697	<.0001
Weighting	yes	**Drug*Inhibitor**	0	0	0
Normalization	yes				

Table A.73. Linear mixed effects model parameters for 2,4-DNP inhibition of A-K-AMCA uptake. Model without [drug]^2 term, with weighting and normalization.

Variability Parameter	Estimate	Fixed Effect	Estimate	Standard Error	p-value
Day	0.000434	**Intercept**	0.02064	0.01306	0.2122
Rep (Day)	0.000044	**Drug**	1.0053	0.05893	<.0001
Residual	0.0749	**Drug^2**	0	0	0
AIC	-161.6	**Inhibitor**	-0.02529	0.005093	<.0001
Weighting	yes	**Drug*Inhibitor**	-0.3526	0.0671	<.0001
Normalization	yes				

Table A.74. Linear mixed effects model parameters for 2,4-DNP inhibition of A-K-AMCA uptake. Model without [drug]^2 and drug*inhibitor terms, with weighting and normalization.

Variability Parameter	Estimate	Fixed Effect	Estimate	Standard Error	p-value
Day	0.000433	**Intercept**	0.03058	0.01351	0.1085
Rep (Day)	0.000031	**Drug**	0.7612	0.04152	<.0001
Residual	0.09847	**Drug^2**	0	0	0
AIC	-141.8	**Inhibitor**	-0.04224	0.004669	<.0001
Weighting	yes	**Drug*Inhibitor**	0	0	0
Normalization	yes				

Linear Mixed Effects Models for Cefadroxil Inhibition of A-K-AMCA Uptake

Table A.75. Linear mixed effects model parameters for cefadroxil inhibition of A-K-AMCA uptake. Full model with weighting and normalization.

Variability Parameter	Estimate	Fixed Effect	Estimate	Standard Error	p-value
Day	0	**Intercept**	0.001156	0.00115	0.4205
Rep (Day)	2.75E-06	**Drug**	0.9737	0.04382	<.0001
Residual	0.02857	**Drug^2**	0.06589	0.08867	0.4601
AIC	-330.9	**Inhibitor**	0.02032	0.001377	<.0001
Weighting	yes	**Drug*Inhibitor**	-0.01233	0.02	0.5397
Normalization	yes				

Table A.76. Linear mixed effects model parameters for cefadroxil inhibition of A-K-AMCA uptake. Full model without weighting and with normalization.

Variability Parameter	Estimate	Fixed Effect	Estimate	Standard Error	p-value
Day	0	**Intercept**	-0.00519	0.009862	0.6515
Rep (Day)	5.90E-05	**Drug**	1.0229	0.06571	<.0001
Residual	0.001964	**Drug^2**	0.05444	0.06722	0.421
AIC	-217.9	**Inhibitor**	0.0278	0.00269	<.0001
Weighting	no	**Drug*Inhibitor**	-0.02709	0.008628	0.0025
Normalization	yes				

Table A.77. Linear mixed effects model parameters for cefadroxil inhibition of A-K-AMCA uptake. Model without drug*inhibitor term, with weighting and normalization.

Variability Parameter	Estimate	Fixed Effect	Estimate	Standard Error	p-value
Day	0	**Intercept**	0.001275	0.001138	0.3789
Rep (Day)	2.79E-06	**Drug**	0.9678	0.0466	<.0001
Residual	0.02829	**Drug^2**	0.05508	0.08652	0.5266
AIC	-336.6	**Inhibitor**	0.02002	0.001283	<.0001
Weighting	yes	**Drug*Inhibitor**	0	0	0
Normalization	yes				

Table A.78. Linear mixed effects model parameters for cefadroxil inhibition of A-K-AMCA uptake. Model without [drug]^2 term, with weighting and normalization.

Variability Parameter	Estimate	Fixed Effect	Estimate	Standard Error	p-value
Day	0	**Intercept**	0.001003	0.001113	0.4624
Rep (Day)	2.58E-06	**Drug**	0.996	0.03188	<.0001
Residual	0.02843	**Drug^2**	0	0	0
AIC	-333.4	**Inhibitor**	0.02023	0.001367	<.0001
Weighting	yes	**Drug*Inhibitor**	-0.00939	0.01955	0.6326
Normalization	yes				

Table A.79. Linear mixed effects model parameters for cefadroxil inhibition of A-K-AMCA uptake. Model without [drug]^2 and drug*inhibitor terms, with weighting and normalization.

Variability Parameter	Estimate	Fixed Effect	Estimate	Standard Error	p-value
Day	0	**Intercept**	0.001117	0.001092	0.4139
Rep (Day)	2.63E-06	**Drug**	0.9884	0.02768	<.0001
Residual	0.0281	**Drug^2**	0	0	0
AIC	-339.2	**Inhibitor**	0.02	0.001278	<.0001
Weighting	yes	**Drug*Inhibitor**	0	0	0
Normalization	yes				

Linear Mixed Effects Models for Gly-Gln Inhibition of A-K-AMCA Uptake

Table A.80. Linear mixed effects model parameters for Gly-Gln inhibition of A-K-AMCA uptake. Full model, with weighting and normalization.

Variability Parameter	Estimate	Fixed Effect	Estimate	Standard Error	p-value
Day	0	**Intercept**	0.000501	0.001106	0.6814
Rep (Day)	1.53E-06	**Drug**	0.9794	0.0341	<.0001
Residual	0.03613	**Drug^2**	0.09866	0.05589	0.0802
AIC	-506.1	**Inhibitor**	0.00052	0.000188	0.0066
Weighting	yes	**Drug*Inhibitor**	-0.0281	0.004556	<.0001
Normalization	yes				

Table A.81. Linear mixed effects model parameters for Gly-Gln inhibition of A-K-AMCA uptake. Full model, without weighting and with normalization.

Variability Parameter	Estimate	Fixed Effect	Estimate	Standard Error	p-value
Day	0	**Intercept**	0.006877	0.01377	0.6517
Rep (Day)	4.06E-04	**Drug**	0.9535	0.04599	<.0001
Residual	0.003443	**Drug^2**	0.08968	0.02958	0.003
AIC	-316.2	**Inhibitor**	-0.0006	0.002212	0.7871
Weighting	no	**Drug*Inhibitor**	-0.00699	0.004684	0.1382
Normalization	yes				

Table A.82. Linear mixed effects model parameters for Gly-Gln inhibition of A-K-AMCA uptake. Model without drug*inhibitor term, with weighting and normalization.

Variability Parameter	Estimate	Fixed Effect	Estimate	Standard Error	p-value
Day	1.56E-06	**Intercept**	0.002502	0.001147	0.1172
Rep (Day)	0.00E+00	**Drug**	0.8698	0.03261	<.0001
Residual	0.04698	**Drug^2**	0.09911	0.06355	0.1216
AIC	-482	**Inhibitor**	0.000057	0.000194	0.77
Weighting	yes	**Drug*Inhibitor**	0	0	0
Normalization	yes				

Table A.83. Linear mixed effects model parameters for Gly-Gln inhibition of A-K-AMCA uptake. Model without [drug]^2 term, with weighting and normalization.

Variability Parameter	Estimate	Fixed Effect	Estimate	Standard Error	p-value
Day	1.55E-06	**Intercept**	-0.00023	0.00122	0.8632
Rep (Day)	1.23E-06	**Drug**	1.0208	0.02614	<.0001
Residual	0.03635	**Drug^2**	0	0	0
AIC	-505.2	**Inhibitor**	0.000557	0.000197	0.0054
Weighting	yes	**Drug*Inhibitor**	-0.02792	0.004582	<.0001
Normalization	yes				

Table A.84. Linear mixed effects model parameters for Gly-Gln inhibition of A-K-AMCA uptake. Model without [drug]^2 and drug*inhibitor term, with weighting and normalization.

Variability Parameter	Estimate	Fixed Effect	Estimate	Standard Error	p-value
Day	4.18E-06	**Intercept**	0.001684	0.001398	0.3147
Rep (Day)	0.00E+00	**Drug**	0.9139	0.02171	<.0001
Residual	0.0467	**Drug^2**	0	0	0
AIC	-483.6	**Inhibitor**	0.000102	0.000208	0.6252
Weighting	yes	**Drug*Inhibitor**	0	0	0
Normalization	yes				

Michaelis-Menten Flow Cytometry Data

Table A.85. Flow cytometry data for Michaelis-Menten kinetic analysis

Drug Conc. (μM)	Day	Rep	Normalized Fluorescence 37°C	Normalized Fluorescence 4°C
1	121808	1	0.0674	0.0594
5	121808	1	0.5072	0.1983
10	121808	1	0.7699	0.3424
20	121808	1	1.0000	0.5960
1	121908	1	0.1953	0.0683
5	121908	1	0.4508	0.2069
10	121908	1	0.6611	0.3180
20	121908	1	1.0072	0.4303
1	121908	2	0.1853	0.0719
5	121908	2	0.4904	0.1631
10	121908	2	0.8056	0.2204
20	121908	2	0.9928	0.1232
1	11609	1	0.1247	0.2541
5	11609	1	0.3960	0.4704
10	11609	1	0.7731	0.8802
20	11609	1	1.0000	0.1628
1	11609	2	0.1718	0.2929
5	11609	2	0.2175	0.5454
10	11609	2	0.7450	0.7090

APPENDIX B

PCR ARRAY DATA

Table B.1. Human drug transporters PCR array gene table

Position	UniGene	GenBank	Symbol	Description
A01	Hs.429294	NM_005502	ABCA1	ATP-binding cassette, sub-family A (ABC1), member 1
A02	Hs.134585	NM_173076	ABCA12	ATP-binding cassette, sub-family A (ABC1), member 12
A03	Hs.226568	NM_152701	ABCA13	ATP-binding cassette, sub-family A (ABC1), member 13
A04	Hs.421202	NM_001606	ABCA2	ATP-binding cassette, sub-family A (ABC1), member 2
A05	Hs.26630	NM_001089	ABCA3	ATP-binding cassette, sub-family A (ABC1), member 3
A06	Hs.416707	NM_00350	ABCA4	ATP-binding cassette, sub-family A (ABC1), member 4
A07	Hs.131686	NM_080283	ABCA9	ATP-binding cassette, sub-family A (ABC1), member 9
A08	Hs.489033	NM_000927	ABCB1	ATP-binding cassette, sub-family B (MDR/TAP), member 1
A09	Hs.158316	NM_003742	ABCB11	ATP-binding cassette, sub-family B (MDR/TAP), member 11
A10	Hs.287827	NM_000443	ABCB4	ATP-binding cassette, sub-family B (MDR/TAP), member 4
A11	Hs.404102	NM_178559	ABCB5	ATP-binding cassette, sub-family B (MDR/TAP), member 5
A12	Hs.107911	NM_005689	ABCB6	ATP-binding cassette, sub-family B (MDR/TAP), member 6
B01	Hs.391464	NM_004996	ABCC1	ATP-binding cassette, sub-family C (CFTR/MRP), member 1
B02	Hs.55879	NM_033450	ABCC10	ATP-binding cassette, sub-family C (CFTR/MRP), member 10
B03	Hs.652267	NM_032583	ABCC11	ATP-binding cassette, sub-family C (CFTR/MRP), member 11
B04	Hs.410111	NM_033226	ABCC12	ATP-binding cassette, sub-family C (CFTR/MRP), member 12
B05	Hs.368243	NM_000392	ABCC2	ATP-binding cassette, sub-family C (CFTR/MRP), member 2
B06	Hs.463421	NM_003786	ABCC3	ATP-binding cassette, sub-family C (CFTR/MRP), member 3
B07	Hs.508423	NM_005845	ABCC4	ATP-binding cassette, sub-family C (CFTR/MRP), member 4
B08	Hs.368563	NM_005688	ABCC5	ATP-binding cassette, sub-family C (CFTR/MRP), member 5
B09	Hs.460057	NM_001171	ABCC6	ATP-binding cassette, sub-family C (CFTR/MRP), member 6
B10	Hs.159546	NM_000033	ABCD1	ATP-binding cassette, sub-family D (ALD), member 1
B11	Hs.76781	NM_002858	ABCD3	ATP-binding cassette, sub-family D (ALD), member 3

Table B.1–continued

B12	Hs.94395	NM_005050	ABCD4	ATP-binding cassette, sub-family D (ALD), member 4
C01	Hs.9573	NM_001090	ABCF1	ATP-binding cassette, sub-family F (GCN20), member 1
C02	Hs.480218	NM_004827	ABCG2	ATP-binding cassette, sub-family G (WHITE), member 2
C03	Hs.413931	NM_022437	ABCG8	ATP-binding cassette, sub-family G (WHITE), member 8
C04	Hs.76152	NM_198098	AQP1	Aquaporin 1 (Colton blood group)
C05	Hs.455323	NM_001170	AQP7	Aquaporin 7
C06	Hs.104624	NM_020980	AQP9	Aquaporin 9
C07	Hs.389107	NM_001694	ATP6V0C	ATPase, H+ transporting, lysosomal 16kDa, V0 subunit c
C08	Hs.496414	NM_000052	ATP7A	ATPase, Cu++ transporting, alpha polypeptide (Menkes syndrome)
C09	Hs.492280	NM_000053	ATP7B	ATPase, Cu++ transporting, beta polypeptide
C10	Hs.632177	NM_017458	MVP	Major vault protein
C11	Hs.952	NM_003049	SLC10A1	Solute carrier family 10 (sodium/bile acid cotransporter family), member 1
C12	Hs.194783	NM_000452	SLC10A2	Solute carrier family 10 (sodium/bile acid cotransporter family), member 2
D01	Hs.436893	NM_005073	SLC15A1	Solute carrier family 15 (oligopeptide transporter), member 1
D02	Hs.518089	NM_021082	SLC15A2	Solute carrier family 15 (oligopeptide transporter), member 2
D03	Hs.75231	NM_003051	SLC16A1	Solute carrier family 16 , member 1 (monocarboxylic acid transporter 1)
D04	Hs.75317	NM_006517	SLC16A2	Solute carrier family 16 , member 2 (monocarboxylic acid transporter 8)
D05	Hs.500761	NM_004207	SLC16A3	Solute carrier family 16 , member 3 (monocarboxylic acid transporter 4)
D06	Hs.84190	NM_194255	SLC19A1	Solute carrier family 19 (folate transporter), member 1
D07	Hs.30246	NM_006996	SLC19A2	Solute carrier family 19 (thiamine transporter), member 2
D08	Hs.221597	NM_025243	SLC19A3	Solute carrier family 19, member 3
D09	Hs.117367	NM_003057	SLC22A1	Solute carrier family 22 (organic cation transporter), member 1
D10	Hs.436385	NM_003058	SLC22A2	Solute carrier family 22 (organic cation transporter), member 2
D11	Hs.567337	NM_021977	SLC22A3	Solute carrier family 22 (extraneuronal monoamine transporter), member 3
D12	Hs.369252	NM_004790	SLC22A6	Solute carrier family 22 (organic anion transporter), member 6
E01	Hs.485438	NM_006672	SLC22A7	Solute carrier family 22 (organic anion transporter), member 7

Table B.1–continued

E02	Hs.266223	NM_004254	SLC22A8	Solute carrier family 22 (organic anion transporter), member 8
E03	Hs.502772	NM_080866	SLC22A9	Solute carrier family 22 (organic anion/cation transporter), member 9
E04	Hs.459187	NM_004213	SLC28A1	Solute carrier family 28 (sodium-coupled nucleoside transporter), member 1
E05	Hs.367833	NM_004212	SLC28A2	Solute carrier family 28 (sodium-coupled nucleoside transporter), member 2
E06	Hs.591877	NM_022127	SLC28A3	Solute carrier family 28 (sodium-coupled nucleoside transporter), member 3
E07	Hs.25450	NM_004955	SLC29A1	Solute carrier family 29 (nucleoside transporter), member 1
E08	Hs.569017	NM_001532	SLC29A2	Solute carrier family 29 (nucleoside transporter), member 2
E09	Hs.653218	NM_006516	SLC2A1	Solute carrier family 2 (facilitated glucose transporter), member 1
E10	Hs.167584	NM_000340	SLC2A2	Solute carrier family 2 (facilitated glucose transporter), member 2
E11	Hs.419240	NM_006931	SLC2A3	Solute carrier family 2 (facilitated glucose transporter), member 3
E12	Hs.532315	NM_001859	SLC31A1	Solute carrier family 31 (copper transporters), member 1
F01	Hs.221847	NM_018976	SLC38A2	Solute carrier family 38, member 2
F02	Hs.195155	NM_033518	SLC38A5	Solute carrier family 38, member 5
F03	Hs.112916	NM_000341	SLC3A1	Solute carrier family 3 (cysteine, dibasic and neutral amino acid transporters, activator of cysteine, dibasic and neutral amino acid transport), member 1
F04	Hs.502769	NM_002394	SLC3A2	Solute carrier family 3 (activators of dibasic and neutral amino acid transport), member 2
F05	Hs.1964	NM_000343	SLC5A1	Solute carrier family 5 (sodium/glucose cotransporter), member 1
F06	Hs.130101	NM_014227	SLC5A4	Solute carrier family 5 (low affinity glucose transporter), member 4
F07	Hs.489190	NM_014251	SLC25A13	Solute carrier family 25, member 13 (citrin)
F08	Hs.390594	NM_014331	SLC7A11	Solute carrier family 7 (cationic amino acid transporter, y+ system), member 11
F09	Hs.513797	NM_003486	SLC7A5	Solute carrier family 7 (cationic amino acid transporter, y+ system), member 5
F10	Hs.351571	NM_003983	SLC7A6	Solute carrier family 7 (cationic amino acid transporter, y+ system), member 6

Table B.1–continued

F11	Hs.513147	NM_003982	SLC7A7	Solute carrier family 7 (cationic amino acid transporter, y+ system), member 7
F12	Hs.632348	NM_182728	SLC7A8	Solute carrier family 7 (cationic amino acid transporter, y+ system), member 8
G01	Hs.408567	NM_014270	SLC7A9	Solute carrier family 7 (cationic amino acid transporter, y+ system), member 9
G02	Hs.46440	NM_005075	SLCO1A2	Solute carrier organic anion transporter family, member 1A2
G03	Hs.449738	NM_006446	SLCO1B1	Solute carrier organic anion transporter family, member 1B1
G04	Hs.504966	NM_019844	SLCO1B3	Solute carrier organic anion transporter family, member 1B3
G05	Hs.518270	NM_005630	SLCO2A1	Solute carrier organic anion transporter family, member 2A1
G06	Hs.7884	NM_007256	SLCO2B1	Solute carrier organic anion transporter family, member 2B1
G07	Hs.311187	NM_013272	SLCO3A1	Solute carrier organic anion transporter family, member 3A1
G08	Hs.235782	NM_016354	SLCO4A1	Solute carrier organic anion transporter family, member 4A1
G09	Hs.352018	NM_000593	TAP1	Transporter 1, ATP-binding cassette, sub-family B (MDR/TAP)
G10	Hs.502	NM_000544	TAP2	Transporter 2, ATP-binding cassette, sub-family B (MDR/TAP)
G11	Hs.519320	NM_003374	VDAC1	Voltage-dependent anion channel 1
G12	Hs355927	NM_003375	VDAC2	Voltage-dependent anion channel 2
H01	Hs.534255	NM_004048	B2M	Beta-2-microglobulin
H02	Hs.412707	NM_00194	HPRT1	Hypoxanthine phosphoribosyltransferase 1 (Lesch-Nyhan syndrome)
H03	Hs.546356	NM_012423	RPL13A	Ribosomal protein L13a
H04	Hs.544577	NM_002046	GAPDH	Glyceraldehyde-3-phosphate dehydrogenase
H05	Hs.520640	NM_001101	ACTB	Actin, beta
H06	NA	NA	HGDC	Human Genomic DNA Contamination
H07	NA	NA	RTC	Reverse Transcription Control
H08	NA	NA	RTC	Reverse Transcription Control
H09	NA	NA	RTC	Reverse Transcription Control
H10	NA	NA	PPC	Positive PCR Control
H11	NA	NA	PPC	Positive PCR Control
H12	NA	NA	PPC	Positive PCR Control

Table B.2. MCF10A human drug transporter array C_T values (cycle threshold) and corresponding gene expression levels.

Position	Symbol	Average C_T	Normalized Expression Level
A1	ABCA1	35.36	7.48E-07
A2	ABCA12	20.41	2.36E-02
A3	ABCA13	30.23	2.61E-05
A4	ABCA2	27.02	2.41E-04
A5	ABCA3	25.08	9.29E-04
A6	ABCA4	30.30	2.49E-05
A7	ABCA9	26.85	2.72E-04
A8	ABCB1	34.31	1.54E-06
A9	ABCB11	36.47	3.44E-07
A10	ABCB4	29.69	3.80E-05
A11	ABCB5	29.47	4.43E-05
A12	ABCB6	23.49	2.79E-03
B1	ABCC1	23.36	3.05E-03
B2	ABCC10	26.29	4.00E-04
B3	ABCC11	28.37	9.45E-05
B4	ABCC12	32.26	6.39E-06
B5	ABCC2	25.68	6.10E-04
B6	ABCC3	21.20	1.36E-02
B7	ABCC4	24.67	1.24E-03
B8	ABCC5	23.54	2.69E-03
B9	ABCC6	33.12	3.52E-06
B10	ABCD1	26.20	4.26E-04
B11	ABCD3	23.08	3.71E-03
B12	ABCD4	28.40	9.30E-05
C1	ABCF1	24.62	1.28E-03
C2	ABCG2	33.44	2.82E-06
C3	ABCG8	32.95	3.97E-06
C4	AQP1	30.27	2.53E-05
C5	AQP7	27.72	1.49E-04
C6	AQP9	27.35	1.92E-04
C7	ATP6V0C	21.59	1.04E-02
C8	ATP7A	24.63	1.27E-03
C9	ATP7B	27.88	1.33E-04
C10	MVP	22.04	7.63E-03
C11	SLC10A1	27.91	1.30E-04
C12	SLC10A2	32.78	4.46E-06
D1	SLC15A1	34.63	1.23E-06
D2	SLC15A2	31.22	1.31E-05
D3	SLC16A1	23.60	2.58E-03
D4	SLC16A2	29.95	3.17E-05
D5	SLC16A3	26.71	3.00E-04
D6	SLC19A1	26.82	2.77E-04
D7	SLC19A2	22.82	4.45E-03
D8	SLC19A3	26.66	3.11E-04
D9	SLC22A1	29.43	4.56E-05

Table B.2–continued

D10	SLC22A2	29.51	4.30E-05
D11	SLC22A3	30.76	1.81E-05
D12	SLC22A6	33.39	2.92E-06
E1	SLC22A7	37.20	2.08E-07
E2	SLC22A8	37.27	1.98E-07
E3	SLC22A9	31.84	8.53E-06
E4	SLC28A1	35.64	6.14E-07
E5	SLC28A2	31.01	1.52E-05
E6	SLC28A3	23.57	2.63E-03
E7	SLC29A1	24.37	1.52E-03
E8	SLC29A2	26.06	4.69E-04
E9	SLC2A1	25.71	6.00E-04
E10	SLC2A2	31.87	8.36E-06
E11	SLC2A3	26.73	2.96E-04
E12	SLC31A1	21.50	1.11E-02
F1	SLC38A2	20.27	2.60E-02
F2	SLC38A5	30.50	2.16E-05
F3	SLC3A1	22.37	6.05E-03
F4	SLC3A2	19.37	4.85E-02
F5	SLC5A1	28.97	6.27E-05
F6	SLC5A4	28.72	7.45E-05
F7	SLC25A13	23.14	3.55E-03
F8	SLC7A11	21.83	8.81E-03
F9	SLC7A5	19.25	5.28E-02
F10	SLC7A6	23.34	3.09E-03
F11	SLC7A7	24.52	1.37E-03
F12	SLC7A8	26.24	4.14E-04
G1	SLC7A9	32.18	6.74E-06
G2	SLCO1A2	38.04	1.16E-07
G3	SLCO1B1	34.60	1.26E-06
G4	SLCO1B3	31.30	1.24E-05
G5	SLCO2A1	30.25	2.57E-05
G6	SLCO2B1	30.65	1.95E-05
G7	SLCO3A1	23.88	2.12E-03
G8	SLCO4A1	24.51	1.37E-03
G9	TAP1	26.56	3.31E-04
G10	TAP2	21.76	9.27E-03
G11	VDAC1	17.64	1.61E-01
G12	VDAC2	19.58	4.19E-02

Table B.3. HMEC human drug transporter array gene expression levels

Well	Sample Name	Avg C_T	Normalized Expression Level
A1	ABCA1	27.87	4.01E-04
A2	ABCA12	24.57	3.59E-03
A3	ABCA13	30.60	6.92E-05
A4	ABCA2	28.15	3.67E-04
A5	ABCA3	28.49	3.27E-04
A6	ABCA4	27.80	5.09E-04
A7	ABCA9	30.62	9.21E-05
A8	ABCB1	33.42	5.19E-06
A9	ABCB11	32.02	1.31E-05
A10	ABCB4	31.79	3.42E-05
A11	ABCB5	31.44	1.96E-05
A12	ABCB6	24.93	5.26E-03
B1	ABCC1	25.44	2.32E-03
B2	ABCC10	27.35	5.54E-04
B3	ABCC11	31.21	4.27E-05
B4	ABCC12	35.05	5.37E-06
B5	ABCC2	30.85	7.76E-05
B6	ABCC3	25.49	2.52E-03
B7	ABCC4	30.15	2.83E-04
B8	ABCC5	25.32	2.23E-03
B9	ABCC6	32.47	8.43E-05
B10	ABCD1	27.31	8.88E-04
B11	ABCD3	23.80	6.32E-03
B12	ABCD4	29.80	1.50E-04
C1	ABCF1	24.70	3.47E-03
C2	ABCG2	33.05	1.56E-05
C3	ABCG8	32.18	1.77E-05
C4	AQP1	30.92	7.21E-05
C5	AQP7	27.46	6.77E-04
C6	AQP9	30.41	9.63E-05
C7	ATP6V0C	21.59	2.85E-02
C8	ATP7A	26.33	1.10E-03
C9	ATP7B	29.24	1.54E-04
C10	MVP	23.60	9.34E-03
C11	SLC10A1	29.33	1.51E-04
C12	SLC10A2	32.33	1.16E-05
D1	SLC15A1	28.96	1.79E-04
D2	SLC15A2	28.03	3.74E-04
D3	SLC16A1	25.94	1.82E-03

Table B.3–continued

D4	SLC16A2	29.09	2.10E-04
D5	SLC16A3	27.67	4.96E-04
D6	SLC19A1	29.35	1.58E-04
D7	SLC19A2	25.21	2.21E-03
D8	SLC19A3	32.51	2.54E-05
D9	SLC22A1	31.17	4.20E-05
D10	SLC22A2	29.38	1.03E-04
D11	SLC22A3	27.20	6.67E-04
D12	SLC22A6	32.98	7.04E-06
E1	SLC22A7	37.75	7.22E-07
E2	SLC22A8	30.78	1.44E-05
E3	SLC22A9	32.85	1.91E-05
E4	SLC25A13	32.44	2.87E-05
E5	SLC28A1	30.74	7.17E-05
E6	SLC28A2	27.89	3.31E-04
E7	SLC28A3	27.00	8.81E-04
E8	SLC29A1	27.51	4.77E-04
E9	SLC29A2	21.70	2.61E-02
E10	SLC2A1	32.28	1.53E-05
E11	SLC2A2	28.49	3.20E-04
E12	SLC2A3	25.10	3.18E-03
F1	SLC31A1	22.37	1.48E-02
F2	SLC38A2	29.93	8.64E-05
F3	SLC38A5	24.14	4.84E-03
F4	SLC3A1	22.64	1.56E-02
F5	SLC3A2	25.64	1.65E-03
F6	SLC5A1	32.05	5.56E-05
F7	SLC5A4	24.97	2.61E-03
F8	SLC7A11	27.35	5.60E-04
F9	SLC7A5	22.18	2.03E-02
F10	SLC7A6	25.12	2.69E-03
F11	SLC7A7	28.02	4.51E-04
F12	SLC7A8	27.00	1.20E-03
G1	SLC7A9	33.50	8.99E-06
G2	SLCO1A2	32.80	7.73E-06
G3	SLCO1B1	31.04	2.62E-05
G4	SLCO1B3	32.63	2.30E-05
G5	SLCO2A1	30.51	6.98E-05
G6	SLCO2B1	30.41	4.13E-05
G7	SLCO3A1	24.86	3.19E-03
G8	SLCO4A1	28.55	2.59E-04

Table B.3–continued

G9	TAP1	27.95	4.01E-04
G10	TAP2	24.45	4.15E-03
G11	VDAC1	20.30	6.69E-02
G12	VDAC2	20.51	5.63E-02

REFERENCES

1. S. Ito and J. Alcorn. Xenobiotic transporter expression and function in the human mammary gland. Adv Drug Deliv Rev. 55:653-665 (2003).

2. P. J. McNamara and M. Abbassi. Neonatal exposure to drugs in breast milk. Pharm Res. 21:555-566 (2004).

3. American Academy of Pediatrics Committee on Drugs. Transfer of drugs and other chemicals into human milk. Pediatrics. 108:776-789 (2001).

4. J. C. Fleishaker. Models and methods for predicting drug transfer into human milk. Adv Drug Deliv Rev. 55:643-652 (2003).

5. J. C. Fleishaker, N. Desai, and P. J. McNamara. Factors affecting the milk-to-plasma drug concentration ratio in lactating women: physical interactions with protein and fat. J Pharm Sci. 76:189-193 (1987).

6. P. O. Anderson. Drug use during breast-feeding. Clin Pharm. 10:594-624 (1991).

7. P. J. McNamara, D. Burgio, and S. D. Yoo. Pharmacokinetics of cimetidine during lactation: species differences in cimetidine transport into rat and rabbit milk. J Pharmacol Exp Ther. 261:918-923 (1992).

8. K. L. Audus, R. L. Bartel, I. J. Hidalgo, and R. T. Borchardt. The use of cultured epithelial and endothelial cells for drug transport and metabolism studies. Pharm Res. 7:435-451 (1990).

9. V. S. Toddywalla, F. W. Kari, and M. C. Neville. Active transport of nitrofurantoin across a mouse mammary epithelial monolayer. J Pharmacol Exp Ther. 280:669-676 (1997).

10. G. Merino, J. W. Jonker, E. Wagenaar, A. E. van Herwaarden, and A. H. Schinkel. The breast cancer resistance protein (BCRP/ABCG2) affects pharmacokinetics, hepatobiliary excretion, and milk secretion of the antibiotic nitrofurantoin. Mol Pharmacol. 67:1758-1764 (2005).

11. H. D. Soule, T. M. Maloney, S. R. Wolman, W. D. Peterson Jr, R. Brenz, C. M. McGrath, J. Russo, R. J. Pauley, R. F. Jones, and S. C. Brooks. Isolation and characterization of a spontaneously immortalized human breast epithelial cell line, MCF-10. Cancer Res. 50:6075-6086 (1990).

12. M. Matsuda, J. A. Lockefeer, and N. D. Horseman. Aldolase C/zebrin gene regulation by prolactin during pregnancy and lactation. Endocrine. 20:91-100 (2003).

13. J. L. McManaman and M. C. Neville. Mammary physiology and milk secretion. Adv Drug Deliv Rev. 55:629-641 (2003).

14. J. Debnath, S. K. Muthuswamy, and J. S. Brugge. Morphogenesis and oncogenesis of MCF-10A mammary epithelial acini grown in three-dimensional basement membrane cultures. Methods. 30:256-268 (2003).

15. B. Margolis and J. P. Borg. Apicobasal polarity complexes. J Cell Sci. 118:5157-5159 (2005).

16. L. A. Lapierre. The molecular structure of the tight junction. Adv Drug Deliv Rev. 41:255-264 (2000).

17. D. A. Nguyen and M. C. Neville. Tight junction regulation in the mammary gland. J Mammary Gland Biol Neoplasia. 3:233-246 (1998).

18. D. A. Nguyen, A. F. Parlow, and M. C. Neville. Hormonal regulation of tight junction closure in the mouse mammary epithelium during the transition from pregnancy to lactation. J Endocrinol. 170:347-356 (2001).

19. K. S. Zettl, M. D. Sjaastad, P. M. Riskin, G. Parry, T. E. Machen, and G. L. Firestone. Glucocorticoid-induced formation of tight junctions in mouse mammary epithelial cells in vitro. Proc Natl Acad Sci U S A. 89:9069-9073 (1992).

20. A. M. Marshall, V. P. Pai, M. A. Sartor, and N. D. Horseman. In vitro multipotent differentiation and barrier function of a human mammary epithelium. Cell Tissue Res. (2008).

21. M. C. Neville and C. T. Walsh. Effects of xenobiotics on milk secretion and composition. Am J Clin Nutr. 61:687S-694S (1995).

22. C. Yeaman, K. K. Grindstaff, and W. J. Nelson. New perspectives on mechanisms involved in generating epithelial cell polarity. Physiol Rev. 79:73-98 (1999).

23. J. Debnath and J. S. Brugge. Modelling glandular epithelial cancers in three-dimensional cultures. Nat Rev Cancer. 5:675-688 (2005).

24. J. L. Blum, M. E. Zeigler, and M. S. Wicha. Regulation of rat mammary gene expression by extracellular matrix components. Exp Cell Res. 173:322-340 (1987).

25. C. Hagios, A. Lochter, and M. J. Bissell. Tissue architecture: the ultimate regulator of epithelial function? Philos Trans R Soc Lond B Biol Sci. 353:857-870 (1998).

26. M. J. Bissell and D. Bilder. Polarity determination in breast tissue: desmosomal adhesion, myoepithelial cells, and laminin 1. Breast Cancer Res. 5:117-119 (2003).

27. V. Wong, D. Ching, P. D. McCrea, and G. L. Firestone. Glucocorticoid down-regulation of fascin protein expression is required for the steroid-induced formation of tight junctions and cell-cell interactions in rat mammary epithelial tumor cells. J Biol Chem. 274:5443-5453 (1999).

28. V. C. Fogg, C. J. Liu, and B. Margolis. Multiple regions of Crumbs3 are required for tight junction formation in MCF10A cells. J Cell Sci. 118:2859-2869 (2005).

29. J. DiRenzo, S. Signoretti, N. Nakamura, R. Rivera-Gonzalez, W. Sellers, M. Loda, and M. Brown. Growth factor requirements and basal phenotype of an immortalized mammary epithelial cell line. Cancer Res. 62:89-98 (2002).

30. Y. Li, J. Pan, J. L. Li, J. H. Lee, C. Tunkey, K. Saraf, J. C. Garbe, M. Z. Whitley, S. A. Jelinsky, M. R. Stampfer, and S. A. Haney. Transcriptional changes associated with breast cancer occur as normal human mammary epithelial cells overcome senescence barriers and become immortalized. Mol Cancer. 6:7 (2007).

31. L. M. Reid and D. M. Jefferson (eds.). Mammalian Cell Culture, Plenum Publishing Company, , 1984.

32. C. Bertram and R. Hass. MMP-7 is involved in the aging of primary human mammary epithelial cells (HMEC). Exp Gerontol. 43:209-217 (2008).

33. J. P. Mathur (ed.). Mammalian Cell Culture : The use of Serum-Free Hormone Supplemented Media, Plenum Plublishing Company, New York, London, 1984.

34. D. Barnes. Attachment Factors in Cell Culture, In J. P. Mathur (ed.), Plenum Publishing Company, New York, 1984.

35. S. P. Ethier, R. M. Summerfelt, K. C. Cundiff, and B. B. Asch. The influence of growth factors on the proliferative potential of normal and primary breast cancer-derived human breast epithelial cells. Breast Cancer Res Treat. 17:221-230 (1991).

36. Q. Guo, W. Tang, N. Kokudo, Y. Sugawara, K. Miki, H. Karako, X. Qu, M. Nakata, Y. Fujita-Yamaguchi, and M. Makuuchi. Epidermal growth factor-mediated growth control of confluent mammary epithelial cells cultured on artificial basement membrane. Int J Mol Med. 16:395-399 (2005).

37. D. A. Groneberg, F. Doring, M. Nickolaus, H. Daniel, and A. Fischer. Renal assimilation of short chain peptides: visualization of tubular peptide uptake. Pharm Res. 19:1209-1214 (2002).

38. S. Tavelin, J. Grasjo, J. Taipalensuu, G. Ocklind, and P. Artursson. Applications of epithelial cell culture in studies of drug transport. Methods Mol Biol. 188:233-272 (2002).

39. D. L. Purich. Contemporary Enzyme Kinetics and Mechanism, Academic Press, New York, 1983.

40. Y. Zhang, C. Bachmeier, and D. W. Miller. In vitro and in vivo models for assessing drug efflux transporter activity. Adv Drug Deliv Rev. 55:31-51 (2003).

41. Claus-Michael Lehr (ed.). Cell Culture Models of Biological Barriers; in-Vitro Test Systems for Drug Absorption and Delivery, Taylor & Francis, London and New York, 2002.

42. G. Pan and W. F. Elmquist. Mitoxantrone Permeability in MDCKII Cells Is Influenced by Active Influx Transport. Mol Pharm. 4:475-483 (2007).

43. P. M. Gerk, R. J. Kuhn, N. S. Desai, and P. J. McNamara. Active transport of nitrofurantoin into human milk. Pharmacotherapy. 21:669-675 (2001).

44. F. W. Kari, R. Weaver, and M. C. Neville. Active transport of nitrofurantoin across the mammary epithelium in vivo. J Pharmacol Exp Ther. 280:664-668 (1997).

45. P. M. Gerk, C. Y. Oo, E. W. Paxton, J. A. Moscow, and P. J. McNamara. Interactions between cimetidine, nitrofurantoin, and probenecid active transport into rat milk. J Pharmacol Exp Ther. 296:175-180 (2001).

46. J. Alcorn, X. Lu, J. A. Moscow, and P. J. McNamara. Transporter gene expression in lactating and nonlactating human mammary epithelial cells using real-time reverse transcription-polymerase chain reaction. J Pharmacol Exp Ther. 303:487-496 (2002).

47. K. Ito, H. Suzuki, T. Horie, and Y. Sugiyama. Apical/basolateral surface expression of drug transporters and its role in vectorial drug transport. Pharm Res. 22:1559-1577 (2005).

48. Y. Sai and A. Tsuji. Transporter-mediated drug delivery: recent progress and experimental approaches. Drug Discov Today. 9:712-720 (2004).

49. A. L. Givan. Flow Cytometry : First Principles, Wiley-Liss, New York, 2001.

50. M. G. Macey. Flow cytometry. :290 (2007).

51. J. P. Robinson, Z. Darzynkiewicz, and H. A. Crissman. Flow Cytometry, Academic Press, San Diego, 1994.

52. W. T. Beck, T. M. Grogan, C. L. Willman, C. Cordon-Cardo, D. M. Parham, J. F. Kuttesch, M. Andreeff, S. E. Bates, C. W. Berard, J. M. Boyett, N. A. Brophy, H. J. Broxterman, H. S. Chan, W. S. Dalton, M. Dietel, A. T. Fojo, R. D. Gascoyne, D. Head, P. J. Houghton, D. K. Srivastava, M. Lehnert, C. P. Leith, E. Paietta, Z. P. Pavelic, and R. Weinstein. Methods to detect P-glycoprotein-associated

multidrug resistance in patients' tumors: consensus recommendations. Cancer Res. 56:3010-3020 (1996).

53. W. T. Ambrosius. Topics in Biostatistics, Humana Press, Totowa, N.J., 2007.

54. R. C. Littell, R. C. Littell, W. W. Stroup, and R. J. Freund. SAS for linear models, fourth edition. (2002).

55. C. T. Wittwer, K. M. Ririe, R. V. Andrew, D. A. David, R. A. Gundry, and U. J. Balis. The LightCycler: a microvolume multisample fluorimeter with rapid temperature control. BioTechniques. 22:176-181 (1997).

56. T. B. Morrison, J. J. Weis, and C. T. Wittwer. Quantification of low-copy transcripts by continuous SYBR Green I monitoring during amplification. BioTechniques. 24:954-8, 960, 962 (1998).

57. R. Higuchi, G. Dollinger, P. S. Walsh, and R. Griffith. Simultaneous amplification and detection of specific DNA sequences. Biotechnology (N Y). 10:413-417 (1992).

58. R. Higuchi, C. Fockler, G. Dollinger, and R. Watson. Kinetic PCR analysis: real-time monitoring of DNA amplification reactions. Biotechnology (N Y). 11:1026-1030 (1993).

59. O. Sabek, M. T. Dorak, M. Kotb, A. O. Gaber, and L. Gaber. Quantitative detection of T-cell activation markers by real-time PCR in renal transplant rejection and correlation with histopathologic evaluation. Transplantation. 74:701-707 (2002).

60. M. C. Neville, T. B. McFadden, and I. Forsyth. Hormonal regulation of mammary differentiation and milk secretion. J Mammary Gland Biol Neoplasia. 7:49-66 (2002).

61. S. Zakelj, I. Legen, M. Veber, and A. Kristl. The influence of buffer composition on tissue integrity during permeability experiments "in vitro". Int J Pharm. 272:173-180 (2004).

62. P. M. Gerk, L. Hanson, M. C. Neville, and P. J. McNamara. Sodium dependence of nitrofurantoin active transport across mammary epithelia and effects of dipyridamole, nucleosides, and nucleobases. Pharm Res. 19:299-305 (2002).

63. M. J. Bissell, A. Rizki, and I. S. Mian. Tissue architecture: the ultimate regulator of breast epithelial function. Curr Opin Cell Biol. 15:753-762 (2003).

64. Y. Izumi, T. Hirose, Y. Tamai, S. Hirai, Y. Nagashima, T. Fujimoto, Y. Tabuse, K. J. Kemphues, and S. Ohno. An atypical PKC directly associates and colocalizes at the epithelial tight junction with ASIP, a mammalian homologue of Caenorhabditis elegans polarity protein PAR-3. J Cell Biol. 143:95-106 (1998).

65. L. A. Doyle, W. Yang, L. V. Abruzzo, T. Krogmann, Y. Gao, A. K. Rishi, and D. D. Ross. A multidrug resistance transporter from human MCF-7 breast cancer cells. Proc Natl Acad Sci U S A. 95:15665-15670 (1998).

66. R. I. Freshney. Culture of Animal Cells : A Manual of Basic Technique, Wiley-Liss, New York, 1994.

67. J. Paul. Cell and Tissue Culture, Churchill Livingstone; distributed in the U.S.A. by Longman, Edinburgh; New York, 1975.

68. American Society for Cell Biology, D. W. Barnes, and J. P. Mather. Animal Cell Culture Methods, Academic Press, San Diego, 1998.

69. G. H. Rothblat and V. J. Cristofalo. Growth, Nutrition, and Metabolism of Cells in Culture, Academic Press, New York, 1972; 1977.

70. M. Garcia-Escarp, V. Martinez-Munoz, I. Sales-Pardo, J. Barquinero, J. C. Domingo, P. Marin, and J. Petriz. Flow cytometry-based approach to ABCG2 function suggests that the transporter differentially handles the influx and efflux of drugs. Cytometry A. 62:129-138 (2004).

71. Y. Xiao, R. Davidson, A. Smith, D. Pereira, S. Zhao, J. Soglia, D. Gebhard, S. de Morais, and D. B. Duignan. A 96-well efflux assay to identify ABCG2 substrates using a stably transfected MDCK II cell line. Mol Pharm. 3:45-54 (2006).

72. E. J. Wang, C. N. Casciano, R. P. Clement, and W. W. Johnson. In vitro flow cytometry method to quantitatively assess inhibitors of P-glycoprotein. Drug Metab Dispos. 28:522-528 (2000).

73. I. Ivnitski-Steele, R. S. Larson, D. M. Lovato, H. M. Khawaja, S. S. Winter, T. I. Oprea, L. A. Sklar, and B. S. Edwards. High-throughput flow cytometry to detect selective inhibitors of ABCB1, ABCC1, and ABCG2 transporters. Assay Drug Dev Technol. 6:263-276 (2008).

74. H. Minderman, A. Suvannasankha, K. L. O'Loughlin, G. L. Scheffer, R. J. Scheper, R. W. Robey, and M. R. Baer. Flow cytometric analysis of breast cancer resistance protein expression and function. Cytometry. 48:59-65 (2002).

75. Q. Wang, R. Strab, P. Kardos, C. Ferguson, J. Li, A. Owen, and I. J. Hidalgo. Application and limitation of inhibitors in drug-transporter interactions studies. Int J Pharm. 356:12-18 (2008).

76. L. A. Doyle and D. D. Ross. Multidrug resistance mediated by the breast cancer resistance protein BCRP (ABCG2). Oncogene. 22:7340-7358 (2003).

77. C. J. Henrich, H. R. Bokesch, M. Dean, S. E. Bates, R. W. Robey, E. I. Goncharova, J. A. Wilson, and J. B. McMahon. A high-throughput cell-based assay for inhibitors of ABCG2 activity. J Biomol Screen. 11:176-183 (2006).

78. Q. Mao and J. D. Unadkat. Role of the breast cancer resistance protein (ABCG2) in drug transport. AAPS J. 7:E118-33 (2005).

79. A. Feofanov, S. Sharonov, I. Kudelina, F. Fleury, and I. Nabiev. Localization and molecular interactions of mitoxantrone within living K562 cells as probed by confocal spectral imaging analysis. Biophys J. 73:3317-3327 (1997).

80. B. L. Abbott. ABCG2 (BCRP) expression in normal and malignant hematopoietic cells. Hematol Oncol. 21:115-130 (2003).

81. A. Poirier, T. Lave, R. Portmann, M. E. Brun, F. Senner, M. Kansy, H. P. Grimm, and C. Funk. Design, data analysis, and simulation of in vitro drug transport kinetic experiments using a mechanistic in vitro model. Drug Metab Dispos. 36:2434-2444 (2008).

82. P. J. Smith, H. R. Sykes, M. E. Fox, and I. J. Furlong. Subcellular distribution of the anticancer drug mitoxantrone in human and drug-resistant murine cells analyzed by flow cytometry and confocal microscopy and its relationship to the induction of DNA damage. Cancer Res. 52:4000-4008 (1992).

83. H. Daniel and G. Kottra. The proton oligopeptide cotransporter family SLC15 in physiology and pharmacology. Pflugers Arch. 447:610-618 (2004).

84. I. Rubio-Aliaga and H. Daniel. Mammalian peptide transporters as targets for drug delivery. Trends Pharmacol Sci. 23:434-440 (2002).

85. P. Luckner and M. Brandsch. Interaction of 31 β-lactam antibiotics with the H+/peptide symporter PEPT2: analysis of affinity constants and comparison with PEPT1. European Journal of Pharmaceutics and Biopharmaceutics. 59:17-24 (2005).

86. D. A. Groneberg, F. Doring, S. Theis, M. Nickolaus, A. Fischer, and H. Daniel. Peptide transport in the mammary gland: expression and distribution of PEPT2 mRNA and protein. Am J Physiol Endocrinol Metab. 282:E1172-9 (2002).

87. M. Klapper, H. Daniel, and F. Doring. Cytosolic COOH terminus of the peptide transporter PEPT2 is involved in apical membrane localization of the protein. Am J Physiol Cell Physiol. 290:C472-83 (2006).

88. K. L. Parker, J. S. Lazo, L. S. Goodman, A. Gilman, and L. L. Brunton. Goodman & Gilman's the Pharmacological Basis of Therapeutics, McGraw-Hill, New York, 2006.

89. F. Doring, T. Michel, A. Rosel, M. Nickolaus, and H. Daniel. Expression of the mammalian renal peptide transporter PEPT2 in the yeast Pichia pastoris and applications of the yeast system for functional analysis. Mol Membr Biol. 15:79-88 (1998).

90. U. Wenzel, D. Diehl, M. Herget, and H. Daniel. Endogenous expression of the renal high-affinity H+-peptide cotransporter in LLC-PK1 cells. Am J Physiol. 275:C1573-9 (1998).

91. P. S. Burton, R. A. Conradi, N. F. Ho, A. R. Hilgers, and R. T. Borchardt. How structural features influence the biomembrane permeability of peptides. J Pharm Sci. 85:1336-1340 (1996).

92. A. Ruhl, S. Hoppe, I. Frey, H. Daniel, and M. Schemann. Functional expression of the peptide transporter PEPT2 in the mammalian enteric nervous system. J Comp Neurol. 490:1-11 (2005).

93. S. T. Dieck, H. Heuer, J. Ehrchen, C. Otto, and K. Bauer. The peptide transporter PepT2 is expressed in rat brain and mediates the accumulation of the fluorescent dipeptide derivative beta-Ala-Lys-Nepsilon-AMCA in astrocytes. Glia. 25:10-20 (1999).

94. D. A. Groneberg, F. Doring, P. R. Eynott, A. Fischer, and H. Daniel. Intestinal peptide transport: ex vivo uptake studies and localization of peptide carrier PEPT1. Am J Physiol Gastrointest Liver Physiol. 281:G697-704 (2001).

95. D. A. Groneberg, I. Rubio-Aliaga, M. Nickolaus, F. Doring, A. Fischer, and H. Daniel. Direct visualization of peptide uptake activity in the central nervous system of the rat. Neurosci Lett. 364:32-36 (2004).

96. M. Ries, U. Wenzel, and H. Daniel. Transport of cefadroxil in rat kidney brush-border membranes is mediated by two electrogenic H+-coupled systems. J Pharmacol Exp Ther. 271:1327-1333 (1994).

97. W. Akarawut, C. J. Lin, and D. E. Smith. Noncompetitive inhibition of glycylsarcosine transport by quinapril in rabbit renal brush border membrane vesicles: effect on high-affinity peptide transporter. J Pharmacol Exp Ther. 287:684-690 (1998).

98. K. Saar, R. Mahlapuu, E. Laidmae, A. Valkna, U. Kahl, E. Karelson, and U. Langel. Characterisation of a new chimeric ligand for galanin receptors: galanin(1-13)-[D-Trp(32)]-neuropeptide Y(25-36)amide. Regul Pept. 102:15-19 (2001).

99. P. M. Bahadduri, V. M. D'Souza, J. K. Pinsonneault, W. Sadee, S. Bao, D. L. Knoell, and P. W. Swaan. Functional characterization of the peptide transporter PEPT2 in primary cultures of human upper airway epithelium. Am J Respir Cell Mol Biol. 32:319-325 (2005).

100. I. Rubio-Aliaga and H. Daniel. Peptide transporters and their roles in physiological processes and drug disposition. Xenobiotica. 38:1022-1042 (2008).

101. J. Yang, G. Zhou, X. Cao, Quanli, and J. Dong. Study on the Fluorescence Characteristics of Alkaline Degradation of Cefadroxil, Cephradine, Cefotaximum Sodium and Amoxicillini. Anal Lett. 31:1047 (1998).

102. A. Biegel, I. Knutter, B. Hartrodt, S. Gebauer, S. Theis, P. Luckner, G. Kottra, M. Rastetter, K. Zebisch, I. Thondorf, H. Daniel, K. Neubert, and M. Brandsch. The renal type H+/peptide symporter PEPT2: structure-affinity relationships. Amino Acids. 31:137-156 (2006).

103. D. A. Kafetzis, C. A. Siafas, P. A. Georgakopoulos, and C. J. Papadatos. Passage of cephalosporins and amoxicillin into the breast milk. Acta Paediatr Scand. 70:285-288 (1981).